Development of an Experimental Methodology for Appraising the Dynamic Response of Tethered Tidal Turbines.

Stephanie Eugenia Ordonez Sanchez

Submitted in fulfilment of the requirements for the
Degree of Doctor of Philosophy
Department of Mechanical and Aerospace Engineering
University of Strathclyde

June, 2013

Signed:

Date:

Acknowledgements

I cannot thank enough all the people that supported me during the development of this thesis. I will try to mention each of you who played an important role throughout my PhD studies but please do not get offended if you are not here because those who know me already know that I am a very distracted person.

Firstly, I would like to thank my supervisors Mr. Cameron Johnstone, Dr. Andrew Grant and Dr. Gary Connor, without your help this thesis would not exist. Also thanks to the rest of the ESRU team but specially to Tom McCombes, Sam Rose and Gavin Murphy; I am deeply sorry if I stole your bright ideas but if you had not shared them with me I would probably had not finished my degree. I would also like to thank Prof. AbuBakr Bahaj and Dr. Paul Tuohy for their useful recomendations that greatly improved this thesis.

I would also like to express my gratitude to the mechanical engineering technical department. Jim, Niall, Andy, Steve, and so on. Many thanks for your patience, help and advice during the experimental phase of my PhD work. Similarly, many thanks to the technical team of DMEM and NAME department.

I also like to thank my dearest friends in Glasgow: Maria Carla, Shazad, Asma, Konstanze and the Mexican team in Glasgow. I really appreciate all the help and support given during my PhD thesis. But also many thanks for being so nice with me and making my life easier in a foreign country.

No me alcanzan las palabras para agradecer el apoyo que mi mamá, mi papá, Carlos y Paty me han brindado no sólo durante esta etapa de mi vida sino siempre. La admiración que tengo hacia ustedes me ayudo a pasar muchos obstáculos y escribir una tesis de doctorado. Su apoyo me dio el coraje para avanzar y llegar a la meta final. Igualmente, agradezco a mis tíos y primos. Tener una familia así siempre me motivo a terminar mis metas. Gracias por su apoyo y cariño incondicional.

Finalmente, me gustaría agradecer el apoyo que me dio Ger. Creo que eres la persona que sabe mejor cuán difícil fue obtener este logro. Muchas gracias por aguantarme en los momentos más difíciles y brindarme ayuda y palabras de motivación en cada momento - “ya sabes lo de siempre”.

Abstract

This thesis makes a comparison of different station keeping structures to support tidal energy converters. It was observed that the use of flexibly tethered turbines would be beneficial due to low material costs and the capability to permit the turbine's self alignment to the flow regime. However, because of the uncertainties over their dynamic behaviour, it was considered that an analysis of response in a range of conditions was essential before they could be considered as practical station keeping system.

Firstly, a static analysis was carried out for both rigid and flexible foundations. Thereafter, the thesis presents the development of an experimental methodology to study the dynamic response of tethered tidal energy converters. In this methodology, the alignment and oscillations of the three main rotational angles (i.e. roll, pitch and yaw), estimated over a period of time, were taken as the fundamental metrics of system behaviour. The analysis was extended into the frequency domain in order to estimate the intensity of the parameters that affect the turbine and its condition (e.g. blade failure, excessive backlash or misalignment, vortex shedding, etc.)

Within the methodology development a series of steps were specified, based on established protocols related to similar concepts (for example EquiMar) where parameters such as the selection of test facilities, blockage ratio limits or safety factors in applied loads were discussed. Instruments to measure the dynamic motion of turbines were specified, along with other instruments to measure power, thrust, angular velocity and flow speed. The final steps in the methodology denoted methods to analyse the acquired signals.

In order to verify the feasibility of the methodology, a series of experiments were carried out at various turbine models scales. Firstly, small turbine models were installed on a zero turbulence tow tank and a flume tank with significant levels of turbulence, under controlled conditions and at similar flow velocities. To compare the dynamic responses, studies were undertaken for a larger turbine deployed in the natural turbulence of an open tidal site and in a turbulent river stream affected by marine traffic.

This thesis concludes that the methodology proposed is suitable to characterise the dynamic response of tethered devices at various model scales. The results presented showed the advantages and disadvantages of using various turbine configurations. Therefore, this methodology can be used develop and validate analytical models that predict the dynamic response of flexibly moored turbines.

Contents

1 Introduction **1**

1.1 Introduction 1

1.2 Motivation and Objectives 1

1.3 Problem Statement 5

1.4 Hypothesis 7

1.4.1 Objectives 7

1.5 Thesis Outline 7

2 Literature Review **9**

2.1 Introduction 9

2.1.1 Deep Water Access 10

2.1.2 Minimum Cost 11

2.1.3 Water Column Effects 13

2.2 Foundations for Offshore Wind Turbines 15

2.2.1 Pile Foundations 15

2.2.2 Gravity Based Foundations (GBFs) 16

2.2.3 Flexible Moorings 17

2.3 Foundations for Wave Energy Converters (WECs) 20

2.3.1 Converter Type 21

2.3.2 Environmental Conditions 21

2.3.3 Material . . . 23
2.3.4 Mooring line configurations . . . 24
2.3.5 Footprint . . . 26
2.3.6 Bathymetry . . . 26
2.4 Anchors . . . 27
2.5 Summary and Conclusions . . . 30

3 Assessing Mooring Requirements for Tidal Energy Converters 33
3.1 Motivation and Objectives . . . 33
3.2 Foundations Applied to TECs . . . 34
3.3 Rotor Configurations . . . 36
3.3.1 Single Rotor Configuration . . . 36
3.3.2 Contra Rotating . . . 38
3.3.3 Side by Side Rotors . . . 39
3.4 Static Analysis of Support Structures . . . 40
3.4.1 Turbine Capacity, Dimensions and Environmental Effects . . . 40
3.4.2 Allowable Load and Displacement . . . 44
3.5 Results and Discussion . . . 46
3.5.1 Elements Dimensions and Displacement . . . 46
3.5.2 Material Cost . . . 48
3.5.3 Stress Analysis . . . 51
3.5.4 Footprint . . . 57
3.6 Conclusions and Final Remarks . . . 57

4 Methodology to Evaluate the Dynamic Response of Tethered Turbines 60
4.1 Motivation . . . 60
4.2 Methodology Description . . . 62

4.3 Facilities 64
4.4 Mechanical Design 66
4.4.1 Rotor Selection 68
4.4.2 Airfoil Selection 69
4.4.3 Scale Parameters 72
4.4.4 Rotor Hubs, Shafts and Bearings 73
4.4.5 Mechanical Control 74
4.4.6 Buoyancy 75
4.4.7 Rigid Structure 75
4.5 Instrumentation and Data Collection 76
4.5.1 Dynamic Response and Vibration 76
4.5.2 Structural Loads 79
4.5.3 Angular Velocity, Flow Velocity and Power 80
4.5.4 Installation and Electrical Connection 80
4.5.5 Calibration of sensors 82
4.5.5.1 Accelerometer/Inclinometer 82
4.5.5.2 Torque and Thrust Gauges 83
4.5.6 Data Logger and Sampling Rate 83
4.6 Signal Processing 85
4.6.1 Filters 85
4.6.2 Time Domain Analysis 87
4.6.3 Frequency domain analysis 89
4.6.4 Windowing 90
4.7 Mechanical Vibration Analysis 92
4.7.1 Rotational Velocities 94
4.7.2 Bearing Failure Detection 95

4.7.3 Von Karman Vortex 96

4.7.4 Vibration Tolerance Chart 97

4.8 Concluding Comments 98

5 Initial Evaluation of the Methodology to Evaluate the Dynamic Response of Tidal Turbines 99

5.1 Motivation and Objectives 99

5.2 Prototype Design 100

5.2.1 Facilities 100

5.2.2 Mechanical Design of Small Scale CRR 101

5.2.3 Instrumentation 103

5.2.4 Signal Processing 105

5.3 Flume and Tow Tank Experiments 105

5.3.1 Time Domain: Roll, Pitch and Yaw Motions 106

5.3.2 Frequency domain: Roll, Pitch and Yaw Vibrations 111

5.4 Summary 118

6 Dynamic Response Assessment of Tethered TECs on a Non-Turbulent Environment 119

6.1 Motivation and Objectives 119

6.2 Rotor Selection and Blade Manufacture 121

6.2.1 Blade Manufacture 121

6.2.2 Material Tensile Strength Tests 122

6.2.3 BEM Analysis 123

6.2.4 Stress analysis 126

6.3 Mechanical Design, Instrumentation and Other Features 128

6.4 Results and Discussion of the Dynamic Response 130

6.4.1 Dynamic Response: SR Turbines 130

6.4.2 Dynamic Response: CRR Turbines 138
6.4.3 Dynamic Response: SSR Turbines 145
6.5 Blade Failure Results and Discussion 148
6.5.1 Dynamic Response: SR Turbines 148
6.5.2 Dynamic Response: CRR Turbines 150
6.5.3 Dynamic Response: SSR Turbines 150
6.6 Summary 153

7 Dynamic Response Assessment of Scaled Up Tethered Turbines 156

7.1 Motivation and Objectives 156
7.2 Site Specification 158
7.3 Mechanical Design of the 3-4 CRR Turbine 158
7.4 Support Mechanism 162
7.5 Instrumentation 165
7.6 System Performance 169
7.7 Results and Discussion of the Dynamic Response in the Sound of Islay 169
7.7.1 Dynamic Response in Time Domain 169
7.7.2 Mechanical Vibrations in Frequency Domain 171
7.8 Results and Discussion of the Dynamic Response in the River Thames 173
7.8.1 Flow Speed 173
7.8.2 Turbulence Intensity 174
7.8.3 Dynamic Response in Time Domain: Roll 175
7.8.4 Dynamic Response in Time Domain: Pitch 177
7.8.5 Dynamic Response in Time Domain: Yaw 177
7.8.6 Frequency Domain Analysis: Roll 179
7.8.7 Frequency Domain Analysis: Pitch 183
7.8.8 Frequency Domain Analysis: Yaw 183

7.9 Summary 195

8 Implication to Operation of Tethered Turbines at Full Scale 197

8.1 Tethered Turbine Configurations 197

8.2 Small and Medium Scale Tethered Tidal Turbines 199

8.3 Vibration Analysis of Small and Medium Scale Tethered Tidal Turbines . . . 202

8.4 Final Assessment of Tethered Tidal Turbines 203

9 Conclusions and Recommendations 205

9.1 Conclusions 205

9.2 Contributions 207

9.3 Recommendations 208

9.3.1 Tolerance Charts and Condition Monitoring 209

A Drawings 210

B Existent Models to Evaluate Tethered Turbine Rotors 222

B.1 Dynamic Analysis Models to Study Tethered Wind Turbines 222

B.2 Hydrodynamic Software Packages 223

B.3 Blade Element Momentum 224

C Results 227

C.1 Probability Density Functions 227

C.2 Frequency Domain Analysis 227

Bibliography 232

List of Figures

1.1 Some of the Structural Concepts studied by Masters and Orme (2006): a) Pile Foundation, b) Gravity Based Foundation and c) Tethered Turbine. Figures based on Masters and Orme (2006). 3

1.2 Turbines studied by a)Francis and Hamilton (2007) and b)Mackie (2008) . Figures taken from Francis and Hamilton (2007) and Mackie (2008). 4

2.1 UK's Tidal Resource, taken from Marine Environmental Resource (2011). . 11

2.2 North Channel and South West of Islay, taken from Marine Environmental Resource (2011). 12

2.3 Separation of costs estimated by Polagye and Previsic (2006). 12

2.4 Cash Flow, taken from CJ Day Associates (2001). 13

2.5 Flow Velocity Profile. 14

2.6 OWTs a) Monopile b) GBF c) Flexible Mooring. 15

2.7 Mooring Configurations Studied by Bulder et al. (2003): a) Spread Mooring and b)TLM. 19

2.8 Mooring Configuration Studied by (Fulton, 2007). 20

2.9 Mooring Configurations: a) Single Catenary Mooring and b) Spread Taut Leg Mooring 25

2.10 Southwest of Islay Seabed Sediments, taken from Marion Harrald and Davies (2010). 27

2.11 West of Colonsay Seabed Sediments, taken from Marion Harrald and Davies (2010). 28

2.12 Drag Embedment Anchor. 28

2.13 Drag in Plate Anchors. 29

2.14 Driven Pile Suction Anchor. 29

2.15 Drilled and Grouted Anchor. 30

3.1 Diversity of Support Structures used in TECs. 35

3.2 Single Rotor. 37

3.3 Horizontal and Vertical Stabilizers. 37

3.4 Contra Rotating Rotor. 39

3.5 Side by Side Rotor. 40

3.6 Flow diagram for static analysis. 41

3.7 15m rotor diameter tidal converter. 42

3.8 Structural Supports: a)Pile Foundation, b) Minipile, c)Quadpod and d)Flexible Mooring. 45

3.9 Member deflections of the a Minipile Foundation at $3\,^{\mathrm{m}}/_{\mathrm{s}}$. 48

3.10 Member deflections of the a Tripod at $3\,^{\mathrm{m}}/_{\mathrm{s}}$. 49

3.11 Estimated Material Costs for each Structural Support. 50

3.12 Floater Diameter. 50

3.13 Stress Analysis of Pile Foundation at $3\,^{\mathrm{m}}/_{\mathrm{s}}$. 52

3.14 Principal Stress of a Tripod ($3\,^{\mathrm{m}}/_{\mathrm{s}}$). 54

3.15 Principal Stress of a Quadpod ($2\,^{\mathrm{m}}/_{\mathrm{s}}$). 55

3.16 Axial Stress of a Tripod (45 deg) at $2\,^{\mathrm{m}}/_{\mathrm{s}}$. 56

3.17 Taut Leg Configuration Footprint. 58

4.1 Linear and Rotational Motions of a Tethered Turbine. 63

4.2 Methodology Pipeline. 65

4.3 Examples of tank tests facilities: a) Flume Tank and b) Tow tank. 66

4.4 Flow Diagram of the Mechanical Design 67

4.5 Representation of fluid streamlines, pressure and velocities of: a) Tidal turbines and b) Propellers. 68

4.6 Inverted properties of the propellers when used as rotors: a) rotor and b)propeller. 69

4.7 Power Coefficient for Wind Turbines Related to: a) Twist Distribution and b) Airfoil Type. Taken from Hau (2006) 70

4.8 NACA 44xx. 71

4.9 NREL S814. 72

4.10 Example of a small scaled prototype. 76

4.11 Flow diagram of the Instrumentation Module. Refer to "Goto A" in Figure 4.4. 77

4.12 Roll, Pitch and Yaw Motions. 78

4.13 Inclinometer Motions. 78

4.14 Wheatstone Bridge. 80

4.15 Amplifiers 81

4.16 Final CRR tidal model. 81

4.17 Inclinometer Calibration. 82

4.18 Calibration Curves: a) Strain Gauge and b)Torque Gauge. 84

4.19 Flow Diagram of the Signal Processing Tools 86

4.20 Filtered Signal. 87

4.21 Skewness: a)symmetric, b) positive skewness and c) negative skewness. . . . 88

4.22 Types of Kurtosis: a) leptokurtic, b) platykurtic and c) mesokurtic. Based on Spiegel and Stephens (1999). 89

4.23 Windowing. 91

4.24 Window functions: a) Hann and b) Hamming. 92

4.25 Rectangular Window applied to a signal of the tethered TEC. 92

4.26 Hamming Window applied to a signal of the tethered TEC. 93

4.27 Hann Window applied to a signal of the tethered TEC. 93

4.28 Bearing failure. 96

4.29 Von Karman Vortex. 97

4.30 Vibrational Tolerance Chart. Taken from Goldman (1999). 98

5.1 Propeller and Hub Section. 102

5.2 Small Scale Turbine in Operation. 103

5.3 Data Acquisition. 105

5.4 Roll Motion: Mean and 1D Standard Deviation. 107

5.5 Probability Density Functions of a) 2-2 C and b) 3-4 C from Roll Motion in the Flume Tank. 108

5.6 Pitch Motion: Mean and 1D Standard Deviation. 108

5.7 Probability Density Functions of a) 2-2 C and b) 3-4 C from Pitch Motion in the Flume Tank. 109

5.8 Yaw Motion: Mean and 1D Standard Deviation. 109

5.9 Probability Density Functions of a) 2-2 C and b) 3-4 C from Yaw Motion in the Flume Tank. 110

5.10 Roll Peak Frequencies of 2-2C at $0.4\,\mathrm{m/s}$: a) Tow Tank and b) Flume Tank. . . 112

5.11 Roll Peak Frequencies of 3-4C at $0.4\,\mathrm{m/s}$: a) Tow Tank and b) Flume Tank. . . 113

5.12 Pitch Peak Frequencies of 2-2C at $0.4\,\mathrm{m/s}$: a) Tow Tank and b) Flume Tank. . 114

5.13 Pitch Peak Frequencies of 3-4C at $0.4\,\mathrm{m/s}$: a) Tow Tank and b) Flume Tank. . 115

5.14 Yaw Peak Frequencies of 2-2C at $0.4\,\mathrm{m/s}$: a) Tow Tank and b) Flume Tank. . 116

5.15 Yaw Peak Frequencies of 3-4C at $0.4\,\mathrm{m/s}$: a) Tow Tank and b) Flume Tank. . . 117

6.1 Specimen. 122

6.2 Specimens after tensile strength test: a) Test 2 and b) Test 4. 123

6.3 Stress vs Strain Curves: a) Test 2 and b) Test 4. 124

6.4 Typical thermoplastic stress-strain behaviour. 124

6.5 C_p curves for SR Turbines with different Number of Blades: a) 2 Bladed, b) 3 Bladed, c) 4 Bladed and d) 5 Bladed, from BEM. 125

6.6 Blade Loads: a) Normal Load and b) Tangential Force. 126

6.7 Maximum Von Mises Stress. 127

6.8 Von Mises Stress Distribution. 127

6.9 Displacement Distribution. 128

6.10 Maximum displacement at the blade tip. 128

6.11 Fixing mechanism: a) 3 Bladed Configuration and b) Pitch Setting Sketch. . . 129

6.12 Roll motion of a)3 Bladed Single Rotor Turbine and b)5 Bladed Single Rotor Turbine. 131

6.13 Roll Energy Spectrum of the 3 Bladed Single Rotor Turbine at: a)$0.5\,^{\mathrm{m}}/_{\mathrm{s}}$ and b)$0.8\,^{\mathrm{m}}/_{\mathrm{s}}$. 132

6.14 Pitch Energy Spectrum of the 3 Bladed Single Rotor Turbine at: a)$0.5\,^{\mathrm{m}}/_{\mathrm{s}}$ and b)$0.8\,^{\mathrm{m}}/_{\mathrm{s}}$ 133

6.15 Roll Energy Spectrum of the 5 Bladed Single Rotor Turbine at: a)$0.6\,^{\mathrm{m}}/_{\mathrm{s}}$ and b)$0.8\,^{\mathrm{m}}/_{\mathrm{s}}$. 134

6.16 5 Bladed Single Rotor Turbine during Yaw Motion. 134

6.17 Yaw Energy Spectrum of: a)3 Bladed Single Rotor Turbine and b)5 Bladed Single Rotor Turbine at $0.8\,^{\mathrm{m}}/_{\mathrm{s}}$. 135

6.18 Roll Energy Spectrum of the a) 3 Bladed Single Rotor Turbine and b) 5 Bladed Single Rotor Turbine at$0.8\,^{\mathrm{m}}/_{\mathrm{s}}$. 136

6.19 Experimental C_p and C_t curves for SR Turbines with different Number of Blades: a) 2 Bladed, b) 3 Bladed, c) 4 Bladed and d) 5 Bladed. 137

6.20 3-3 Contra Rotating Rotor Turbine in Roll Motion 138

6.21 3-4 Contra Rotating Rotor Turbine in Roll Motion. 139

6.22 Roll Energy Spectrum of: a) 2-3 Contra Rotating Rotor Turbine and b)3-3 Contra Rotating Rotor Turbine at $0.6\,^{\mathrm{m}}/_{\mathrm{s}}$. 140

6.23 Roll Energy Spectrum of the 3-3 Contra Rotating Rotor Turbine at $0.8\,^{\mathrm{m}}/_{\mathrm{s}}$. . . 140

6.24 Roll Energy Spectrum of the 3-4 Contra Rotating Rotor Turbine at $0.6\,^{\mathrm{m}}/_{\mathrm{s}}$. . . 141

6.25 Pitch Energy Spectrum of the 2-3 Contra Rotating Rotor Turbine at $0.6\,^{\mathrm{m}}/_{\mathrm{s}}$. . 141

6.26 Pitch Energy Spectrum of the 3-4 Contra Rotating Rotor Turbine at $0.8\,^{\mathrm{m}}/_{\mathrm{s}}$. . 141

6.27 3-4 Contra Rotating Rotor Turbine in Yaw Motion. 142

6.28 Yaw Energy Spectrum of the 3-3 Contra Rotating Rotor Turbine at $0.8\,^{\mathrm{m}}/_{\mathrm{s}}$. . . 142

6.29 Torsion Energy Spectrum of: a) 3-3 Contra Rotating Rotor Turbine and b) 3-4 Contra Rotating Rotor Turbine at $0.8\,^{\mathrm{m}}/_{\mathrm{s}}$. 143

6.30 Experimental C_p and C_t curves for CRR Turbines with different Number of Blades: a) 2-3 Configuration, b) 3-3 Configuration and c) 3-4 Configuration. . 144

6.31 Side by Side Rotor Turbines in Pitch Motion. 145

6.32 Side by Side Rotor Turbines Yaw Motion. 146

6.33 Roll Energy Spectrum of the 3-3 Side by Side Rotor Turbine at $0.5\,\mathrm{m/s}$ 146

6.34 Yaw Energy Spectrum of the 3-3 Side by Side Rotor Turbine at $0.5\,\mathrm{m/s}$. 146

6.35 Roll Energy Spectrum of the 2-2 Side by Side Rotor Turbine at $0.5\,\mathrm{m/s}$. 147

6.36 Pitch Energy Spectrum of the 2-2 Side by Side Rotor Turbine at $0.5\,\mathrm{m/s}$. . . . 147

6.37 Yaw Energy Spectrum of the 2-2 Side by Side Rotor Turbine at $0.5\,\mathrm{m/s}$. 148

6.38 Experimental C_p and C_t curves for SSR Turbines with different Number of Blades: a) 2-2 Configuration and b) 3-3 Configuration. 149

6.39 3 Bladed Single Rotor Turbine in Roll Motion at $0.6\,\mathrm{m/s}$ during blade failure. 150

6.40 Roll Energy Spectrum of the : a) 3 Bladed Single Rotor Turbine at $0.6\,\mathrm{m/s}$ and b)5 Bladed Single Rotor Turbine at $0.8\,\mathrm{m/s}$. 151

6.41 2-3 Contra Rotating Rotor Turbine in Pitch Motion at $0.8\,\mathrm{m/s}$ during blade failure. 151

6.42 Pitch Energy Spectrum of the 2-3 Contra Rotating Rotor Turbine at $0.8\,\mathrm{m/s}$. The case (a) represents the spectrum of the device with a blade failure. The case (b) represents the same case before the turbine has suffered any damage. 152

6.43 3-3 SSR at $0.8\,\mathrm{m/s}$: a) Before Blade Failure and b) After Blade Failure. 152

6.44 Roll Energy Spectrum of the 3-3 Side by Side Rotor Turbine at$0.8\,\mathrm{m/s}$. 153

7.1 Sound of Islay: Installation Area. 159

7.2 River Thames: Installation Area. 160

7.3 Contra-Rotating Turbine's Generator. 161

7.4 Peak Power Tracking Flux Diagram , based on Gitano-Briggs (2010). 162

7.5 3-4 CRR turbine installation in the Sound of Islay. 163

7.6 3-4 CRR turbine installation in the River Thames. 164

7.7 Turbine Installation from the Wellington Ship and Instrumentation. 166

7.8 "S" type load cell, model 620, taken from Vishay Measurements Group (1989). 167

7.9 Magnetic Relays on Turbine. 167

7.10 Resistive Element. 168

7.11 System Performance. 169

7.12 Performance Curves of a 1.1m rotor diameter 3-4 CRR Turbine: a) Cp vs. TSR and b) Ct vs. TSR. 170

7.13 Roll of Turbine and Surface Buoy. 171

7.14 Pitch of Turbine and Surface Buoy. 172

7.15 Frequency domain analysis of: a) Roll and b) Pitch. The energy spectrums were obtained at average flow velocity conditions of $0.5\,{}^{\mathrm{m}}/_{\mathrm{s}}$. 173

7.16 Flow Velocity measured during the Spring+3 tidal cycle. 174

7.17 Turbulence Intensity : a) Ebb Cycle and b) Flood Cycle. 175

7.18 Roll: Mean and 1D Standard Deviation. The bars in blue represent "flood conditions" and the bars in brown represent "ebb conditions". 176

7.19 Roll Motion: a) Neap+3 (flood) and b) Spring (ebb). 176

7.20 Pitch : a) Mean and b) Standard Deviation. The bars in blue represent "flood conditions" and the bars in brown represent "ebb conditions". 177

7.21 Pitch Motion: a) Neap+2 (ebb) and b) Spring (ebb). 178

7.22 Yaw : a) Mean and b) Standard Deviation. The bars in blue represent "flood conditions" and the bars in brown represent "ebb conditions". 179

7.23 Yaw Motion: a) Neap+2 (flood) and b) Neap+2 (ebb). 180

7.24 Roll Motion Vibration Level. 181

7.23 Roll Motion Vibration Level. (Cont) 182

7.24 Roll energy spectrums of the tidal cycle. 184

7.24 Roll energy spectrums of the tidal cycle. (Cont.) 185

7.24 Roll energy spectrums of the tidal cycle. (Cont.) 186

7.24 Roll energy spectrums of the tidal cycle. (Cont.) 187

7.25 Pitch Motion Vibration Level. 187

7.25 Pitch Motion Vibration Level. (Cont.) 188

7.26 Pitch energy spectrums of the tidal cycle. 189

7.26 Pitch energy spectrums of the tidal cycle. (Cont.) 190

7.27 Yaw Motion Vibration Level. 191

7.27 Yaw Motion Vibration Level. (Cont.) 192

7.28 Yaw energy spectrums of the tidal cycle. 193

7.28 Yaw energy spectrums of the tidal cycle. (Cont.) 194

7.28 Yaw energy spectrums of the tidal cycle. (Cont.) 195

B.1 Control volume around a wind turbine rotor, based on Hansen (2008) 224

B.2 Resultant Projection of Lift and Drag Forces,based on Manwell et al. (2009) . 225

B.3 BEM Algorithm, based on Hansen (2008) 226

C.1 2-2 C: a) Flume Tank and b) Tow Tank 228

C.2 2-3 C: a) Flume Tank and b) Tow Tank 228

C.3 3-3 C: a) Flume Tank and b) Tow Tank 229

C.4 3-4 C: a) Flume Tank and b) Tow Tank 229

C.5 2-3 C Flume Tank FFT's: a) Roll b) Pitch and c) Yaw 230

C.6 2-3 C Tow Tank FFT's: a) Roll b) Pitch and c) Yaw 230

C.7 3-3 C Flume Tank FFT's: a) Roll b) Pitch and c) Yaw 231

C.8 3-3 C Tow Tank FFT's: a) Roll b) Pitch and c) Yaw 231

List of Tables

1 Nomenclature xviii

1 Nomenclature. (Cont.) xix

1 Nomenclature. (Cont.) xx

1 Nomenclature. (Cont.) xxi

1 Nomenclature. (Cont.) xxii

3.1 Power Extracted at Optimum Conditions. 43

3.2 Member Dimensions (Structural Frameworks) in mm. 47

3.3 Member Dimensions (Piles and Mooring Lines) in mm. 47

3.4 FEA Results (Structural Frameworks). 51

3.5 FEA Results (Pile Designs). 51

3.6 Positive and Negative characteristics of each of the Support Structures studied in this Chapter. 59

4.1 Vibration Causes. Various Sources (e.g. Goldman (1999) and Piersol and Paez (2002)) 95

5.1 Blockage Factor. 101

5.2 Propeller Characteristics. 101

5.3 Solidity of the Contra Rotating Turbines (Propellers). 101

5.4 Design Parameters. 102

6.1 VeroBlue Resin Properties, taken from (Object-Geometries, 2010). 122

6.2 Optimum Operational Conditions of SR Turbines according to BEM theory. . 125

6.3 Solidity of the Contra Rotating Turbines (S814). 129

6.4 SR Turbine Mean and Standard Deviation. 135

6.5 CRR Turbine Mean and Standard Deviation. 142

6.6 SSR Turbine Mean and Standard Deviation. 145

6.7 Mean and Standard Deviation of various blade failure cases. 149

7.1 Time Domain Characteristics at the sea trials. 171

7.2 River Thames Tidal Cycles. 174

7.3 Detected Wave Strikes on the River Stream. 174

7.4 Highest Vibrations on the same Tidal Cycle. 195

8.1 Advantages and disadvantages of several tethered turbine configurations. . . . 200

8.2 3-4 Contra Rotating Turbine Mechanical Vibrations. 202

Nomenclature

- A = Swept area of the rotor.
- B = Number of Blades.
- c = Chord length of a foil.
- C = Number of pulse counts.
- C_d = Drag coefficient.
- C_l = Lift coefficient.
- C_n= Normal coefficient.
- C_p= Power Coefficient.
- C_t= Thrust Coefficient.
- C_T = Tangential coefficient.
- D = Diameter (e.g rotor, bearing elements, or pile) or Drag force.
- $DC_{current}$ = Direct Current.
- e = Pitch diameter of the cage.
- f = Frequency (e.g. bearing element or vortex shedding).
- F_a = Axial factor.
- F_d = Drag force per unit length.
- $F_{friction}$ = Friction force.
- F_{static} = Static Load.
- F_r = Radial factor.
- F_n = Normal force.
- F_t = Tangential force.
- g = Gravity.
- H = Hertz.
- L= Length of the member/ Lift force.

Table 1: Nomenclature

- mm = Millimeter.
- m = Meter (unit).
- m = Object's mass.
- $^{\mathrm{m}}/_{\mathrm{s}}$= Meter per second.
- N = Newton.
- N = Number of sampled data.
- P = Power Extracted.
- Pa = Pascal.
- Q = Torque.
- r = Radial distance.
- $R_{1,2}$= Resistor in an electrical circuit.
- Re = Reynolds Number.
- s = Second.
- St = Strouhal Number.
- T = Thrust.
- T_x = Shear stress relative to the x direction.
- T_y = Shear stress relative to the y direction.
- t = Wall thickness.
- v = Flow velocity.
- V = Volt.
- V_{out} = Expected Voltage.
- V_{in} = Input Voltage.
- V_{max}= Maximum voltage output of the roll (x), pitch (y) and yaw (z) motion.
- V_{min}= Minimum voltage output of the roll (x), pitch (y) and yaw (z) motion.

Table 1: Nomenclature. (Cont.)

- W = Watt.
- $x_{i,k,n,m}$ = Data values (e.g. $i = 1, 2, ..., N$).
- x_k= Original numbers in time numbers.
- X = Sensor value.
- $\mathrm{Y(s)}$= Output signal of the transfer function.
- y_m= Transformed complex numbers after the FFT is carried out.
- Z = Number of rolling elements (balls).
- $^\circ$ = Degree (angle).
- $^\circ\mathrm{C}$ = Centigrade.

Greek Letters

- α= Angle of attack or Angle of contact.
- δ= Lateral displacement.
- θ= Angle of taut mooring line or local geometrical pitch angle.
- μ = Friction coefficient of the material / Mean.
- ρ = Water Density.
- σ = Standard Deviation or Rotor Solidity.
- ϕ = Angle formed between the rotor plane and the relative velocity of the fluid.
- ω = Angular velocity.
- Ω= Ohm.

Abbreviations

- ANOVA = Analysis of Variance tests.
- ADCP = Acoustic Doppler Current Profile.
- ADV = Acoustic Doppler Velocimeter.
- BEM = Blade Element Momentum.

Table 1: Nomenclature. (Cont.)

- BPFI = Rolling Element Pass Frequency of the Inner Race.
- BPFO = Rolling Element Pass Frequency of the Outer Race.
- BSF = Roller Element Frequency.
- CAD = Computer-Aided Design.
- CFD = Computational Fluid Dynamic.
- CoRMaT = Contra Rotating Marine Current Turbine.
- CRR = Contra Rotating Rotor.
- DFT = Discrete Fourier Transform.
- ESRU = Energy Systems Research Unit.
- FB = Front Brake.
- FEA = Finite Element Analysis.
- FFT = Fast Fourier Transform.
- FIR = Finite Impulse Response.
- FTF = Fundamental Train Frequency.
- IIR = Infinitive Impulse Response.
- GBF = Gravity Based Foundation.
- EMEC = European Marine Energy Center.
- EquiMar = Equitable Testing and Evaluation of Marine Energy Extraction Devices.
- NACA = National Advisory Committee for Aeronautics.
- NREL = National Renewable Laboratory.
- OWT = Floating Wind Turbine.
- PLA = Port London Authorities.
- PMW = Pulse Width Modulator.
- rpm = Revolutions Per Minute.

Table 1: Nomenclature. (Cont.)

- SALM = Single Anchor Leg Moorings.
- SCADA = Supervisory Control and Data Acquisition.
- SP-Tool = Signal-Processing Tool.
- SR = Single Rotor.
- SSR = Side by Side Rotor.
- UTS = Ultimate Tensile Strength.
- WEC = Wave Energy Converter.
- TEC = Tidal Energy Converter.
- TLM = Tension Leg Mooring.
- TSR = Tip Speed Ratio.

Table 1: Nomenclature. (Cont.)

Chapter 1

Introduction

1.1 Introduction

What are the benefits of using a tethered turbine? What is the dynamic response of a flexible moored turbine? Which type of rotor system would be the most feasible in terms of dynamics and vibrations? This thesis addresses the above general questions by means of a statical analysis of four rigid foundations and a taut mooring configuration at two flow conditions. The issues of normal, axial and shear stresses, material costs and device footprint are discussed in the thesis. Since the study of a flexibly moored turbine (i.e. device fixed to the seabed by means of mooring lines) is complicated due to its uncertain dynamic response, a methodology to study this behaviour was proposed in this thesis which was used to analyse tethered tidal energy converters (TECs). Model turbines are equipped with accelerometers in order to provide information related to their three main rotational angles (e.g. roll, pitch and yaw). The same information is used to study the mechanical vibrations of the devices in various flow conditions. The aim is to apply the same analytical methodology to the analysis of scaled up devices moored to the seabed.

1.2 Motivation and Objectives

There exist several key limitations in current knowledge related to structural support systems for tidal turbines. Specifically, studies reported by Masters and Orme (2006) and CJ Day Associates (2001) have found both positive and negative aspects of using rigid or flexible moored foundations for tidal turbines. Masters and Orme (2006) reported a comparative study between different structural concepts based on manufacture, installation and mainten-

ance (Figure 1.1); however, the study does not provide quantitative evidence to support the conclusions of the report; thus, the suitability of each configuration in each case is hard to assess. CJ Day Associates (2001) studied the design and deployment costs of pile foundations and tethered devices. In contrast to the work of Masters and Orme (2006), CJ Day Associates (2001) reported valuable information about the installation, maintenance costs, profits, taxes, cash flow, and the debt coverage during a period of 10 years for each of the structural systems utilising a $5\,\mathrm{m}$ rotor diameter turbine in a $20\,\mathrm{m}$ water depth location. However there is a lack of information on the environmental conditions, the materials and the configurations considered for each structural support.

Several key limitations in current knowledge relating to the dynamics of tethered turbines are identified:

- At the beginning of this research, there was sparse availability of information related to the dynamics and vibrations of such devices. Studies undertaken by Francis and Hamilton (2007) and Mackie (2008) have reported on the development of floating tethered turbines (Figure 1.2); however, since there is no dedicated software available to simulate the dynamics of the turbines coupled to mooring configurations, these studies did not cover all aspects of their operation. In Francis and Hamilton (2007), the dynamics of the mooring line arrangements were investigated, but the rotodynamics of the turbine were not included. Mackie (2008) reported experimental investigations related to a small scale tethered turbine; however, the results only discussed heave motions of single rotor devices and no other dynamic motions were reported.

- The above studies only contemplated floating devices with a specific rotor configuration; for example, the report of Francis and Hamilton (2007) contemplated the use of a counter rotating device with 2 blades in each rotor. The available information was limited to specific rotor configurations and there was no evidence of the use of alternative configurations which could improve its performance.

- Finally, results comparing the dynamics and vibrations of small scale devices to scaled up tethered turbines have not been reported in the literature. This is partially due to limitations on laboratory conditions where academic research is undertaken, in terms of testing devices over a significant range of scales.

Thus, the main objective of this thesis is to create a methodology to investigate the dynamic response and mechanical vibrations of tethered devices of various configurations in terms of their three main rotational angles: roll, pitch and yaw. The responses are analysed in time domain to compare the oscillations and alignment of the devices at various flow velocities and environmental conditions. A frequency domain analysis is then used to identify the inherent

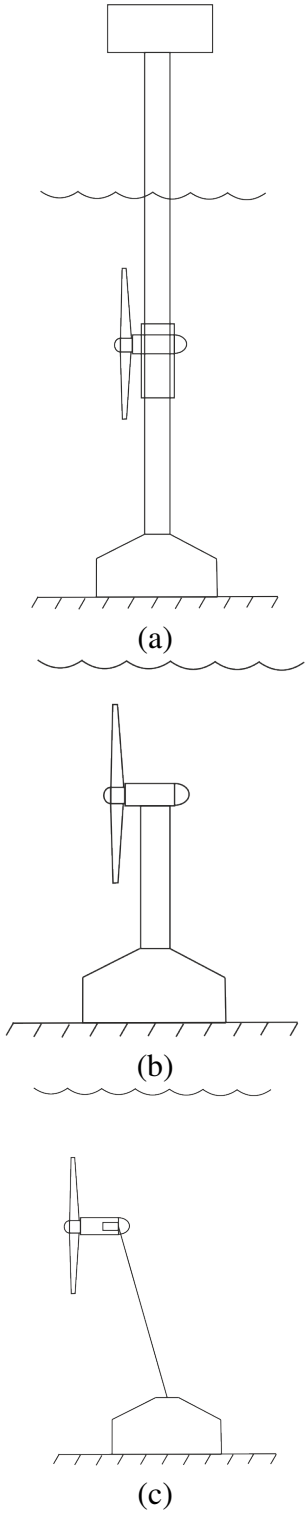

Figure 1.1: Some of the Structural Concepts studied by Masters and Orme (2006): a) Pile Foundation, b) Gravity Based Foundation and c) Tethered Turbine. Figures based on Masters and Orme (2006).

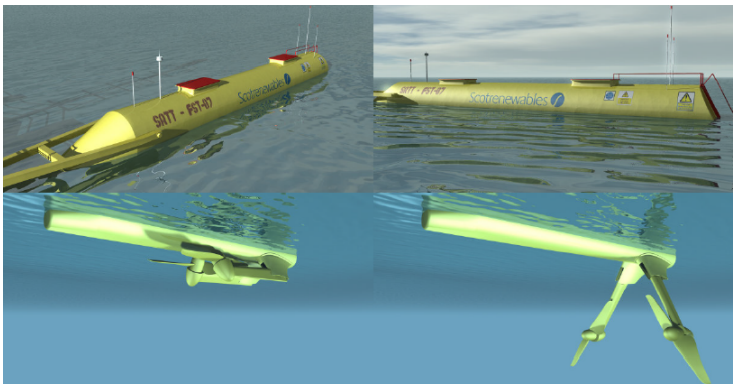

(a)

(b)

Figure 1.2: Turbines studied by a)Francis and Hamilton (2007) and b)Mackie (2008) . Figures taken from Francis and Hamilton (2007) and Mackie (2008).

mechanical vibrations of the devices and their variations as the flow conditions are exacerbated. To that end, various small scale tethered systems were designed and tested under repeatable conditions in order to compare the dynamic motions of various rotor systems, which might be employed within tidal energy technology. The impact as the devices are scaled up is then investigated with the dynamic analysis of a larger tidal turbine working in two different real environments: sea and river regimes. Therefore, the following specific objectives were established in order to address the current limitations of tidal technology, and, in consequence, facilitate the exploitation of marine renewable energy in the future.

- To investigate the effects of using rigid foundations and flexibly moored devices in terms of mechanical properties, device footprint and material costs in various environmental conditions.
- To investigate the feasibility of using a quadpod or tripod framework as an alternative to use a single pile.
- To design and integrate a methodology in order to explore the dynamic response and mechanical vibrations of small scale tethered turbines operated in laboratory conditions.
- To investigate the dynamic and mechanical vibration performance of different rotor configuration in a tidal turbine (e.g. single rotor, contra-rotating rotors and counter-rotating rotors) and, understand the vibration characteristics of each of them in a range of flow conditions.
- To investigate the effects of scaling up a tethered tidal device in real sea conditions and to compare its dynamic response and mechanical vibrations with a similar turbine installed within a turbulent river regime.

1.3 Problem Statement

The use of tidal technology provides several advantages with respect to other renewable resources. For example, the tidal currents are predictable and, consequently, it is possible to know when the turbines would be able to extract energy from the tides and also the amount of energy that would be available. This is not possible with renewable resources with random behaviour; for example, waves or wind. In recent years, the development of tidal technology has increase substantially.

Tidal turbines have been mainly categorised according to the manner in which they extract energy: *horizontal axis turbines*, *vertical axis turbines* and *oscillating hydrofoils*. Horizontal

turbines extract energy from a rotor (e.g. shaft) that is aligned parallel to the tidal resource. Vertical axis turbines yield the energy from a shaft which is mounted perpendicular to the flow direction. Oscillating hydrofoils are equipped with foils that do not rotate around a shaft but, move up and downwards or forward and backwards accordingly (EMEC, 2012).

Tidal technology can also be categorised in terms of its structural support systems. Currently, three main groups can be considered: *pile foundations*, *gravity based foundations* and *flexibly moored configurations*. Comparative studies have shown that pile foundations (e.g. Figure 1.1(a)) involve high costs and long periods of time are therefore required to recoup revenues (CJ Day Associates, 2001). Flexibly moored foundations (i.e. tethered turbines) are considered to be the most attractive in terms of costs; however, the most effective mooring configurations have yet to be established. Given this lack of maturity, a preliminary literature review of foundations used in wind and wave technologies which share similarities to tidal turbines has been undertaken in order to understand the positive and negative effects of the wide range of mooring arrangements that have been proposed recently (Chapter 2).

Gravity foundations (e.g. Figure 1.1(b)) have been widely used as support systems in current tidal turbines. However, there is still discussion as to which type of gravity foundation is the most adequate in terms of mechanical stresses and material costs. A static analysis is required in order to quantitatively identify the mechanical and cost differences between these foundations. Chapter 3 presents this static analysis.

Although researchers might suggest that a tethered turbine (e.g. Figure 1.1(c)) is an attractive option to exploit the tidal resource, the necessary dynamic is relatively challenging since the dynamic behaviour of such turbines is unknown. Current computational programs (Orcina (2012) or Ansys (2012)) are able to estimate the dynamics of mooring lines. However, it is also necessary to provide information about the turbine's motions. This thesis proposes to address such limitations and presents a experimental methodology in order to study the dynamic responses of various tethered turbines in terms of its main rotational angles (roll, pitch and yaw). Also, it is not known whether the mechanical components (e.g. the shaft, generator, bearings and so forth) may suffer high vibrations under turbulent flow conditions. This will be investigated with the use of small scale prototypes that are flexibly moored during their operation (as presented in Chapters 4, 5 and 6).

Since most of the current research relating to tidal turbines is carried out in laboratory conditions which are usually restricted in dimensions and scope, this thesis also presents investigations of dynamics and vibrations of a scaled-up turbine installed in real world environments (e.g. at sea and in a river estuary). This analysis characterises the dynamic and mechanical effects in the tidal turbines due to turbulent flows, including external sources such as ship washes and debris in the water as discussed in Chapter 7.

1.4 Hypothesis

This thesis argues that by developing an experimental methodology that studies the dynamic response and mechanical vibrations (related to the three main rotational angles: roll, pitch and yaw), the feasibility of different configurations of tethered turbines can be explored in several environmental conditions (i.e. turbulent tidal flows in combination with common marine disturbances).

1.4.1 Objectives

- Asses the use of rigidly mounted turbines against tethered turbines in terms of its mechanical properties, footprint and material costs.
- Explore a methodology to assess the dynamic response and mechanical vibrations of tidal tethered devices.
- Study the dynamic responses of small scale turbines composed of several rotor configurations composed with different number of blades operating at several flow velocities.
- Analyse the impact on the dynamic response of tethered turbines when blade failure occurs.
- Investigate the dynamic response of a scaled up tethered turbine when tested in real conditions and the influence of random impacts caused by the surrounding environment (e.g. marine traffic).
- Analyse the implications of utilising the operational behaviour of small scale prototypes in full scale systems.

1.5 Thesis Outline

The structure of this thesis is organised as follows:

- Chapter 2 provides an overview of different concepts, approaches, and applications required to understand the problem of tethered devices following the principles of similar renewable energy converters. The chapter surveys and discusses related technologies and their applicability to tidal technology.

- Chapter 3 presents a static evaluation of several structural concepts (based on the literature review) utilising a horizontal axis turbine (i.e. structural concepts shown in 1.1). The study presents a comparison of footprint, material costs and mechanical properties such as normal and axial stresses in each of the structures.

- Chapter 4 proposes a methodology to study the dynamic response and mechanical vibrations of flexibly moored turbines.

- Chapter 5 presents the initial evaluation of various configurations of contra rotating tethered turbines under different flow conditions in terms of its dynamics and vibrations.

- Chapter 6 presents a dynamic and vibration evaluation of rotor configurations moored as tethered devices under various flow rates. This chapter also presents an evaluation of blade failure modes by applying rapid prototyping techniques to create blade profiles for tidal configurations.

- Chapter 7 presents the dynamic response and vibrations of a scaled up tethered turbine installed in real environments and its correlation with small scale devices.

- Chapter 8 presents a comparison on the behaviour of small and medium scale turbines to relate its implications on full scale systems. This chapter also presents an overall assessment of tethered turbines.

- Finally, conclusions and recommendations for future work are presented in Chapter 9.

Chapter 2

Literature Review

This chapter presents a summary of the current state-of-the-art in support foundations used in offshore renewable technologies, especially for Offshore Wind Turbines (OWTs) and Wave Energy Converters (WECs). From the above information, it was found that much of the knowledge can be applicable in the foundation design stages for TECs. The literature gives an insight into the problems arising when different foundation types are employed in these marine technologies. Several parameters and limitations that are considered when designing and studying mooring structures for OWTs and WECs are presented. Finally, the similarities and differences between tidal technology and the aforementioned offshore renewable technologies are summarised at the end of this chapter.

2.1 Introduction

The development of TECs has rapidly accelerated during recent years. Initial attempts of extracting energy from the tidal streams by means of horizontal axis turbines can be found in Macnaughton et al. (1993), Fraenkel (2007) and Hammerfest Strom (2012b). Notably, Fraenkel (2007) developed the *Seaflow* turbine which was capable of producing 300 kW. This turbine was deployed 3km North-West of Lynmouth on the North Devon coast. The Hammerfest Strom Blue Energy turbine was also rated at 300 kW. It was deployed near the small town of Kvalsund in Norway in order to provide electricity to 30 homes close to the deployment site. Both turbines were successfully tested around 2003 as "proof of concept" technologies. Since then, the number of tidal turbine developments has increased rapidly.

In a report by Connor et al. (2008), the authors estimated that by 2011, around 25 devices had been tested at least for 1 year in sea/river conditions. Of course many turbines have failed

during the first trial stages or the developers had not met their targets; as with any other novel technology, such mistakes provide an insight of the key research areas that require further study. In that regard, the research of tidal technology has been mainly focused on:

- the hydrodynamic performance of the rotor turbines
- power take-off mechanisms
- wake propagation of the tidal devices for array formations
- materials; and,
- station keeping systems.

Initially at least, the station keeping system does not imply difficulties in the development of tidal converters since the structures can simply be based on similar concepts used by wind turbine technologies (e.g. pile foundations). However, it has recently been found that the marine energy resource is vast in deeper waters which are not accessible to pile-mounted turbines. In addition, the variability of the tidal resource throughout the water column will have certain implications for the converter's performance. These factors are further discussed in detail in the forthcoming subsections.

2.1.1 Deep Water Access

Many places around the UK coast-line have been identified as suitable areas for tidal energy extraction (Figure 2.1). For example, locations such as the Pentland Firth (Figure 2.1, point A), the region around Orkney (Figure 2.1, point B) and the region in the south of the Shetland Isles (Figure 2.1, point C) can reach velocities equal or higher than $3\,{}^{\mathrm{m}}/_{\mathrm{s}}$ (Marine Environmental Resource, 2011). Aside from the northern isles (e.g. Orkney and Shetland), a substantial tidal resource can be found in some parts of the North Channel (Figure 2.2). Currents exceeding $1\,{}^{\mathrm{m}}/_{\mathrm{s}}$ can be found in the area between the Isle of Islay, Mull of Kintyre (Figure 2.2, point A) and Torr head (Nihoul, 1982) (Figure 2.2, point B). The downside about these areas is that the depths vary greatly: from 30 to $100\,\mathrm{m}$.

Two energetic tidal sites can be found to the south-west of the Isle of Islay (Marion Harrald and Davies, 2010). Off the Rhinns of Islay (Figure 2.2, point C), the annual average tidal resource is estimated of $5.9\,{}^{\mathrm{kW}}/_{\mathrm{m}^2}$ where water depths range from 30 to $50\,\mathrm{m}$. In comparison, the available annual mean resource off Oa Peninsular (Figure 2.2, point D) can be up to $5.7\,{}^{\mathrm{kW}}/_{\mathrm{m}^2}$ but water depths oscillate between 50 and $100\,\mathrm{m}$. Near the westerly shore, from 2 to

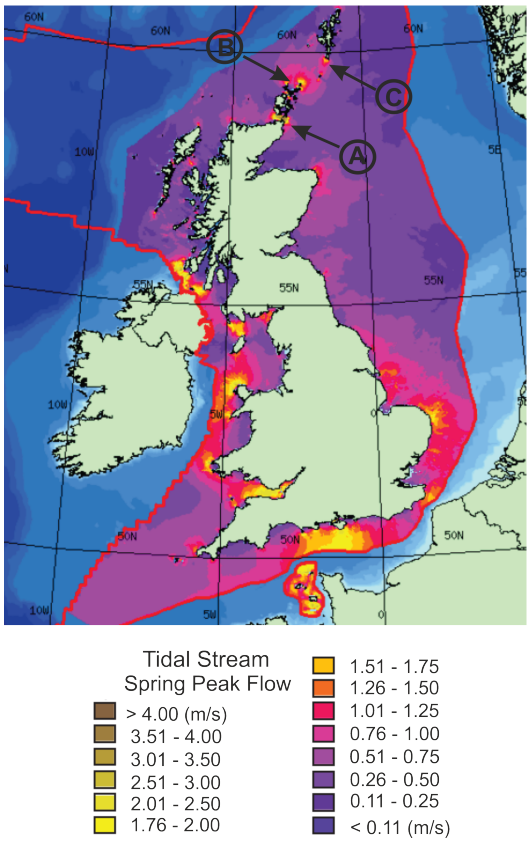

Figure 2.1: UK's Tidal Resource, taken from Marine Environmental Resource (2011).

$3\,\mathrm{km}$, the water depths are approximately $50\,\mathrm{m}$. And from 3 to $8\,\mathrm{km}$ the water depths increase gradually up to $100\,\mathrm{m}$.

Similar patterns are also found in areas outside the UK. For example, Morton (2004) reported that most of the tidal energy source available in Ireland is located in places with water depths of more than $50\,\mathrm{m}$. Thus, the information presented in this section suggests that ways must be found to access the resource in deeper areas.

2.1.2 Minimum Cost

Polagye and Previsic (2006) undertook an estimation of the overall costs associated with a tidal turbine and its monopile foundation. As depicted in Figure 2.3, it can be observed that most of the costs are associated to the material quantities, where 33% of the material consists of steel, which is primary, used in the turbine and in the monopile.

Estimations done by CJ Day Associates (2001) have shown that it is possible to generate affordable electricity from marine currents by implementing tethered configurations. Figure 2.4 shows the estimations of the cash flow recovery period comparing a tidal turbine supported

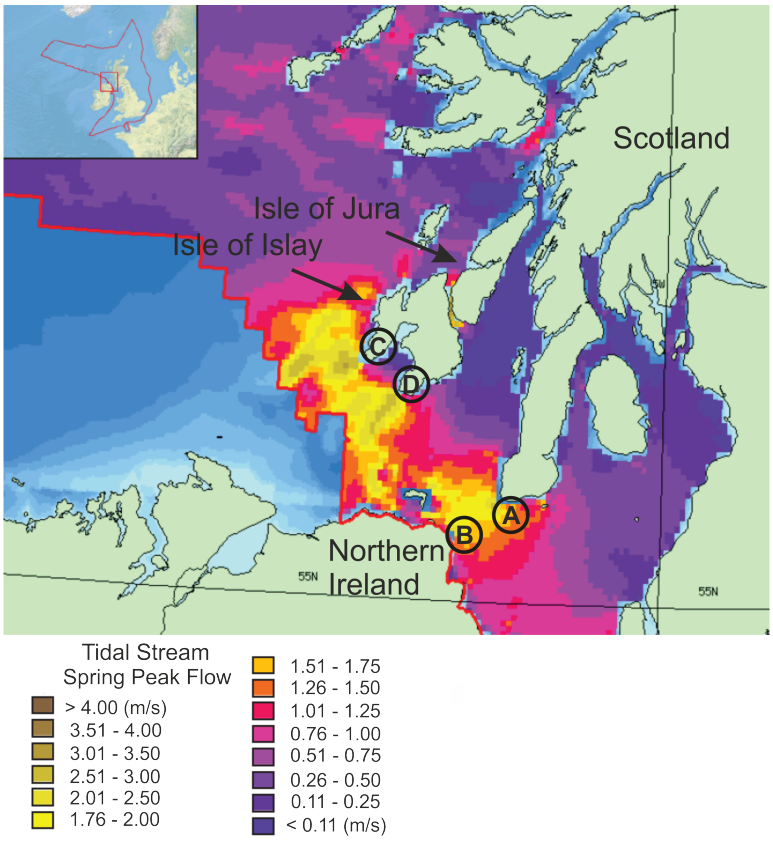

Figure 2.2: North Channel and South West of Islay, taken from Marine Environmental Resource (2011).

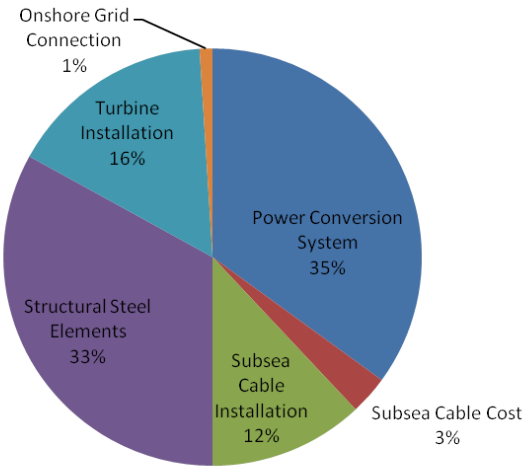

Figure 2.3: Separation of costs estimated by Polagye and Previsic (2006).

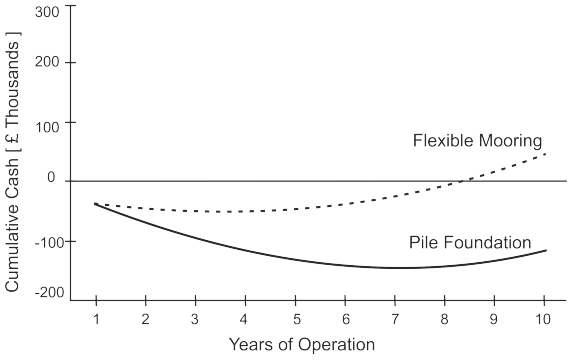

Figure 2.4: Cash Flow, taken from CJ Day Associates (2001).

by a pile configuration and a flexible moored system. It can be observed that the recovery of the investment can be reached in a period of 7 years; meanwhile, investors must wait several more years to start looking at the generated cash from the rigidly moored turbines. The calculations considered an energy tariff of $6\,\mathrm{p}/\mathrm{kWh}$.

If submerged support structures are used to install TECs (e.g. Figures 1.1(b) and (c)), water depths will have unsubstantial influence on installation costs. This will no hold true if pile foundations are used (e.g. Figures 1.1(a)). The use of vessels will change according to mass and volume, therefore, this will modify installation costs significantly(Masters and Orme, 2006). Moreover, operation and maintenance requirements will increase the costs associated to rigidly mounted structures. The reason is that the environmental conditions will induce fatigue or corrosion problems on the structures which will require routinary inspections, as stated by Rangel-Ramírez and Sørensen (2008).Therefore, the installation, maintenance and recovery procedure's cost is likely to be reduced if a flexible mooring is considered as the station keeping mechanism. This is because tethered devices will need smaller transport vessels than those required by pile foundation systems. Furthermore, due to the dimensions and weight of the rigid foundation systems, multiple vessels might need to assist in the deployment of the devices in the seabed. Finally, the performance of the TECs is affected by the hydrodynamics of the tidal resource as described in the following section.

2.1.3 Water Column Effects

The water column is mainly affected by the bathymetry of the site (as discussed in subsection 2.3.4) and the roughness of the seabed. The friction that the seabed layer creates and the roughness intensity slows down the flow closer to the sea-floor; therefore, Dawson (1983) recommends to approximate the speed flow variation as a $1/7^{\mathrm{th}}$ power law (Figure 2.5). The flow velocity can be considered to be an acceptable approximation if a device is deployed in a

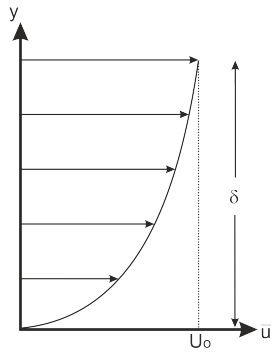

Figure 2.5: Flow Velocity Profile.

sheltered location; however, high energy wave densities may induce particle accelerations into the flow which will affect the power factor correlation at the surface area. Also, if the seabed is composed of large bathymetric features (e.g. rocks), the flow is affected by turbulence downstream and over the seabed.

An investigation carried out by Norris and Dronio (2007) investigated both effects: the turbulence and the wave induced particle velocities. The investigations were carried out in a $45\,\mathrm{m}$ depth site on the *Falls of Warness* located in the *west of Eday*, UK. Wave penetrations of up to $15\,\mathrm{m}$ down below the free surface were found at the site. In addition, the turbulence penetrated as far as $13\,\mathrm{m}$ height. These estimations implied that the 'non penetrated area' occupied $13\,\mathrm{m}$ of distance around the mid part of the water column.

Similarly, Gooch et al. (2009) determined with the use of Acoustic Doppler Current Profilers (ADVs) the velocity profiles and turbulent kinetic energies on several sites at the *Puget Sound* in *Washington, USA*. The study revealed that the turbulent kinetic energy intensities were strongest close to the seabed and were increased in the presence of strong flow currents. Thomson et al. (2010) reported that the turbulent intensity of such area was of around 10% during strong tides.

It is therefore concluded that the ideal location to avoid 'contaminated flow stream' and extract the maximum amount of energy is localized approximately on the central third of the water column. Thus, if sites of more than $50\,\mathrm{m}$ depth are considered, the use of gravity based foundations (GBFs) or monopiles will be compromised. However, the use of tethered moorings can also be problematic in some cases. Thus, a study of the advantages and disadvantages while using each of the structural types (i.e, pile foundations, GBF and tethered systems) in common offshore technologies (i.e, OWTs and WECs) is presented in the following sections. Also the applicability of each of the structural systems to TEC technology is described.

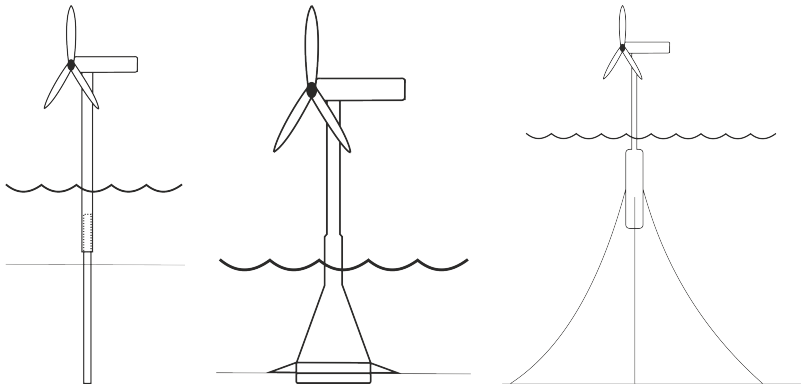

(a) (b) (c)

Figure 2.6: OWTs a) Monopile b) GBF c) Flexible Mooring.

2.2 Foundations for Offshore Wind Turbines

Because of the larger amounts of kinetic energy and the decrease of the visual impact in offshore sites, the installation of OWTs has become popular in recent years, but considerable challenges arise with the use of them. There is the need to access the resource to be found in deeper water areas. The severe weather conditions, which can produce winds of $50\,\mathrm{m/s}$ (Suzuki et al., 2011) or more in high wave density areas generate larger forces that must be accepted by the structural design. As a consequence, the rigid foundations (e.g. piles) require larger outer diameters and lengths which become difficult to deploy and transport. Thus, the use of floating OWTs has been recently investigated as an alternative to produce efficient and low cost clean energy. The three main structural concepts considered in offshore wind technology therefore comprise:

- *Pile Foundations* (Figure 2.6(a))
- *Gravity Based Foundations* (Figure 2.6(b)); and
- *Flexible Moorings* (Figure 2.6(c)).

A brief description of each of these structural configurations is given in the following sections.

2.2.1 Pile Foundations

Pile foundations are currently the most common structural concept to support OWTs (Figure 2.6(a)). According to the turbine's operation, the impact loads in the structure are mainly horizontal; therefore, the cyclic loading is almost unidirectional (Byrne and Houlsby, 2006). As a consequence, a delayed response caused by forces applied to the structure through time

is generated in the pile. Such response is referred to as hysteresis and can be minimised by increasing the stiffness of the structure itself (Bai, 2003).

As the water depth increases and the environmental conditions become substantially tempestuous, the dimensions of the piles must be increased to withstand the overturning moments created by the turbine loads. These dimensions can become as large as $4.9\,\mathrm{m}$ in diameter and lengths of $21\,\mathrm{m}$ into the seabed (Byrne and Houlsby, 2006). Zaayer (2003) showed that as the diameter of the column increases, the natural frequencies of the structure move close to the high spectrum side making it more difficult to tune, and, therefore, resonant problems can be present in the configuration. Currently the maximum depth where pile foundations are installed is about $30\,\mathrm{m}$ (Fulton, 2007). It is thus probable that monopiles will only be installed in shallow locations with no influence of high breaking waves to keep them economically feasible (Byrne and Houlsby, 2006). Similar conclusions can be expected for tidal turbine devices which generate similar forces as those of OWTs. Additionally, scour protection must be employed in any pile construction installed on sandy places. This is because the continuous movement of the stream flow removes the sea grains in the vicinity of the column creating a continuous weakening in the underground structural support (Westgate and DeJong, 2005).

Finally, the costs involved during the installation and construction are of significant importance. It must be considered that the use of pile foundations generates an extra cost due to the surface piercing in a rocky place. During installation procedures the length of the tower can induce extra problems for accurate positioning of the structure on the seabed. Dynamic positioning systems must be used during installation procedures and highly specialized large vessels are needed to transport the components (Malhotra, 2011).

2.2.2 Gravity Based Foundations (GBFs)

These structures rely on their own weight to provide sufficient strength to withstand the corresponding loads. The GBFs can be constructed using steel or concrete. In the case of steel, further research in coating techniques must be undertaken since corrosion reduces the material life. In this thesis, GBFs are subdivided into two main groups:

- ***Space Frames.*** These structures consist of several struts. The number of struts and dimensions vary accordingly to specific designs and conditions. For example, a space frame might be designed with a square or a triangular base. Their use certainly reduces the diameter of the main strut since the loads are distributed through the metallic frame. If large turbines are to be installed, such foundations are easier to tune and avoid resonance problems; however, high levels of hysteresis might be presented as the push

and pull of the loads is counteracted by the opposite footings. Tubular joints can also exhibit high levels of stress under operation. Both problems can be overcome by increasing the dead-weight of the structure or the separation between tripod bases (Byrne and Houlsby, 2006).

Up to date, not many OWT projects have utilised space frames, due to the fact that these structures are significantly heavy. Thus, its manoeuvrability becomes a problem during installation procedures (Zaayer, 2003). TEC foundations fixed to the seabed by means of space frames might represent a better approach since the turbines are likely to be deployed closer to the seabed or in the worst case scenarios, in the middle third of the water column. Thus, the forces experienced by space frames will be less affected by breaking waves.

- ***Concrete GBFs.*** This type of structure comprises a substantial amount of concrete to provide sufficient weight in the foundation to withstand the aero/hydrodynamic forces, as depicted in Figure 2.6(b). Seabed preparation is relatively simple compared to monopile foundations. For instance, Vø lund (2005) shows that the production costs decrease by half when employing concrete GBFs. Moreover, Zaayer (2003) has demonstrated that the same amount of structural mass is required for a 3 or a $6\,\mathrm{MW}$ device, the reason being that the heave load is the governing force instead of the overturning moment in this type of structure. This also holds true for TECs; since the restraining force is directly related to the mass of the support structure. Vø lund (2005) also states that such constructions are viable for the next generation of larger wind turbines. However, the use of concrete GBFs has negative effects in the environment; for example, high noise levels and sediment dissipation.

Hence, if the turbines are meant to be deployed in shallow areas GBFs might be more suitable structures than pile foundations. However, the wind industry also faces the problem of energetic sites where the water depth is larger than $50\,\mathrm{m}$. In that regard, research concerning the use of flexible moorings for OWTs had gained relevance in recent years. The following subsection gives an insight of the current designs and their characteristics, as described in the literature.

2.2.3 Flexible Moorings

In order to deploy wind turbines in deep water locations, equivalent practices of oil and gas platform installations are being followed by OWT designers. However, unlike offshore fuel structures, the OWT foundations will need to counteract the rotordynamic and aero/hydro

dynamic interactions of the entire system. The station keeping system is required to provide sufficient stability in the most severe environmental conditions.

The disposition of mooring lines and floater sections are the main characteristics of the structural design. The most common mooring configurations are the *catenary*, *taut*, and *tension leg lines*; each of them posses different capabilities and in turn, they are used differently in marine applications. These are briefly summarised below.

- ***Catenary lines.*** The vertical forces are restored by the weight of the line. The anchor is entirely subjected to the horizontal forces, as depicted in Figure 2.7(a) (Harris et al., 2004). If the primary lines lose contact with the seabed, the catenary line properties are lost and the device does not remain on station any longer. Thus, in order to avoid these limitations, the line lengths are very long. The configuration is usually not recommended for shallow water locations (Fulton, 2007). The use of catenary lines might not be adequate on tethered TECs since the influence of the turbulent environment and excessive wave motions might induce excessive surge motions on the system which will force the catenary line to loose its restraining properties.

- ***Taut leg.*** In this arrangement, the anchor is subjected to horizontal and vertical forces; therefore, the restoring force of the system depends entirely on the elasticity of the taut lines (Harris et al., 2004) and as the name suggests, the lines are designed to work under tension (Figure 2.9(b)). This configuration is usually employed in shallow or moderate water depths; thus, the plan area traversed by the taut leg lines (the "footprint" of the system) can be minimised as compared to catenary mooring lines.

- ***Tension leg moorings (TLM).*** These lines are installed at 90 degrees from the seabed; thus, the lines restrain only the heave behaviour of the device. A buoyancy section is usually employed below the wave interaction (Fulton, 2007). Thus, the lines work purely under vertical tension providing a small footprint. Its use is not practical for shallow water locations.

Distinct mooring line variations with various floater configurations have been studied for OWTs. For example, Bulder et al. (2003) analysed an OWT of $115\,\mathrm{m}$ rotor diameter kept on station with a single floater and two distinct mooring line configurations: catenary lines (Figure 2.7(a)) and a TLM (Figure 2.7(b)). It was found that the floater section was reduced from $37\,\mathrm{m}$ diameter , when a catenary line was employed, to $26-30\,\mathrm{m}$ diameter when tension line was used; however, the pretension loads required to avoid slack are high $(3,000\,\mathrm{tonnes})$. However, since the restoring forces in taut leg line arrangements are directly related to the pre-tension of the lines, the draft of the buoyancy sections had to be substantially increased.

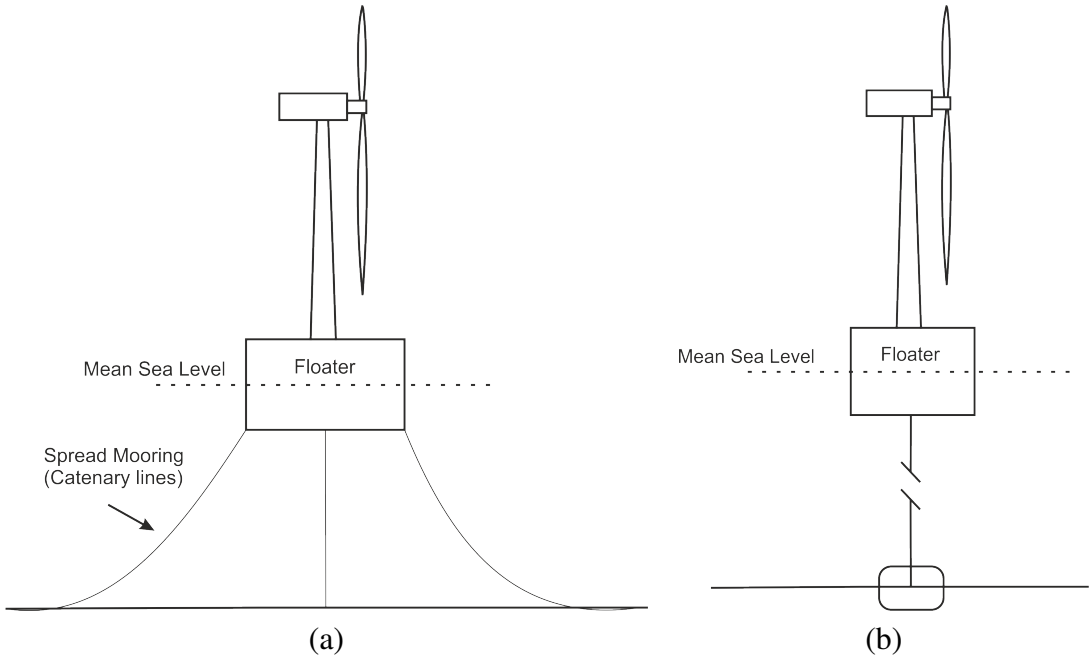

Figure 2.7: Mooring Configurations Studied by Bulder et al. (2003): a) Spread Mooring and b)TLM.

It was also found that it is necessary to tune the system to avoid the high energy range of the wave spectrum which was difficult to achieve with a single floater. The second floater concept studied by Bulder et al. (2003) consisted of a triple floater. The main advantage of this design concept was that it could be modified to tune the system according to the environmental conditions. However, if the platform is meant to be utilised to install two turbines side by side, it was found that the amount of material must increase by 170%.

Fulton (2007) studied a a semi-submerged triangular platform fixed to the seabed by TLMs (Figure 2.8). This study demonstrated that the mast tower of a $5\,\mathrm{MW}$ turbine behaves as a rigid structure according to the natural frequencies obtained. In conclusion, further analytical procedures must be undertaken since the current hydrodynamic computational techniques have not been upgraded to study specifically OWTs. The author stated that the current models would need to include the necessary Froude/Krylov forces and the additional diffraction/radiation models.

Ramachandran et al. (2011) studied the performance of a TLM system consisted of two tensioned lines. As expected, it was found that the surge and heave motions were related to the effects of the rotor thrust and the tension of the lines, respectively. However, oscillations in the pitch motion were found. Even if the response amplitudes were small, it was observed that the pitch motion grew over time, decayed and then grew again. The studies carried out by Lee (2005) demonstrated that TLM configurations present stiff properties in the main rotational modes but soft properties in surge and sway. In the same study, it was found that this

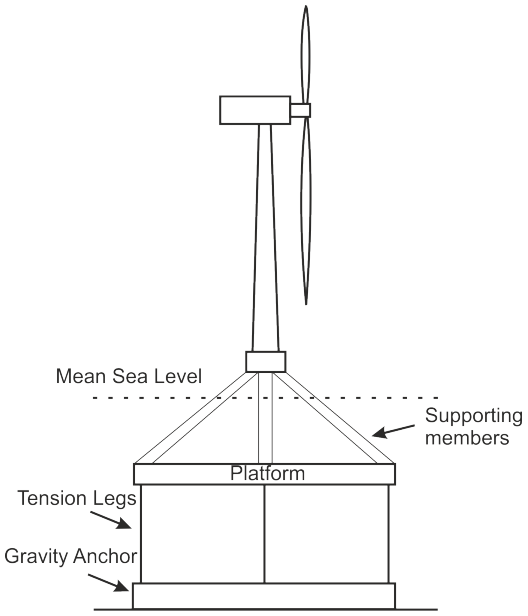

Figure 2.8: Mooring Configuration Studied by (Fulton, 2007).

behaviour was completely opposite to other types of system such as Spar Buoy designs (Lee, 2005). The investigation, which Suzuki et al. (2011) undertook, showed that TLM systems are functional in seismic regions. The results of the research proved that the motions of pitch and heave are short and of small amplitudes; but also, no resonance response was found in the system. Thus, it is probable that TLM configurations would be an adequate solution to fix OWTs in deeper water locations; however, further studies are needed in this matter.

Some of the flexible moored prototypes that are in the development stages are the Sway (Sway, 2012), Hywind (Statoil, 2012) and the Windfloat (Principle Power, 2012) concepts. This technology is being tested in small turbine capacities (~2MW) and the arrangements consist of mainly taut and tension leg configurations. Flexible moorings are complex structures and their use depends on several factors, such as the bathymetry of the site or the environmental conditions. Similarly to OWTs developments, extensive research into mooring lines has been undertaken by WEC developers; thus, the discussion of mooring line properties will continue in the following section.

2.3 Foundations for Wave Energy Converters (WECs)

It has been estimated that the wave resource can provide up to $2,000\,\mathrm{TWh}$ per year world wide (Pelamis, 2012). Thus, the idea of wave energy conversion has regained popularity in recent years. Even more than in tidal conversion, there is a large variety of WEC converters; the Pelamis device was one of the first WECs to be deployed at the European Marine En-

ergy Centre (EMEC) in 2010 (Pelamis, 2012). As discussed in relation to OWTs, the station keeping procedures used by the oil industries cannot be simply transferred to wave energy technology for two main reasons. On the one hand, wave energy conversion will only generate profits on a long term basis in comparison with the oil and gas industry (Johanning et al., 2005); thus, the developers of WECs will need to adjust their finances to produce economically feasible devices. On the other hand, the bathymetry (as defined in section 2.3.6) of the site and sea states are likely to differ from the locations where drilling platforms usually operate (Vickers and Johanning, 2009). Several parameters need to be taken into account for the structural design of flexible moorings and these are related to: *the converter type* (section 2.3.1), *environmental loadings* (Section 2.3.2), *footprint area* (Section 2.3.5), and *bathymetry of the site* (section 2.3.6) (Johanning et al., 2005).

2.3.1 Converter Type

The WEC devices can be subdivided into two main groups: *motion independent* and *motion dependent* converters. Motion dependent devices are the ones that rely on the motion of the mooring lines in order to optimise the power and efficiency of the device. The analysis of such devices is certainly more complicated since natural frequencies of the wave period and the mooring lines required to be coupled while ensuring a low fatigue in the lines (Johanning et al., 2005).

On the other hand, the mooring configuration of motion independent WECs is designed to avoid resonance in the entire system. Resonance can occur if the natural frequencies from the device, which in turn are related to the wave periods, match the natural frequency from the mooring line (Johanning et al., 2005). Consequently, the natural frequencies from the mooring lines must be designed to fall far from the ones of the WEC.

2.3.2 Environmental Conditions

In order to determine the maximum loadings applied to the mooring lines, the maximum environmental loadings of tidal current, wind and wave height and period should be considered on each specific site. The application of such parameters should follow the recent protocols established by the Equitable Testing and Evaluation of Marine Energy Extraction Devices in terms of Performance, Cost and Environmental Impact (EquiMar) (e.g. Ricci et al. (2009), Stallard (2011), Venugopal et al. (2011)). In this particular case, the information should be based according to the environmental characterisation described by Venugopal et al. (2011).

The position of the WEC is calculated for the maximum tension force in the system for extreme environmental conditions.

The analysis of offshore systems generally follows the standards used by the naval industry. The American Petroleum Institute suggests that a static and a transient analyses must be carried out during the design stages (Johanning et al., 2005). In the same document, it was stated that the static analysis is typically undertaken to parameterise the main variables of the system. In this phase, the intact and damaged cases are also considered (i.e. the damaged case is considered when the mooring line gets to a new position of "equilibrium").

The last investigation, (Johanning et al., 2005), pointed out that Det Norske Veritas stated that a quasi-static analysis is sufficient to analyse the mooring line configurations if the water depths do not exceed $200\,\mathrm{m}$, although such a protocol can undoubtedly be applied to renewable energy technologies. That is, the inherent dynamic motions of WECs, OWTs or TEC technologies generate large oscillations and forces in the station keeping systems that affect the performance of the devices. Moreover, the cyclic loadings of the station keeping systems are not considered in the quasi-static analysis. Thus, a dynamic analysis to investigate the structural dynamic interactions coupled with the body motions when considering damping and fluid accelerations is required for the design stages of WECs. The transient analysis will provide an insight of the intact condition and the damaged condition which refers to problems such as the failure of a mooring line, when the device reaches a new stable position (Johanning et al., 2005). Sophisticated tools are currently available to carry out time and frequency domain analysis of WEC devices (e.g. Orcaflex, Ariana-3D, MOSES, AQWA and so forth), which provide information on both dynamic and static analysis modes.

Besides the above, adequate safety factors must be considered when calculating the maximum design load for each static and dynamic condition. The design conditions can be based on the DNV-OS-E301 standards (Johanning et al., 2005) for the partial safety factors of the ultimate limit state and the accidental limit state. The former can be defined as the maximum permanent loads with regular environmental conditions that the structural member can withstand to examine its strength; whereas, the latter is related to the damage occurred during an unexpected event of short duration (Bai, 2003).

The final safety factors can then be obtained from the API RP 2SK standards for the corresponding damaged and intact conditions (Johanning et al., 2005). In addition, reliability tests must be undertaken when the structures are already in the water, similar to the process carried out for wind turbines (Westgate and DeJong, 2005). It must be noted that the converter must be able to withstand the appropriate forces from the harsh environment to cover a minimum design life of 5 years (Harris et al., 2004).

2.3.3 Material

The uncertainty of which material is the most suitable for each mooring line configuration is currently under scientific study. The three main materials that have been considered thus far are: *steel chains*, *wire rope* and *synthetic ropes* (i.e. polyester, nylon, and so on) (Harris et al., 2004).

The utilisation of a single component or a combination of two of them working in the same line is currently studied. The last arrangement is usually referred as a hybrid configuration (e.g. steel rope and nylon, chains and nylon). In addition, a selection of clump weights, springs or floaters have been considered to modify certain mechanical characteristics that influence the dynamic motions and dimensions of the entire configuration (e.g. Fitzgerald and Bergdahl (2007) or Vickers and Johanning (2009)) where some mechanical design considerations are described as follows:

- ***Steel Chain.*** It is suitable to use in catenary configurations due to its weight, stiffness, and bending properties. The disadvantage of utilising chains is that the line should be large enough to avoid lifting of the catenary line in order to preserve the reactive vertical force needed by the converter. In contrast with other configurations, the damping properties (energy dissipation) of the catenary chain lines increment as the pretensions in the line are increased. The latter statement needs further investigation, because the catenary line employed by Vickers and Johanning (2009) presented some lifting at higher pretensions. Corrosion is unquestionably another of the drawbacks when using metals in the support system.

- ***Wire Rope.*** The large amount of strands in wire ropes increases the stiffness of the line; thus, it is capable to withstand higher loads than any other mooring lines. It is also a light weight material with some level of elasticity. The material is ideal for taut leg configuration, S-shapes (as observed in Vickers and Johanning (2009)) or as hybrid configurations. The inconvenience of such material is that the thermal propagation through strands and the drag forces induced by high intensity currents can produce cracks on the mooring line and fracture failures (Savin et al., 2009). Similarly, bending in the line is the most harmful mechanical failure of the system.

  In order to solve the above problem, Savin et al. (2009) investigated a high density jacket compound in special steel wire, named *powerplast*. The compound presented several advantages such as good abrasion while decreasing the scratch and heat deformation. Moreover, the material showed untwisting behaviour in the strands which commonly happens to conventional wire lines (i.e. inner cores twist in opposite directions of the

outside strands). Further coating investigations should be performed in order to avoid premature failure of the lines due to corrosion issues.

- ***Synthetic rope.*** The ropes are comprised of lightweight material and they are considered as adequate materials for deep water locations and taut leg configurations. The main problem associated with synthetic ropes is the hysteric heating created by the friction between the line strands. Hysteresis reduces the mechanical properties of the material; therefore, the mooring lines need to be replaced frequently (Fitzgerald and Bergdahl, 2007). Another problem of synthetic mooring lines working in the free surface is that biofouling is more likely to be developed (Fonseca et al., 2009). If biofouling occurs, it modifies the damping properties of the material. Also, if synthetic lines are closer to a sandy bottom, particles of sand can be deposited between the strands causing a decrease of the life's material. Fish bites can also be an issue in this type of arrangement.

- ***Hybrid configurations.*** Vickers and Johanning (2009) focused on the study of the material's damping properties. It was shown that a hybrid configuration of "chain and nylon" line follows a gaussian trend as the pretension is increased. Since the chain is always lying on the floor, it can be stated that the main damping contributor is the synthetic material. A similar behaviour was presented by the S-shape line composed by floaters. In this configuration, the main source of damping is found to be influenced by the floaters.

  Similarly, Fitzgerald and Bergdahl (2008) studied a composition of a chain and a wire attached to an independent buoy, then the synthetic rope was coupled to the WEC. With this test, it was found that the synthetic line absorbed the entire load from the converter, which in the future, may cause hysteric damping on the line. Further studies are required in order to optimize the line arrangements (e.g. number of mooring lines used in the arrangements).

2.3.4 Mooring line configurations

Separately from the mooring line type and material, the design of the mooring configurations also involves the selection of two important mooring arrangements: *spread* and *single point moorings*. The *single point moorings,* as the name suggests, are integrated by an individual line either attached to the main body or to a floater. The single lines are frequently linked to a turret by means of a swivel; hence, the device has the freedom to weathervane to the flow conditions within its three modes of motion: *roll*, *pitch* and *yaw* (Harris et al., 2004). Single Anchor Leg Moorings (SALM) have typically heavier chains than spread moorings as the reactive force is only provided by an individual line. Spread moorings employ two or more

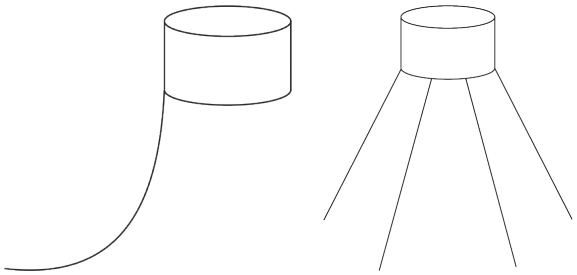

(a) (b)

Figure 2.9: Mooring Configurations: a) Single Catenary Mooring and b) Spread Taut Leg Mooring .

cables in their configurations to divide the forces applied in the mooring configuration.

The use of SALM configurations was studied by Johanning et al. (2006), where lines of 90 to $170\,\mathrm{mm}$ of diameter were coupled to buoys installed in locations with wave heights from 2 to $12\,\mathrm{m}$, wind speeds up to $100\,\mathrm{m/s}$ and superficial current velocity of $2.8\,\mathrm{m/s}$. The same study was undertaken utilising spread moorings, and it was found that the required mooring line sections had a smaller cross sectional area by up to 70% (e.g. 60 to $120\,\mathrm{mm}$ diameter).

Fitzgerald and Bergdahl (2008) made a theoretical comparison of five mooring line configurations to keep on station a cylinder which represented a WEC. The aim of the study was to investigate the effects of the mooring lines and performance of a WEC at the three major motion components: *surge*, *pitch* and *heave*. The analysis showed that any of the catenary arrangements were able to enhance the heave motion of the device, but it was possible to enhance pitch and surge motions with some of the configurations, especially the ones that provide an unrestrained behaviour.

Fonseca et al. (2009) studied a composition of four lines of catenary chains with the top end made of nylon rope connected to the main floater. The calculation was undertaken for environmental conditions with a return period of 100 years. The study demonstrated that if the chains abandon their catenary position and reach a tension state, the elastic region is reached rapidly. This in turn reduces the break load of the system and produces a rapid failure.

Finally, another configuration that should be included in studies related to spread mooring configurations is the TLM. Since TLM configurations completely restrain the heave motion of any system (as mentioned in Section 2.2.3), their use might be restricted to specific WEC designs (e.g. oscillating water columns or overtopping devices), as reported by Harris et al. (2004).

2.3.5 Footprint

In order to generate a significant amount of energy, several WECs will need to be deployed in a confined area to produce maximum energy output from a specific site. Thus, the span area occupied by WECs is a limitation in their performance, contrary to the protocols followed in oil platforms. In this regard, if catenary lines are meant to be used in the mooring structure, Johanning et al. (2006) recommends the use of heavy chains with short line lengths. This helps to reduce the footprint while increasing their stiffness and the natural frequencies of the arrangement. Similarly, Fitzgerald and Bergdahl (2007) proposes the implementation of clumpweights in the mooring arrangement to reduce the span of the line; however, the use of this arrangement increases the mechanical impedance which restricts the motion of the device when subjected to the corresponding forces.

On the contrary, Gao and Moan (2009) recommends increasing at least to double the footprint of the anchors in order to reduce the extreme tension loads. By employing this method, the dimensions of the required buoy will be significantly smaller if surface buoys are meant to be used. In consequence, the costs of anchors and the buoys will be significantly reduced but a large amount of energy yield might be penalised. Thus, an exhaustive cost analysis considering each circumstance must be undertaken to identify if the revenues obtained by the extracted power will be significantly reduced by the mooring configuration costs.

2.3.6 Bathymetry

As discussed in Section 2.1.1, the seabed properties (commonly termed as *bathymetry*) determine the anchoring systems. These anchoring mechanisms are further discussed in Section 2.4. Specifically, the variation of the ocean sea bed varies greatly at different locations. It has been found that locations in the south west of the Isle of Islay, the water depths range from $10\,\mathrm{m}$ to $30\,\mathrm{m}$ in the south west headland to up to $100\,\mathrm{m}$ in the south east headland. The sea bed is mainly composed of sand and sandy gravel between Loch Indaal and offshore of the two headlands. In the areas to the west side of the Rinns and the south west the sea floor is similarly composed (Marion Harrald and Davies, 2010). In the same document, the Mull of Kintyre seabed is said to be composed mainly of muddy sand and gravel. The water depth varies between 50 and $100\,\mathrm{m}$ (Figure 2.10).

Similar bed properties were identified in the areas of West of Colonsay (e.g. sand and gravels); however, solid rock has been found in sites like the West of Tiree (Figure 2.11). Johanning and Wolfram (2005) have reported that various locations with high wave energy densities are composed of rocky sea floors. Therefore, it is important to identify the seabed character since

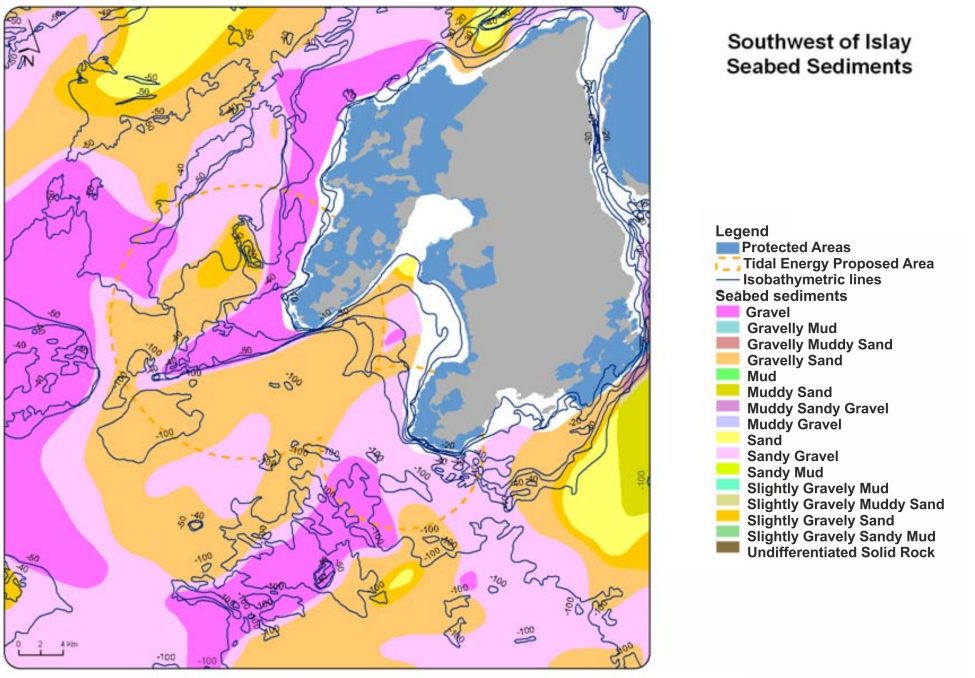

Figure 2.10: Southwest of Islay Seabed Sediments, taken from Marion Harrald and Davies (2010).

this determines the anchoring type suitable for each particular case.

2.4 Anchors

The selection of the appropriate anchoring mechanism is not a trivial process and may substantially affect the economics of the mooring configuration. It has been found that the anchors are usually the most expensive component of the entire station keeping structure (Huang and Aggidis, 2008). Parameters to consider during their selection are the holding capacity required and the soil component. It must be noted that in comparison to oil platforms, maintenance and replacement of components should not be undertaken prior than 5 years (Johanning et al., 2006). Thus, if the chosen anchor has a very high holding capacity the recovery or recycling procedures will become extremely difficult and expensive.

Due to a lack of standards related to anchoring systems for WECs, the current protocols to follow are those of the oil, gas and fishing industries. The main anchoring systems that might be used in the wave energy industry according to Huang and Aggidis (2008) and Fulton et al. (2005) are:

- ***Drag embedment anchor.*** Primarily used in catenary configurations (Figure 2.12). The anchor withstands horizontal loads and the weight of the chain usually provides the

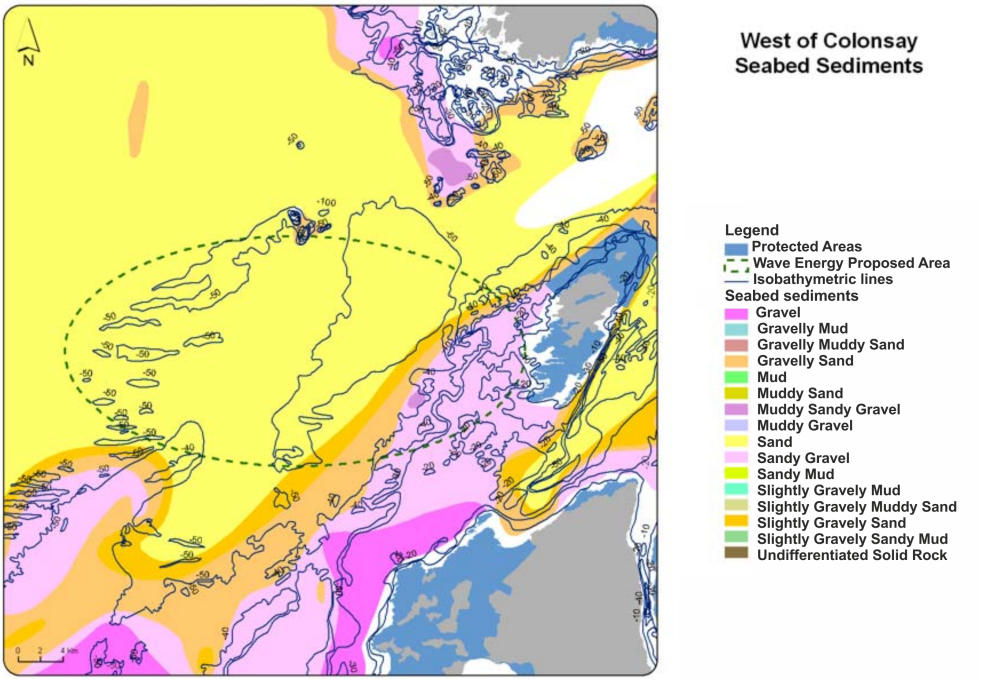

Figure 2.11: West of Colonsay Seabed Sediments, taken from Marion Harrald and Davies (2010).

resistance of the vertical loads created by the device (Fitzgerald and Bergdahl, 2007). The material properties of the mooring lines may not be compatible with the anchoring system. For example, fibre ropes cannot withstand abrasion created by such fixings.

- ***Drag in plate anchors.*** These types of anchors counteract the vertical forces not only due to their weight (Figure 2.13), but also due to their embedment within the layers of soil which create a bond between them (PelaStar, 2012). According to (Fitzgerald and Bergdahl, 2007), clay is the ideal soil type to install this kind of anchors; but, PelaStar (2012) considers that this anchor system can also be applied in silt and sand conditions. According to (Fulton, 2007), it is usually used in conjunction with catenary mooring

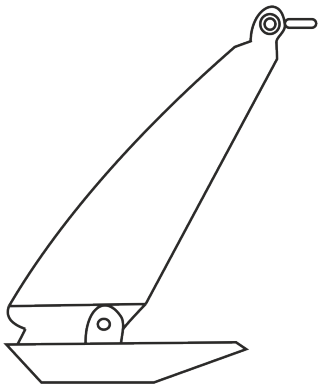

Figure 2.12: Drag Embedment Anchor.

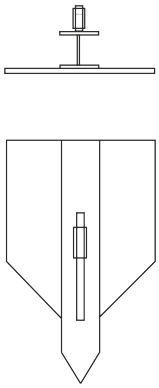

Figure 2.13: Drag in Plate Anchors.

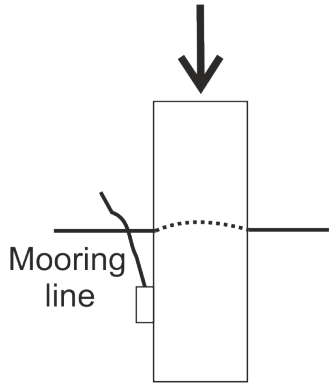

Figure 2.14: Driven Pile Suction Anchor.

configurations; however, PelaStar (2012) has studied the possibility of utilising them for TLM configurations.

- ***Driven pile suction anchor.*** This type of anchor is able to resist horizontal and vertical loads due to the pressure difference into the ground (Figure 2.14). The anchor mechanism creates the necessary friction force between the pile and soil. The main drawback for this anchoring system is present during the recovery procedures. For instance, given the high water pressure, recovery operations require large and costly infrastructure. Their installation depends entirely on the soil type. They usually become very expensive in deep water locations (Fulton, 2007). And if the seabed consists of a rocky base the installation becomes economically infeasible.

- ***Gravity based anchor.*** This anchor type is also referred to a vertical load anchor since the reactive load is counteracted by the dead weight of the structure (Figure 2.8). The main advantage of its use is that no soil preparation is required and the anchor can be installed in any location disregarding the sea floor properties (e.g. sandy, rocky, or clay

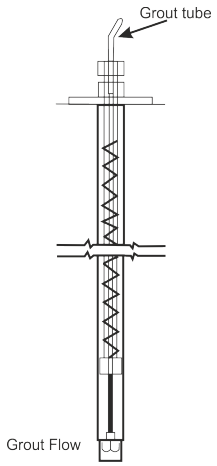

Figure 2.15: Drilled and Grouted Anchor.

seabed) (Fulton, 2007). In the study carried out by Fitzgerald and Bergdahl (2007), it was found that the use of a vertical load anchor can have a certain influence on the floater's behaviour; however, this can be minimised by the implementation of spring behaviour in the line.

- ***Drilled and grouted anchor.*** This anchoring type provides both horizontal and vertical holding capacity (Figure 2.15). According to the investigation of EPRI (2006), this type of anchor is ideal for rocky or hard clay seabed. The same author also states that the penetrations of the pile are usually in the range of 15 to $20\,\mathrm{m}$. Thus, the use of such foundation will imply larger installation and transportation costs.

It is apparent that a deep study of soil properties must be carried out before any deployment operation is planned. The study should be carried out through several layers of the sea floor since the soil properties change along the seabed (Marion Harrald and Davies, 2010). Also, continuous monitoring must be undertaken to study the performance and settlement of the anchoring systems. It has been found in some cases that the situation becomes rather complicated and, in consequence, positioning mistakes may take place (Vickers and Johanning, 2009).

2.5 Summary and Conclusions

This chapter presented a summary of the support foundations used for OWTs and WECs. The main differences between OWTs, WECs and TECs can be related to the environmental load that each converter must resist. Although, the installation locations are very similar to each other, the foundation design of OWTs and WECs must take into account the maximum wind,

wave and current loads in their static/dynamic analysis. This does not hold true for TECs, in most of the cases, as the loads are less damaging. It is clear that if GBFs are utilised for TECs, the structures are less exposed to extreme wind or wave conditions. And, the foundation type that will be exposed to major effects of wind or wave conditions is a pile foundation long enough to reach the surface (e.g. Seagen (Marine Current Turbines, 2012)). In particular cases for TECs, a flexible mooring is used as discussed in the following chapters.

It can be concluded that OWTs are related to TECs to a greater extent than they are to WECs. Since the rotordynamic and horizontal cyclic loads generated by wind and tidal turbines are similar, it is likely that the structural effects are, in consequence, similar. Thus, analogous protocols to build pile foundations for TECs should be followed. If pile foundations are applied to TECs the electrical components of the machine could possibly be located outside the marine environment. Additionally for maintenance requirements, due to the configuration of the structure, it is possible to lift the entire device to the surface, if the pile structure extends far enough. Finally, the design of a pile structure can be considered to be straightforward while providing a small footprint.

The above comments are also applicable to GBFs. As discussed in section 2.2.2, the use of space frames can also be appropriate for TECs; however, issues related to hysteresis in the struts might be present in the structure. The required frameworks will be bulky and heavy, and the use of concrete GBFs might be an adequate alternative. Since the devices should be deployed at water depths close to the middle third of the water column, it might be possible to have mini-pile foundations to provide the required security to the structure. Given these limitation, the length of the members of the structures will not change as the device is installed in deeper water locations; however, the maintenance, installation and retrieval procedures become more complicated as the water depths increase.

The last option that is increasingly being studied is to deploy OWTs in deeper water is the use of mooring lines. The application of mooring lines for WECs has been investigated over many years. Therefore, the use of that information can be of benefit to the design of TECs. In this context, it has been observed that the main problem with the use of mooring lines is the requirement to restrict the footprint area of the device. It is probable that tethered TECs will employ taut leg moorings since:

- they can be considered to be motion independent devices (differently from WECs); and,
- taut line configurations can be designed to utilise a smaller span area. This cannot be achieved when catenary lines are used in an array. The use of clumpweights or heavier mooring lines offer limited improvements and can produce external effects such as damping.

If the use of mooring lines is a feasible solution for the station keeping systems of renewable offshore energy converters, the selection of components is certainly more complicated than when using rigid foundations. The use of different materials in the mooring lines affects the mechanical properties of the station keeping system and, similarly, the efficiency of the devices. Likewise, the number of lines used in the mooring arrangement is an important factor in the overall costs of the device. Finally, it is also observed that the anchor systems are defined in accordance with the bathymetry of the sites, and a careful study of the bathymetry of the desired site is required before any deployment activity.

For flexibly moored devices, transportation and installation procedures should decrease in complexity even in deep water locations. Although there is still strong uncertainty over the best procedures to install tethered devices on the seabed (e.g. the number of mooring lines, types of anchors, materials involved, etc.), one of the greatest concerns is the dynamic response of the machines in the natural environment. This also involves the reaction of the mooring lines during the tidal cycles. Slack water periods, followed by the initiation of ebb and flood periods with their corresponding eddy fluctuations can cause tangling and knotting of the lines, not to mention the power cables fastened to the device. The footprint area of the system will vary depending on the decided arrangement. In contrast with rigid foundations, there are many mooring options for tethered devices.

The output of the literature review underpins knowledge that is applicable to the structural design of tidal turbines in general. As it was observed, several concepts are applicable to these devices; therefore, the next chapter will present a study of various types of support structures for TEC technology. Properties such as materials and the stresses in the structural members can give an insight into the limitations and restrictions for each case.

Chapter 3

Assessing Mooring Requirements for Tidal Energy Converters

The previous chapter described the investigations of the properties and limitations of several station keeping systems that are used to install OWTs and WECs. The last chapter also discussed the use of similar foundations for TECs. It was conjectured that the use of rigid foundations in TECs would represent an acceptable solution in some locations. However, if the turbines are to be deployed in deeper waters, as is likely to happen in the foreseeable future given the resource locations, tidal technology should consider the use of flexible moorings with similar arrangements to those proposed for OWT and WEC technology. The aim of this chapter is therefore to present an overview of the loads generated by a TEC and the effects of using various foundations. It conducts a static analysis of five structural systems: pile and minipile foundations, two framework structures and a tethered mooring. The results indicate the forces, stresses and deflections involved in a medium size horizontal axis tidal converter at two flow velocity conditions. The study also quantifies the amount of material utilised by each configuration. Finally, the chapter summarises the consequences of using each type of configuration in TECs.

3.1 Motivation and Objectives

The main objective of this chapter is *to study five structural systems to support a* $15\,\mathrm{m}$ *rotor diameter horizontal axis turbine*. The conveyed analysis considers a location in $40\,\mathrm{m}$ water depth and two flow conditions of $2\,\mathrm{m/s}$ and $3\,\mathrm{m/s}$.

The structural types considered in this analysis are:

- pile foundations,
- minipiles,
- tripods,
- quadpods; and,
- taut leg mooring foundations.

A finite element analysis is carried out, where possible, in order to quantify the normal and shear stresses in each of the members of the foundation, the deflections of the structural parts and, by a process of iteration, the dimensional characteristics of the structural parts that are required for a successful foundation.

This chapter is thus divided into six sections, where Section 3.2 presents the current status of foundations utilised by horizontal axis marine turbines; Section 3.3 discusses the utilisation of several rotor arrangements in tidal turbine designs; Section 3.4 comprises a static analysis of five marine structures to support a TEC of $15\,\mathrm{m}$ rotor diameter; Section 3.5 includes the results, discussion and conclusions of the static analysis; the summary and final remarks of the chapter are in Section 3.6.

3.2 Foundations Applied to TECs

EMEC (2012) states that approximately 58 tidal devices are under development around the globe. These fall into three configurations, by which TECs extract power from the marine currents (*horizontal and vertical-axis* turbines and *oscillating hydrofoils*). Another method to classify TECs is according to their station keeping system. In this context, Figure 3.1 shows the relative proportions of the station-keeping systems utilised by various types of TECs under development based on the information found in the EMEC site (EMEC, 2012).

It can be observed that similar support mechanisms to those utilised in OWTs and WECs have been employed for tidal technologies.

The most representative structural concepts are summarised below.

- **Pile foundation**. The first stage of the Openhydro tidal turbine (Connor et al., 2008) and both Seaflow and Seagen turbines (Fraenkel, 2007) employed pile structures to support

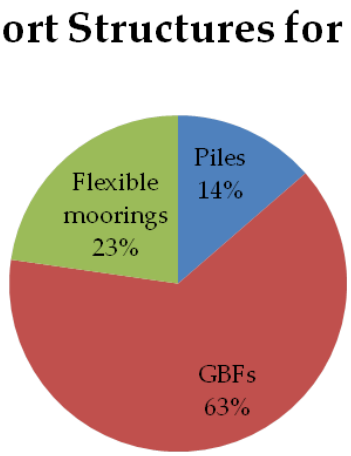

Figure 3.1: Diversity of Support Structures used in TECs.

their turbines (e.g. Figure 3.8(a)). Openhydro, the open centre ducted turbine, was installed with a twin piled foundation in the Falls of Warness for testing purposes in 2006 (Openhydro, 2012). Likewise, the 1 MW Seagen Turbine was deployed in Strangford Lough in 2008 and it has been tested for four years (Marine Current Turbines, 2012).

- **GBFs.** An approximate of 65% of the existing tidal turbines are supported by GBFs (e.g. Figure 3.8(b) and (c)). Representative cases include the space framed design of the Blue Energy Concept by Hammerfest Strom (Hammerfest Strom, 2012a), the TGL turbine (Connor et al., 2008) and the Swantechnology turbines (Swanturbines, 2012). The use of GBF can also be observed in the Verdant Power Turbine (Verdant Power, 2012) or the Beluga 9 Turbine (Alstom, 2012).

- **Flexible Moorings.** Devices employ different configurations of mooring line structures but each of them are similar to the ones described for OWTs and WECs (e.g. Figure 3.8(d)). For instance, Evopod (Oceanflow Energy, 2012) and the SR250 (Scotrenewables, 2012) are floating devices fixed to the seabed by a combination of catenary and taut mooring lines. The Contra Rotating Marine Turbine (CoRMaT) (Nautricity, 2012) and TidEL (SMD, 2012) utilise similar mooring line structures but in this case, the turbines are completely submerged. The main difference between the two systems is the rotor arrangement and the location of the buoyant sections utilised for tensioning. A description of each rotor configuration is undertaken in the following sections.

3.3 Rotor Configurations

The rotor arrangement of a horizontal axis tidal turbine can vary according to the number of blades in it and in the disposition of the rotor configuration. For example, a turbine can extract energy with the use of coaxial, co-planar or single rotor designs. These mechanisms correspond to more familiar devices such as helicopter, aircraft and ship rotor/propeller designs. However, their implementation in turbine design brings a different set of operational characteristics. The next subsection provides a detailed examination of the options, with particular regard to the implications for loads transferred to the support structure of a TEC.

3.3.1 Single Rotor Configuration

The simplest of all the configurations employs a single rotor (SR) device (Figure 3.2). The main problem with this rotor does not lie with the converter itself but in the dynamic response. In a helicopter, a tail rotor is usually employed to counter act the torque developed by the main rotor (Johnson, 1994). Alternatively, horizontal and vertical stabilisers are commonly employed to counter-act the aero/hydro dynamic forces that affect the longitudinal (pitch) and lateral (roll) motions in boats and aeroplanes (Figure 3.3).

Similarly, the use of SRs in tethered marine turbines must consider the use of such techniques to balance the forces and avoid severe dynamic motions. As reviewed in Section 3.2, the only tethered device aiming to exploit a tidal resource via a SR configuration is the Evopod, a semi-submerged device moored to the seabed by catenary lines that allow the turbine to move freely and weathervane with the flow.

The experimental stages included $1/40^{\text{th}}$ scale prototypes and experimental tests near the Portaferry Marine Laboratory in Strangford Narrows. These experimental studies revealed low power oscillations over a period of time (Mackie, 2008); however, the stabilising structure designed to prevent large oscillations is likely to induce a large drag on the system. If as in this case a turbine is close to the free surface; it is likely that the hydrodynamic forces created by wave-current interactions will induce fatigue on the blades due to cyclic loading (Galloway et al., 2011) and possible vibration problems. It is possible that the costs associated with tidal turbine blades will be higher than those used already on wind turbines.

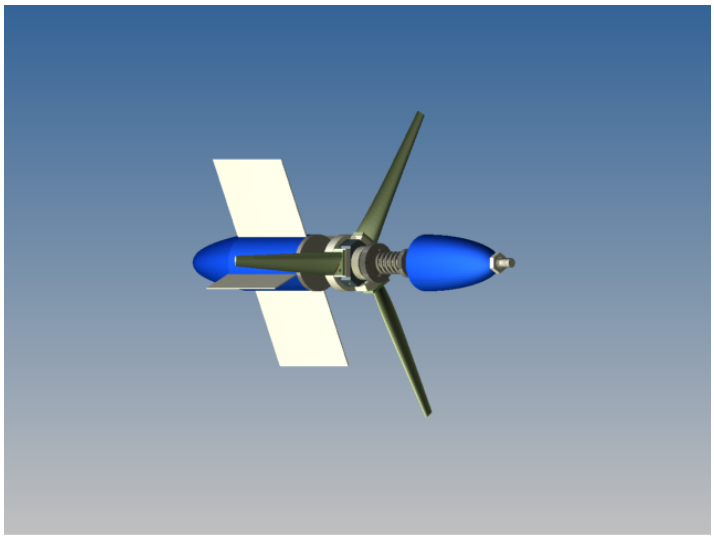

Figure 3.2: Single Rotor.

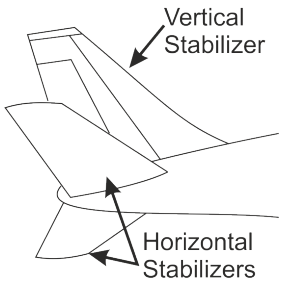

Figure 3.3: Horizontal and Vertical Stabilizers.

3.3.2 Contra Rotating

The contra rotating rotor (CRR) consists of co-axial upstream and a downstream set of blades (Figure 3.4). The rotors turn in opposite directions to induce torque compensation. CRRs have been previously employed by shipping and aviation industries (Johnson, 1994).

Ghassemi (2009) has demonstrated, in the shipping industry context, that contra rotating rotors reduce the reactive torque in the shaft and increase the efficiency of the system itself. Moreover, CRRs provide the required power with smaller rotor diameters (especially important in shallow water applications); whilst the noise and vibrations produced are lower than the ones observed in traditional single rotors (Jukola and Ronkainen, 2006). The enhancement in performance allows ships to reduce the fuel consumption during operations.

The aviation industry has used them to increase the manoeuvrability of helicopters due to torque and moment of inertia reduction which simplifies control mechanisms (Chen and McKerrow, 2007). The author found that an increase of stability in hover is obtained when using this type of rotor configuration. The most significant inconvenience found with the use of CRR machines is that the mechanical design is complex and the machine's design and production costs considerably increase.

In the offshore industry for marine renewables, a tethered device has been developed using a CRR. (Clarke et al., 2007b) carried out the first tests with a $1/30^{\text{th}}$ scale device in a tow tank. In order to prove the feasibility of the concept and to obtain the performance curves, the prototype was tested at different velocities with a rigid mooring attached to the towing carriage. The next phase involved sea trial testing for a $1/10^{\text{th}}$ scale device (Clarke et al., 2007a). In this stage the effects of blade-blade interactions were measured, and they showed that it was viable to produce a design with very moderate blade interactions.

The main concern regarding the CRR configuration is the complexity of the machine since it might be possible to have larger vibration effects on the device; however, the benefits of using a CRR configuration are not only related to the torque balance properties. Other investigations have found that the wake propagation behind the propeller is different from that of an isolated rotor which allows the deployment of more devices in a constrained area (O'Doherty et al., 2009). Furthermore, (O'Doherty et al., 2009) demonstrated that the power generation increased 13% with respect to a conventional single rotor. Therefore, further investigations in the stability and vibration performance of SR and CRR turbines will be undertaken in the forthcoming chapters.

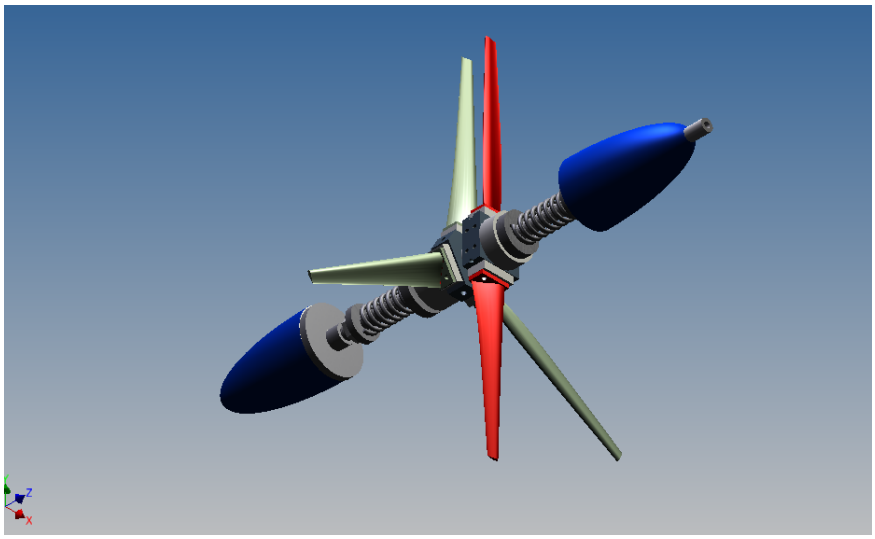

Figure 3.4: Contra Rotating Rotor.

3.3.3 Side by Side Rotors

In contrast to the CRR, side by side rotors (SSRs) use two co-planar rotors in the system. The torque is counter acted by the opposite angular motion of both rotors. Side by side rotors (also called Tandem systems) are extensively used in the aviation industry. The main implication in using such devices in TECs is that the rotors require a large supporting structure which is likely to induce extra drag in the system.

In the marine renewable context, the use of SSRs appears to be a good solution since the energy extracted is doubled compared to CRR or SR devices. However, since the system comprises two rotors on its configuration, the loading imposed on the structural support is doubled. If GBFs are used, the structural support costs might remain the same for a single or a SSR turbine (as stated in Section 2.2.2), however, if a tethered system is considered, the system costs might increase substantially (as reported in Section 2.2.3).

Two SSR tethered TECs are being developed as discussed in Section 3.2 *SR205* and *TidEl*. The development of the SR205 floating tidal turbine started approximately in 2003. Francis and Hamilton (2007) reports a study carried out for $^1/_{14}{}^{\text{th}}$, $^1/_{16}{}^{\text{th}}$ and $^1/_{7}{}^{\text{th}}$ scaled prototypes. The author's studies include the description of a numerical modelling of the platform and, in consequence, the structural design of the complete SR205 device. It includes a description of the mooring mechanism employed and a computational analysis to simulate the mooring line dynamics. Unfortunately, no experimental data about mechanical vibrations or oscillations of the device in the deployment areas were included in the report.

Brief information of the TidEl's development plan has been publicly released by Soil Machine Dynamics Ltd (SMD, 2012); however, theoretical studies made by Vanzwieten et al. (2006)

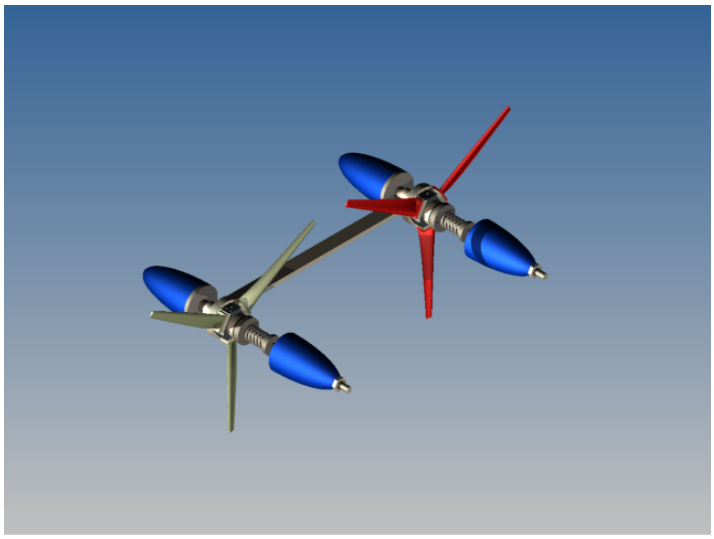

Figure 3.5: Side by Side Rotor.

have produced a mathematical model to simulate the effects of tethering a SSR turbine similar to the TidEL configuration. The second part (VanZwietena et al., 2006) included strategies to control orientation and depth. The analytical strategies seemed to be effective and, indicated stability at low velocities of $0.3\,\mathrm{m/s}$, but the analysis was not backed up by experimental validation of the prototype.

3.4 Static Analysis of Support Structures

In this thesis, the static analysis of structures is carried out through the stress analysis suite of *Autodesk Inventor Professional 2011*. Before the analysis is undertaken, several design parameters, must be considered: *the turbine capacity, boundary conditions of the model and the established criteria limits* (as detailed in the following subsections). Results are compared with respect to their mechanical properties (e.g. normal and axial stresses), required material and footprint. The analysis follows a similar methodology to the one stated by Johanning et al. (2006). Figure 3.6 depicts a flow diagram describing the static analysis methodology.

3.4.1 Turbine Capacity, Dimensions and Environmental Effects

This study is based on the rotor specifications found in Batten et al. (2006); therefore, a full size horizontal axis tidal turbine of $15\,\mathrm{m}$ rotor diameter is employed throughout the analysis. According to the comparisons of two blade profiles studied in Batten et al. (2006), the blade profile NACA 61-8xx presents 12% more power than the NACA 63-2xx. Therefore, properties

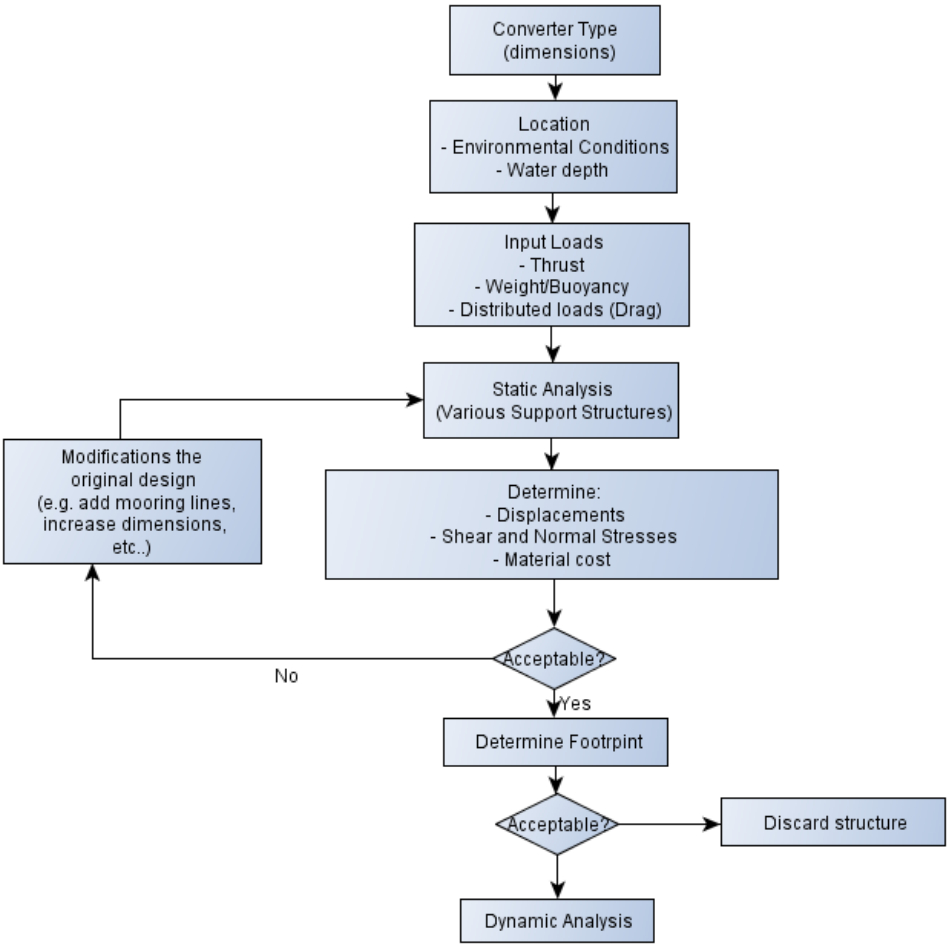

Figure 3.6: Flow diagram for static analysis.

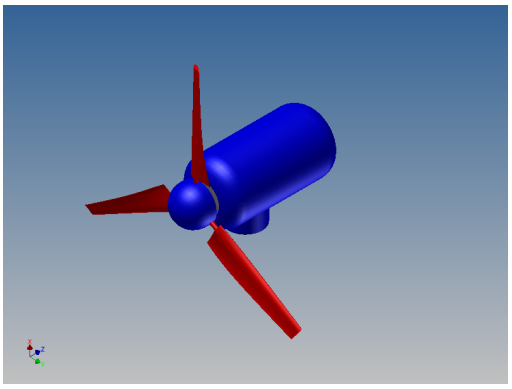

Figure 3.7: 15m rotor diameter tidal converter.

such as power, thrust and torque are based on the characteristics of a 3 bladed NACA 61-8xx tidal turbine.

As established by the Betz's law (Hansen, 2008), a turbine cannot extract completely the kinetic energy from the flow fluids. Therefore, the energy yield is limited by the C_p coefficient which is expressed as the ratio of the available power and the power extracted by the turbine. The C_p of each turbine is thus based on several factors; that is, the blade profile characteristics and the environmental conditions of each specific site. Hence, the calculation of the power output is determined by:

$$\mathrm{P} = 0.5\rho A C_p V_{flow}^3 \tag{3.1}$$

where P is the calculated power generated (predicted) of the specified turbine, and ρ represents the density of salt water. A value of $1025\,{}^{kg}/_{m^3}$ is employed in this thesis (Patel, 1989). A corresponds to the swept area of the rotor, and V_{flow} expresses the undisturbed flow velocity.

As the turbine extracts energy from the fluid, a pressure drop is generated over the axial direction of the turbine rotor (Figure 4.5), which is known as *thrust force*. Similarly to the power extracted, the thrust force is related to a thrust coefficient (C_t). The thrust coefficient varies in accordance with the flow velocity and the rotor's angular velocity; and it is measured with respect to the rotor plane (wake centre) (Frohboese and Schmuck, 2010). In an equation which considers an ideal wind turbine (Hansen, 2008) the thrust is calculated as:

$$\mathrm{T} = 0.5\rho A C_t V_{flow}^2 \tag{3.2}$$

where T is the calculated thrust load of the turbine, ρ represents the density of the seawater, A is the swept area of the rotor, and V_{flow} denotes the unidirectional flow velocity.

Flow velocity	Power	Torque	Thrust
2 m/s	318 kW	29 kN m	272 kN
3 m/s	1075 kW	65.5 kN m	611 kN

Table 3.1: Power Extracted at Optimum Conditions.

The coefficients C_t and C_p are usually related to the local rotational velocity of the rotor through a non-dimensional parameter called Tip Speed Ratio (TSR). In order to obtain the maximum power output, the turbine must operate at its ideal TSR. For example, Batten et al. (2006) establish that the optimum C_p coefficient for the NACA 61-8xx is reached at a TSR of 4.3. The TSR is calculated as follows:

$$\mathrm{TSR} = \frac{\omega R}{V_{flow}} \tag{3.3}$$

where TSR corresponds to the relation between the blade tip speed and the flow velocity (V_{flow}), ω symbolises the angular velocity of the rotor in radians per second and R represents the radius of the rotor. Thus, according to the TSR, the optimum values of C_p and C_t in relation to the TSR of this specific turbine were established as 0.44 (Batten et al., 2008) and 0.75 (Batten et al., 2006) , respectively. In order to carry out a complete static analysis, it is necessary to calculate the torque (Q) generated by the turbine. The torque force is obtained as:

$$\mathrm{Q} = {}^{\mathrm{P}}/_{\omega} \tag{3.4}$$

where P indicates the theoretical extracted power (eq. 3.1), and ω is equated to the angular velocity in radians per second. Specifically, the power, torque and thrust calculated for the purpose of this thesis at 2 and $3\,{}^{\mathrm{m}}/_{\mathrm{s}}$ are found in Table 3.1.

An approximation of the turbine's weight is added to the calculations of the performance characteristics. Since the turbine blades are considered to be neutrally buoyant, the total weight of the system is essentially the nacelle's weight. Thus, the nacelle's weight is extrapolated from 4C Offshore (2012), where the weight of a wind turbine's nacelle of $500\ \mathrm{kW}$ is quoted. Considering the same generator for both 2 and $3\,{}^{\mathrm{m}}/_{\mathrm{s}}$. the total weight is assumed as $380\ \mathrm{kN}$ (in air). Even if the generator will also provide buoyancy, this is considered to be of a minor scale.

The weight of the turbine is considered in each of the calculations where the centre of gravity lines up with the main support. In special cases, the weight of the turbine exerts a bending moment on the pile (and on the pile foundation), or the weight is neglected in tethered turbines. The reason to not consider the weight in a tethered system is because some devices are

designed to work as neutrally buoyant systems as in Ordonez-Sanchez et al. (2010) and SMD (2012). Anchoring mechanisms such as suction plates or sub structural monopile foundations (Figure 2.6(a)) are not considered in the calculations. The utilisation of such sub-structural elements are specified as fixed constrains.

The drag force generated by each of the structural members is also considered in the analysis. The distributed drag force is calculated as:

$$F_d = 0.5\rho D C_d V_{flow}^2 \tag{3.5}$$

where F_d denotes the drag per unit length of the beam/pile, D indicates the outer beam/pile diameter, and C_d is the corresponding drag coefficient. A drag coefficient of 1.2 is considered in the calculations (according to Patel (1989)); however, it must be noted for future calculations that the drag coefficient decreases according to rough surfaces or turbulent conditions as stated by White (1991). The structures to be studied are depicted in Figure 3.8.

3.4.2 Allowable Load and Displacement

Two limit criteria are considered in the structural analysis of rigid structures:

1. The stresses in the structural members should not reach ***the maximum yield stress of the material***. In this case, mild steel is considered as the material of beams and piles (Figure 3.8(a) and (b)); thus, a yield stress criterion of $250\,\mathrm{MPa}$ is established for this calculations. If one of the structural members exceeds such a limit, the next dimension of beams/piles is applied until this criteria is met. The database of the beams included in the *Autodesk Frame Analysis* comprises beams of up to $1.2\,\mathrm{m}$ in outside diameter. Beyond this, the aspect ratio of the outside diameter of the pile, D, versus the wall thickness, t, followed a relation of $\frac{D}{t} = 27$, according to Jardine (2009).

2. ***The allowable deflection of piles and beams***. Standards for pile foundations indicate that the maximum lateral displacement (δ) should not exceed $25.4\,\mathrm{mm}$, as suggested by Mokwa (1999). The criterion that it is utilised to study the frame members follows a relation of $\delta = \frac{L}{120}$, according to Johnson (2010), where L corresponds to the length of the member.

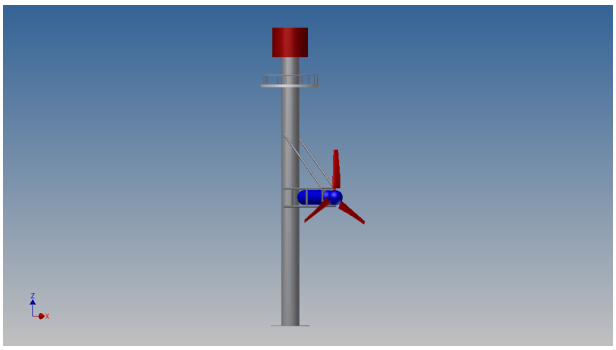

(a)

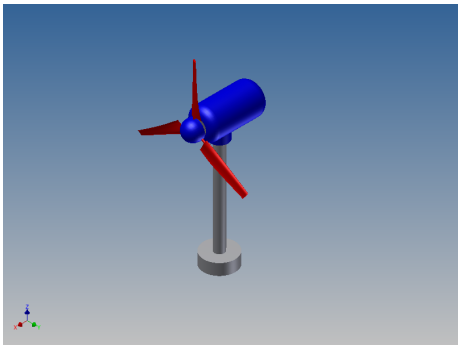

(b)

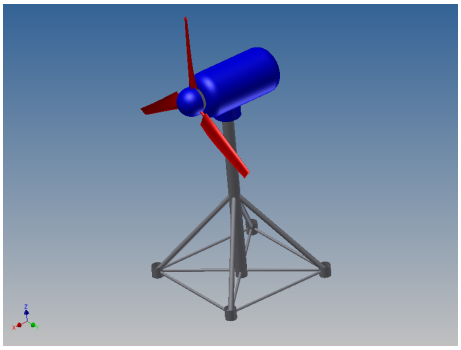

(c)

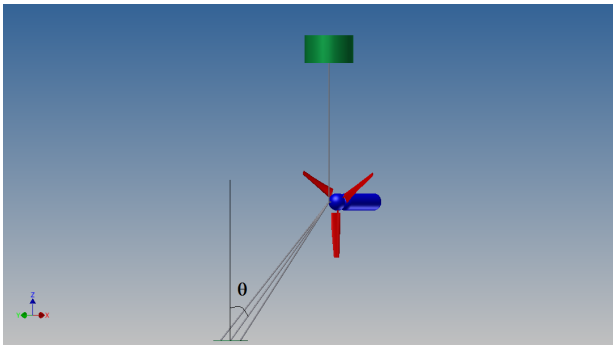

(d)

Figure 3.8: Structural Supports: a)Pile Foundation, b) Minipile, c)Quadpod and d)Flexible Mooring.

3.5 Results and Discussion

The following sections include the results for the five configurations considered in this static analysis. The sections are subdivided into five parts where the structural systems are compared in terms of material costs, stresses and footprint area.

3.5.1 Elements Dimensions and Displacement

As mention at the beginning of Section 3.4, a finite element analysis was undertaken through the stress analysis suite of Autodesk Inventor. An iterative process was followed to find the beam/pile configuration which would require minimum amount of material while following the criteria established in Section 3.4.2 (e.g. maximum deflection of piles of 25.4mm). The concluding dimensions of the beam/pile members are shown in Tables 3.2 and 3.3.

It is clearly observed that the beams/piles require an increment in the member dimensions as the flow velocities increase throughout the tidal cycle. According to the results shown on Table 3.3, pile foundations require a pile of $3.6\,\mathrm{m}$ for moderate water flows; but, as the environmental conditions become more severe, the outer diameter should be increased at least to $5\,\mathrm{m}$ in order to prevent severe deflections. By comparing the last results to similar pile foundation designs (e.g. Seaflow installation), it can be observed that these calculations suggest that the pile structure used for the Seagen turbine should be wider than the current design (e.g. which at the present time is of 2.1m of outside diameter (Fraenkel, 2005)). Differences between current designs and the results presented in this thesis could have occurred due to library restrictions of Autodesk Inventor. In this thesis it was suggested that members larger than $1200\,\mathrm{mm}$ should follow a relationship of $\delta = \frac{L}{120}$ (as explained in Section 3.4.2). Therefore, it is likely that wall thickness differences have arisen between these calculations and the information on Fraenkel (2005).

Three structural framework configurations are displayed in Table 3.2. Two cases consider a tripod and a quadpod structure where the inclined members form an angle of 45 degrees with the horizontal axis which creates a base of $15\,\mathrm{m}$ diameter. A third case considered a tripod with a steeper angle in the crosswise beam members. The base size of the tripod for this case is $10\,\mathrm{m}$ diameter. Due to the large stresses located in the frameworks, the required outer diameters of the frame members increased by 1.65 times when flows increase from 2 to $3\,\mathrm{m/s}$ for a tripod with a base of $15\,\mathrm{m}$ diameter (i.e. $762\,\mathrm{mm}$to $1269\,\mathrm{mm}$). The change in frame elements is smaller in quadpod configurations, where the outer diameter increases only by 1.33 times. As expected, the outer diameters of the members are minimised if the number of members increases in the structural system. It should be noted that at low velocities the

Framework Configuration	Tripod 45deg (2m/s)	Tripod 45deg (3m/s)	Tripod 33deg (2m/s)	Tripod 33deg (3m/s)	Quadpod 45deg (2m/s)	Quadpod 45deg (3m/s)
Main Member (Out. Diam.)	762	1269	762	1067	762	1016
Wall Thickness	30	30	30	30	30	30
Inclined Member (Out. Diam.)	457	508	457	457	457	457
Wall Thickness	30	30	30	30	30	30
Base Member (Out. Diam.)	244	244	244	244	244	244
Wall Thickness	12.5	12.5	12.5	12.5	12.5	12.5
Max. Deflection	**63.43**	**45.46**	**61.33**	**58.32**	**59**	**61.32**

Table 3.2: Member Dimensions (Structural Frameworks) in mm.

Pile and Flexible Mooring Config.	Pile (2m/s)	Pile (3m/s)	Minipile (2m/s)	Minipile (3m/s)	Taut Leg (2m/s)	Taut Leg (3m/s)
Main Member (Out. Diam.)	3600	5000	1500	1900	38	63
Wall Thickness	129	190	60	70		
Max. Deflection	**25.60**	**28.00**	**23.66**	**23.32**		

Table 3.3: Member Dimensions (Piles and Mooring Lines) in mm.

structural member dimensions do not change in any of the three framework configurations, the reason is that due to the structural members available in the software library, the use of a smaller member would exceed the criteria established in Section 3.4.2. However, it can be observed that the deflection of the member of the quadpod configuration is lesser than that of both tripods (Tables 3.2).

In respect to the estimation of minipile structures, it is deduced that the foundation requires an increase of 27% in the outer diameter at flow velocities of $3\,\mathrm{m/s}$. This makes minipiles a safer option if the device is meant to be installed within turbulent flows where current velocity might increase by 50%. Finally, the analysis suggests that mooring line diameters must be increased by 66% if the stream velocity rises from 2 to $3\,\mathrm{m/s}$, and the turbines are installed as tethered devices.

Figures 3.9 and 3.10 show the lateral displacement of a minipile and a structural framework during flow conditions of $3\,\mathrm{m/s}$, respectively. A displacement of about $7\ \mathrm{mm}$ is observed in one of the diagonal members of the tripod (Figure 3.10); this was expected since the direction of the flow creates higher loads in this member; additionally, the thrust force creates an additional force that must be supported mainly by that member.

Unlike rigid structures, the deformation of the mooring line is not quantified in the static

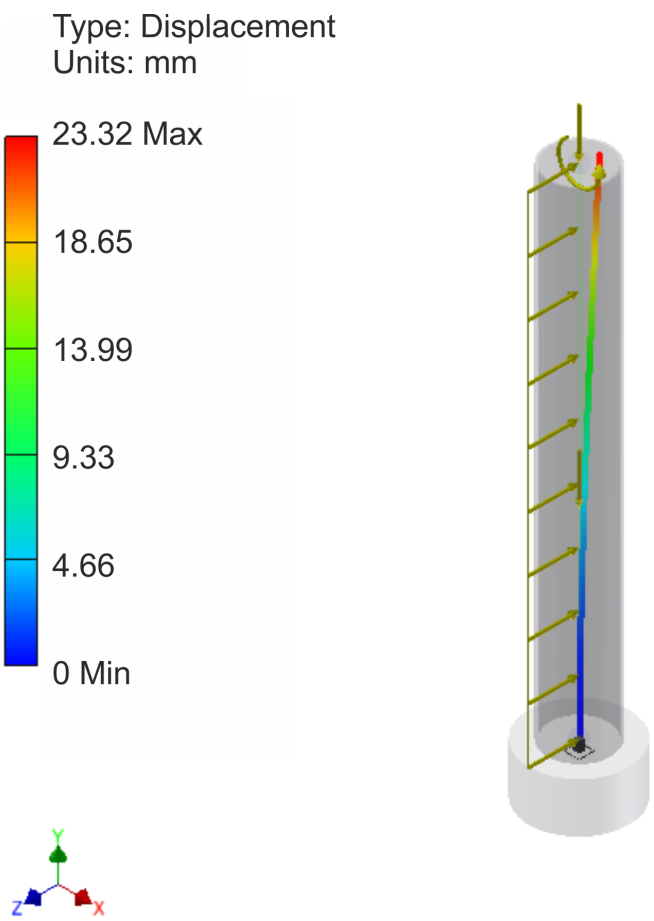

Figure 3.9: Member deflections of the a Minipile Foundation at $3\,^{\mathrm{m}}/_{\mathrm{s}}$.

analysis. The breaking load dictates the amount of load that the mooring lines are able to withstand. The main parameter for line selection is the breaking load of the corresponding line.

3.5.2 Material Cost

In Vø lund (2005) and Harris et al. (2004), the authors carry out cost estimations of structural support systems and materials for OWTs and WECs, respectively. The material considered for rigid structures in this static analysis is mild steel with a cost of $1.5\,^{\mathrm{euros}}/_{\mathrm{kg}}$ (Vø lund (2005)); whereas the costs of the mooring lines are approximate values of steel wire ropes. Thus, the mooring lines are based on a cost of 52 to $76\,^{\mathrm{euros}}/_{\mathrm{m}}$, as presented in Harris et al. (2004). The use of buoyant systems was also included in the material cost estimation. The information of the buoyancy costs was obtained through private communications. Therefore, it is evident in Figure 3.11 that pile foundations are, as expected, the most expensive station keeping systems in general. For instance, a pile foundation requires 21 times more steel than framework structures, as quantified for flows of $3\,^{\mathrm{m}}/_{\mathrm{s}}$.

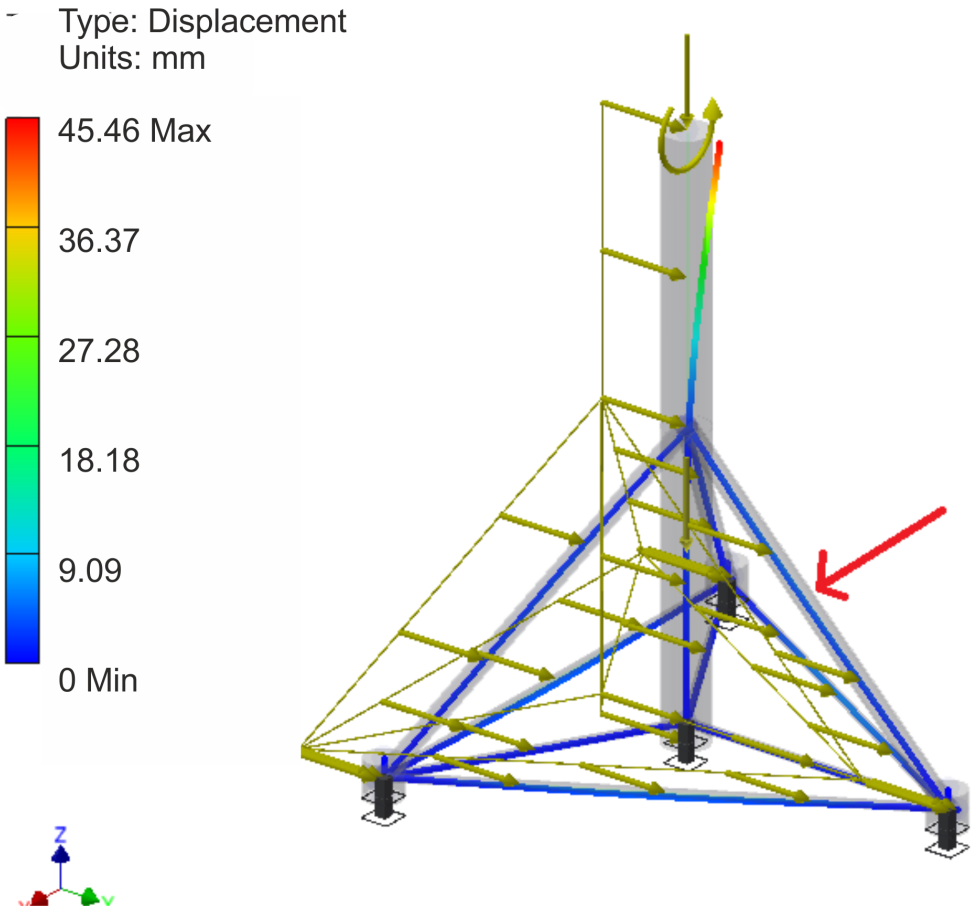

Figure 3.10: Member deflections of the a Tripod at $3\,{}^{\mathrm{m}}/_{\mathrm{s}}$.

Structural Type/ Flow Condition	2 m/s	3m/s
Pile Foundation	€661,700	€1,288,998
Minipile	€47,880	€70,989
Tripod (45°)	€45,656	€68,586
Tripod (33°)	€29,420	€34,504
Quadpod (45°)	€55,673	€59,906
Taut Leg	€6,721	€13,949

Figure 3.11: Estimated Material Costs for each Structural Support.

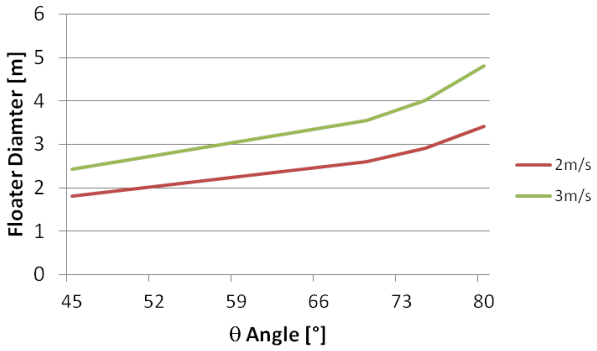

Figure 3.12: Floater Diameter.

As observed in Table 3.3, in order to meet the established criteria, the outer diameter of the minipile increases 27% in the calculations for flow conditions of $3\,\mathrm{m/s}$. This is directly reflected in the calculated material costs. Generally the smaller sections are required for quadpod structures. In this case, the changes between flows of 2 and $3\,\mathrm{m/s}$ remain the same; whereas the material employed for tripods with a base of $15\,\mathrm{m}$ increases by 11% when the calculations are carried out for environmental conditions of $3\,\mathrm{m/s}$. It is found that tripod structures with steeper crossbeams (configurations with a base of $10\,\mathrm{m}$) are almost 100% cheaper than the other tripod arrangement (base of $10\,\mathrm{m}$) or 15% cheaper than the quadpod system.

In regard to flexible moorings, the costs increase by 45% as the calculations are undertaken for flow streams of $3\,\mathrm{m/s}$. In spite of an increase in the line diameter, the costs of the mooring lines are still lower than for rigid structures (Figure 3.11). Moreover, the costs could be further reduced if synthetic mooring lines are considered in the configuration. The main disadvantage of this station keeping system is the surface buoy. As depicted in Figure 3.12, the requirements of the system vary according to the angle, θ, established in the static calculations. It is found that as steeper angles (Figure 3.8) are established as input in the analysis, the demands on the buoyant sections increase proportionally.

Mechanical Properties (Mpa)	Tripod 45deg (2m/s)	Tripod 45deg (3m/s)	Tripod 33deg (2m/s)	Tripod 33deg (3m/s)	Quadpod 45deg (2m/s)	Quadpod 45deg (3m/s)
Max Deflection [mm]	**63.43**	**45.46**	**61.33**	**58.32**	**59.00**	**61.32**
Max Normal Stress (Smax)	238.30	234.30	166.80	189.80	166.80	205.80
Min Normal Stress (Smin)	40.80	99.60	6.40	19.00	9.20	23.80
Max Axial Stress	47.33	106.20	7.88	21.04	9.62	24.65
Min Axial Stress	-47.33	-106.20	-22.46	-47.57	-13.79	-28.36
Max Shear Stress (Tx)	4.06	7.07	0.38	0.39	0.96	0.94
Min Shear Stress (Tx)	5.78	-8.70	-1.98	-2.04	-1.68	-1.93
Max Shear Stress (Ty)	7.03	12.25	8.07	15.47	8.12	13.55
Min Shear Stress (Ty)	-6.77	-14.59	-8.12	-13.26	-8.11	-16.18
Moment (Mx) [Nm]	1.60	4.11	2.07	4.72	0.61	1.58
Moment (My) [Nm]	0.44	0.77	0.21	0.22	0.18	0.21
Moment (Mz) [Nm]	0.02	0.03	0.02	0.03	0.03	3.47

Table 3.4: FEA Results (Structural Frameworks).

Mechanical Properties (Mpa)	Pile (2m/s)	Pile (3m/s)	Minipile (2m/s)	Minipile (3m/s)
Max Deflection [mm]	25.60	28.00	23.66	23.32
Max Normal Stress (Smax)	15.04	24.29	46.38	59.87
Min Normal Stress (Smin)	0.00	0.00	-1.71	-0.58
Max Axial Stress	0.00	0.00	-1.40	-1.31
Min Axial Stress	-3.93	-3.85	-2.55	-64.02
Max Shear Stress (Tx)	0.00	0.00	0.00	-0.94
Min Shear Stress (Tx)	-1.72	-3.32	0.00	-2.10
Max Shear Stress (Ty)	0.00	0.00	-2.00	0.00
Min Shear Stress (Ty)	0.00	0.00	-2.48	-3.03
Moment (Mx) Nm	0.03	0.07	-4.57	-10.93
Moment (My) Nm	22.40	93.52	-0.03	-0.07
Moment (Mz) Nm	0.00	0.00	0.00	0.00

Table 3.5: FEA Results (Pile Designs).

3.5.3 Stress Analysis

The maximum and minimum stresses for each of the structures are summarised in Tables 3.4 and 3.5. The main objective is to locate the affected areas of each structure member where failures can occur. Obviously, the higher the stresses, the lower number of cycles that are required for a structural part to fail.

Following the established criteria, it is shown in Table 3.5, that the pile foundations have lower magnitudes of maximum and minimum normal stresses for the same load conditions. Moreover, the shear stresses calculated for the pile are lower in magnitudes. No shear stresses (T_y) are obtained in the 'y' axis; however, this is expected since the flow stream is considered to be uniformly horizontal in the 'x' axis. Thus, the maximum shear stress obtained (T_x) had a magnitude of $-3.32\,\mathrm{MPa}$ and it is located in the fixed constraint of the pile foundation.

A second case is studied for the pile with an outer diameter of $3.5\,\mathrm{m}$ with a flow velocity of $3\,\mathrm{m/s}$. The results show that the lateral displacement at the top section increases by 2.5 times (i.e. to $63.3\,\mathrm{mm}$). The maximum normal stress remains at a low value of $42.81\,\mathrm{MPa}$. A shear stress of $4.04\,\mathrm{MPa}$ is found in the same conditions. However, the anchor system needs

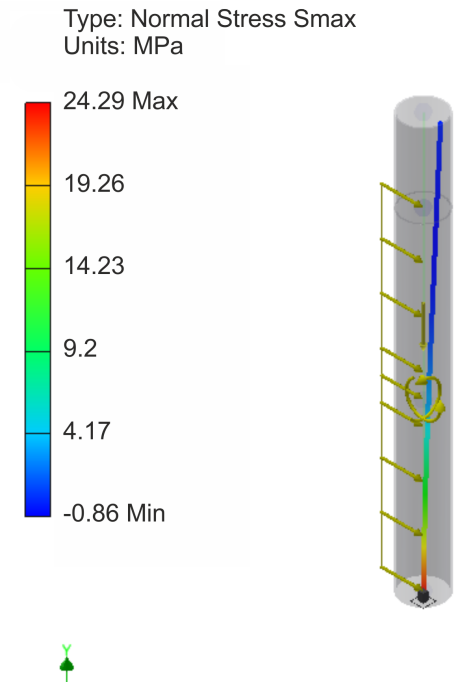

Figure 3.13: Stress Analysis of Pile Foundation at $3\,^{\mathrm{m}}/_{\mathrm{s}}$.

reinforcement due to the substantial increase of the overturning moment (2 times higher than for the condition of $2\,^{\mathrm{m}}/_{\mathrm{s}}$).

The principal stresses calculated for the mini-pile foundations are clearly higher than those obtained for monopile structures (Table 3.5). Similarly to the study performed for the monopile foundations, the corresponding loads of flows at $3\,^{\mathrm{m}}/_{\mathrm{s}}$ are applied to the mini-pile foundation designed for flow conditions of $2\,^{\mathrm{m}}/_{\mathrm{s}}$. As a result, an increment of 2.25 times is found in the top displacement. As distinct to the results obtained with monopiles (as discussed above), the resulting maximum principal stress has a severe increment of 2.28 times ($107.4\,\mathrm{MPa}$). As mentioned in Section 2.2.2, the advantage of using a concrete GBF foundation is that the same structure can withstand severe load changes without presenting failure in the system. Furthermore, it is expected that the shear stresses calculated are considerably higher than those of pile foundations because of the smaller outer diameters utilised in the minipile members. Hence, the main characteristic identified in mini-pile foundations is that the overturning moment about the y axis is considerably lower ($-11\,\mathrm{Nm}$) that the one calculated for monopile structures ($93\,\mathrm{Nm}$). Hence, the anchoring subsystem presents less structural requirements.

As in the previous study cases, the velocity of the flow is considered to be uniform and unidirectional in the analysis. During the structural framework calculations, the drag forces created in each of the members are allocated such that one of the cross beams absorbs most of the

load (e.g. Figure 3.14). The objective is to analyse extreme cases, especially for the quadpod arrangement where the load is probably spread between 2 cross beams as the tide approaches and the other two beams when the flow changes direction. Therefore, the consequences of studying this case intend to identify the affected areas in both structural framework configurations.

Principal stresses on the tripod are significantly high when the diagonal beams are fixed with a 45 degree inclination with respect to the base. Principal stresses therefore reduce as the inclination of the members decreases to 33 degrees; however, Table 3.2 shows that in order to satisfy the established criteria (described in Section 3.4.2), the outer diameter of the crossbeam members has to be increased by 11% with flow velocities of $3\,^{\mathrm{m}}/_{\mathrm{s}}$. Thus, the resultant maximum principal stress is reduced by 23% from the 45 degree tripod to the 33 degree tripod configurations.

As expected, the principal stresses were 14% lower in the quadpod space frames of 45 degree than the tripod configuration with the same crossbeam angle. In summary, the maximum principal stresses are identified in the main strut and in the inclined beam which withstands the entire load. Figures 3.14 and 3.15 depict the maximum principal stresses of a tripod at 33 degree and a quadpod at flow conditions of $3\,^{\mathrm{m}}/_{\mathrm{s}}$ and $2\,^{\mathrm{m}}/_{\mathrm{s}}$, respectively.

Similarly, the maximum and minimum axial stresses are identified in the diagonal members. The tripod with inclined beams of 45 degrees has the highest tension stresses of 106 MPa at flow conditions of $3\,^{\mathrm{m}}/_{\mathrm{s}}$. Meanwhile, the maximum value obtained for the quadpod configuration is 25 MPa. Tripod configurations with diagonal members of 33 degrees present a maximum axial stress of 21.04 MPa, 6 times lower than that observed in the other tripod configuration. Axial stresses are of low magnitude in the tripod configuration with crossbeams with an angle of 33 degrees. The element with highest axial stresses is located in the base section (Figure 3.16) since the cross beam has a stiffer strut; thus, the calculated stress does not go beyond the established criteria.

A summary of the maximum stress characteristics for each of the configurations can be found in Tables 3.4 and 3.5. It must be noted that the shear stresses calculated for each of the structural framework configurations are of small magnitude (e.g. maximum at 15.47 MPa). The maximum overturning moment calculated in these structures has a value of 4.72 Nm (Figure 3.4). Thus, it is clear that due to the dispersion of loads created in the structural framework configurations, the overturning moment is minimised with respect to the pile and minipile foundations (Figure 3.5).

A static analysis is undertaken for a taut mooring line configuration without using Autodesk Inventor since the platform considers frame members, and an approximation of wire or syn-

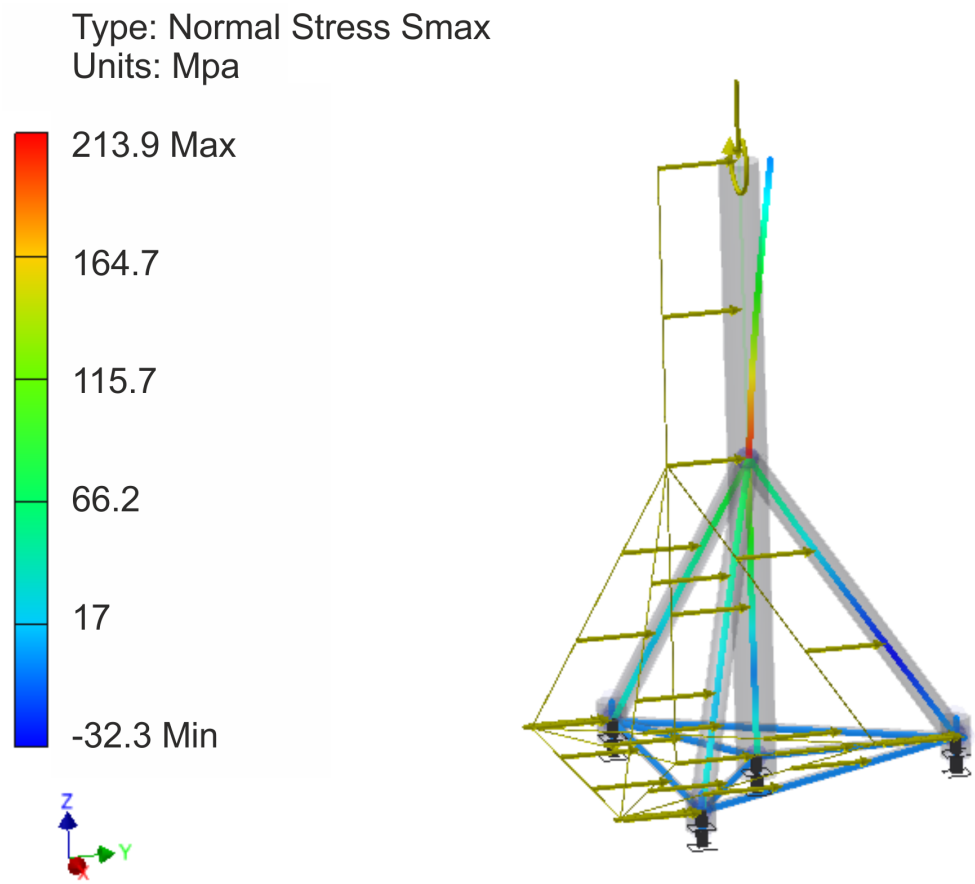

(a)

Figure 3.14: Principal Stress of a Tripod ($3\,{}^{\mathrm{m}}/_{\mathrm{s}}$).

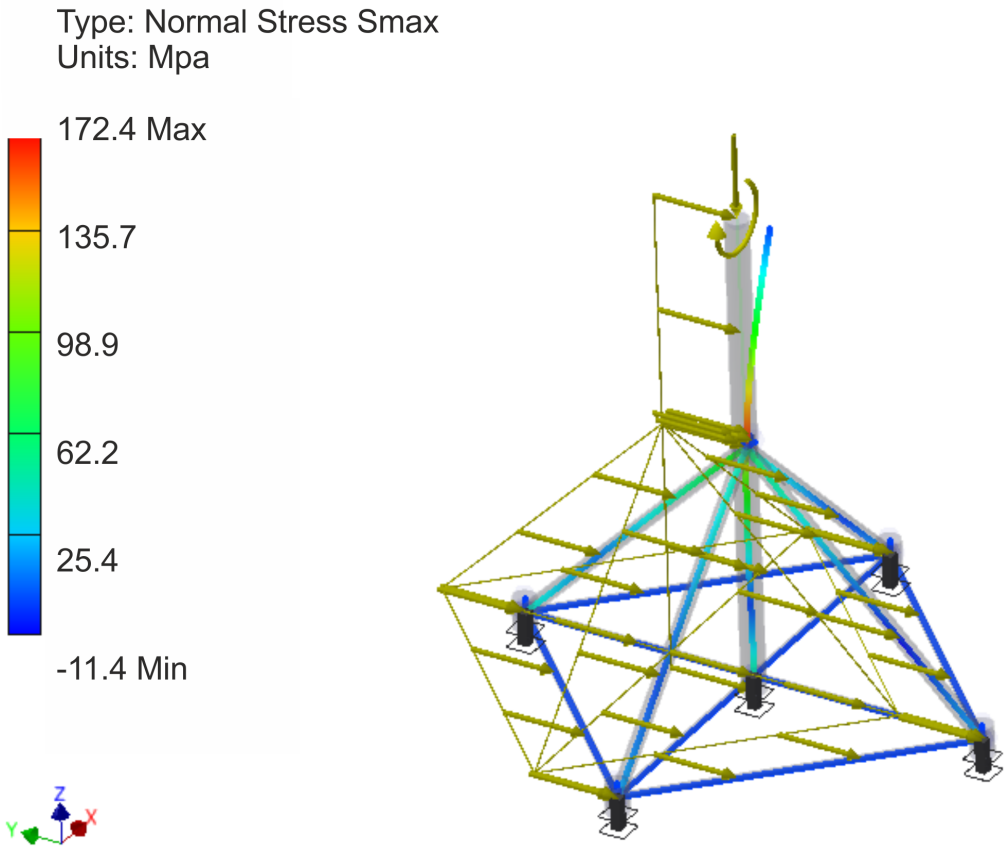

(b)

Figure 3.15: Principal Stress of a Quadpod ($2\,{}^{\mathrm{m}}/_{\mathrm{s}}$).

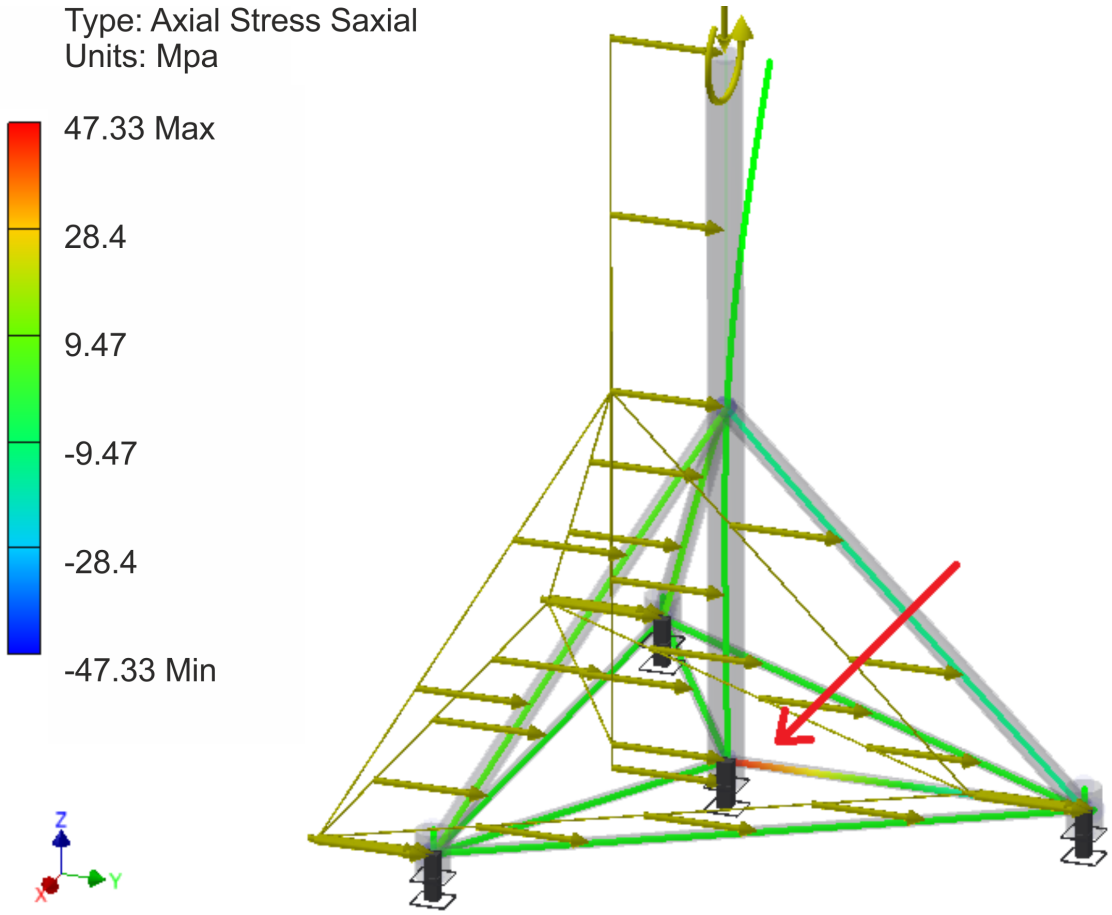

Figure 3.16: Axial Stress of a Tripod (45 deg) at 2 $^{m}/_{s}$.

thetic ropes is not possible. Thus, the main mechanical properties calculated in this analysis are related to the axial stresses in the lines. The axial stresses calculated for the mooring lines are $800\,\mathrm{MPa}$ and $780\,\mathrm{MPa}$ for both cases of $2\ ^{\mathrm{m}}/_{\mathrm{s}}$ and $3\ ^{\mathrm{m}}/_{\mathrm{s}}$, respectively. These data are obtained when using mooring line diameters of $38\,\mathrm{mm}$ and $63\,\mathrm{mm}$ (Table 3.3). Clearly, these are significantly higher in comparison with stresses in rigid foundations. However, due to the lack of information on the dynamic motions of the device and the line, the study cannot provide further information.

From this study, the feasibility of using rigid foundations is demonstrated. If the load requirements increase according to the site characteristics, the pile foundations or beam members can be reinforced or increased in size in order to withstand such forces. The stiffness of the structures provides a solid foundation to the TEC, with minimum influence on their performance. This might not be the case for tethered devices, since it is possible that the dynamic responses of devices have high impact on the mooring lines and on their performance as observed in the literature review related to OWTs in Section 2.2.3.

3.5.4 Footprint

As observed in Figure 3.8, the rigid foundations do not generate a large footprint, especially pile structures. However, the flexible mooring device studied in this work occupies a larger span area in the sea bed than rigid foundations. The footprint area can therefore be reduced if the angle θ (Figure 3.8(d) and 3.12) is reduced to smaller values.

In Figure 3.12, it is observed that the volume of the buoyancy must be increased by approximately 70% in order to provide the required upward force of the system when the current speed increases from 2 to $3\ ^{\mathrm{m}}/_{\mathrm{s}}$. Moreover, it is observed in Figure 3.17, that as the angle θ is increased, the footprint area can be reduced significantly. These calculations are undertaken for taut leg mooring lines; if catenary lines are considered in the station keeping system, the footprint area increases substantially (in this study, catenary lines are not considered and therefore, they are proposed as future work as described in Chapter 8).

3.6 Conclusions and Final Remarks

As reviewed in the literature survey of this chapter, piles and GBFs are frequently used in current tidal technology. Developers, are also considering the use of flexible moorings as station keeping mechanisms. The latter requires care in the selection of a suitable rotor arrangement; for example, *single*, *contra rotating* and *side by side rotors*. Each of them provides

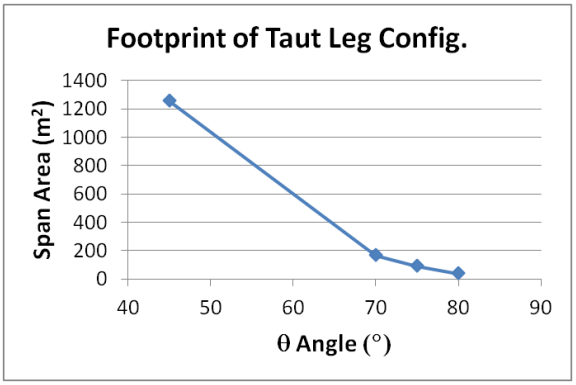

Figure 3.17: Taut Leg Configuration Footprint.

several advantages and disadvantages when used for helicopters, aircrafts or ships; however, the performance of them in TECs is a different matter. This chapter carried out a static structural analysis of current off-shore foundations in order to study, understand and determine the implications of using each of them. Two criteria were proposed in the investigation:

1. The maximum displacement of each structural member would not exceed $25.4\,\mathrm{mm}$ in pile foundations and the maximum deflection in structural frameworks should not go beyond the length of the member divided by 120.

2. The stresses should not exceed the yield strength of the material.

The results were presented in terms of the mechanical properties, device footprint and material costs. A summary of the outcomes and comparison between the studied support structures is presented in Table 3.6.

Piles and mini-piles showed lower shear stresses than structural frameworks in general due to the large cross sectional areas; this has several advantages since buckling problems could be reduced. Another advantage was that they were not subjected to tensile and compressive loads which could affect the members under cyclic loading. The main disadvantage identified in the use of monopiles was related to the material costs. That is, the material costs of installing a pile foundation were calculated to be 21.5 times higher compared to quadpod space frames designed for flow velocities at $3\,\mathrm{m/s}$. Likewise, the costs were 400 times higher than those determined for a tethered configuration (with the same flow conditions, and no anchoring foundations considered) even at low water depths of $40\,\mathrm{m}$.

The study in this chapter also compared the use of two frameworks (tripods and quadpods). The loads on a quadpod are widely spread and smaller sections of the members stand the same loads; therefore, the normal and shear stresses are lesser in this configuration. Because of the larger amount of material used for a quadpod, they proved to be less economic than tripod

Structural Type/ Flow Condition	Advantages	Disadvantages
Pile Foundation	Low mechanical stresses on the system. Not subjected to a change of tensile and compressive loads. Small footprint.	Significant material costs associated with this structure. Costs vary with water depth variations. Large overturning moment.
Minipile	Submerged rigid structure with the lowest mechanical stresses. Small footprint	Large overturning moment.
Tripod (33deg)	Lowest material costs compared to other rigid structures. Small footprint. A change on the environmental conditions only affects the main structural member.	Low overturning moments. Large mechanical stresses. Tensile and compressive loads which lead to hysteresis problems.
Quadpod	Lower mechanical stresses on the components compared with other framework structures. A change on the environmental conditions requires a minimum increase of the structural members. Low footprint. Less expensive when using in higher flow velocity currents (>3 m/s).	Low overturning moments. Large mechanical stresses. Tensile and compressive loads lead to hysteresis problems.
Taut Leg	Lowest material costs compared to rigid structures.	Footprint can become substantially large. High stresses on the mooring lines which will required to be changed frequently. Dynamic motions might affect the structural system.

Table 3.6: Positive and Negative characteristics of each of the Support Structures studied in this Chapter.

configurations when used in low flow velocity conditions (e.g.$2\,^{\mathrm{m}}/_{\mathrm{s}}$). At higher flow velocities (e.g. $3\,^{\mathrm{m}}/_{\mathrm{s}}$) the quadpod configuration shows to be the most adequate solution. Since the height of this structures will be subjected to the tidal turbine design, the amount of material will be different for each location.

Tethered turbines are the most economically attractive as shown in Figure 3.11. The loads increase greatly if the site has stronger currents, but, the material costs are still much lower than for rigid foundations. The main disadvantage concerns the buoyancy demands and the device footprint. There is a compromise to be struck between footprint area (which should be minimised) and buoyancy (which reduces footprint area but is costly).

The use of a static analysis for tethered devices is not sufficient to ensure the viability of a flexible mooring system. A dynamic analysis in the mooring lines and the device itself must be undertaken before any installation is proposed. Thus, a methodology to quantify the dynamic motions of tethered tidal turbines is presented in Chapter 4.

Chapter 4

Methodology to Evaluate the Dynamic Response of Tethered Turbines

Following the structural analysis of various support foundations, it was concluded that tethered systems for TECs could potentially be more effective than rigid foundations for two reasons. Firstly, a substantial reduction of materials is achieved when mooring lines are utilised. Secondly, a reduction in the use of barges, DP vessels and cranes could improve costs of installation and recovery, as seems to be the case for floating OWTs. However, success or failure of tethered turbines would depend upon their largely unknown dynamic response characteristics. Therefore, this chapter proposes a methodology to evaluate dynamic interactions of tethered devices. The mechanical design and instrumentation of model tethered turbines are described. The results obtained from tests are then evaluated in both time and frequency domains.

4.1 Motivation

The main property of rigid foundations is that they ensure stable positioning of the rotor when the turbine is exposed to severe environmental conditions. The use of a stiff foundation decreases the possibility of resonance problems. The efficiency of TECs supported by rigid structures primarily depends on the efficiency of the turbine and the power take off mechanism. A FEA technique is adequate to provide an insight into the principal stresses, element deflections and material sizing in each of the components.

The static analysis carried out on tethered devices gave an insight into several parameters including the dimensions and lengths of the mooring line sections, anchoring capacity and

footprint area, but it did not consider dynamic behaviour. The dynamic response of these devices is uncertain, and the motions of the turbine may affect the behaviour of the mooring lines. Also, the coupling of mooring lines and TEC can lead to a resonant system if the natural frequencies of the device are not known. Additionally, the mechanical vibration levels may be higher or more difficult to control in tethered devices than those of rigid systems.

Common hydrodynamic software used widely by naval and marine scientists provides information on both dynamic and static analysis of mooring line structures (e.g. Orcina (2012), Bureau Veritas and MCS (2012), Ansys (2012), Ultramarine (2012)). However, this software is usually employed to analyse mooring line characteristics or dynamic couplings of wave energy converters (Fitzgerald and Bergdahl (2007), Vickers and Johanning (2009)) which do not normally incorporate large rotordynamic machines. Offshore wind turbine developers have proposed several methods to couple the motions of floating wind turbines using the above mentioned software. For example, Wayman et al. (2006) and Jonkman and Buhl (2007b) based their studies on coupling several modules. To study the rotordynamics of the turbine, one of the modules determines the aerodynamics and structural dynamics of the turbine and the tower section, employing the program FAST developed by NREL. The algorithm includes modes of motion of structural sections such as blades and tower leading to a 22 to 24 DOF system, depending on its characteristics (e.g. the number of blades, control systems, etc.). Then, this system is coupled to a hydrodynamic module to determine the added mass and damping properties of the ballast section to be used. Finally, a quasi-static analysis is linked to the previous modules to estimate the properties of the mooring line sections. Other examples are presented in Appendix C which considers different suites in their analysis.

The computational techniques used for wind turbines might be considered appropriate for the study of tidal energy converters and in some respects they are; but for modelling of complete systems the differences are substantive. For tethered tidal systems a dedicated dynamic analysis is required, to determine their behaviour through a series of tidal states. In this case, the analytical methods used nowadays have not been fully validated with empirical data to support a theoretical analysis (e.g. Mackie (2008), Francis and Hamilton (2007) and Vanzwieten et al. (2006)).

Therefore, this chapter outlines an experimental methodology to study the dynamic response of tethered turbines. Testing and evaluation of marine energy conversion systems has received considerable attention in the recent past, culminating in the publication of the findings from the European Commission EquiMar project (EquiMar, 2012). The steps outlined below follow the general ethos of the EquiMar protocols, but are set in the specific context of tethered tidal energy converters.

The mechanical design process described here is primarily focused on the selection of com-

ponents of small scale devices, designed to be tested over short periods of time. A series of such tests, carried out at various scales, is described in the following chapters. However, the rest of the processes can be scaled and made appropriate for the testing and analysis of both small and large scale devices. In particular, the guidelines related to instrumentation and signal processing techniques used to evaluate the dynamic response of the turbines are relevant to the analysis of systems at any scale and in any test environment.

The remainder of this chapter is organised as follows: The general methodology is described in Section 4.2, the selection of facilities is described in Section 4.3 and the mechanical design process for tethered turbines is described in Section 4.4. Instrumentation and data acquisition systems are described in Section 4.5. Section 4.6 reviews the signal processing techniques in general, and as used in this study. A review of mechanical vibrations in rotary machines is given in Section 4.7. And Section 4.8 presents the concluding comments of the developed methodology.

4.2 Methodology Description

Since the variety of tethered tidal turbine designs have increased lately (Section 3.2), it is important to assess the stability and the consequences of using each turbine configuration in terms of its dynamic response. It is well known that the dynamic response of a system can be studied by means of its linear (e.g. surge, sway and heave) and rotational motions (e.g. roll, pitch and yaw). Since the dominant force on a TEC device is driven by its thrust load, it is likely that sway motion will be insignificant; in contrast, due to the turbulent nature of the flow, yaw alignment can change severely throughout the tidal cycle. Therefore, significant power looses will be expected (Galloway et al., 2011).

Since the up and down motions of a turbine are limited by the station keeping system to a minimum; heave motions will have insignificant influence on power loss. However, an incorrect weight distribution on the turbine arrangement or high wave energy densities could lead to severe pitch motions resulting in grievous power losses. Finally, as stated in Section 2.3.3, some mooring line material will be damaged if severe twisting is imposed (which will be caused by roll motions); also, fatigue will be induced by frequent snap loads (cause by surge motions created by wave or debris interactions). Since surge will be directly affected by the nature of the environment and not by the device itself, it was established that the key parameters to measure were the three main rotational angles: roll, pitch and yaw.

A series of steps must be followed before the measurement of these parameters is undertaken. Thus, Figure 4.2 depicts the sequential steps of the proposed methodology. These are sum-

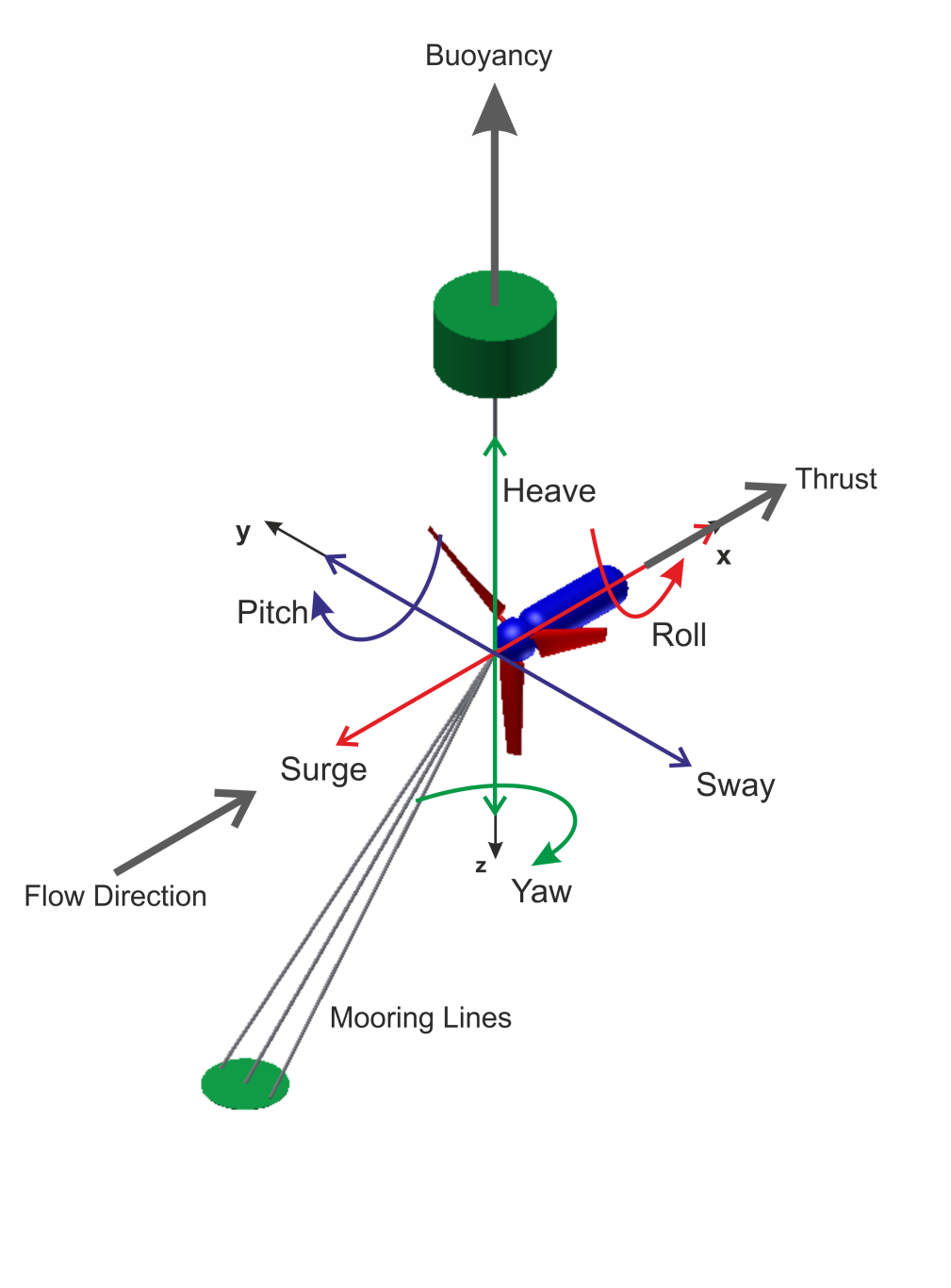

Figure 4.1: Linear and Rotational Motions of a Tethered Turbine.

marised below, in some cases a component in the Figure is expanded later as a flow diagram at the beginning of the appropriate section (see Figures 4.4, 4.11 and 4.19).

1. The initial step is to evaluate the available test facilities in order to undertake an appropriate mechanical design of scaled prototypes (Section 4.3).

2. The next stage is to use this required information for the mechanical design of the test prototypes. This considers the expected loads and dimensional limitations imposed by the test facilities, leading to decisions on materials and rotor and bearing sizes. Subsequently, dimensions of structural elements and (where appropriate) buoyant sections can be calculated (Section 4.4).

3. The instrumentation required to obtain the fundamental characteristic parameters of tidal turbines (such as thrust, shaft torque and angular velocity, along with the inflow velocity) must now be specified. The structural loads on key components may need to be monitored. And for a tethered prototype, dynamic response is important and further sensing capabilities should be installed in the device (such as accelerometers - see Section 4.5).

4. Data obtained from the sensors is characterised by using signal processing techniques in order to measure the variation of key parameters in both time and frequency domains. Data sampling rates will be selected based on the capabilities of the primary sensors and in anticipation of resonant frequencies in the system (Section 4.6).

5. These signals could then later be related in vibration analyses via spectral parameters to the vibration modes of rotary machines, blade/structure interactions or other frequency-dependent effects (Section 4.7).

4.3 Facilities

The first parameter that must be established in the methodology is the selection of an appropriate test facility. This is of course largely dependent on the stage of development and the physical size of the device under investigation. There are difficult choices to be made with all test programmes, particularly at model scale, and these are discussed at some length in EquiMar (McCombes et al., 2010). Further work in documenting and comparing test facilities is proceeding under the European Commission MaRINEt programme MARINET (2012).

For aero/hydro dynamic component testing, wind tunnels should not be ignored as a relatively cheap and accessible option. The use of air as the working fluid will of course affect the

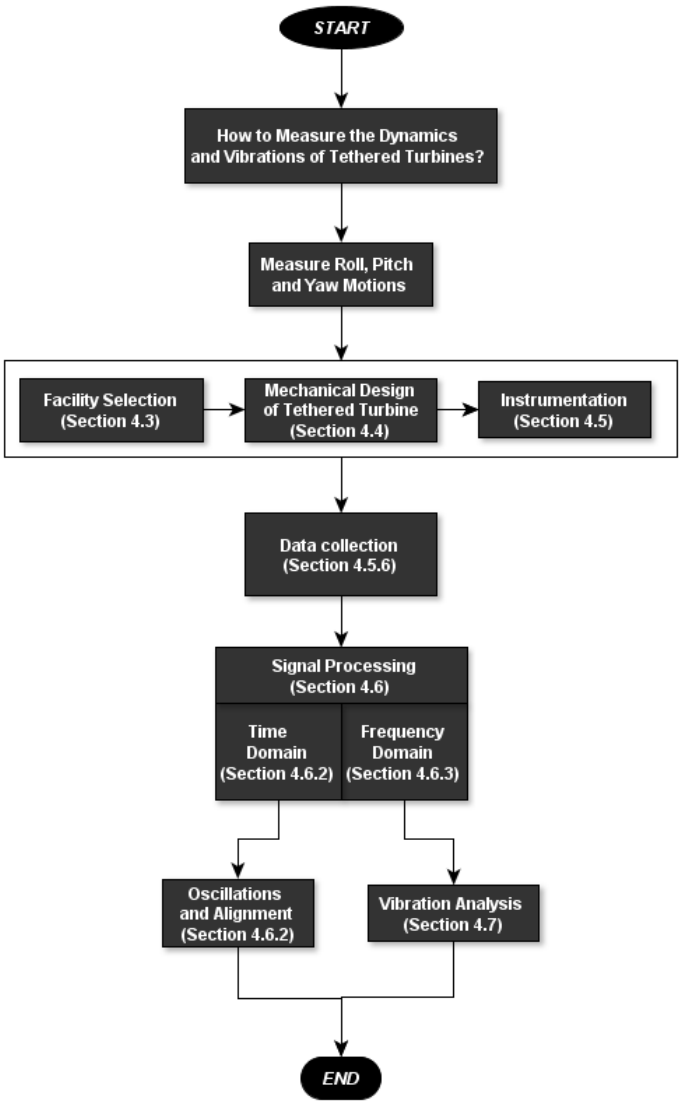

Figure 4.2: Methodology Pipeline.

(a) (b)

Figure 4.3: Examples of tank tests facilities: a) Flume Tank and b) Tow tank.

Reynolds number, but with any test other than at full scale Reynolds scaling will need to be taken into consideration anyway (see Section 4.4.3). If the experimental work is focused on small scale tests, tow/flow or flume tank (Figure 4.3) facilities can be employed to explore the performance of a tethered tidal turbine. If wave environments must be considered, the facilities should include a wave making facility capable of generating regular and preferably irregular wave profiles.

At larger scales there are a small number of flumes and towing tanks available, but the size of model that can be accommodated remains limited and it may be preferable to go to a scaled outdoor test site. External sites suitable for model testing are starting to appear, to complement full-scale test facilities such as EMEC. In all cases, the inflow conditions must be carefully quantified with the use of ADCPs or Acoustic Doppler Velocimeters (ADVs), throughout the test programme.

Therefore, the mechanical design of the test prototypes is based on the dimensions and capabilities of the test facilities. The forthcoming sections describe the component selection and the mechanical design.

4.4 Mechanical Design

The flow diagram of the mechanical design process is depicted in Figure 4.4.

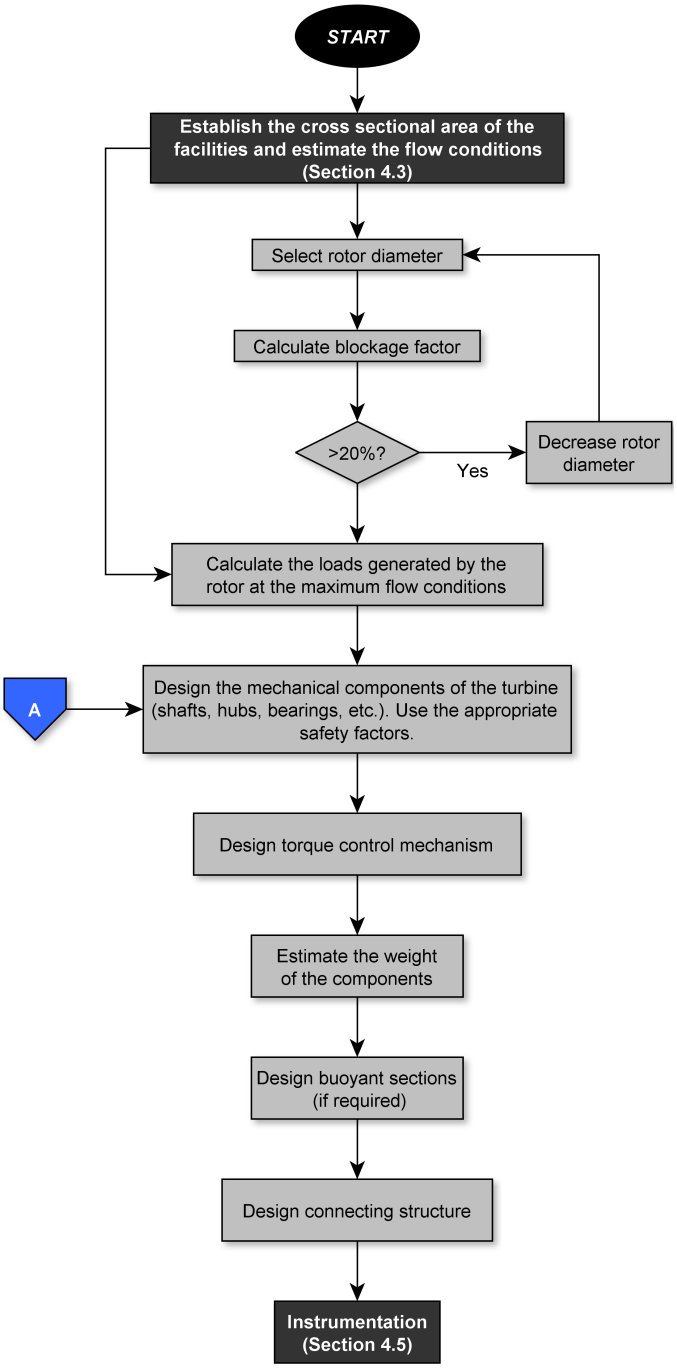

Figure 4.4: Flow Diagram of the Mechanical Design

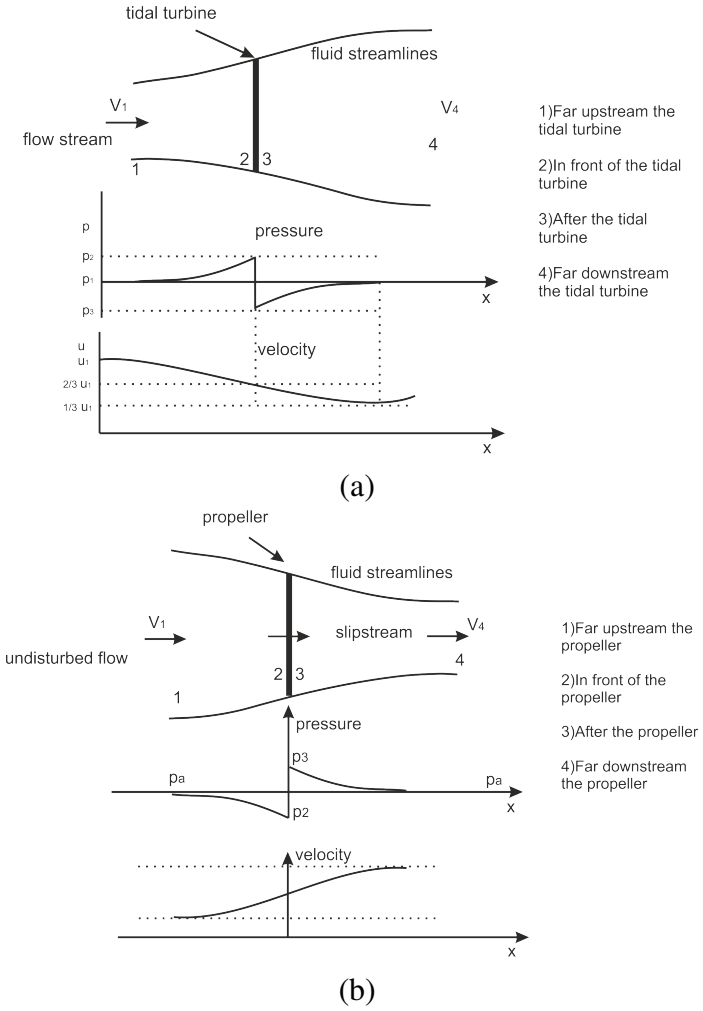

Figure 4.5: Representation of fluid streamlines, pressure and velocities of: a) Tidal turbines and b) Propellers.

4.4.1 Rotor Selection

Propellers and rotors are utilised in various rotordynamic machines; although they share similarities, functionalities and the effects on the slipstream region, velocity and pressure gradients within the working fluid are propagated differently (Figure 4.5).

For initial testing at small scale for proof of concept it may be attractive and more cost effective to use propellers as the prime movers in experimental tests, given the availability of a wide range of standard propellers in model shops at a reasonable price. Since both rotor and propeller systems follow the same theoretical operational basis where the thrust and power output is driven by lift and drag vectors created by a blade profile, the use of propellers might suffice to confirm the initial viability of a suggested prototype. However, when a propeller is transposed to work as a rotor, the trailing edge works as a leading edge (Figure 4.6). Therefore the performance of the resulting turbine is compromised by the deficiencies in the blade

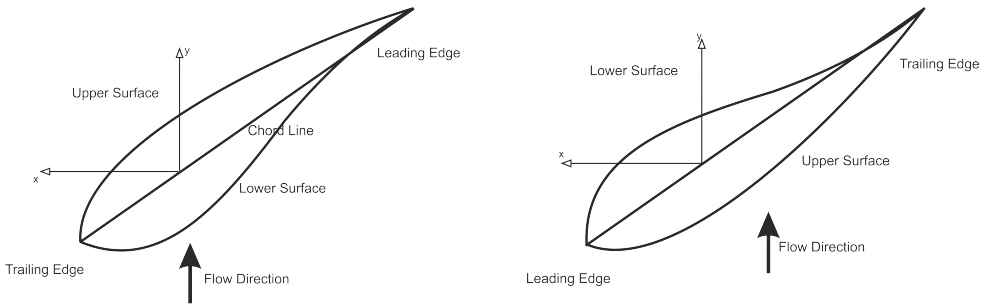

Figure 4.6: Inverted properties of the propellers when used as rotors: a) rotor and b)propeller.

profile. If a contra-rotating turbine is under investigation, pusher propellers can be obtained to represent one of the rotors.

A crucial factor to be considered in the selection of rotor diameter is the blockage ratio. This parameter relates the swept area of the rotor to the cross sectional area of the corresponding channel of the test facility being used. High blockage can affect the accuracy of test results, as first recognised many years ago in wind tunnel work. Empirical correction factors have been derived for moderate blockage factors, and these work fairly well. The matter is discussed in detail in the recent EquiMar protocols: Stallard (2011) quantifies the effect of blockage on turbine C_p , which can exceed values of 1 when the blockage ratio is greater than 20%. This will primarily limit the scope of indoor laboratory facilities, but proximity to the seabed or the free surface may also cause problems in sea trials (Section 2.1.3).

4.4.2 Airfoil Selection

For most cases progressing beyond the proof of concept stage, it is possible to choose the aerofoil shape of the rotor. For tidal turbines the blade profile, chord and twist distributions can be based on current designs used in wind turbines, since the fundamental fluid dynamic behaviour is identical. The first wind turbine designs contemplated the use of similar aerofoils to those used on aircraft wings. With the time it was identified that improvements must be made, due to performance losses caused by roughness and stalling issues (Hau, 2006). As designs for wind turbines evolved, a combination of blade profile, twist and chord distribution was found to maximise the energy yield, as illustrated in Figure 4.7.

In general one would expect the rotor geometry for any marine turbine to be checked and refined by Blade Element theory, as practiced by established wind (and now increasingly, marine) turbine designers. This process enables accurate prediction of performance and gives an insight into the effectiveness of control methods, by stall and/or pitch regulation (Appendix C).

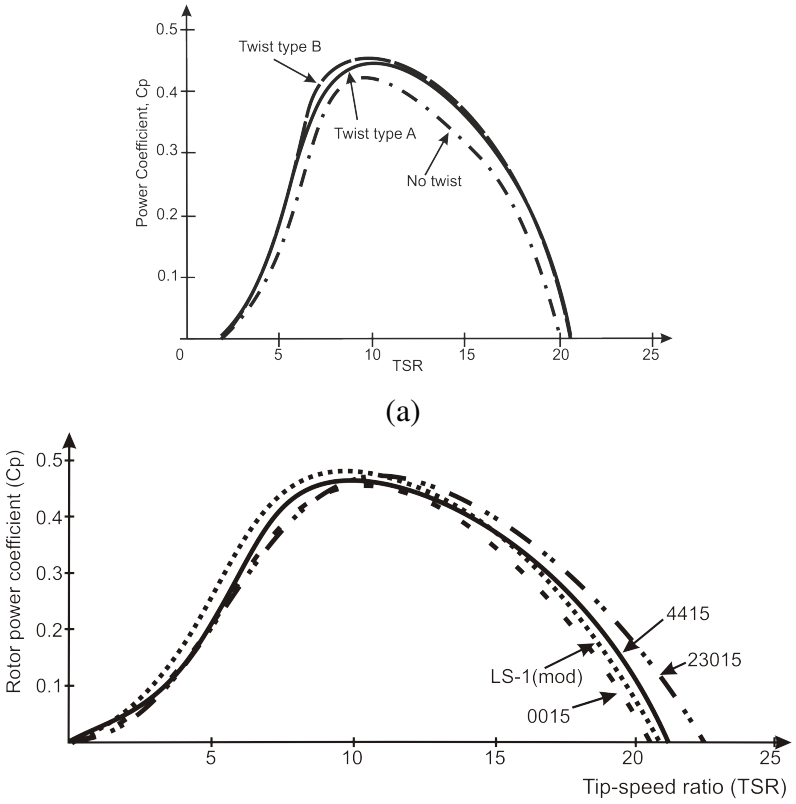

Figure 4.7: Power Coefficient for Wind Turbines Related to: a) Twist Distribution and b) Airfoil Type. Taken from Hau (2006)

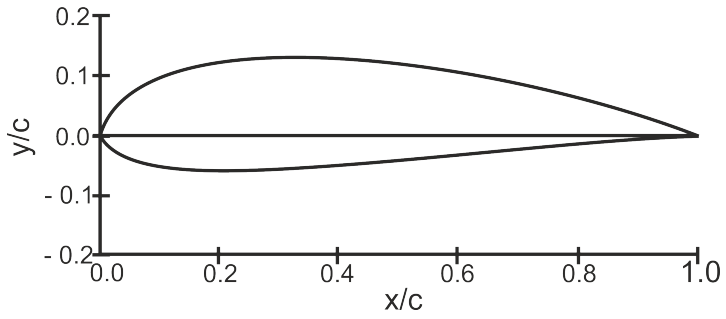

Figure 4.8: NACA 44xx.

The most common blade types utilised in the wind industry are the NACA 44xx (Henriques et al., 2009) and NACA 63xxx (Hochart et al., 2008). series. In the USA the National Renewable Laboratory (NREL) has also developed a series of aerofoils for wind turbines. The characteristic shape is substantially different as depicted in Figures 4.8 and 4.9.

Developers of tidal energy converters have followed a similar path. Currently there is not much evidence to compare each blade profile on TECs. Molland et al. (2004) studied the performance characteristics in a cavitation tunnel of four different airfoils used in TECs. Profiles included were the NACA 4415, NACA 6615, NACA 63-215 and NACA 63-815. The results were then compared to information available from XFoil analysis and existing wind tunnel experimental data. The results showed that the lift coefficients did not change substantially from the experimental wind tunnel tests but there was a slight reduction in drag coefficient as the relative velocity was increased. This is perhaps consistent with expectations at an increased Reynolds number.

On the other hand, Clarke et al. (2005) used the NREL S814 in their contra rotating marine turbine (CoRMaT). The initial investigations included the analysis of power and thrust curves. Tangler and Somers (1995) stated that one of the main advantages of the NREL S814 is its insensitivity to roughness enabling the aerofoil to maintain a high lift coefficient with a low drag coefficient (Somers, 1997). Finally, the S814 design employs a thick root section in order to withstand high axial loads and bending moments (Somers and Tangler, 1995). Such an attribute is found to be beneficial in TEC designs, because of the high density of the working fluid the loading regime is very different from that on wind turbines. It is apparent that blades for TECs tend to have greater chord length and thickness than their wind turbine equivalents, an extreme case being the Tocardo turbine (Tocardo, 2012).

Integrity of the rotor blades is likely to be a major design issue for TECs at all scales. A stress analysis should also be carried out before any experiment is undertaken in order to study the feasibility of the material and blade section working under the corresponding conditions.

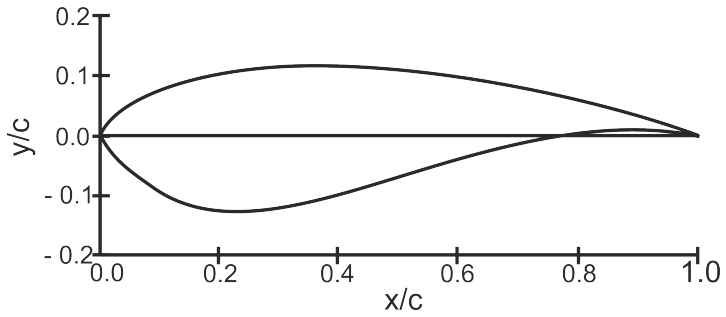

Figure 4.9: NREL S814.

4.4.3 Scale Parameters

The two dimensionless parameters most relevant to the testing of TECs are the Froude number (Fr) and the Reynolds number (Re), defined by the expressions:

$$Re = \frac{c(r)V_{rel}}{v} \tag{4.1}$$

$$Fr = \frac{V_{flow}}{\sqrt{gL}} \tag{4.2}$$

where c corresponds to local chord at the radial position r. v is related to the kinematic viscosity of the fluid and V_{rel} is the relative velocity in the blade section. g corresponds to the acceleration due to gravity and L is related to the water depth. Fr relates to the behaviour of the free surface and Re concerns the flow of fluid around a submerged body. For complete dynamic similarity, any model tests should be carried out at identical values of Fr and Re, referred to the full-size prototype. However, similarity of ambient flow field states such as turbulence intensity should also be considered during the tests.

Since Fr is related to water surface elevation, this scaling parameter must be used if wave motions are included in the experimental programme. While Fr scaling is relatively easy to achieve, Re scaling is not and complete dynamic similarity is practically impossible, as has long been recognised in model testing of ship hulls by naval architects. For TECs the situation is perhaps not so difficult: many are fully immersed well below the free surface and Froude effects are negligible. But with tethered devices, they may be quite significant. Some designs incorporate buoyant elements close to or even on the free surface and the turbines themselves may be influenced by wave motion. So the relevant scaling parameters are ultimately determined by the physical design of the TEC in question.

Whatever the configuration, Reynolds number is a key parameter in determining the perform-

ance of the turbine rotor. Tests on small models will almost inevitably be conducted at values of Re which are too low for dynamic similarity with full scale. The likely effect on aerofoil sections are well documented (Molland et al., 2004), consisting of a small reduction in peak lift coefficients and a significant increase in drag. For a turbine rotor, this results in a reduction in power coefficient throughout the range of operation, meaning that performance predictions from model tests will be somewhat conservative. Fortunately the overall effects of reducing the Reynolds number are moderate and progressive in nature.

Reynolds number effects may also be observed in the flow over static components of a TEC system, particularly where curved or rounded surfaces are present. For a tethered TEC, inequality of drag coefficients between model and full scale may affect predictions of flow-induced forces on structural elements.

Turbulence is not governed by any dimensionless number. However, the ratio of the turbulent eddies relative to the size of the prototype could be compared to the full size characteristics. Since this is an extremely difficult process, turbulence intensities between laboratory and real case scenarios should be compared. In this case, it has been found that flume tanks are capable of generating turbulence intensities similar to tidal test sites. For example, Rose et al. (2010) reported a turbulence intensity of 7% in a flume tank; meanwhile, Gooch et al. (2009) measured an average value of 10% at the *Puget Sound* in *Washington*, as discussed in Section 2.1.3.

A further relevant parameter is the cavitation number,

$$\sigma = \frac{P_L - P_0}{0.5\rho V_{flow}} \tag{4.3}$$

where P_L corresponds to local pressure, P_0 is related to the reference static pressure, V_{flow} is the flow velocity and ρ corresponds to the density of the fluid. This principally concerns the performance of the turbine rotor, where low local static pressures may produce cavitation bubbles on blade surfaces. Where rotors are in close proximity to the free surface cavitation may be a problem and should be investigated. Scaled models can be tested in cavitation tunnels in representative conditions, making appropriate allowance for blockage effects in the confined working section.

4.4.4 Rotor Hubs, Shafts and Bearings

Before commencing the design of these components, it is necessary to establish the forces applied in the system under the most severe operational conditions. Typically, the forces

acting on a tidal turbine rotor are axial (the blades of course are subjected to both axial and tangential forces). Thus, the rotor bearings must be chosen primarily to support this thrust load. However, velocity shear gradients or misalignment of the rotor may give rise to bending moments, which must also be taken into account. Time-averaged values for these loads can be produced from Blade Element theory or simple static analysis. A major advantage of tethered turbines over many pile or gravity-based devices is that the main thrust load does not reverse. Some load reversal may take place near times of slack water, but the forces will be very small. Safety factors should be included in the mechanical design and they should be chosen based on established standards such as the IEC 61400-2 (Sinclair and Bowen, 2008).

Miniature plastic bearings might be considered in order to avoid corrosion issues at least during small scale testing; however, they are not capable of withstanding high axial forces, so conventional stainless steel bearings would be the normal choice, specified to handle the (substantial) thrust load. For larger scale turbine, composite bearings can be used due to their ability to withstand large forces using two surfaces lubricated with a viscous film (SKF Group, 2012). The rotor hubs and shafts can then be designed accordingly. The process is the same as in the design of other large rotating machines, and specialised mechanical design procedures are well established (e.g. Budynas and Nisbett (2011)).

4.4.5 Mechanical Control

It is assumed that a tethered device should be able to weathervane to the flow satisfactorily; thus, mechanical control of device pitch or yaw should not be necessary. However, there may be issues with the power transmission cable from the device, which must necessarily follow one of the mooring lines and must be prevented from twisting as the device moves in response to the reversals of tidal flow. Special measures may need to be taken to address this potential problem. At small scales with short-term tests in a laboratory there should be no difficulty as any power cable will be light and flexible.

Torque control should be incorporated in the design even at small scales, since the power capture will depend on the load applied to the turbine. This will allow the turbine to be operated over a range of tip speed ratios and hence power coefficients. If the turbine has multiple rotors, it may be necessary to equalise their torques in order to ensure a stable dynamic response of the complete system.

Typically a small electromagnetic dynamometer may be incorporated within the rotor; however, for small scale devices, it might be difficult to employ an electromechanical power take-off given the limited dimensions. Other options might be contemplated such as a mechanical

system using springs and a friction disc. This would require careful design to enable a sufficiently sensitive adjustment.

For larger scale devices with an electrical power take-off system, various control options are available and the situation is relatively straightforward.

4.4.6 Buoyancy

All tethered tidal turbines will require buoyancy in the system, to maintain the rotor at the required level above the sea bed. The buoyant elements may be fully submerged or surface piercing, and could use dynamic effects in addition to displacement to produce the required upward forces. They must be designed to avoid possible power loss due to misalignment with the flow; that is, the trim of the device must be controlled. Model testing of such TECs might progress through a number of stages: initially perhaps the rotors might be supported by a rigid structure, which is then progressively replaced by more flexible elements until the full tethered system is reproduced.

In some designs the device is fully submerged and the turbine system is neutrally buoyant. A substantial buoyancy chamber must then be integrated to the turbine itself, the shaping of which is critical to ensure low drag and provide stability. The design of such buoyant elements is a major part of the overall process, and further development is needed.

4.4.7 Rigid Structure

For a tethered TEC, the function of the rigid structure is simply to connect the rotor system with the buoyancy chambers, and to provide an attachment to the mooring. Where the structure is surface-piercing a large structure might be desirable to mitigate disturbances from surface waves, but for a fully submerged device compactness and light weight are desirable: the latter to minimise the requirements for buoyancy around the rotor assembly and reduce the momentum on the mooring system. Clearly the design of the structural components will be determined by the configuration of the device itself. Loads borne by the rigid structure will of course comprise the thrust load produced by the fluid stream, with added unsteady forces from turbulence and (perhaps) wave action. These must be determined from a combination of model testing and structural analysis, with appropriate factors of safety included.

The device configuration for a model at very small scale may differ significantly from a full-scale prototype. An example illustrated below shows a small contra-rotating turbine model

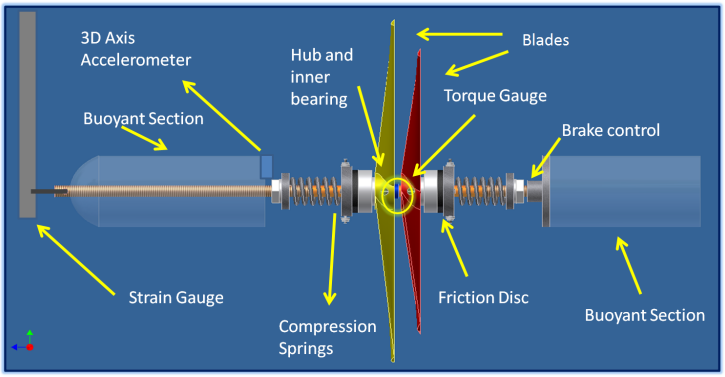

Figure 4.10: Example of a small scaled prototype.

with mechanical power take-off and flotation chambers front and rear to give neutral buoyancy. The bulky and poorly streamlined appearance is largely dictated by experimental requirements and the effects of scale: the space consumed by instrumentation is comparatively large, as is the volume required for buoyancy.

4.5 Instrumentation and Data Collection

The purpose of instrumentation is to provide the necessary data for evaluation of the TEC, in terms of its performance in the most general sense of the word. This covers the efficiency of energy conversion, dynamic response and station-keeping, and structural integrity under the most severe operational conditions. Thus for a tethered TEC, prototypes should be equipped with sensors to measure their dynamic response (Section 4.5.1), thrust and shaft torque magnitudes (Section 4.5.2). The angular speed of the rotors must also be measured (Section 4.5.3), along with the flow velocity of the chosen test facility (Section 4.5.3). If the turbine is equipped with an electrical power take off mechanism, electrical current and voltage measurements should be included (Section 4.5.3). Data loggers should be selected to record the data at the appropriate frequencies. A flow diagram that describes the process can be seen in Figure 4.11.

4.5.1 Dynamic Response and Vibration

For a tethered turbine, stability is a primary concern. It requires to be studied in a number of contexts: the behaviour of the system under nominally steady flow, where natural frequencies of oscillation may be detected; in turbulent flow typical of natural tidal streams, where misalignments should be self-correcting; and at slack water, where the turbine must swing round

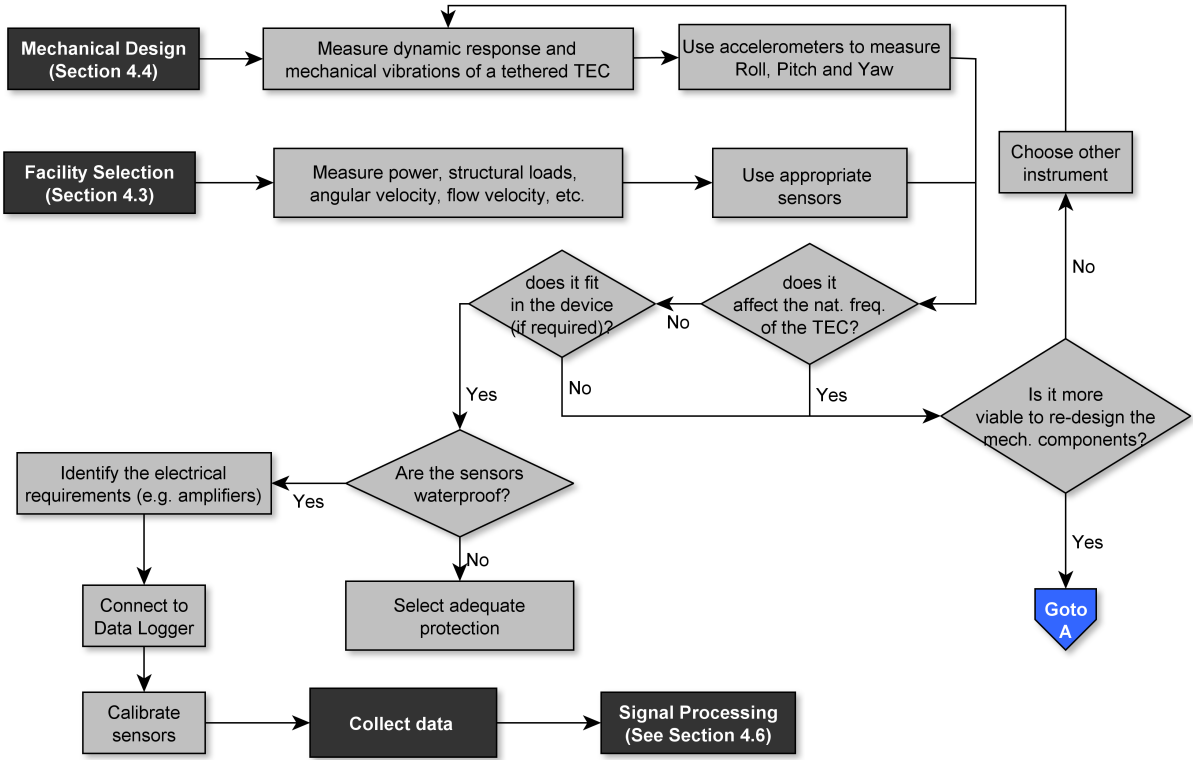

Figure 4.11: Flow diagram of the Instrumentation Module. Refer to "Goto A" in Figure 4.4.

in a controlled manner to re-align itself with the reversing flow. These requirements can be met by measuring the three rotational angles (roll, pitch and yaw) as shown in Figure 4.12.

In order to measure inclination, electronic accelerometers or inclinometers might be used. The former measures the tilt angles of the instrument with respect to gravitational force (Figure 4.13). The operating principle is that of a piezoelectric system and electrical responses are obtained according to inertial changes and the data can utilised as degrees (°) or analogue values to measure shock and vibration. 3D axis accelerometers are not be influenced by linear motions since they are calibrated as global coordinate systems. Moreover, the sensors are compact and can be incorporated into small test models.

Inclinometers can also be implemented to measure rotational angles. For example, 3D axis gyroscopes could be used as indicators of roll, pitch and yaw presented as $^{\circ}/_{s}$. Similarly to accelerometers, the output data can be used to measure vibrations and they can also be found in compact versions. Frequency response of both systems is more than adequate to cover the oscillations anticipated in this application.

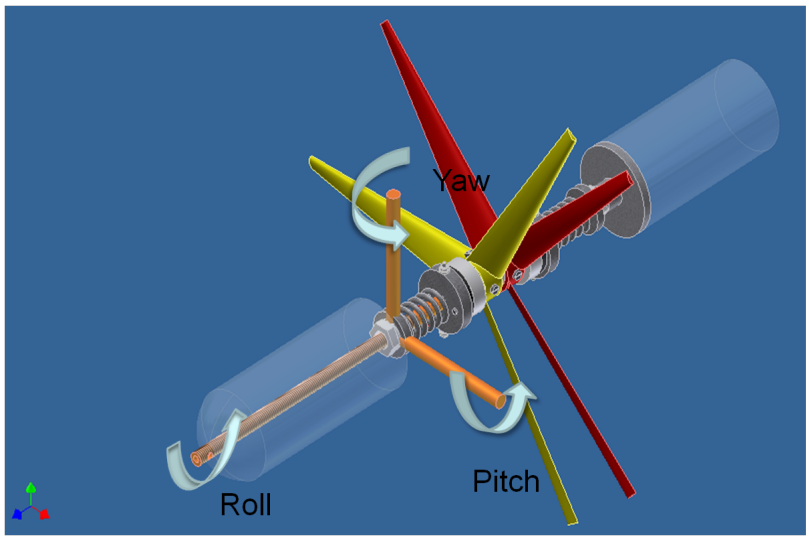

Figure 4.12: Roll, Pitch and Yaw Motions.

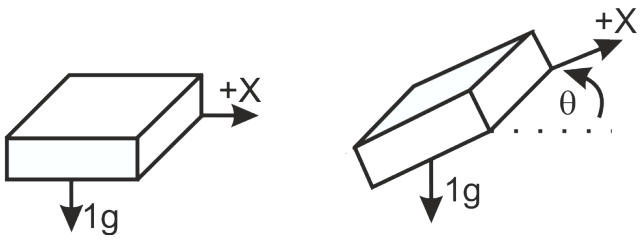

Figure 4.13: Inclinometer Motions.

4.5.2 Structural Loads

The primary loads on a tethered TEC originate from the drag force due to the tidal stream, and the upthrust generated by buoyancy. These must be borne by the mooring system and (in part at least) by other structural elements within the device. Forces on rotor blades are very large for tidal turbines, and for tethered systems may be exacerbated by misalignment and instability. It is therefore desirable to monitor these forces, using either slip rings or telemetry to extract signals from the blades as they rotate. On a small test model, the physical space available may make this difficult or even impossible.

Load measurement is usually carried out using strain gauges or purpose-built load cells incorporating resistors or piezo-electric elements. Strain gauges are compact, robust and provide a linear response over a wide range of frequencies. They operate by measuring changes in the electrical resistance of a small element, so can be disturbed by temperature fluctuations. In marine applications the presence of large volumes of water tends to ensure stability, but of course presents its own problems in terms of sealing. The size of the strain gauge has to be considered during the design stages; very small gauges are available for specialised applications but should be avoided if possible as they are flimsy and can suffer from instability and fatigue.

The last two parameters to be considered are gauge pattern and resistance. Strain gauges can be used as single gauges or rosettes. Rosette configurations are essentially arrangements of two or four strain gauges, the use of a single gauge is usually contemplated only if there is limited space in the specimen. Multiple strain gauge configurations can be installed as $90\,^{\circ}$, $45\,^{\circ}$, $60\,^{\circ}$ or stacked rosettes. The main difference lies in the number of resistors connected to the circuit. The resistance of gauges ranges between $120\,\Omega$ and $1000\,\Omega$, with higher resistance giving greater accuracy in measurement; however, the use of $120\,\Omega$ resistors suffices for most applications. Ideally a full Wheatstone bridge configuration should be used at the location where strain is to be measured; where space is limited, half or even quarter bridges are installed on site, with 'dummy' gauges located elsewhere to make up the remainder of the bridge. Temperature effects may then influence the accuracy of the data produced.

If a mechanical power take-off is employed, the shaft torque can be measured in a number of ways. Specially designed torque gauges may be obtained for fitting to the rotor shaft, generally using strain gauge elements to produce an electrical signal. In small models, bearing friction will be an unduly dominant feature and needs to be minimised. Ideally any torque measuring system should be configured to include friction from rotating bearings.

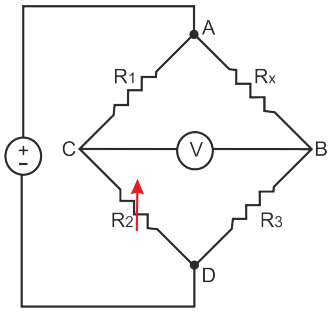

Figure 4.14: Wheatstone Bridge.

4.5.3 Angular Velocity, Flow Velocity and Power

These quantities concern the performance of the device and the computation of non-dimensional coefficients such as C_p and C_t. Angular velocity of the rotors can be measured with Hall effect or proximity sensors. These are widely used in industry, but their installation might be difficult in small models and water ingress is always a problem. Magnetic reed switches are an alternative and their installation may be less complicated.

The method used for measurement of the flow velocity of course depends on the nature of the test facility. In a towing tank the carriage speed will be controlled via the drive train, but an independent monitoring system might be advisable. In a flume tank question of velocity distribution and turbulence arise: conditions within the working section should be investigated prior to the test programme, using ADVs or other 'point' measuring devices. During tests, continuous monitoring of velocity at a single reference point may suffice. In sea trials, data from one or more ADCPs should be recorded throughout the test period.

Flow meters installed in the turbine itself are a possibility (they are common practice on wind turbines), but these will inevitably be affected by the device itself and could really only serve to signal changes in flow conditions. If the test site is affected by wave motions then the requisite data should be gathered during the test, using output from ADCPs or other methods (i.e. wave gauges or rider buoys).

Finally, instrumentation to record electrical power output (where appropriate) should be installed. This is normally a straightforward task, incorporating shunts and dump loads.

4.5.4 Installation and Electrical Connection

Before the selection of the instruments is finalised, it must be ascertained that they are sufficiently small and light that they do not affect natural frequencies or otherwise influence the

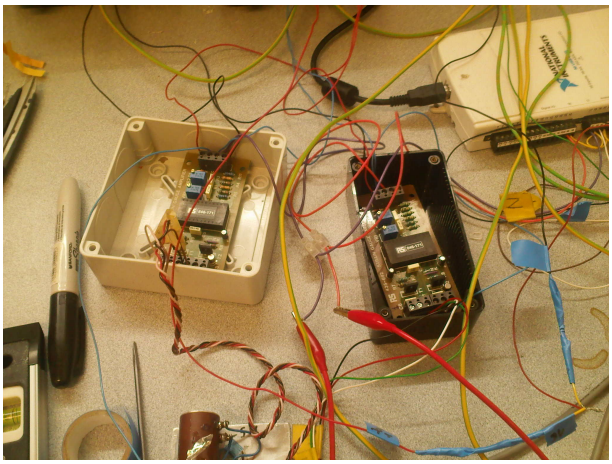

Figure 4.15: Amplifiers

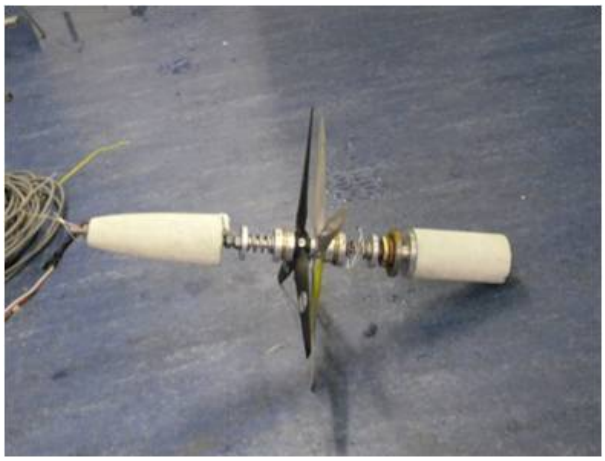

Figure 4.16: Final CRR tidal model.

dynamic response of the system. This is of course a particular consideration for small models. If the sensors are not waterproof, the necessary protection should be applied without modifying the operation of the sensor, and the system tested by submergence for a long period of time in order to confirm viability.

Instruments must be supplied by the correct input voltage and the output signals amplified where necessary (likely in the case of strain gauge systems, where outputs are usually only a few mV), before the data are transmitted to loggers. Figure 4.15 illustrates typical strain gauge amplifiers, which for small models can be situated remotely.

In such a situation, twisted shielded cables should be employed to minimise external electronic noise; these should be grounded to a common point. For a tethered TEC it is important that the data cables do not exert any force upon the test model: they should be led along the mooring line, to allow the device to move freely about the three main rotational axes. Figure 4.16 shows the described configuration applied to a small contra-rotating test model.

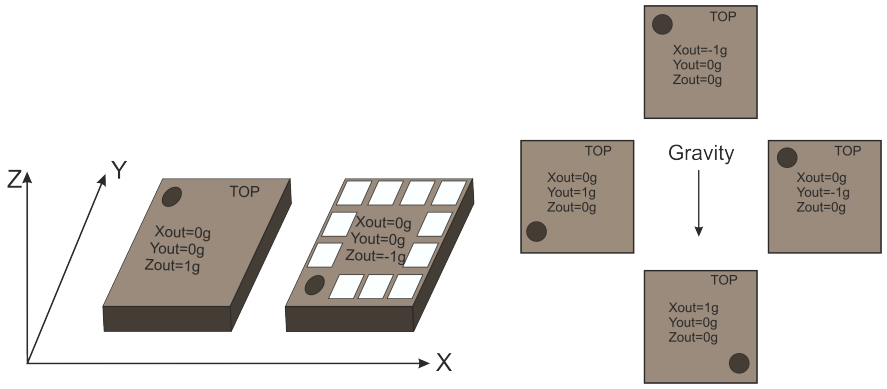

Figure 4.17: Inclinometer Calibration.

4.5.5 Calibration of sensors

In many cases, instruments are calibrated by the manufacturer. It is perhaps prudent to check these calibrations, particularly if operating conditions are near the extremes of the operating range. For bespoke systems of course calibration is essential. The process is not simply to relate electrical signals to physical effects, but to ensure that the responses are repeatable and do not drift with time to an unacceptable extent. As examples, calibration tests for three instruments used in forthcoming experiments are described in the following subsections.

4.5.5.1 Accelerometer/Inclinometer

The calibration of an accelerometer or inclinometer is challenging due to its small dimensions, it being difficult to position the mounting board with spirit levels. As illustrated in Figure 4.17, a rotation of the instrument is required to obtain the maximum and minimum values of each tilt position. In some cases, these represent the 0 g and 1 g positions (Analogue Devices, 2007), being $0\,g$ when zero gravity is affecting the corresponding axis and $1\,g$ when the axis is directly aligned with the vertical. The system is very sensitive to small disturbances and vibration, addressed by choosing a quiet location and repeating calibration procedures several times to ensure accuracy.

Once the calibration is carried out, the analogue voltage signals were related to roll pitch and yaw by means of the equations 4.4, 4.5 and 4.6 in order to obtain the corresponding measurement of the angular positions.

$$Roll = (\frac{180}{\pi})(\frac{Vx_{out} - Vx_{min}}{Vx_{max} - Vx_{min}}) \tag{4.4}$$

$$Pitch = (\frac{180}{\pi})(\frac{Vy_{out} - Vy_{min}}{Vy_{max} - Vy_{min}}) \tag{4.5}$$

$$Yaw = (\frac{180}{\pi})(\frac{Vz_{out} - Vz_{min}}{Vz_{max} - Vz_{min}}) \tag{4.6}$$

where $\mathrm{roll},\ \mathrm{pitch}$ and yaw are expressed in degrees; V_{out} indicates the output voltage obtained during the data acquisition; V_{max} and V_{min} are related to the maximum and minimum voltages obtained from the calibration. The uncertainty obtained from the calibration tests was 0.002% for each of the calibration procedures.

4.5.5.2 Torque and Thrust Gauges

The calibration of two strain gauge systems was carried out with test weights, checked by precise measurement before the calibration process started. The calibration curves obtained are depicted in Figures 4.18(a) and (b). The uncertainty of the measurement obtained was 0.004% on the thrust gauge and 0.04% on the torque gauge, again as the average of the standard error of three calibration procedures. It will be seen that the response from both was linear, as expected. Calibration procedures was also done before and after in order to find drift values. It was found a drift of 0.04% and 1% for the strain and torque gauge, respectively. General information related to the calibration and uncertainty analysis of instruments can be found in the EquiMar protocols (McCombes et al., 2010).

4.5.6 Data Logger and Sampling Rate

One of the most important rules of signal processing techniques is the "Nyquist-Shannon Sampling Theorem", stating that the sampling rate of the acquired data must be at least twice the expected peak frequencies (Chitode, 2009). For tests on tethered turbines, it is expected that the signal will be mainly related to the rotational speeds of the turbine and blade passing frequencies (see Section 4.7). Compared to rotating machines in general, this might be regarded as the low frequency part of the spectrum (Section 4.6), the sampling rates in the region of 30 to $500\,\mathrm{Hz}$ should be adequate. This is well within the capabilities of modern data loggers. As always, there will be some compromise between logging frequencies, storage capacity and file sizes.

The determination of the sample size and duration of tests should refer to established protocols and standards, in this case these parameters should be referred to EquiMar protocols

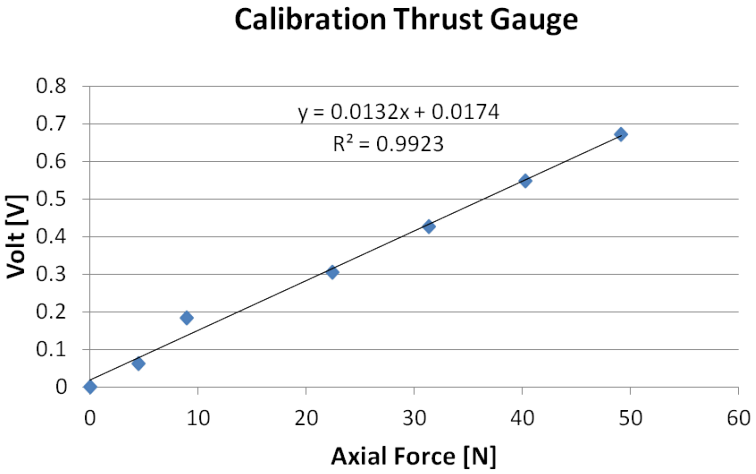

(a)

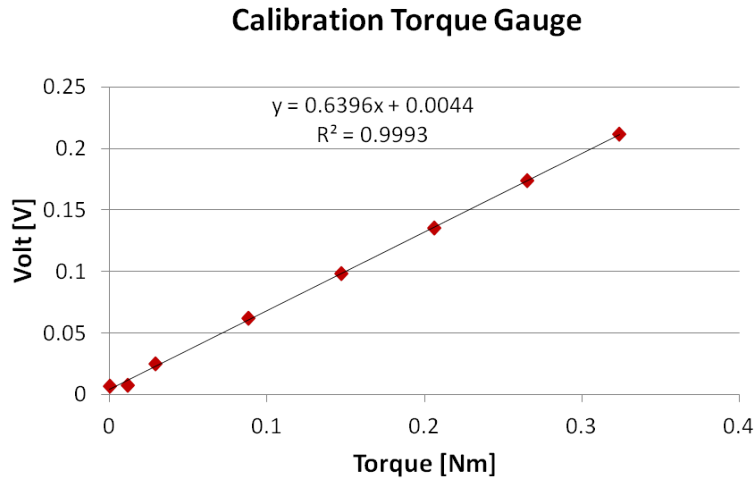

(b)

Figure 4.18: Calibration Curves: a) Strain Gauge and b)Torque Gauge.

(EquiMar, 2012).For example, McCombes et al. (2010) establish that the sample size should follow the following relationship:

$$n = \left(s/U_c\right)^2 \tag{4.7}$$

where n is the number of samples, s is the sample standard deviation and U_c is the interval in which there is a confidence interval of 95%. This means that the variability of the data should not be greater than 5%.

This is easily achievable in circulating flume tanks where the data can be analysed with auto-regression techniques. This means that a running mean (k) can be instantly compared to the k-1 test. In the case of single tests, such as the ones undertaken in tow tanks, care should be taken. Even if the sampling frequency is large enough to generate a mean is greater than 1, this is considered as a single experiment (McCombes et al., 2010) . Therefore, data can be collected and compared between the number of sets until the threshold has been satisfied.

If periodicity of the signal is being monitored, three analysis can be undertaken. First, the average of the cycles can be determined. Secondly, spectral moments should be considered from zero to order 2 with a 5% convergence. The thirds analysis is similar to the former analysis, but in this case window functions should be applied before spectral moments are calculated (McCombes et al., 2010).

4.6 Signal Processing

After the mechanical design and the instrumentation are defined, the next section describes the methodology to process the data obtained from the instrumentation. The analysis is divided into time and frequency domain techniques; where simple statistical methods are employed to quantify the variations in the time domain and Fourier Transform techniques are utilised to study the vibration effects in the machines. The flow diagram that describes the process is shown in Figure 4.19.

4.6.1 Filters

Filtering techniques are usually applied before the statistical measurements are calculated. The reason is to remove any noise that could influence the signal output; for example, the noise generated by electromechanical appliances and/or a large sampling acquisition rate are

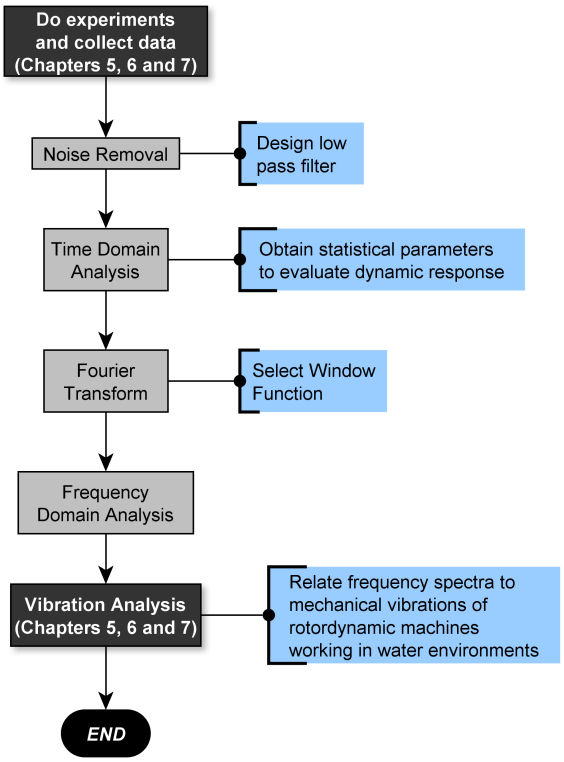

Figure 4.19: Flow Diagram of the Signal Processing Tools

potential sources of signal contamination (Schilling and Harris, 2005). Therefore, signals are frequently filtered at one or various stages during the signal-processing strategy. Filters can be implemented in analogue or digital forms. Analogue filters employ resistors and capacitors between the input signal and the acquisition system; however, these filters are usually sensitive to environmental conditions (i.e. temperature). As digital filters are implemented throughout mathematical operations they are highly flexible and are neglected by external noise effects (Chitode, 2009). Therefore, digital filters were employed to process the output sensor signals in this thesis.

There are two types of digital filters available: the infinite impulse response (IIR) and the finite impulse response (FIR) (Schilling and Harris, 2005). The main difference is that the FIR filter is a non-recursive filter (i.e. systems with an open loop)). Whereas, the IIR filter is a recursive filter (Harris, 2003) (i.e. the system works as a close loop). The main advantage of an IIR filter is that it utilises less mathematical operations, delivers a higher quality processed signal and has high flexibility; however, due to the unstable nature of IIR filters, high-level processing techniques must be employed in its design (Schilling and Harris, 2005). Therefore, stable and less-complex FIR filters are chosen in the filter design procedure in this thesis.

The signal-processing '*filter design and analysis tool*' (SPTool) available in Matlab 2009/2010, was used to design the required filters. The designed filter involves low pass filters with a variety of cut off specifications (i.e. according to the sampling rate). A Hamming Window

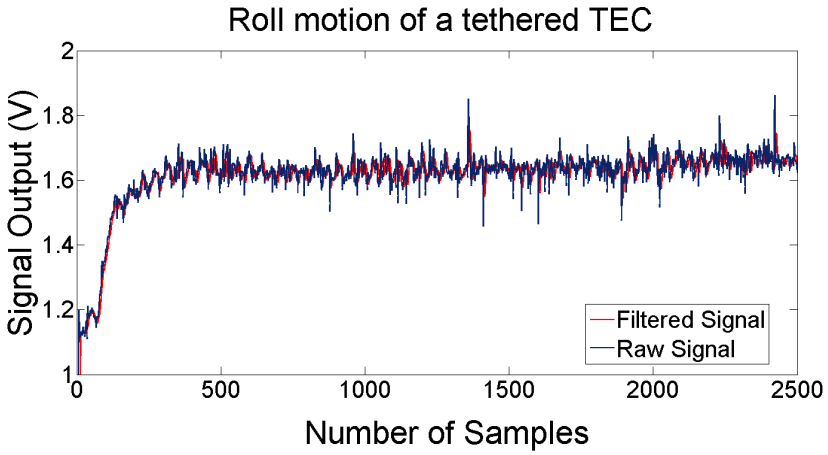

Figure 4.20: Filtered Signal.

was selected for the designed filter. After such parameters are determined, the coefficients obtained from the SPTool can be described by equation 4.8.

$$Y(s) = \frac{b(1) + b(2)s^{-1} + ... + b(n+1)s^{-n}}{a(1) + a(2)s^{-1} + ... + a(m+1)s^{-m}} \tag{4.8}$$

where $Y(s)$ corresponds to the output signal of the transfer function, b and a represent the numerator and denominator coefficients, respectively. And n and m are power coefficients. In this case, only the numerator part of the function is employed while the denominator is set to 1 due to the intrinsic nature of FIR filters (Kehtarnavaz and Kim, 2005). An example of a signal with and without noise effects is presented in Figure 4.20.

4.6.2 Time Domain Analysis

The data obtained from the transducers depends on the amplitude of the fluctuating signal throughout a certain time length. This data can be classified into several types: *stationary, non-stationary, deterministic, random* and *mixed data* (Piersol and Paez, 2002). The main differences between the *stationary* and *non stationary* data are that they do or do not oscillate with time, respectively. If such a signal follows a periodic sequence, the evaluated data can be considered as *deterministic.* However, *random* signals do not adopt sinusoidal patterns and their analysis is more difficult. If a variation of several types of signal applies to the data form, then this can be classified as *mixed* data.

It is assumed that stationary data is expected in the repeatable environment of the laboratory; however, due to possible imbalance in the turbine prototypes and other unknown dynamic responses, mixed data can also become visible in the results. For example, the angular velocity

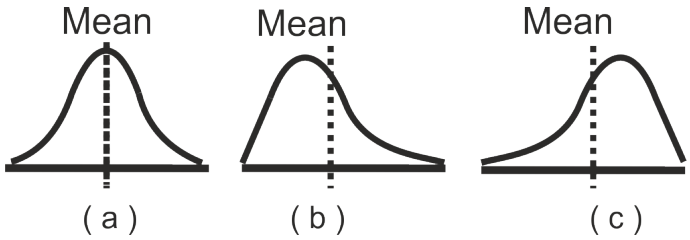

Figure 4.21: Skewness: a)symmetric, b) positive skewness and c) negative skewness.

of the rotors can be considered stationary and deterministic since the rotational speed of a rotor should remain invariant during short operational periods; but a non-stationary and random behaviour might be present in the presence of roll and pitch motions, due to oscillations of the device. This particular response might be intensified if the device is deployed in highly turbulent flows with additional influence from wave interactions. The following mathematical functions describe the performance of the device in order to evaluate its oscillations in a time domain basis:

$$\mu = \frac{1}{N}\sum_{i=0}^{N-1} x_i \tag{4.9}$$

$$\sigma^2 = \frac{1}{N-1}\sum_{i=0}^{N-1} (x_i - \mu)^2 \tag{4.10}$$

where μ and σ represent the mean and standard deviation respectively, N is the number of data items sampled and, x_i corresponds to each of the data values $(i = 1, 2, ..., N)$.

Skewness and kurtosis measures can also be used to characterise the dynamic response of the turbine in the time domain. Skewness is the degree of symmetry or asymmetry of a distribution. According to its the length of the tail, the distribution is called skewed to the right (positive skewness) or skewed to the left (negative skewness) (Figure 4.21). Moreover, the measure of kurtosis can be used to define the peakedness of a distribution (e.g. Figure 4.22). Formulation and tolerances of both measures should be applied as indicated by McCombes et al. (2010), in this case skewness values should fall around 0; meanwhile, kurtosis should fall around 3 with a 5% of error. In order to establish if the dynamic responses are acceptable, combinations of yaw and pitch deviations should not be greater than 7.5° as reported by Galloway et al. (2011). Roll motions can be argued to be adequate if the system achieves a stability point without exceeding 360° (a complete revolution).

Other statistical tools can be applied to asses quality of the data. McCombes et al. (2010) stablish that standard methods such as the Student's t-Test or the Chauvenet's criteria can be

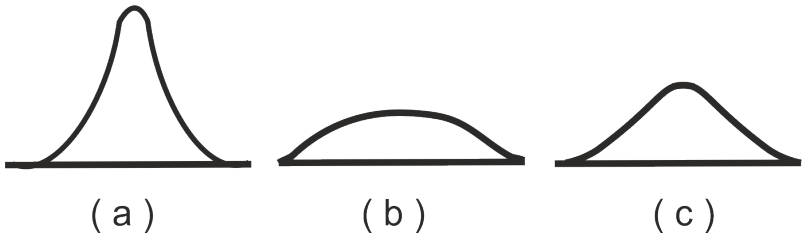

Figure 4.22: Types of Kurtosis: a) leptokurtic, b) platykurtic and c) mesokurtic. Based on Spiegel and Stephens (1999).

used to identify if the data falls within expected range of values. However, according to the facility selected, it is possible that the tests must be carried several times (i.e. depending on the tow tank length, tow velocity used, sampling frequency, etc.); therefore, the variability of the results between experiments should also be estimated. In this case, one-way analysis of variance tests should be applied. As rule of thumb, if the probability is less than 0.05, the tests are statistically significant.

4.6.3 Frequency domain analysis

The characteristic parameters of a signal can be obtained through a frequency domain analysis. In contrast to a time domain signal, when a spectral analysis is undertaken, the energy of the data is dissipated in bandwidths. Distinctive frequencies are identified in the spectrum which can be correlated to the particular behaviour of any linear or rotary machine (Piersol and Paez, 2002).

The frequency domain representation of the data can be evaluated by means of the Discrete Fourier Transform (DFT). The DFT is a transformation of discrete time functions on a finite domain. Fast Fourier Transform (FFT) algorithms are usually implemented to calculate DFTs. FFT algorithms are usually presented as functions in common high-level programming suites (e.g. MATLAB or Mathematica). There are three possible formulations to compute the FFT transformation, summarised in the following equations(Heinzel et al., 2002):

$$y_m^{(1)} = \sum x_k exp(-2\pi i \frac{mk}{N}) \tag{4.11}$$

$$y_m^{(2)} = \frac{1}{\sqrt{N}} y_m^{(1)} \tag{4.12}$$

$$y_m^{(3)} = \frac{1}{N} y_m^{(1)} \tag{4.13}$$

where y_m denotes the transformed complex numbers when the FFT is undertaken, x_k symbolises the original numbers in time domain , and N is the total number of items of sampled data. The formulation used in programming packages usually computes the FFT using eq. 4.11; however, its application should not be assumed as straightforward. The main postulation of the FFT algorithm is that the acquired data are correlated with a period of a sinusoidal function. Generally this assumption is invalid as the data are acquired for a limited period of time. Therefore, signal processing techniques are usually applied to compensate for the effects of the FFT assumptions.

According to (Heinzel et al., 2002), the output of an FFT analysis is commonly scaled in terms of Volts (V) or by the power spectral density ($\mathrm{V}/\sqrt{\mathrm{Hz}}$) which indicates how the power of a time series is distributed with frequency. In the case of the accelerometer mentioned in Section 4.5.5.1, the signal output given in volts also represents acceleration measurements (0 to 1g, being 1g the value of $9.81\,\mathrm{m/s^2}$). Therefore, the frequency spectrum can be scaled in terms of acceleration ($\mathrm{m/s^2}$) or in terms of velocity ($\mathrm{m/s}$) and displacement (m) by using the following expressions:

$$V = \frac{A}{2\pi f} \tag{4.14}$$

$$D = \frac{A}{(2\pi f)^2} \tag{4.15}$$

where A, V and D represent the amplitude of the frequency (f) in terms of acceleration, velocity and displacement , as stated by Piersol and Paez (2002).

4.6.4 Windowing

The implementation of window functions is commonly adopted with the computation of the FFT. There is a wide range of window functions that are employed in signal processing; for example, the rectangular, hamming and hanning windows. Each of them are described by different functions and they can be primarily differentiated by their capability of smoothing discontinuities of the signal, the narrowness of the bandwidth and the side lobs (smaller peaks beside the main peak - these are usually design to be as small as possible), thus, the peak frequencies can be identified with more precision (Figure 4.23).

The mathematical functions that describe some of the window functions are as follows:

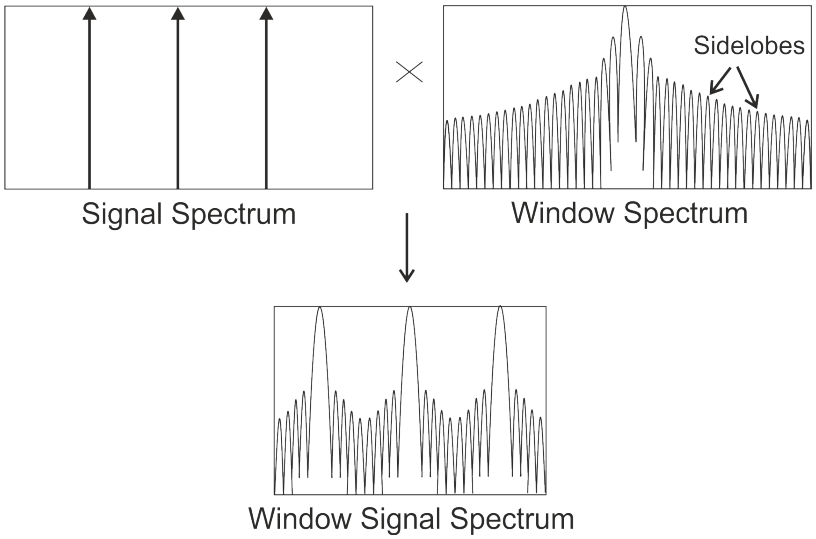

Figure 4.23: Windowing.

Rectangular Window:

$$w(\mathrm{n}) = 1 \tag{4.16}$$

Hanning Window (Hann):

$$w(\mathrm{n}) = 0.5(1 - \cos(\frac{2\pi - \mathrm{n}}{\mathrm{N} - 1})) \tag{4.17}$$

Hamming Window:

$$w(\mathrm{n}) = 0.54 - 0.46(\cos(\frac{2\pi\mathrm{n}}{\mathrm{N} - 1})) \tag{4.18}$$

where, N corresponds to width (samples) and n represents an integer with values of $0 \leq \mathrm{n} \leq (\mathrm{N} - 1)$. As it can be observed the most basic window function is the rectangular. The basic operation of this function is to multiply the sinusoidal signal by a value of 1. Thus, the signal is not affected by this function (as seen in Figure 4.25). However, the difference between the other two functions can be visualised in terms of the side lobes (which determine the smoothness of the peak frequencies), as can be depicted in Figure 4.24(b) (Chitode, 2009). In this case, it is recommended that during the signal processing analysis both Hamming and Hann windows are used and then the user decide which one gives better results according to the results obtained in the spectrum. In the case of the accelerometer output, insignificant difference between both functions was obtained, as observed in Figures 4.26 and 4.27; there-

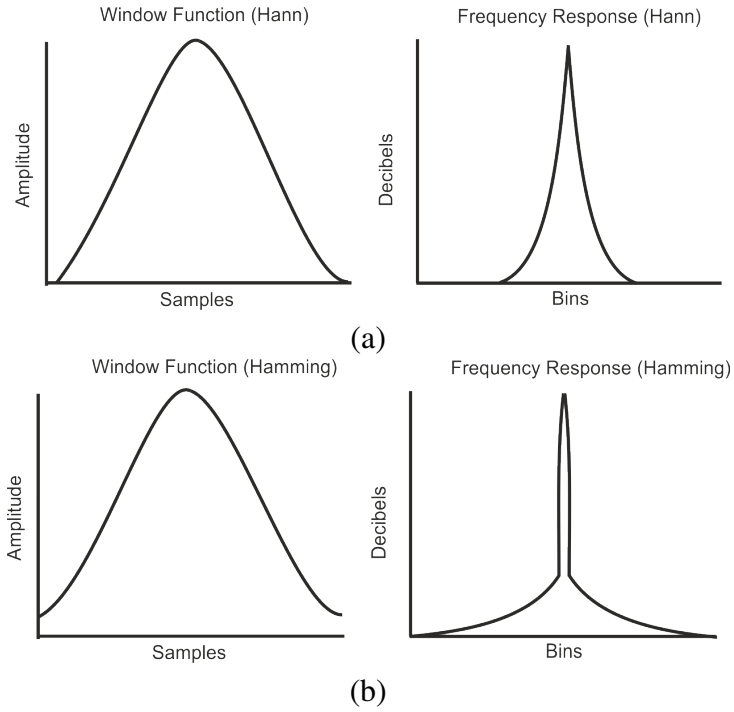

Figure 4.24: Window functions: a) Hann and b) Hamming.

fore, the use of any of them would be acceptable during the signal processing analysis. Other window functions can be studied such as, Barlett or Kaiser (Heinzel et al., 2002); however, the these are not commonly applied.

4.7 Mechanical Vibration Analysis

The dynamic and vibrations of the turbine can be explored based on the results from the signal process. Since the turbines are explored at various velocities (according to the flow velocities

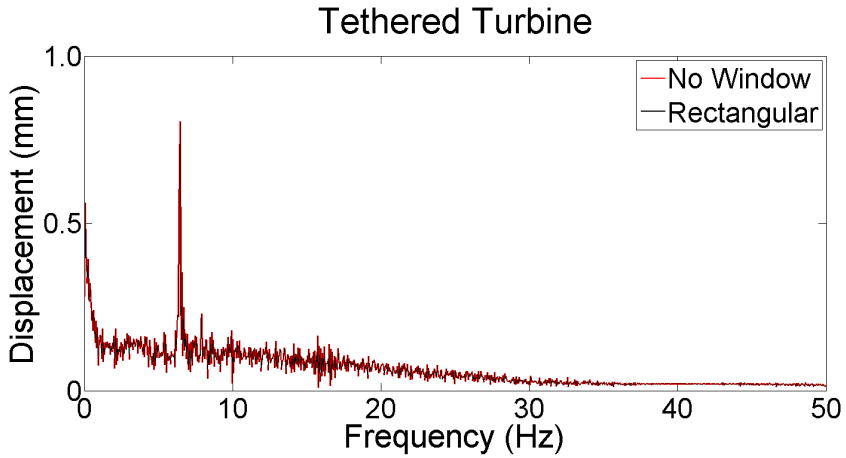

Figure 4.25: Rectangular Window applied to a signal of the tethered TEC.

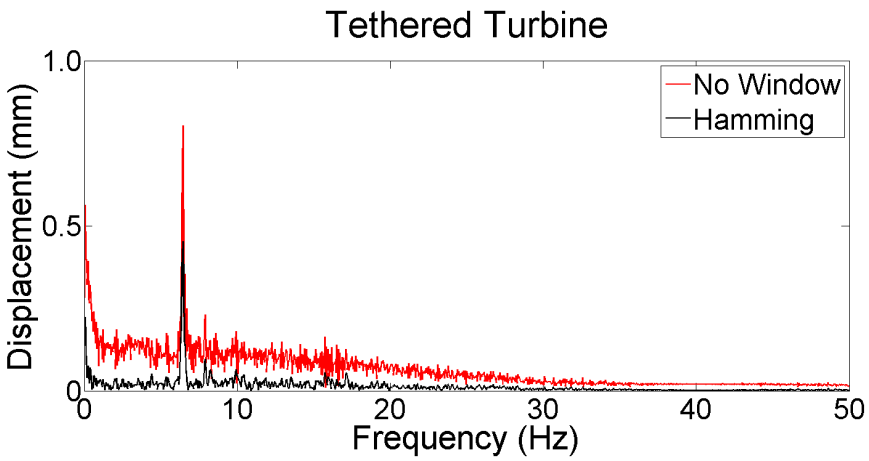

Figure 4.26: Hamming Window applied to a signal of the tethered TEC.

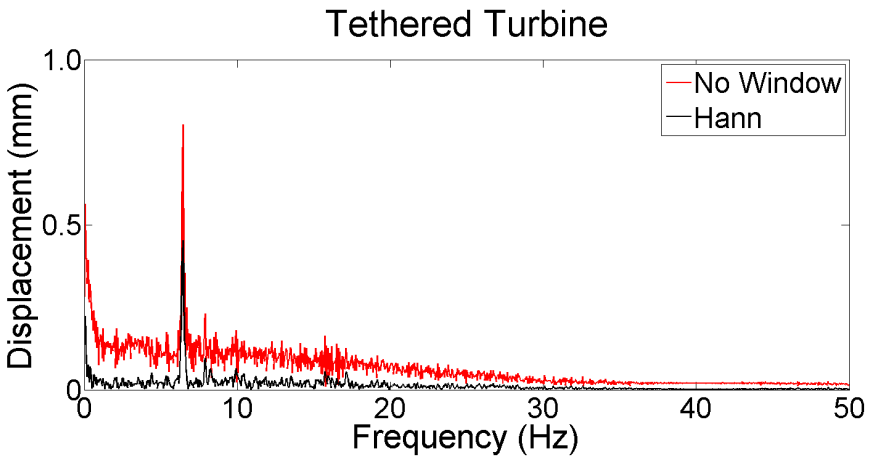

Figure 4.27: Hann Window applied to a signal of the tethered TEC.

of the facilities of through the tidal cycle) a condition monitoring can be carried out as it is commonly done for rotodynamic machines (e.g. pumps or gas turbines) in order to determine the onset of mechanical faults (Rogers (1979) or Stegemann (1998)). Therefore, a preliminary vibration analysis would provide guidance to understand the nature of characteristic or unusual vibration patterns. In order to obtain a measurement of the machine vibrations, accelerometers are usually employed (as described in Section 4.5.5).

The "signatures" or distinctive peak vibrations of the device can normally be correlated to several mechanical aspects. For instance, the presence of the first rotational speed frequency ($1x$) of the rotors is commonly found in the energy spectra. According to the amplitude of such frequency, this characteristic peak can inform if the device is working under normal or abnormal conditions. Faults might be related to excessive mechanical backlash or a bearing failure.

Additional to the typical vibrations occurring on a rotational device, external excitation caused by the working fluid can be present. The shedding of vortices can induced vibrations in the devices, as can turbulent flow or ocean waves (Piersol and Paez, 2002).

4.7.1 Rotational Velocities

The excitement of the first angular speed frequency ($1x$) of a rotor is frequently found in the spectral characteristics of bladed rotational devices such as pumps or fans. If the amplitude or bandwidth of such frequency increases, it usually means that the device is unbalanced (Goldman, 1999). The appearance of sub or super harmonics in the energy spectrum can be related to several mechanical conditions in the system.

For example, if the $2nd$ and $3rd$ angular speed frequencies appear or increase their amplitude in the energy spectra, the response can be associated with a lack of mechanical rigidity and shaft bending, respectively. Therefore, it is important to quantify and register any substantial change on the vibration level to determine if the peak frequency is atypical or has unusual behaviour. To determine the inherent vibrations in the machines, a preventive study is usually undertaken in the rotary system. Generally, the machine is operated at several rotational speeds to detect any amplification in the signal which can be related to a defect or failure. Occasionally it is difficult to identify the vibration sources when two or more frequencies merge into one single peak. These frequencies in the spectrum can be called ghost frequencies and they are usually the most destructive frequencies in a machine due to their nature (Piersol and Paez, 2002).

Table 4.1 contains a summary of the causes of some sub or super harmonics on a rotor dynamic

Frequency	Possible Cause	Remarks/ Other possible causes
1x	Unbalanced	Excess vibration of the machine, during rotational motion the centre of mass of the rotating part does not matches the rotational centre.
1/n	Shaft complication	Shaft Friction.
2x	Play or Backlash in the Machine.	Resonance or loose bearing part (mechanical looseness).
3x	Misalignment and bent shaft	Internal misalignment and machine part.
4x	Coupling problem	Bearing looseness, resonance possibility in slower machines and machine part.
5x	Machine Part	
1/2x	Rub or Oil Whirl	Sub harmonic of the shaft, sleeve bearings, change speed or oil temperature.
Increase in Amplitude	Increase in Turbulence	

Table 4.1: Vibration Causes. Various Sources (e.g. Goldman (1999) and Piersol and Paez (2002))

machine. This table serves as a guide to understand and relate possible characteristics or defects of the studied tidal devices in this thesis. This information is extracted from several specialised sources (Piersol and Paez (2002), Goldman (1999) and Adams (2005)).

4.7.2 Bearing Failure Detection

Due to the short-term usage of the bearings in the laboratory experiments, it was not expected to identify bearing failure in the energy spectra. If the bearing has an existing crack or is not capable of supporting the applied loads (Figure 4.28), failure can be referred to four main frequencies as given by the following equations:

$$BPFO = \frac{1}{2}(Z)(f)(1 - \frac{D}{e}cos(\alpha)) \tag{4.19}$$

$$BPFI = \frac{1}{2}(Z)(f)(1 + \frac{D}{e}cos(\alpha)) \tag{4.20}$$

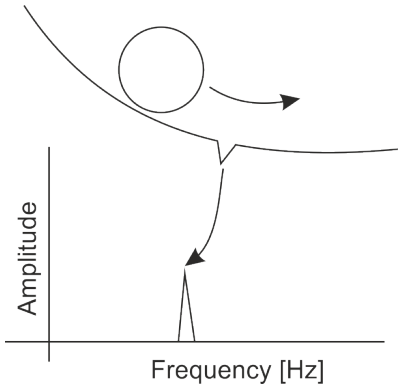

Figure 4.28: Bearing failure.

$$BSF = (f)(\frac{e}{D})(1 - (\frac{D}{e})^2 cos^2(\alpha)) \tag{4.21}$$

$$FTF = \frac{1}{2}(f)(1 - \frac{D}{e}cos(\alpha)) \tag{4.22}$$

where $BPFO$ and $BPFI$ depict the rolling element pass frequency of the outer and inner race respectively. BSF represents the roller element frequencies and FTF depicts the fundamental train frequency of the bearing cage. e is the pitch diameter of the cage (in); D, the rolling element diameter; and f, Z and α denote the rotational speed of the bearing, the number of rolling elements (balls) and the angle contact, respectively (Goldman, 1999).

4.7.3 Von Karman Vortex

Thus far, the frequencies in the energy spectra of the tidal converters can be related to mechanical properties that almost every rotatory machine encounters during operational periods. An additional parameter should be consider if such machine is immersed in a fluid flow, vortex shedding.

The formation of vortices in a device can lead to hazardous vibration effects. This phenomenon is commonly noticed when the flow passes across bluff bodies forming a particular kind of vortices in the wake. The most common example can be observed in the flow across circular cylinders, as depicted in Figure 4.29. Such representative vortex shedding is called *a von Karman vortex street*.

This vortex shedding usually causes a transverse force on members. This in turn creates a dynamic excitation on the structure (Patel, 1989). The appearance of the vortices can be determined through frequency analysis using equation 4.23.

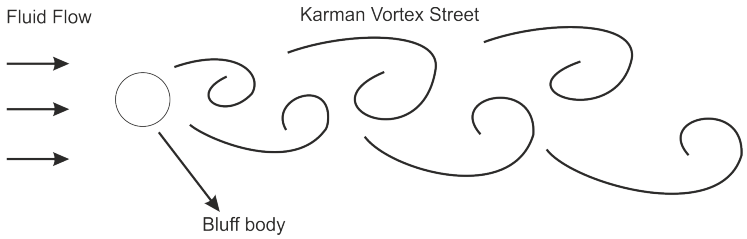

Figure 4.29: Von Karman Vortex.

$$St = \frac{fD}{V_{flow}} \tag{4.23}$$

where St corresponds to the Strouhal number, f represents the frequency, D designates the object's diameter and V_{flow} symbolises the flow velocity. St describes the shedding frequency of the vortices, and it usually falls around a value of 0.2 as observed in White (1991).

As described by Chakrabarti (2002), the use of spoilers can reduce or even eliminate the vibrations of structures due to vortex shedding. These spoilers are used to either break up the vortices just after they have been created or to reduce the chance that they be created by using shrouds or streamline geometries, respectively. In the experiments described in this thesis, streamlined geometries were used in the buoyant sections of the devices (Figure 4.10) and in the strut to support the turbines in either the flow or tow tanks, as described in Section 4.4.7. Even so, the frequencies related to the shed of vortices should be investigated in the vibration analysis, since the structures can resonate with periodic constituents of the wake. Thus, the responses can be determined with a time/frequency domain analysis which will be described on the following section.

4.7.4 Vibration Tolerance Chart

Additionally, the vibration levels presented by the tethered turbines can further be analysed and compared to existent vibrational tolerance charts used for rotordynamic machines and which are available from specialised literature such as Goldman (1999) or from consulting firms dedicated to predictive maintenance of machines; for example, Wowk (2009) or Bradley (2006). In this thesis the chart presented by Goldman (1999) was used throughout the thesis. As mentioned in Section 4.6.3, frequencies and amplitudes from roll, pitch and yaw spectrums can be measured in terms of their intensity and they can be correlated these tolerance charts. In order to relate amplitude of the studied frequencies, this should be scaled as the RMS Displacement, RMS Velocity or RMS Acceleration (as specified in Section 4.6.3). Acceptable limits of vibration are those within fair and rough levels, according to Goldman (1999). The verification of the proposed methodology will be studied in the following chapters.

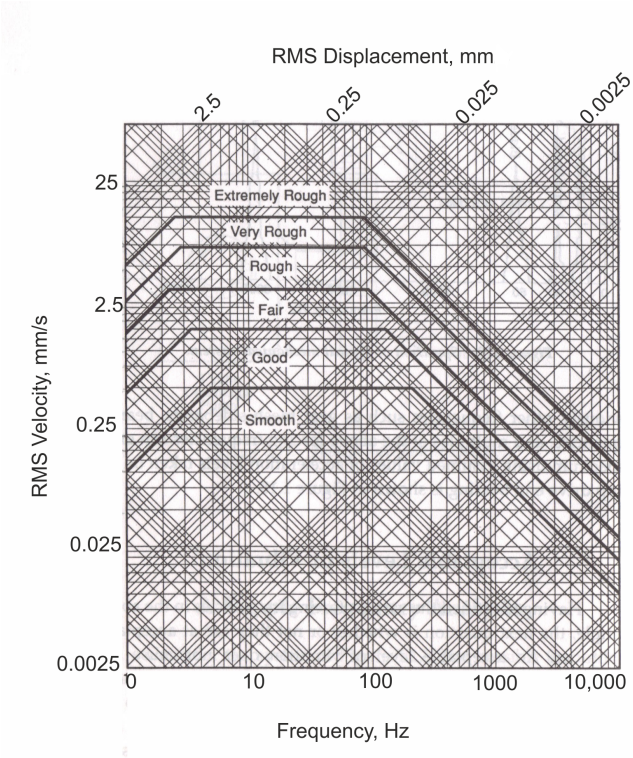

Figure 4.30: Vibrational Tolerance Chart. Taken from Goldman (1999).

4.8 Concluding Comments

This chapter has elaborated a methodology for the evaluation of tethered tidal energy converters, which represent something of a special case. In contrast to gravity based or piled configurations, the issues of stability and dynamic behaviour are of critical importance. The methodology is largely based upon experimental techniques; a purely analytical approach is of course a valid alternative, but difficulties arise with the specification of essential parameters such as added mass and damping.

In any experimental programme the effects of scale are likely to arise, and these have been discussed here. When the characteristics of the mooring system are added to the general hydrodynamic behaviour, it becomes very difficult to make confident predictions from test of complete tethered systems at model scale. Ideally investigations should be carried out at a variety of scales as described in the following chapters.

Chapter 5

Initial Evaluation of the Methodology to Evaluate the Dynamic Response of Tidal Turbines

In the previous chapter a complete methodology was developed to analyse the dynamic oscillations and mechanical vibrations of tethered devices. This chapter therefore verifies and explores the methodology through an initial design and evaluation of the dynamic response of small scale tethered turbines. The turbines' design is based on the regulations established in the previous chapter. Similarly, the turbines are equipped with the sensors specified in the methodology; and, the data is processed in order to undertake a preliminary analysis of the dynamic motions of tethered turbines. In order to compare the results when turbines are tested in turbulent and non turbulent environments, tests were carried out in a towing tank and a flume.

5.1 Motivation and Objectives

The main objective here is to assess and implement the methodology developed in the previous chapter. Therefore, a small scale prototype tidal turbine was designed for this purpose. The main focus was on the evaluation of the dynamic response of contra-rotating turbines given their special characteristics mentioned in Section 3.3.2; but the methodology can be equally applied to analyse single-rotor or turbines with two coplanar rotors. The number of blades was initially chosen according to the models presented by Clarke et al. (2010) and O'Doherty et al. (2009), where, two arrangements of 3-4 and 3-3 blades are considered. The first character

represents the number of blades in the upstream rotor and the second stands for the number of blades in the downstream rotor.

Two additional configurations were considered for these experimental trials. Both were equipped with 2 bladed rotor sections forming 2-3 and 2-2 arrangements. The underlying rationale was that 2-2 rotors will present unbalanced forces due to "shadow effects" as has been observed in single 2-bladed wind turbines (Cotrell, 2002). Hence, the initial experimental phase compared the behaviour of various CRR turbines in turbulent and non turbulent environments at flow velocities of $0.4\,\mathrm{m/s}$.

The remainder of this chapter is organised as follows. Section 5.2 presents the selection of components to design a prototype based on the developed methodology (Chapter 4). Section 5.3 presents the results of the dynamic performance of tethered turbines tested in tow and flume tanks. Finally, Section 5.4 summarises the results of each of the tests and the consequences of applying the proposed methodology on small scaled tethered tidal turbines.

5.2 Prototype Design

5.2.1 Facilities

Following the process outlined in Section 4.3, two facilities were identified within the University of Strathclyde in order to carry out the experimental plan. The flume tank (Figure 4.3(a)) is located at the Department of Civil Engineering. This tank is $30\,\mathrm{m}$ long, $0.92\ \mathrm{m}$ wide and up to $0.40\,\mathrm{m}$ in water depth, and runs at a maximum velocity of approximately $0.4\ \mathrm{m/s}$. The stream in the tank has turbulent intensities of up to 7% according to ADV measurements taken at different points over the sectional area through the length of the channel (Rose et al., 2010). It can be noticed that the turbulence intensity measured on the flume tank is similar to that of real tidal sites, as stated in Section 2.1.3.

The tow-wave tank (Figure 4.3(b)) is located at the Department of Naval Architecture and Marine Engineering. This tank is $21.6\ \mathrm{m}$ long, $1.6\ \mathrm{m}$ wide and $0.65\ \mathrm{m}$ water depth. The towing carriage is equipped with stepper motors to give precise control of towing velocities, ranging from $0.03\,\mathrm{m/s}$ to up to $2\,\mathrm{m/s}$. The tank also features its own wave maker which is capable of generating regular or irregular two dimensional waves.

Tank	Blockage factor
Flume	15.5%
Tow	6%

Table 5.1: Blockage Factor.

Propeller	Diameter (m)	Pitch (m)
2 Bladed	0.28	0.15
2 Bladed (Pusher)	0.28	0.15
3 Bladed	0.28	0.18
3 Bladed (Pusher)	0.28	0.18
4 Bladed	0.28	0.15

Table 5.2: Propeller Characteristics.

5.2.2 Mechanical Design of Small Scale CRR

Blade systems suitable for small-scale turbines are not readily obtainable and would have to be manufactured. Given availability, it was considered that inverted scale model propellers constructed from strand glass/nylon could be utilised to carry out an initial analysis of the methodology and the dynamic response of various CRR types. There was a clear conflict between the need to obtain measurable quantities in the experiments, and the need to keep a blockage ratio below 20% (Section 4.4.1); thus, rotors of approximately $0.3\,\mathrm{m}$ diameter were chosen, and the resultant blockage factors are shown in Table 5.1.

Three counter clockwise propeller types were used during the first experiments: 2 bladed, 3 bladed and 4 bladed. Two clockwise (pusher) propellers (2 bladed and 3 bladed) were included in order to investigate contra rotation effects (Table 5.2). Table 5.2 lists the characteristics of the propellers as given by the manufacturer (Section 4.4.1).

It was found that the Reynolds Number ranges from 3.46×10^4 to 1.85×10^4 (see Section 4.4.2) at velocities of $0.3\ \mathrm{m/s}$ and $1.6\ \mathrm{m/s}$, respectively. The Froude Number varies between 0.119 and 0.634, at the same flow velocities. The solidity of the rotors (calculated as defined by Hansen (2008)) is depicted in Table 5.3.

Precise information about propeller geometry was difficult to obtain and was of limited relev-

Turbine's Configuration	Rotor's Solidity
2-2 C	0.13
2-3 C	0.16
3-3 C	0.19
3-4 C	0.22

Table 5.3: Solidity of the Contra Rotating Turbines (Propellers).

Parameter	Coefficients	
Thrust	$C_t = 0.75$	68 N
Power	$C_p = 0.4$	58 W
Torque		1.26 Nm
Angular velocity	$\lambda = 4$	407 rpm

Table 5.4: Design Parameters.

Figure 5.1: Propeller and Hub Section.

ance in this initial series of tests. To provide estimates of structural loadings, mainly to select appropriate bearings, a TSR of 4 was used and a maximum flow velocity of 1.6 $^{\mathrm{m}}/_{\mathrm{s}}$ was considered in the experiments. Therefore, thrust and torque loads (Section 4.4.4) were calculated using equations 3.2, 3.1 and 3.4 (Table 5.4).

Considering the thrust load to select the bearings and a safety factor of 2 (Section 4.4.4), the maximum force that could possibly act on the bearing was calculated as 136 N. It was found that a miniature SKF stainless steel bearing of $3\mathrm{mm} \times 10\mathrm{mm} \times 4\mathrm{mm}$ (SKF Group, 2012) was adequate to resist the applied loads. The hubs were then designed to fit the bearing dimensions (Section 4.4.4).

Due to the small scale, electrical power take-off systems were not included in the design. Instead, a mechanical brake was designed to fulfil the requirements described in Section 4.4.5. Compression springs were installed on each side of the rotor in order to compress brass friction discs against the rotor hub. The torque was therefore regulated by compressing these springs at various intensities. The turbine design is depicted in Figure 5.1.

A nose cone profile was utilised on the front section of the turbine, while the tail fairing was designed as a normal cylindrical shape (Section 4.4.6). Both sections were constructed from *Dyvinicell H60* with a density of 60 $^{\mathrm{kg}}/_{\mathrm{m}^3}$. An aluminium shaft with a total length of 325 mm and an inside diameter of 3 mm was adopted for the final design (as described in Section 4.4.4). A simple bored hole was located at the front of the shaft in order to connect the flexible mooring to the towing strut (Section 4.4.7).

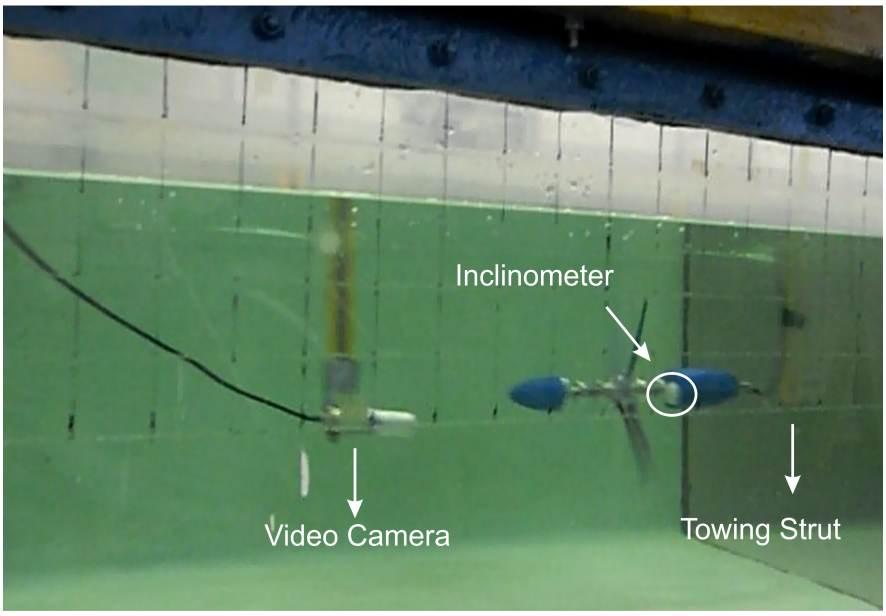

Figure 5.2: Small Scale Turbine in Operation.

Trace wire for fishing purposes was used as the mooring line. The wires were covered by strand nylon to avoid corrosion problems and the load capacity was rated at $100\ \mathrm{kg}$ according to Tronix (2012). Crimps were used to adjust the length between the towing strut and the prototypes. A separation of $50\ \mathrm{mm}$ was employed during the tests, this measurement was determined on site and based on the laboratory conditions. The length of the wire provided sufficient flexibility to the turbine to move throughout the three main rotational angles: roll, pitch and yaw. Using this procedure, it was guaranteed that the only restricted motions were in the heave and sway directions; hence, the CRR turbine would only reflect the motions of a turbine held by flexible moorings. A picture of the turbine during operation can be observed in Figure 5.2. The location of the model in the tank in more detail and final technical drawingscan be found in Appendix A.

5.2.3 Instrumentation

To measure the dynamics and vibrations of the tethered turbine, the accelerometer *ADXL330* (Analogue Devices, 2007) was selected due to its cost effectiveness and its dimensional properties (Section 4.5.1). The device weighs approximately $1\,\mathrm{g}$ and measures $18.5\mathrm{mm} \times 38.3\mathrm{mm} \times 1.5\,\mathrm{mm}$; thus, it does not exert significant inertial effects on the system (Section 4.5.4) and is able to fit easily onto the turbine. The lower frequency limit of the transducer is $0.5\ \mathrm{Hz}$, extending upward to $1600\ \mathrm{Hz}$ for the X and Y axis and $550\ \mathrm{Hz}$ for the Z axis. The sensitivity of the device is $300\,{}^{\mathrm{mV}}/_{\mathrm{g}}$ (Analogue Devices, 2007). Low strain sensitivities enable it to study large displacements of the device.

In order to measure thrust and the shaft torque, two strain gauge systems were installed in the prototypes (Section 4.5.2). A strain gauge to measure axial force (thrust) was implemented in the towing strut. A $90\,^{\circ}$ rosette was employed with resistors of $120\ \Omega$, connected in a Wheatstone bridge formation (Section 4.5.2). The second strain gauge arrangements was employed to measure shaft torque. Due to space restrictions, a quarter Wheatstone bridge was employed for this configuration, and three external gauges were added to complete the full bridge installation.

Due to the small scale of the turbine, it was decided to measure the angular velocity of the rotors independently. A submersible camera was attached behind the turbine in order to measure the angular velocity of the rotors during operation (Section 4.5.3). Since the video camera was able to continuously record video at $25\,{}^{\text{frames}}/_{\text{s}}$, the frames were then separated and translated into Autodesk Inventor. From there, the moving distance of a "marked" blade was measured between frames until the blade would complete an entire revolution (Section 4.5.3). Power was not taken from the device; hence, electrical outputs were not measured.

The accelerometer was mounted in the front buoyant section of the prototype. In order to guarantee a secure fit, the instrument was firstly pinned in each corner to the foam material; afterwards, it was covered with non corrosive silicon as a bonding material in order to prevent water and electronic damage. The torque gauge was located between the rotors in the aluminium shaft (Figure 4.10),while the other strain gauge was mounted on the upper section of the towing strut. Both sets of gauges were protected from water ingress by microcrystalline wax (M-Coat-W-1) (Vishay Precision Group, 2012). The submersible colour camera was installed at the rear of the towing carriage with a spacing of approximately $100\ \text{mm}$ behind the turbine. Waterproof material was not required for this instrument since it is capable of working at depths of up to approximately $30\,\text{m}$ (Section 4.5.4).

A power supply of -5 to $+5\ \text{V}$ fed the amplifiers used for the strain gauges (Section 4.5.4) and the accelerometer. A voltage differential to fed the accelerometer with $3\ \text{V}$ was designed to meet the requirements specified by Analogue Devices, 2007.

The signal and power cables were chosen to be lightweight and flexible (Section 4.5.4). Twisted shielded cables were employed for the overall connection. However, the cables to connect the torque gauge to the data acquisition could not fit in the inside diameter of the designed shaft. So it necessary to re-design the shaft to accommodate the cable, which in turn required a change in the bearing to a deep groove design of $8\text{mm} \times 16\text{mm} \times 5\,\text{mm}$. The rotor hubs were re-configured to accommodate these bearings. The final assembly was submerged in water for 24 hours prior to the experimental phase in order to prove the electronic components.

The calibration procedure presented in the methodology was carried out with the strain gauges

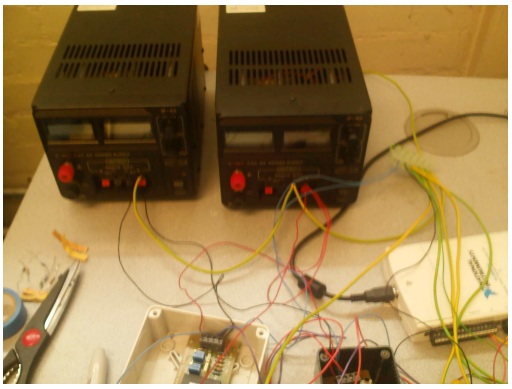

Figure 5.3: Data Acquisition.

used, and the results can be observed in Figure 4.18. The analogue signals of torque, thrust, roll, pitch and yaw were acquired thorough a National Instruments data logger module, NI USB – 6210 module with 16 bits. The data-logger was connected to an Intel(R) Core (TM) 2 Duo (model T7100) processor with a CPU clock speed of 1.8 GHz, with 2 GB of RAM. A USB port sent the signals to Labview 8.5, running under Windows Vista. The final connections can be seen in Figure 5.3. The maximum sampling rate obtained was 40 Hz (Section 4.5.5).The number of samples was determined differently for each facility. In the case of the flume tank, an auto-regression technique was used during the tests to satisfy the requirements established in Section 4.5.6. In comparison, with a working length of 10 meters and a tow carriage velocity of 0.4 m/s, it was determined that three experiments on the tow tank facility fulfilled the requirements of Section 4.5.6. The number of samples was approximately 3000.

5.2.4 Signal Processing

A low pass FIR filter was designed with a Hamming Window (as described in Section 4.6.1); and the data was analysed in both time and frequency domains (Sections 4.6 and 4.7). The results and the appropriate discussion are presented in the following sections.

5.3 Flume and Tow Tank Experiments

The three available modes of motion for a tethered system can affect its performance in various ways. Firstly, if the device rolls continuously, the mooring lines will twist, placing a strain on these and any power or data cables which run in parallel. Secondly, if the devices pitch or yaw with a prominent angle, power losses will occur, as pointed out by Galloway et al. (2011). The following the experimental analysis of 4 CRR turbine arrangements was carried out to analyse

the dynamic response of tethered turbines in general, but also to obtain a basic understanding of the methodology proposed in the previous section. This chapter focuses uniquely on four CRR arrangements:

- 2-2C - 2 bladed rotor upstream and 2 bladed rotor downstream arrangement.
- 3-3C - 3 bladed rotor upstream and 3 bladed rotor downstream arrangement.
- 2-3C - 2 bladed rotor upstream and 3 bladed rotor downstream arrangement.
- 3-4C - 3 bladed rotor upstream and 4 bladed rotor downstream arrangement.

The aim of the first set of tests was to compare the performance of these four configurations in two facilities at low velocities of approximately $0.4\,^{\mathrm{m}}/_{\mathrm{s}}$. The prototypes were firstly installed in a flume tank with a turbulence intensity of approximately 7%. Then, the devices were deployed in a tow tank facility. The tow tank was assumed to have zero free-stream turbulence since it is still water, and sufficient time was allowed between tests to allow any disturbance to disperse. During the experiments, the brake load was set in order to achieve a TSR of 4 in each of the configurations and thrust values were also similar for each condition (Cp ~ 0.88). The following sections present the results of this investigation.

5.3.1 Time Domain: Roll, Pitch and Yaw Motions

From Figure 5.4, it is observed that the variability of the roll motion in the devices is more severe in tests conducted at the tow tank. As mentioned earlier, the blockage ratio of the flume tank is more than double the blockage ratio calculated in the tow tank. It is possible that the flow concentration contributed to minimise the rotational variability of the device in a turbulent environment. Standard deviations are generally larger in the flume tank, as would be expected from the ambient turbulence levels. The mean level of roll is to some extent a function of the imbalance of torque loading on the two rotors, which was not easy to eliminate at such small scale. It is found that the signal quality was affected in the tow tank tests by noise created by stepper motors installed in the towing carriage. As pointed out in Section 4.6.1, this problem could be solved by applying adequate filters. Given the preliminary nature of these tests, the results were initially analysed as raw data but the experimentation undertaken in later chapters considered the use of filters in conjunction with a higher data sampling rate in order to overcome this problem.

Probability density distributions were also studied, as recommended in Section 4.6.2. It can be observed that the distributions for the 2-2 and 3-4 configurations seemed to be symmetrical

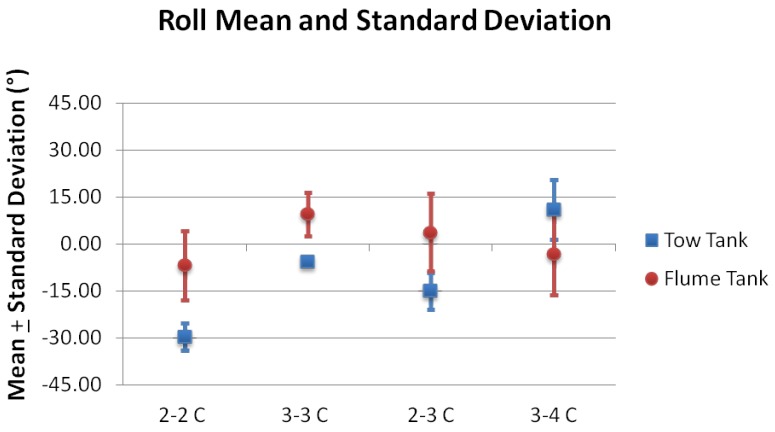

Figure 5.4: Roll Motion: Mean and 1D Standard Deviation.

(Figures 5.5a and b); however, the roll motion of the 3-4 turbine configuration falls about off from the expected value. Similarly, kurtosis values closer to those recommended in the protocol were obtained by the 2-2 turbine configuration. Meanwhile, it can be observed that the 3-4 configuration presents a mesokurtic behaviour.

The 3-4C configuration shows an adequate aligned pitch position when it was tested in the tow tank (Figure 5.6). A balancing problem was found in the other cases; however, as stated before it was expected that the devices would improve their alignment when tested at higher flow speeds. It was noticed that the turbulent flow in the flume tank generated around 1.4 times more pitch oscillation on the prototypes than in non turbulent flows.

The probability density distributions of the 2-2 and 3-4 turbine's pitch motion can be observed in Figure 5.7a and b. Similar to roll motion distributions, skewness and kurtosis values are close to expected values. Again, the distribution of the 3-4 turbine configuration seems to follow a mesokurtic behaviour; meanwhile, the 2-2 C follows a leptokurtic behaviour.

Due to the large blockage ratio the yaw alignment of the 2-2C devices in the flume tank improves significantly. The devices with dissimilar numbers of blades (2-3C and 3-4C) present satisfactory orientation properties in both facilities. It is noticed that the yaw fluctuate 2.7 times more in the tow tank than in the flume tank.

Kurtosis behaviour of both 2-2 and 3-4 turbine configuration of yaw motion follow a leptokurtic conduct (Figure 5.9a and b). Additional figures describing the probability density function of the 2-3 and 3-3 turbine configurations can be found in Appendix C.

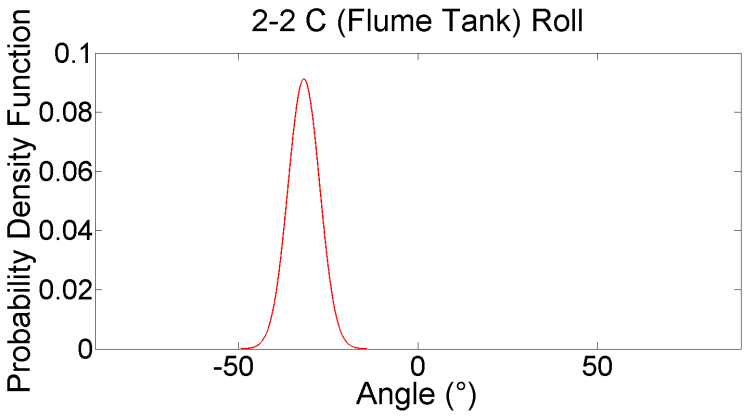

(a) Skewness = -0.08, Kurtosis = 3.22

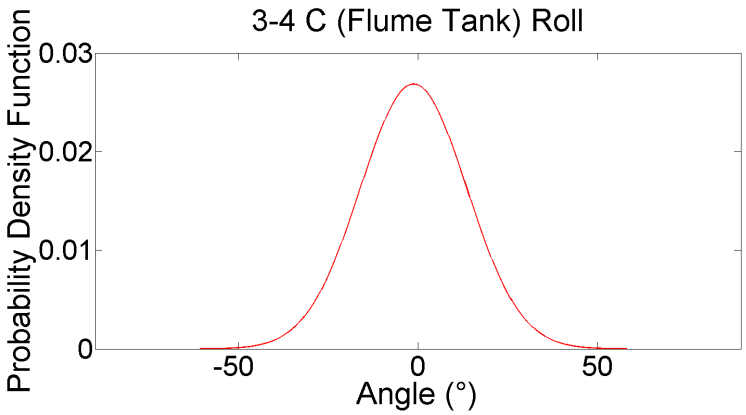

(a) Skewness = 0.24, Kurtosis = 2.54

Figure 5.5: Probability Density Functions of a) 2-2 C and b) 3-4 C from Roll Motion in the Flume Tank.

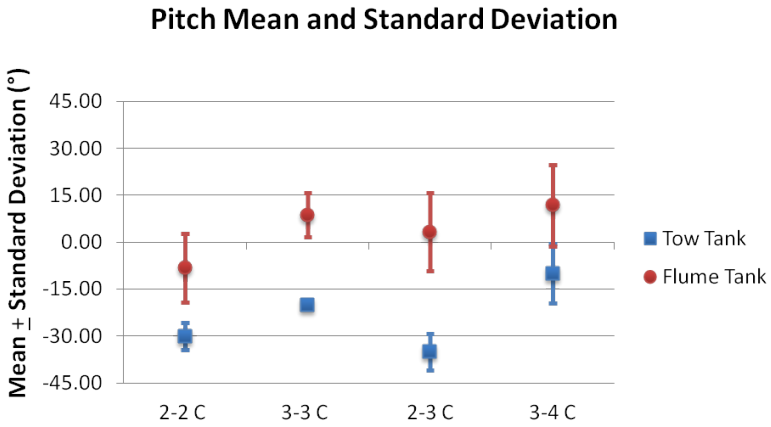

Figure 5.6: Pitch Motion: Mean and 1D Standard Deviation.

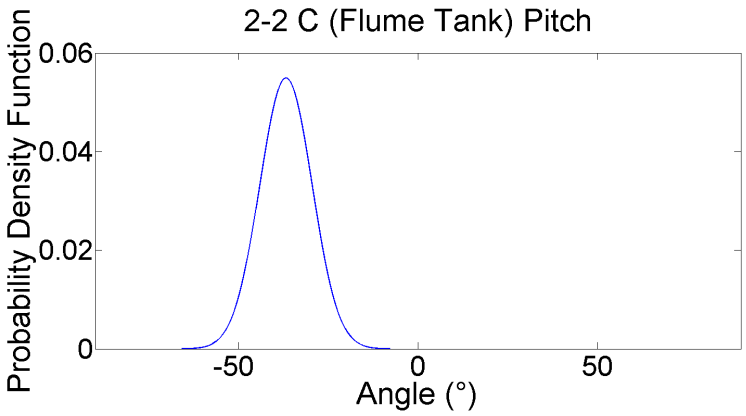

(a) Skewness = 0.18, Kurtosis = 3.22

centering

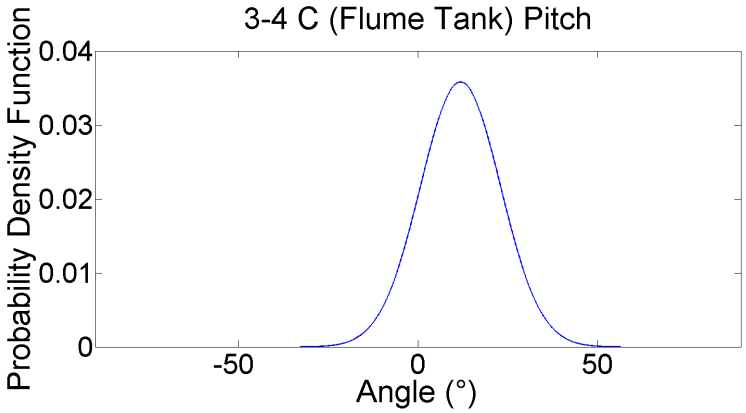

(a) Skewness = -0.57, Kurtosis = 2.47

Figure 5.7: Probability Density Functions of a) 2-2 C and b) 3-4 C from Pitch Motion in the Flume Tank.

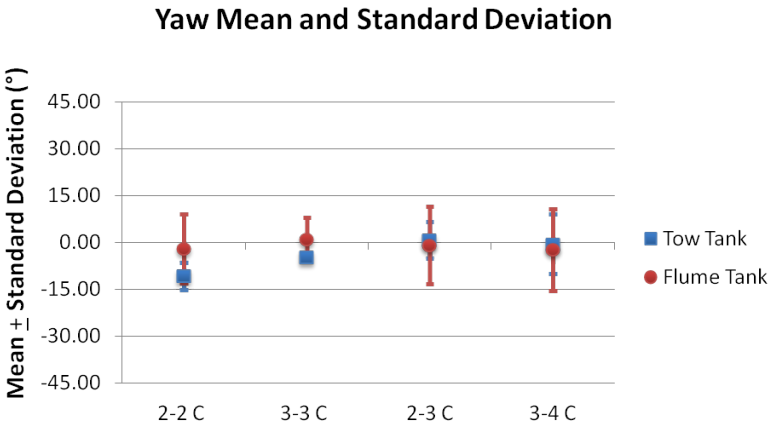

Figure 5.8: Yaw Motion: Mean and 1D Standard Deviation.

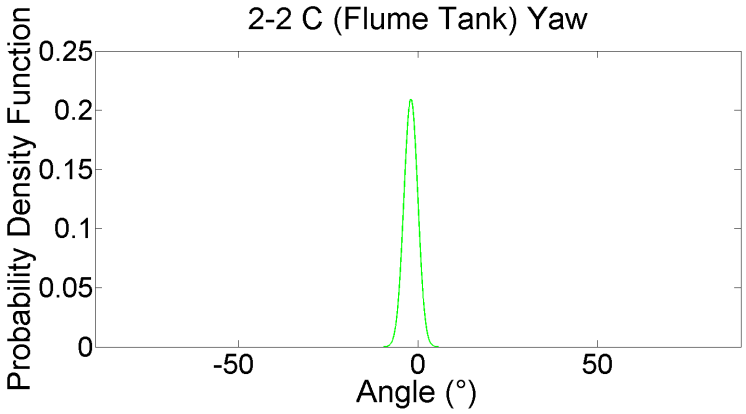

(a) Skewness = 0.18, Kurtosis = 3.22

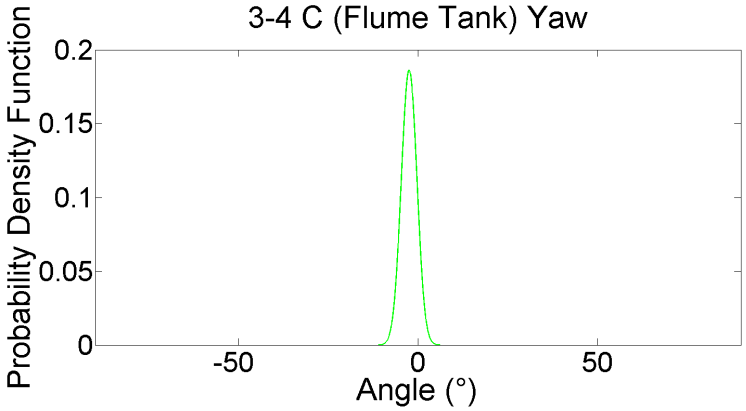

(a) Skewness = -0.57, Kurtosis = 2.47

Figure 5.9: Probability Density Functions of a) 2-2 C and b) 3-4 C from Yaw Motion in the Flume Tank.

5.3.2 Frequency domain: Roll, Pitch and Yaw Vibrations

The following graphs show the energy spectra of each configuration in the three measured dynamic motions. The results are obtained with the use of FFT and signal processing techniques reviewed in the previous chapter. Figures 5.10(a) and (b) show the roll energy spectrum of the 2-2C from the tow and flume tanks respectively. The following terminology is employed to define the peak frequencies of the energy spectra:

- nxu - Frequency corresponding to the upstream rotor.
- nxd - Frequency corresponding to the downstream rotor.
- nxbb - Frequency corresponding to blade interactions (if present),

where n refers to the frequency related to the angular rotor speed. This number can vary according to the sub or super harmonic (e.g. 1, 2, 3, 4, etc,).

It is noticed that the amplitude of the roll peak frequencies is substantially higher in the flume tank energy spectrums than in the tow tank due to the turbulence intensity (as seen in Table 4.1 and discussed by Piersol and Paez (2002)). It is noticed in Figure 5.10(a) that the two peak frequencies appearing on the roll spectrum are related to the unbalancing of the machine ($1x$). When the same device is tested in the tow tank, both peak frequencies are related to shaft friction problems.

Figures 5.11(a) and (b) depict the roll energy spectrum developed by the 3-4C in the flume and tow tanks. Both spectra show that the 3-4C presents several peak frequencies related to the first frequency of the rotor and to the blade interactions of both rotors ($1xbb$). The 3rd sub-harmonic ($3x$) is also visible in the tow tank energy spectrum. This frequency represents a possible misalignment in the device and shaft bending. Moreover, the 4th harmonic is detected in the flume tank spectrum denoting possible resonant problems in the turbine. A similar response is presented by the 2-3C configuration. Again, the first frequency and 2nd sub-harmonic of the rotor are observed in the flume tank spectrum; where, $2x$ represents potential mechanical play or backlash. In the tow tank, the roll energy spectrum of the 2-3C presents the $1x$ frequency and the blade interactions ($1xbb$); however, it is found that the peak frequencies are less clearly defined.

The pitch energy spectra of the 2-2C and 3-4C configurations are observed in Figures 5.12 and 5.13. It is shown in the 2-2C case (Figure 5.12(a)) that the turbulence intensity is again reflected in the spectrum when the device is deployed in the flume tank. The first rotational

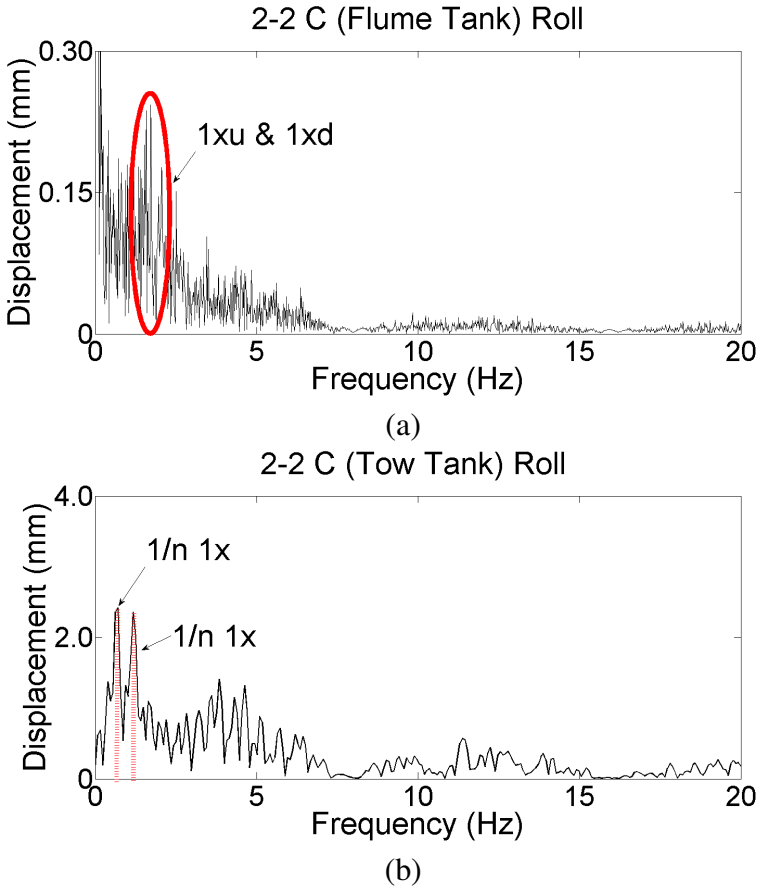

Figure 5.10: Roll Peak Frequencies of 2-2C at $0.4\,{}^{\mathrm{m}}/_{\mathrm{s}}$: a) Tow Tank and b) Flume Tank.

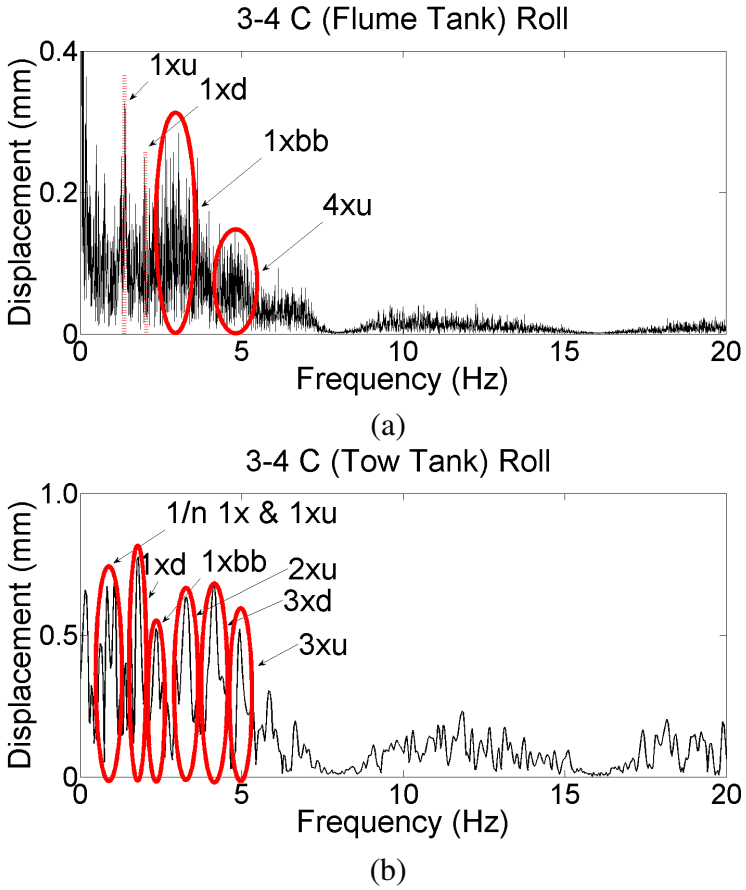

Figure 5.11: Roll Peak Frequencies of 3-4C at $0.4\,{}^{\mathrm{m}}/_{\mathrm{s}}$: a) Tow Tank and b) Flume Tank.

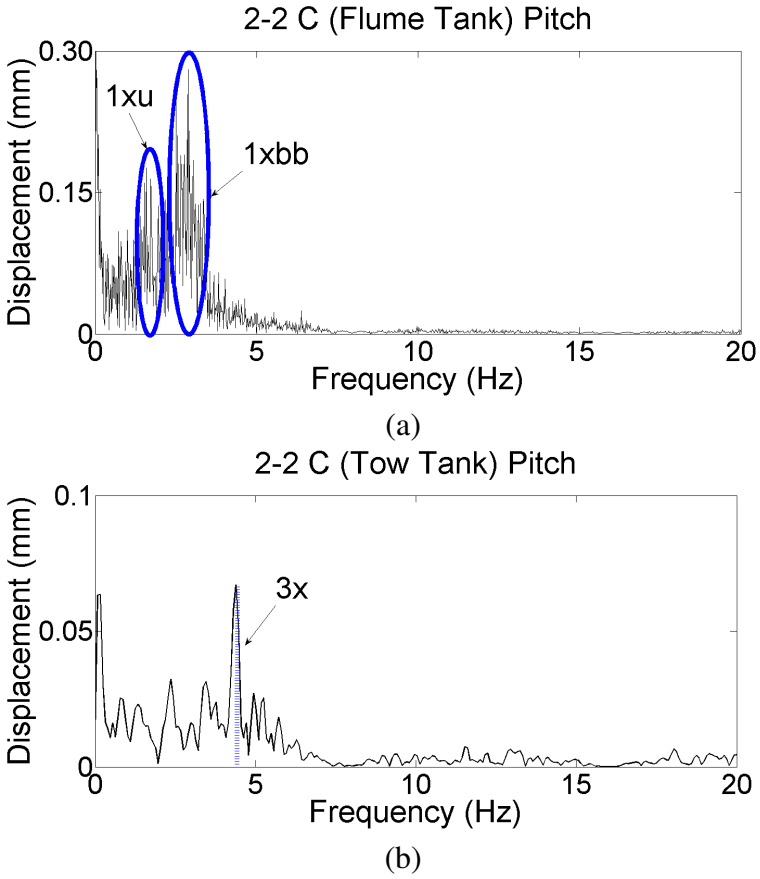

Figure 5.12: Pitch Peak Frequencies of 2-2C at $0.4\,^{\mathrm{m}}/_{\mathrm{s}}$: a) Tow Tank and b) Flume Tank.

frequency of the upstream rotor ($1x$) and the blade interactions ($1xbb$) are observed in Figure 5.12(a). The intensity of both frequencies is considerably lower in the tow tank and the dominant peak frequency here is caused by the third harmonic of the fundamental frequency.

Similarly to the roll spectra, the 3-3C presents defined peaks in the pitch energy spectrum. The amplitude of the peak frequencies is 23% lower than in the roll spectrums and is similar in both test facilities. Two of the important frequencies found in the flume energy spectrum represent mechanical unbalance ($1x$ and $1xbb$).

Figure 5.13(a) shows the pitch energy spectrum of the 3-4C turbine in the flume tank. The first rotational frequency of both rotors is present in the spectrum. Similarly to the roll spectrum, the $4th$ rotational frequency is evident in the spectrum. A sub-harmonic frequency is also found in the pitch spectrum from the flume tank which represents friction on the shaft. In the tow tank spectrum, only the blade interactions' frequency is visible with an amplitude of at least 2 times lower than that observed in the flume tank. Similarly, the 2-3C case presents the first rotational and the blade interaction frequencies in the non turbulent environment. In the turbulent environment, on the other hand, several peak frequencies are detected in the spectrum, i.e. $1x$ and $2x$ of the front and back rotor, plus the sub-harmonic of the rotors.

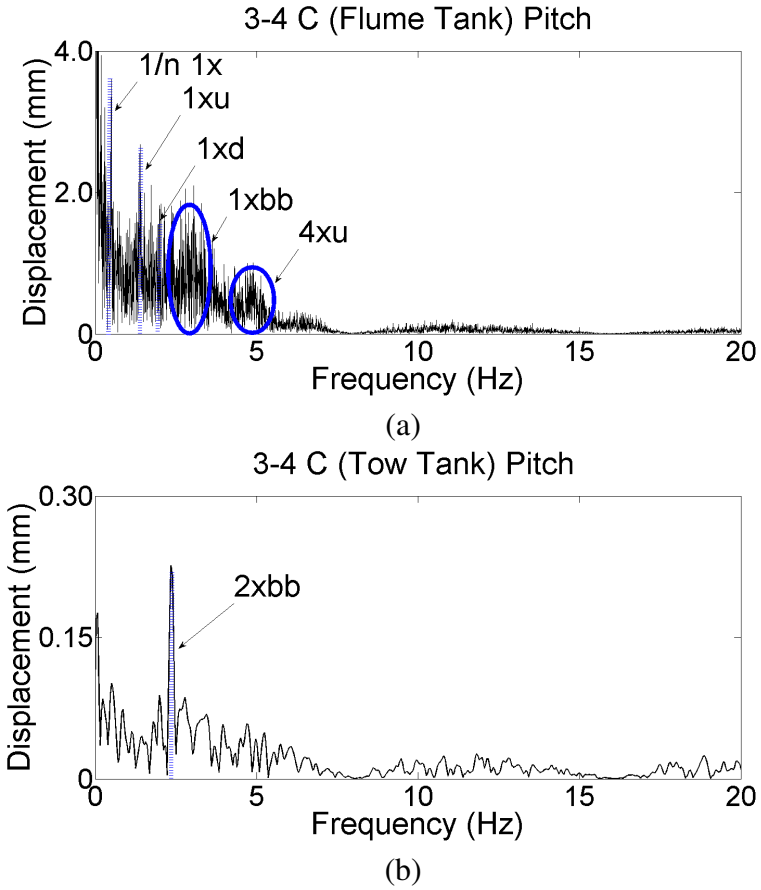

Figure 5.13: Pitch Peak Frequencies of 3-4C at $0.4\,{}^{\mathrm{m}}/_{\mathrm{s}}$: a) Tow Tank and b) Flume Tank.

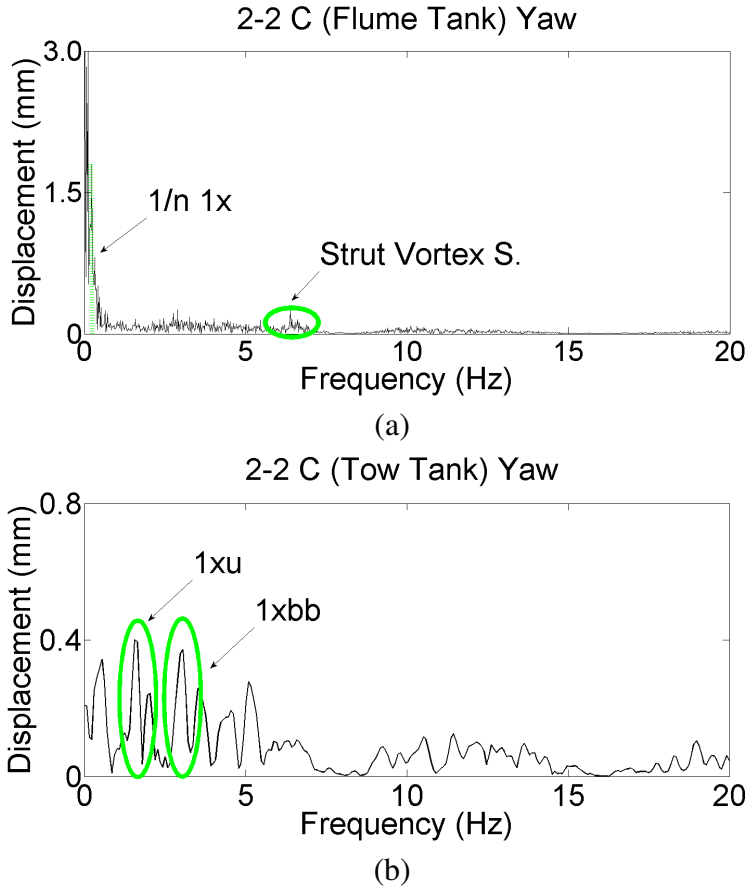

Figure 5.14: Yaw Peak Frequencies of 2-2C at $0.4\,{}^{\mathrm{m}}/_{\mathrm{s}}$: a) Tow Tank and b) Flume Tank.

Finally, Figures 5.14(a) and 5.15(a) demonstrate that the main frequency on the yaw motions in the flume tank corresponds to friction on the shaft (${}^{1}/_{\mathrm{n}}\,1x$). In the tow tank spectra (5.14(b) and 5.15(b)), it is found that the devices present possible unbalanced ($1x$) and mechanical looseness ($2x$); however, the amplitude intensities are 66% lower compared with the roll and pitch energy spectra of the tow tank and up to 3 times lower compared to the roll and pitch energy spectrums of the flume tank.

With the use of the tolerance charts (Section 4.7.4) available in Goldman (1999), it was found that the peak frequencies of the 3-3C and the 3-4C turbines were located in the “rough” section of the charts; while the peak frequencies of the 2-3C and 2-2C were placed in the ”very rough” section of the charts. This information relates to the flume tank tests; but a different pattern was found for the configurations when they were tested in the tow tank. The peak frequencies of the 2-2C were located in the “extremely rough” section of the chart. The peak frequencies for the 3-3C and 3-4C turbines were located in the “very rough” segment and the peak frequencies for the 2-3C were situated in the “rough” segment of the chart.

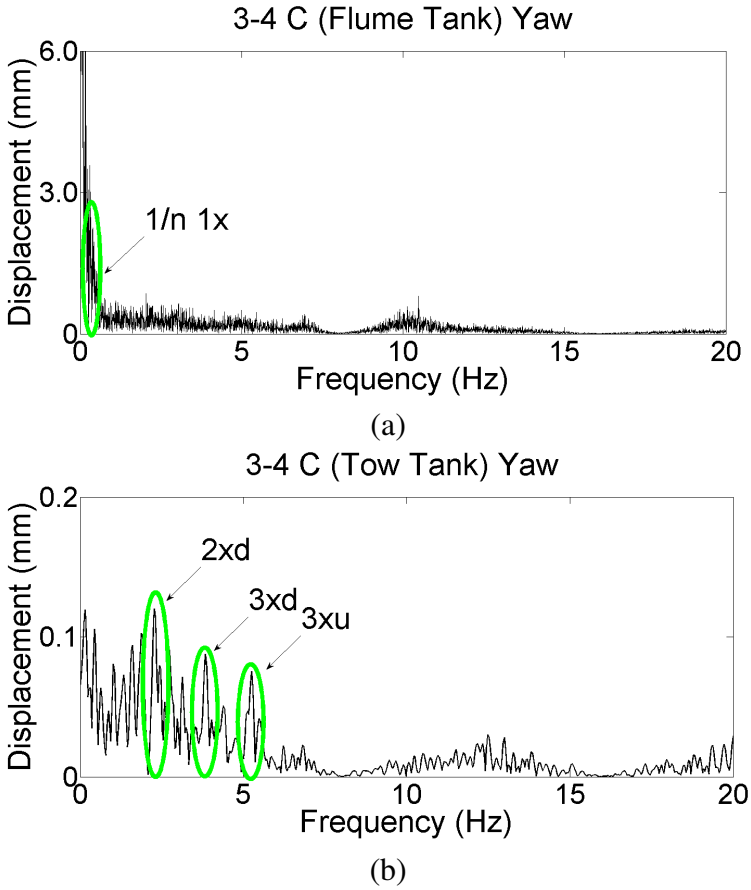

Figure 5.15: Yaw Peak Frequencies of 3-4C at $0.4\,{}^{\mathrm{m}}/_{\mathrm{s}}$: a) Tow Tank and b) Flume Tank.

5.4 Summary

The methodology to measure the general performance, dynamic oscillations and mechanical vibrations of tidal tethered turbines was tested in this chapter. Specifications for small model turbines were drawn up, and the prototypes constructed. Tests were then carried out in a tow tank and a flume, typical of the facilities commonly used for such purpose.

It was found that the variability of the dynamic response of the tethered turbines was higher when the turbines were tested in the flume tank, this was expected due to the high levels of turbulence in the water (7%). But also, the dynamic response of the turbines was affected by the magnitude of the blockage ratio in the flume tank (15%). The pitch motion variability increased by around 40% when the devices were tested in the flume tank, clearly as a result of turbulence. The small separation between the turbine blade tip and the tank floor, also influenced pitch motions. This is due to a high blockage ratio, the blade tip was working at low radial velocity and within turbulent flow conditions which gave rise to instabilities of the turbine. Perhaps surprisingly, yaw alignment was rather better in the flume tank; however, it must be remembered that the flume presented higher blockage ratio conditions which would accelerate the fluid around the turbine, inducing it to align better to the flow. Therefore, care must be taken in tests with large blockage ratios because not only do they tend to increase C_p (as discussed in Section 4.4.1) but also, for tethered turbines they influence yaw alignment. Moreover, it was observed that some turbines presented larger yaw angles or higher mechanical vibrations in the zero turbulent environment, mostly notably the 2-2C turbine. In the general sense, it was found that the methodology provided information that can be used to analyse the dynamic response of tethered TECs. In the following chapters, these principles would be applied to various types of tethered turbines at different scales to further validate the methodology proposed in Chapter 4.

Chapter 6

Dynamic Response Assessment of Tethered TECs on a Non-Turbulent Environment

A methodology to examine the dynamic response of tethered TECs was designed in Chapter 4. In order to demonstrate the value of the methodology, further series of experiments are presented in this chapter. These cover co-axial contra rotating rotors (CRR), in-plane counter rotating rotors or "side by side rotors" (SSR) and single rotors (SR). The rotor blades were constructed to represent accurate scaled model turbines, using rapid prototyping techniques. The tensile strength of the synthetic material was such as to allow the possibility of blade failure at high relative velocities. Observations of blade failure and the accompanying stress analysis therefore formed part of this study. The final results highlight the capabilities and deficiencies of each rotor type according to time and frequency domain characteristics. The implications of using rapid prototyping techniques in the production of small scale TECs are also discussed.

6.1 Motivation and Objectives

As discussed in Section 3.3, rotor technologies in general are based on current knowledge and experience from ship or aviation industries. The peculiarities of marine renewable turbines arise according to particular fluid characteristics or the working purposes of the systems. For use in tethered system, the CRR turbine is again considered. Two additional configurations are studied on this occasion: side by side contra rotating (SSR) configuration and single rotor

(SR) devices.

The main purpose of the work presented in this thesis is to corroborate the applicability of the methodology (Chapter 4) by studying the dynamics and vibrations of these three configurations (with variations of rotor blade numbers) in time and frequency domain techniques. Thus, dynamic oscillations are studied about the three main rotational axes. Additionally, the mechanical vibrations of the systems are analysed in different flow conditions to understand the effects of collateral rotors, in the case of SSRs, or the implementation of lateral and longitudinal stabilisers, in the case of SR turbines.

The initial evaluation of the dynamic response of CRR turbines (Chapter 5) demonstrated that 2-2 C presented an inadequate dynamic response (e.g. prominent yaw angles and mechanical vibrations were located in the "extremely rough" area of the vibration tolerance charts). Thus, this work is focused on investigations of three other CRR prototypes (i.e. 2-3 CRR, 3-3 CRR and 3-4 CRR configurations). In order to avoid confusion during the presentation of the results the following convention is utilised during this chapter:

- nB SR - n Bladed Single Rotor Turbine; where n represents the number of blades (e.g. 1, 2, 3, etc.).
- 2-3 CRR - 2-3 Contra Rotating Rotor Turbine; where the first and second index refers to the upstream and downstream rotor, respectively.
- 3-3 CRR - 3-3 Contra Rotating Rotor Turbine; where the first and second index refers to the upstream and downstream rotor, respectively.
- 3-4 CRR - 3-4 Contra Rotating Rotor Turbine; where the first and second index refers to the upstream and downstream rotor, respectively.
- 2-2 SSR - 2-2 Counter Rotating Rotor Turbine (Side by Side Rotors); where the first and second index refers to the right and left rotor, respectively.
- 3-3 SSR - 3-3 Counter Rotating Rotor Turbine (Side by Side Rotors); where the first and second index refers to the right and left rotor, respectively.

The rotor blades were composed of Veroblue resin as a consequence of the use of rapid prototyping techniques. This allowed the opportunity to induce and observe blade failure during the test programme. Tensile tests were undertaken to obtain the mechanical properties of the blade material in order to complete a stress analysis of the blade profile.

This chapter is organised as follows: Section 6.2 outlines the blade profile selection, the blade manufacturing process, the mechanical properties of the resin utilised and the results of the

blade stress analysis. Section 6.3 describes the mechanical design of the system and the instrumentation used in the test program. Section 6.4 and 6.5 present the results of the dynamic oscillations and mechanical vibrations of the turbine prototypes during normal operation and "blade failure mode", respectively. Finally, a brief summary of the results is given in in Section 6.6.

6.2 Rotor Selection and Blade Manufacture

As in the previous chapter, the rotor diameter was set to $0.3\,\mathrm{m}$ in order to maintain the blockage ratio presented in Section 5.2.2 and the specifications of Section 4.4.1. On this occasion, the experiments were entirely carried out in the towing tank in order to accommodate the dimensions of the SSR turbine configuration. The main difference between the previous activity (Chapter 5) and the work presented in this chapter is that the rotor now used properly configured turbine blades with the NREL S814 airfoil profile (Section 4.4.2). This profile was chosen partly due to its thick root section (Somers and Tangler, 1995), and because of its insensitivity to roughness enabling the aerofoil to maintain a high lift coefficient, as described in Section 4.4.2.

In order to fulfil the specified methodology of Section 4.4.2, a stress analysis was undertaken to assess the performance of the blade material under the specific flow conditions of the tests programme.

6.2.1 Blade Manufacture

A 3D printer was utilised to manufacture the blade sections. During the process, the material (a photo-polymer resin) was spread in a series of layers according to the geometrical properties of the object, creating an accurate profile to a tolerance of $\pm 0.016\,\mathrm{mm}$ (Cognity, 2012). In order to carry out the blade stress analysis, the mechanical properties of the material were obtained from Object-Geometries (2010) and are shown in Table 6.1. It was necessary to verify the information taken from Object-Geometries (2010) for two reasons. Firstly, to the author's knowledge there is no evidence in the present academic literature of the material's stress-strain curves. Secondly, the properties of the object produced will change according to the sequence used to produce the piece. Therefore, four specimens (Figure 6.1) were used to determine the stress-strain characteristics of the Veroblue material; the specimens were printed in the same positions as used for the turbine blades. The results are presented in the following section.

Property	ASTM	Metric	Metric
Tensile Strength	D-638-03	MPa	55.1
Modulus of Elasticity	D-638-04	MPa	2740
Elongation at Break	D-638-05		20%
Flexural Strength	D-790-03	MPa	83.6
Flexural Modulus	D-790-04	Mpa	1983
Compressive Strength	D-695-02	Mpa	79.3
Izod Notched Impact	D-256-06	J/m	23.6
Shore Hardness	Scale D	Scale D	83
Rockwell Hardness	Scale M	Scale M	81
HDT at 0.45 Mpa	D-648-06	C	48.8
HDT at 1.82 MPa	D-648-07	C	44.8
Tg	DMA, E”	C	48.7
Ash Content	NA		% <0.3
Water Absorption	D570-98 24 Hr		1.54%

Table 6.1: VeroBlue Resin Properties, taken from (Object-Geometries, 2010).

Figure 6.1: Specimen.

6.2.2 Material Tensile Strength Tests

The test consisted of the application of a continuous and incremental tensile load to the specimen until failure was presented. Through the entire duration of the process, the corresponding elongation and load applied on the specimen were recorded to determine the strain – stress curves (Rosler et al., 2007). The curves, in turn, were used to obtain mechanical parameters such as the ultimate tensile strength (UTS), the modulus of elasticity, yield strength, the fracture point and so on. The shape of the specimen is depicted in Figure 6.1. Its dimensional characteristics are found in Appendix A.

The results obtained from the four tensile strength tests show a relatively linear behaviour in the first part of the curve. Then, the specimen exhibits necking (Point A, Figures 6.3(a) and (b)), followed by a long process of cold drawing (Point B, Figures 6.3(a) and (b)). Usually during this process the molecules of the thermoplastic materials align to the direction of the applied stress (Rosler et al., 2007). Then, the process continues until the specimen reaches a fully “cold drawn” point where the material presents a “strain hardening” characteristic (Nicholson, 2006). In the case of the Veroblue, the specimen suffers fracture (Point C, Figures

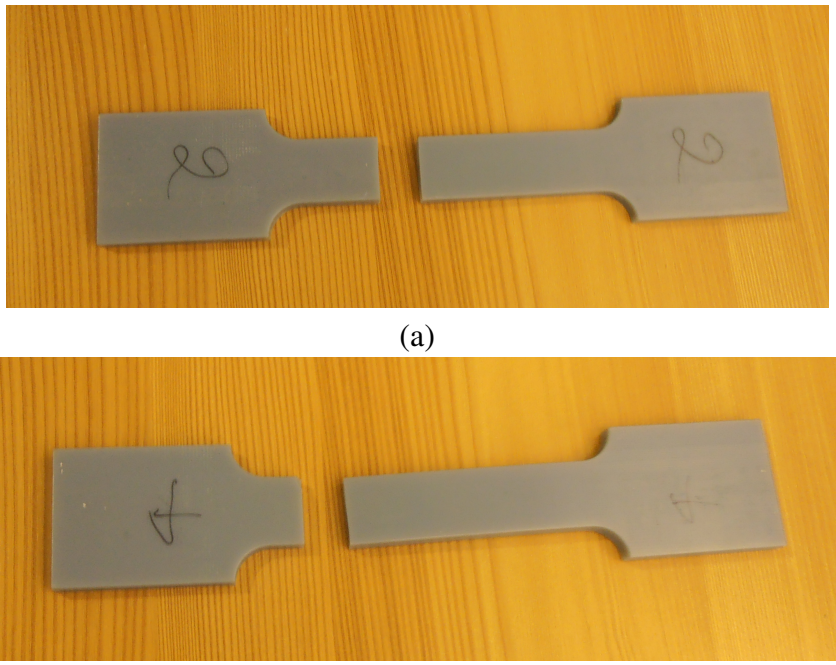

(a)

(b)

Figure 6.2: Specimens after tensile strength test: a) Test 2 and b) Test 4.

6.3(a) and (b)) before reaching the fully cold drawn point, which differs slightly from the normal behaviour presented by polymers (Figure 6.4). Despite this, the stress-strain curves depicted in Figures 6.3(a) and (b) show a typical pattern for thermoplastic materials (Figure 6.4).

Trantina and Nimmer (1994) established that the yield strength of a material is usually found at the point A of Figures 6.3(a) and (b), and that the yield point should be considered as the limit point in the stress analysis instead of the UTS. However, the first part of the stress-strain curve in Figures 6.3(a) and (b) could be considered linear and the modulus of elasticity can be obtained from this region. It was found that the UTS and the modulus of elasticity were 12% and 20% lower than those quoted in Table 6.1, respectively. The next section describes the methods used to evaluate the blade loads for a range of flow conditions.

6.2.3 BEM Analysis

Before a stress analysis is carried out, the external forces applied to the blade profile must be estimated. There are of course a number of techniques to predict the loads on tidal turbine rotors. For time-averaged loads the boundary element model (Baltazar et al., 2005) and the application of the Reynolds Averaged Navier-Stokes equations, usually applied through Computational Fluid Dynamic techniques (O'Doherty et al., 2009), are commonly employed. A relatively simple approach can be utilised, as recommended by the EquiMar protocols (Sec-

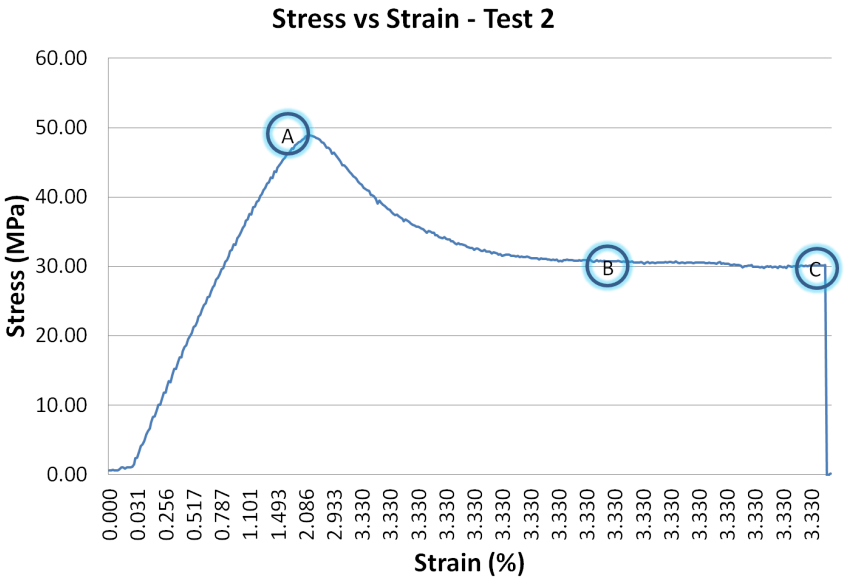

(a)

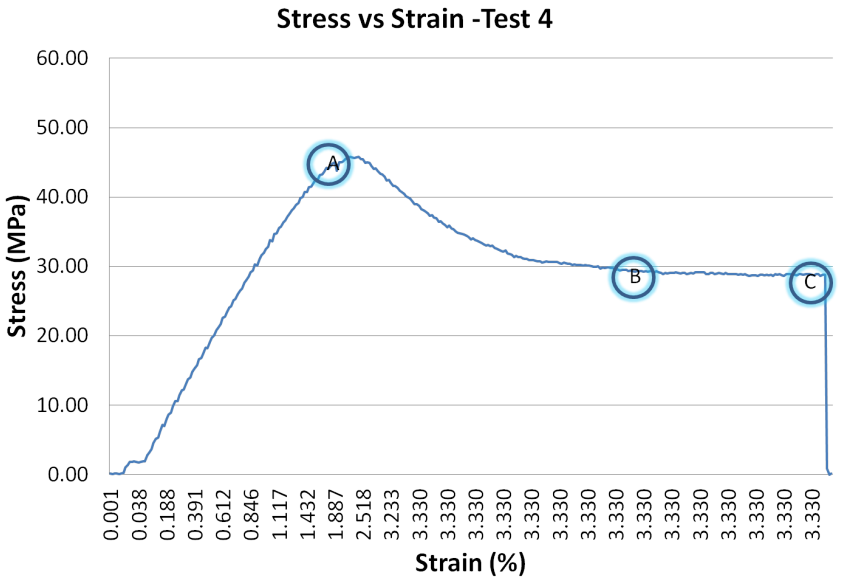

(b)

Figure 6.3: Stress vs Strain Curves: a) Test 2 and b) Test 4.

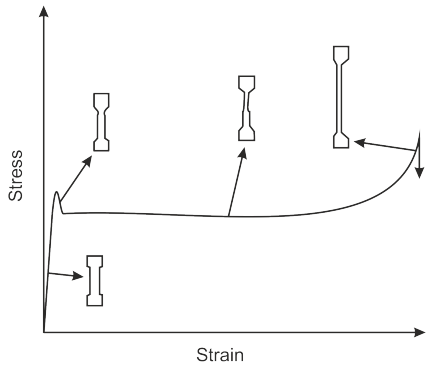

Figure 6.4: Typical thermoplastic stress-strain behaviour.

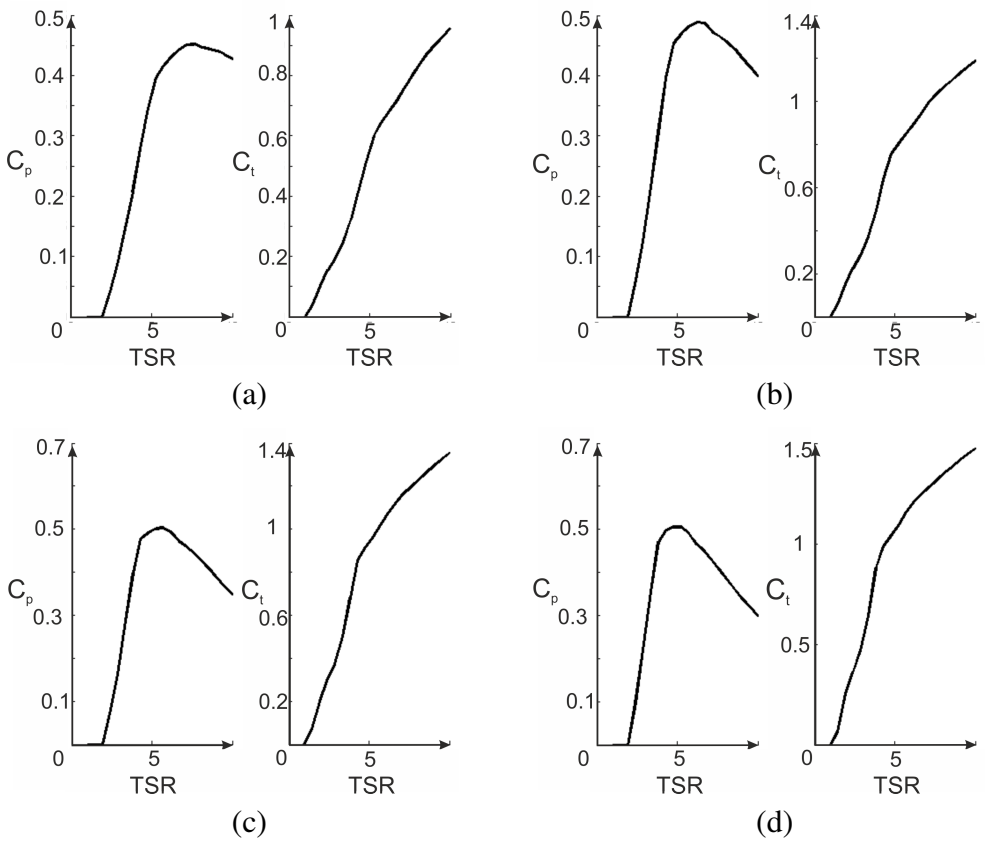

Figure 6.5: C_p curves for SR Turbines with different Number of Blades: a) 2 Bladed, b) 3 Bladed, c) 4 Bladed and d) 5 Bladed, from BEM.

No. Blades	TSR	C_p	C_t
2	7.6	0.45	0.79
3	6.2	0.48	0.89
4	5.7	0.5	1.01
5	5	0.5	1.06

Table 6.2: Optimum Operational Conditions of SR Turbines according to BEM theory.

tion 4.4.4). More complex codes are available for predicting cyclic loads which might arise from misalignment with the flow or velocity shear gradients (Jonkman and Buhl, 2005). But in tidal streams the unsteady loads are likely to be dominated by local turbulence which is much difficult to predict.

In this study, the application of BEM codes permitted the calculation of the steady loads on the blade elements for single-rotor turbines; and at the same time, the prediction of characteristic C_p-λ and C_t-λ curves for each solidity. The optimum operational conditions expected for each of the SR turbines are summarised in Figure 6.5 and Table 6.2.

The corresponding loads were estimated using the optimum TSR values. The concentrated

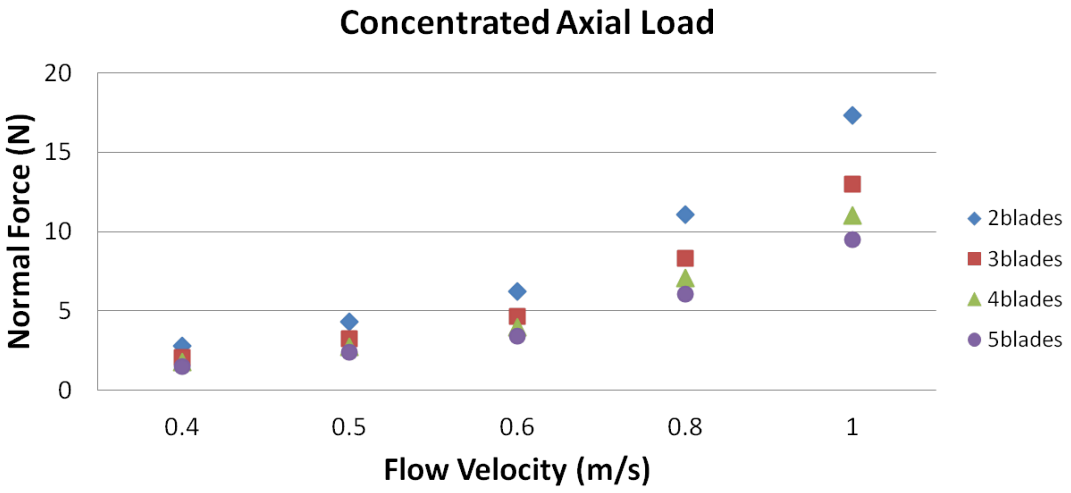

(a)

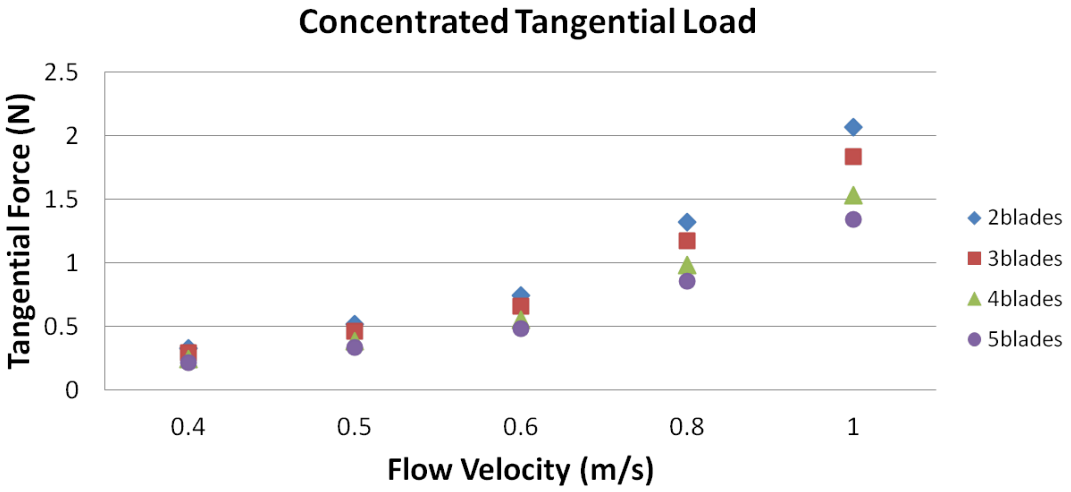

(b)

Figure 6.6: Blade Loads: a) Normal Load and b) Tangential Force.

steady forces are depicted in Figure 6.6(a) and (b). Finally, a stress analysis was carried out to obtain stress distributions along the blade length and to estimate the magnitude of blade deflections. The results of the stress analysis are summarised in the following section.

6.2.4 Stress analysis

Following the procedure outlined in Section 4.4.2, the integrity of the blade profiles was studied through a stress analysis. This was undertaken within the stress analysis suite of Autodesk Inventor 2011 using the information obtained in Sections 6.2.2 and 6.2.3. Two important features were compared throughout the investigation, the stress concentration along the blade and the blade deflection at various flow conditions.

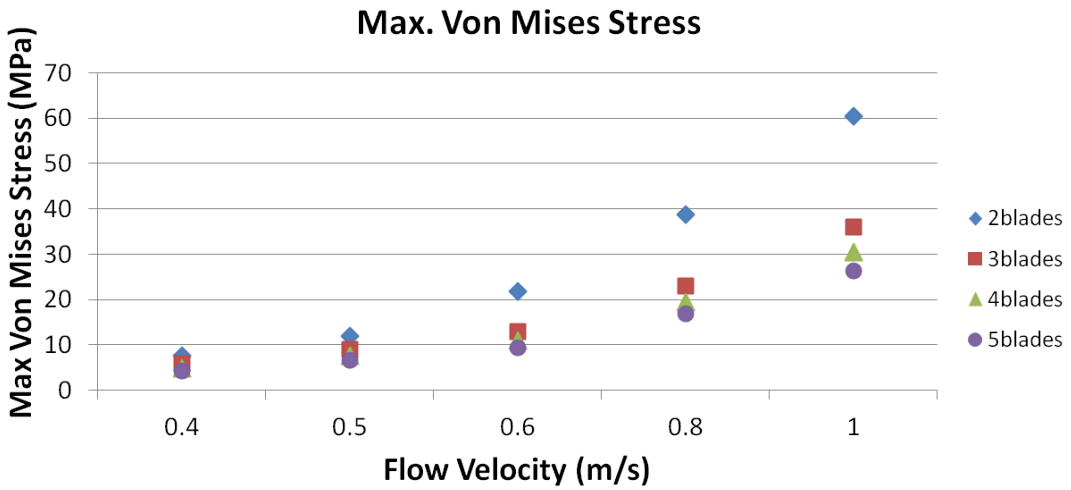

Figure 6.7: Maximum Von Mises Stress.

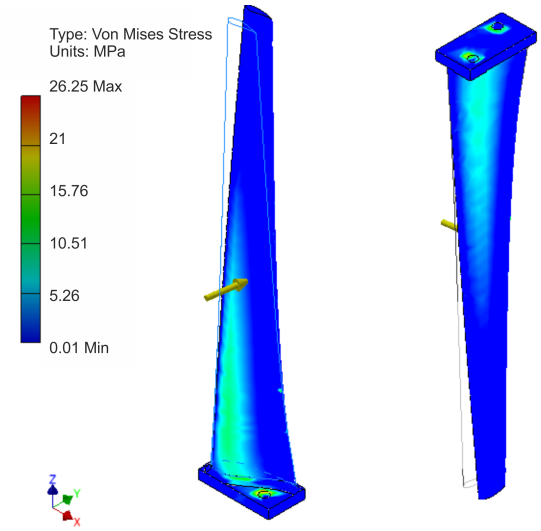

Figure 6.8: Von Mises Stress Distribution.

As stated by (Yuan et al., 2009), the highest bending loads in a turbine blade are usually located at the root connection. The turbine blades used here increased steadily in chord length and thickness from tip to root; the blade root was further reinforced by implementing a fillet between the blade root and the flat plate which attached to the hub.

As expected, the maximum stresses were observed in the 2 bladed SR configuration at a tow speed of 1 $^{\mathrm{m}}/_{\mathrm{s}}$ (Figure 6.7). Significant blade deformation is present at velocities higher than 0.5 $^{\mathrm{m}}/_{\mathrm{s}}$; similar levels of deformation happened at 0.6 $^{\mathrm{m}}/_{\mathrm{s}}$ for the 3 bladed configurations and 0.8 $^{\mathrm{m}}/_{\mathrm{s}}$ for the 4 and 5 bladed arrangements. In Figure 6.7, it is observed that the maximum stress concentration is located at the root section, and in the connection of the blade to the root. Overall, it was concluded that no blade failure would be expected at operational conditions ≤ 0.6 $^{\mathrm{m}}/_{\mathrm{s}}$, except for the 2 bladed SR case.

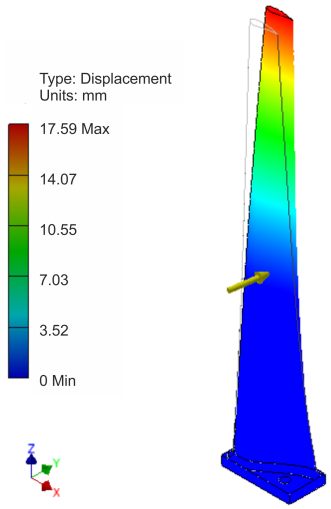

Figure 6.9: Displacement Distribution.

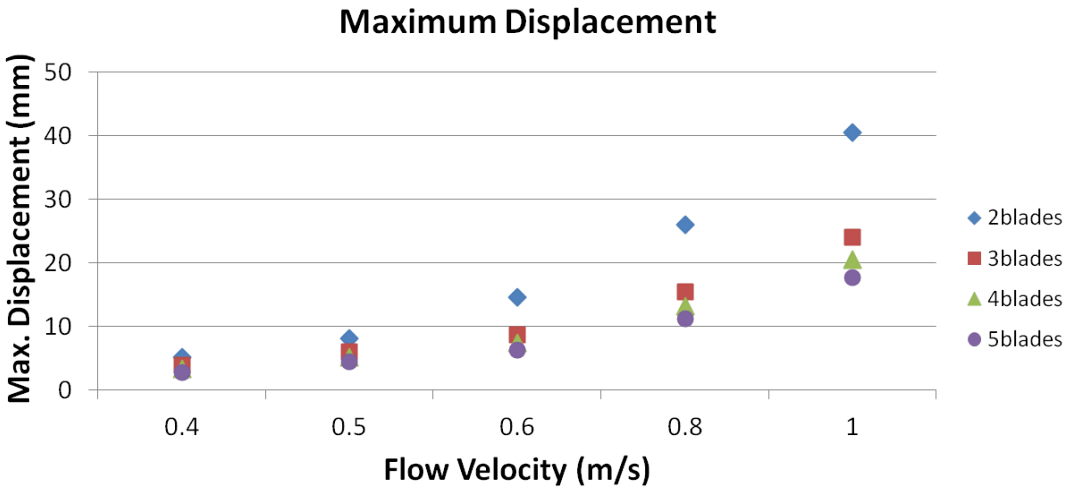

Figure 6.10: Maximum displacement at the blade tip.

As expected, the deflection of the blade increases gradually from root to tip (Figure 6.9). Blade deflections increased progressively with the flow velocity (Figure 6.10).

6.3 Mechanical Design, Instrumentation and Other Features

Following the procedure in Section 4.4.3, the Reynolds number was calculated to range between 4.5×10^4 and 8.97×10^4 for towing speeds of $0.4\,^{\mathrm{m}}/_{\mathrm{s}}$ to $0.8\,^{\mathrm{m}}/_{\mathrm{s}}$, respectively. The Froude Number was calculated to be 0.158 and 0.317, respectively for the same flow conditions.

Turbines' Configuration (S814)	Rotor's Solidity
2B SR	0.04
3B SR	0.07
4B SR	0.09
5B SR	0.11
2-3 CRR	0.11
3-3 CRR	0.13
3-4 CRR	0.16
2-2 SSR	0.04
3-3 SSR	0.07

Table 6.3: Solidity of the Contra Rotating Turbines (S814).

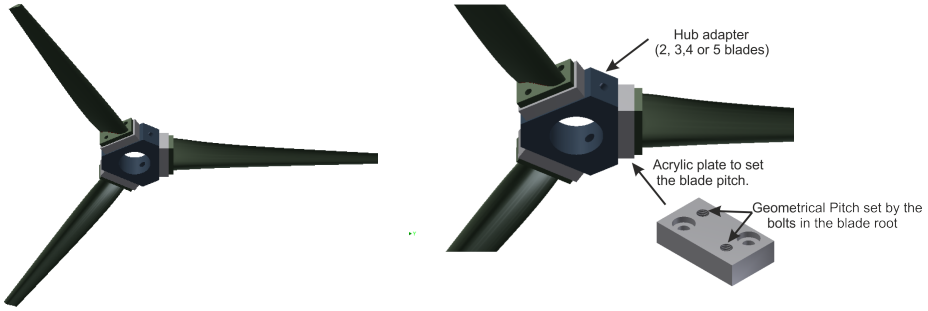

(a) (b)

Figure 6.11: Fixing mechanism: a) 3 Bladed Configuration and b) Pitch Setting Sketch.

The solidity ratio calculated for SR and CRR turbine configurations is depicted in Table 6.3. It is clear that the 3-3 and 3-4 CRR arrangements have the largest solidity ratios amongst all the rotor arrangements (in the same way as those in Chapter 5).

The mechanical design and instrumentation described in the previous experiments (Chapter 5) was once more used here. The hub sections were redesigned to fit up to 5 blades on the rotor. The technical drawings can be found in Appendix A.

In order to provide lateral and vertical stability for the SR prototypes, flat aluminium tails were fitted to the rear buoyant sections of the turbine (Figure 3.2). The vertical tail fin measured $90\,\mathrm{mm} \times 200\,\mathrm{mm}$ and the horizontal fin $75\,\mathrm{mm} \times 105\,\mathrm{mm}$.

Finally, a data acquisition system similar to the one described in Section 4.5.6 was utilised. This time, an Intel(R) Core (TM) 2 Duo (model P7450) processor with a CPU clock speed of 2.13 GHz, with 3.6 GB in RAM running under Windows 7 and Labview 8.5 was employed. A sampling rate of 200 Hz was set throughout the experiments. The reason to use a larger sampling frequency this time than in the experiment undertaken in Chapter 5, was to identify the peak frequencies of each energy spectrum with more clarity. A FIR filter composed of a Hamming Window was included in the signal processing stage (see Section 4.6).

6.4 Results and Discussion of the Dynamic Response

The results of the investigation are discussed in the following sections. As in the previous chapter, the results time domain data are presented in terms of common statistical parameters: mean and standard deviation (Section 4.6.2). The results of the FFT analysis are presented as energy spectra (as discussed in Sections 4.6.3 and 4.7). As before, the terminology refers to $(1x)$ as the angular frequency of the turbine rotor. If several harmonics of the rotational velocity appear in the energy spectra the indication will continue as 2x, 3x, 4x, and so on. So, the following terminology is employed for each rotor type:

- 1xu - Frequency corresponding to the upstream rotor in the case of CRR turbines.
- 1xd - Frequency corresponding to the downstream rotor in the case of CRR turbines.
- 1xbb - Frequency corresponding to blade interactions.
- 1x - Frequency corresponding to the rotor in the case of SR turbines.
- 1xr - Frequency corresponding to the right rotor in the case of SSR turbines.
- 1xl - Frequency corresponding to the left rotor in the case of SSR turbines.

6.4.1 Dynamic Response: SR Turbines

Since the torque created by a single-rotor turbine will tend to generate a continuous rotation of the device, these turbines were equipped with longitudinal and lateral stabilisers. The dimensions of the stabilisers were adequate to compensate the torque generated by 3 bladed SR turbines Figure 6.12(a); but it was not sufficient for rotors with 4 or more blades which generate higher torque (Figure 6.12(b)). However, as observed in the frequency analysis, the use of stabilisers induced mechanical vibrations in the turbines. As visible in Figures 6.13 and 6.15, increasing flow velocity produces resonant frequencies (and related harmonics) which are only seen in tests on single turbines: it is speculated that these may be related to the behaviour of the stabilisers fitted to the turbine. The same peak frequencies appeared in the energy spectra for the same flow velocities, independent of rotor configuration.

3 bladed SR roll and pitch energy spectra exhibit the $1x$ frequency of the rotor's angular velocity (Figure 6.13 and 6.14), becoming more evident as the tow velocity rises. The same is seen in the spectrum of the 5 bladed SR cases (Figure 6.15(a)); however, in this case the time domain results showed a continuous roll for a longer time period before reaching a stable position. Therefore, the amplitude of the spectra becomes muddled (Figure 6.15(b)), showing

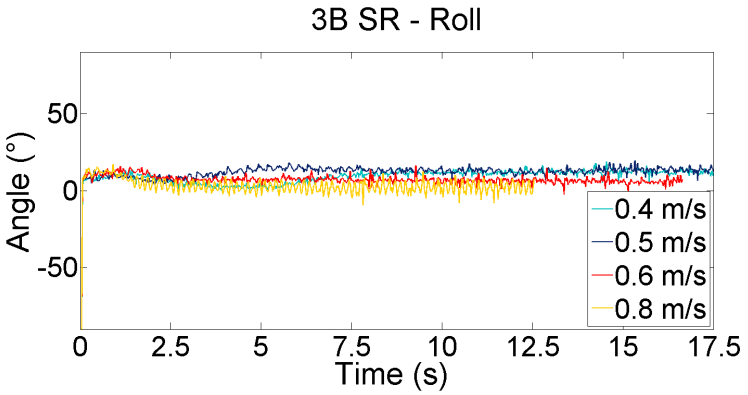

(a)

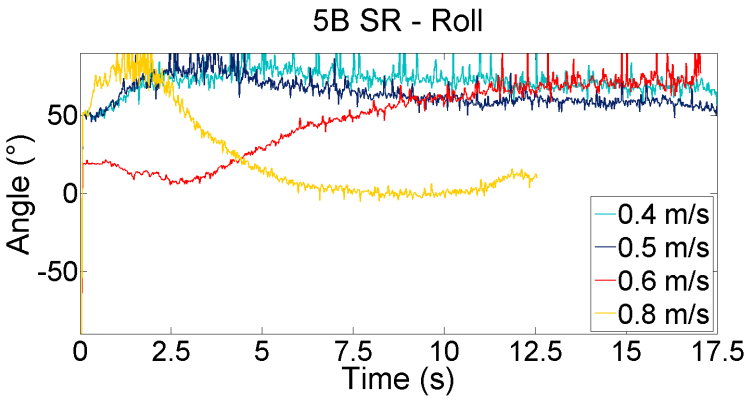

(b)

Figure 6.12: Roll motion of a)3 Bladed Single Rotor Turbine and b)5 Bladed Single Rotor Turbine.

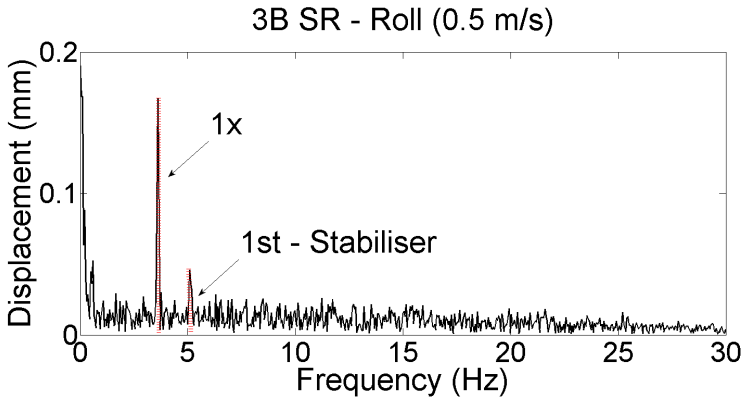

(a)

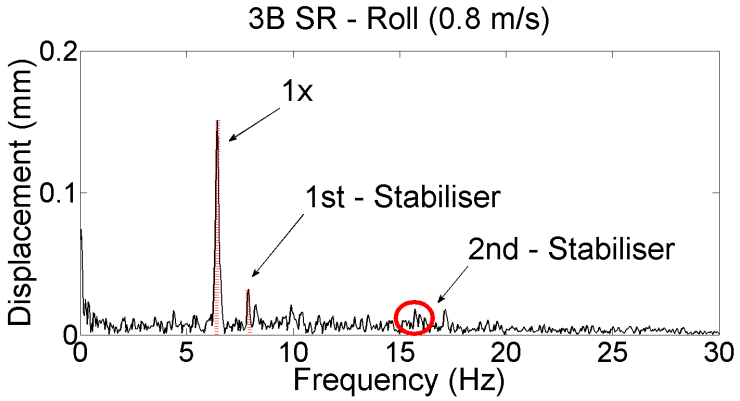

(b)

Figure 6.13: Roll Energy Spectrum of the 3 Bladed Single Rotor Turbine at: a)$0.5\,{}^{\mathrm{m}}/_{\mathrm{s}}$ and b)$0.8\,{}^{\mathrm{m}}/_{\mathrm{s}}$.

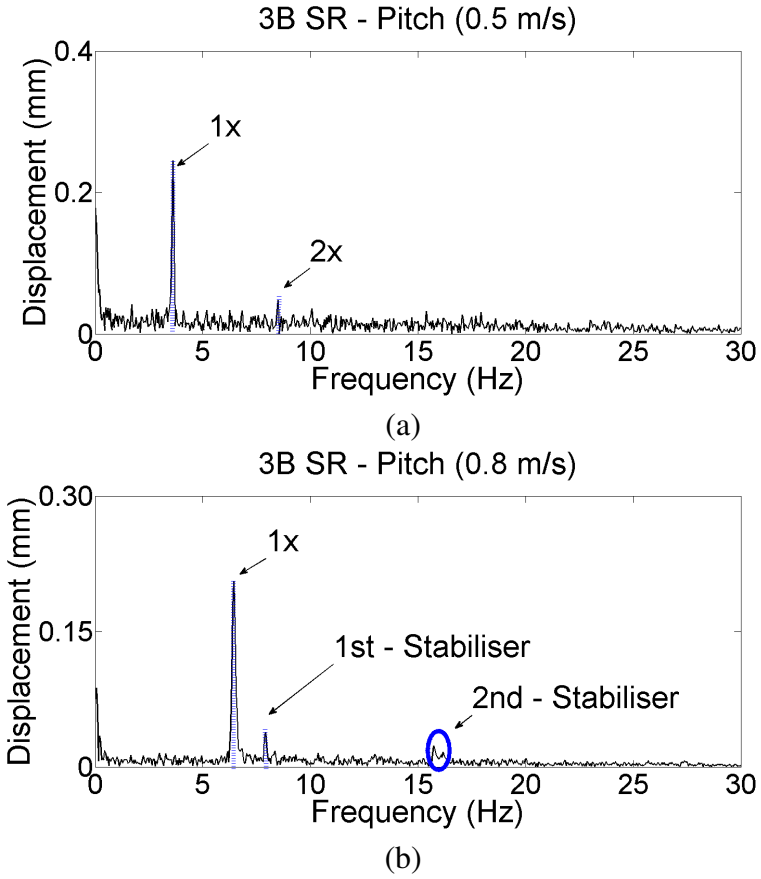

Figure 6.14: Pitch Energy Spectrum of the 3 Bladed Single Rotor Turbine at: a)$0.5\,^{\mathrm{m}}/_{\mathrm{s}}$ and b)$0.8\,^{\mathrm{m}}/_{\mathrm{s}}$

a faulty condition of the turbine's performance. The appearance of other frequencies, such as $2x$ is noted on also visible in some occasions, denoting mechanical backlash. Moreover, the 6th harmonic (suggesting in extreme cases a mechanical failure) is seen in Figure 6.15(b). The shaft torque spectrum exhibits similar frequencies to the roll spectrum (Figure 6.18).

As expected, the turbines aligned more accurately in pitch and yaw as the tow velocity increased (Table 6.4). As distinct from the roll and pitch spectra, Figures 6.17(a) and (b)) indicate mechanical excitation due to hydrodynamic forces (Piersol and Paez, 2002) signified by the existence of $2x$, $3x$, and $5x$ frequencies in the yaw motion.

Finally, it was found that for the SR turbines the values of the coefficients C_p and C_t were around 0.3 and 0.75, respectively. As the turbine aligned to the flow in both pitch and yaw directions, the experimental values of power and thrust approximated to the predictions generated by the BEM; for example, in the case of the 3 bladed SR turbine, the turbine presented C_t values of 0.7 at the highest towing speed as against a predicted value of almost 0.9. C_p values were also lower than predicted, by a similar percentage. C_p and C_t curves of each of the single rotor turbines can be found in Figure 6.19.

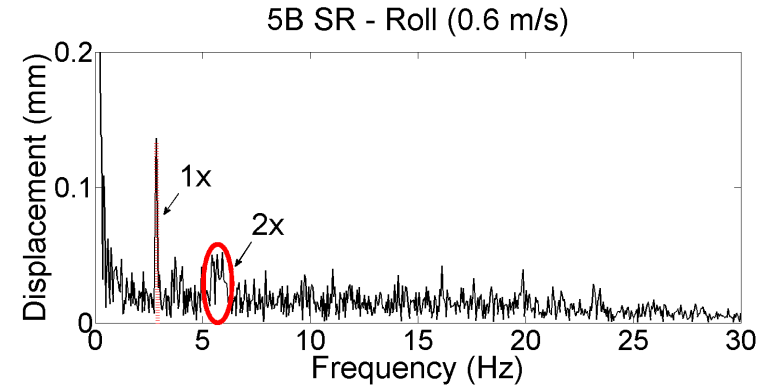

(a)

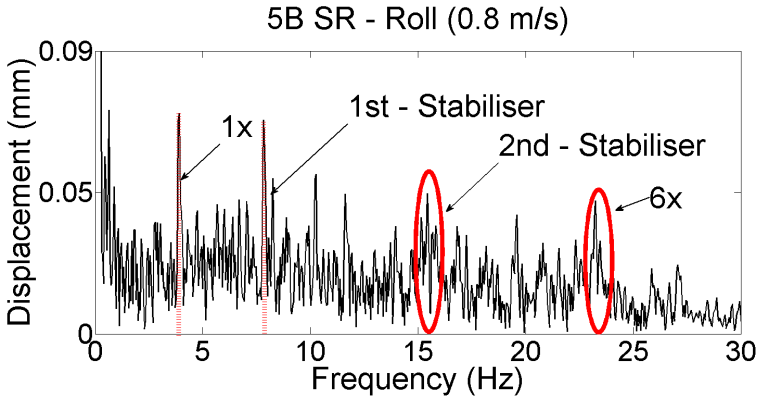

(b)

Figure 6.15: Roll Energy Spectrum of the 5 Bladed Single Rotor Turbine at: a)$0.6\,^{\mathrm{m}}/_{\mathrm{s}}$ and b)$0.8\,^{\mathrm{m}}/_{\mathrm{s}}$.

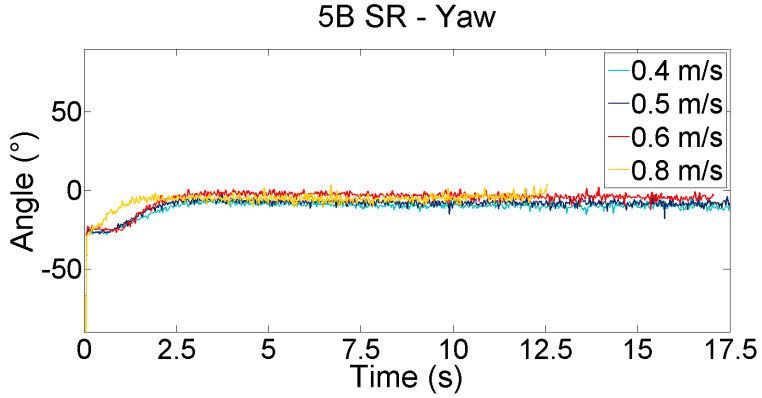

Figure 6.16: 5 Bladed Single Rotor Turbine during Yaw Motion.

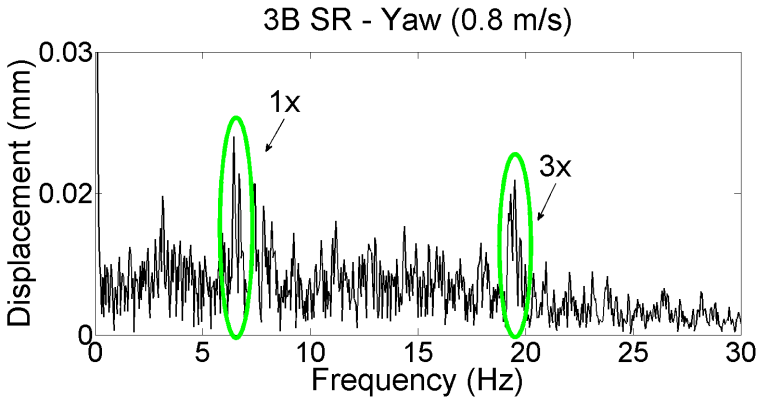

(a)

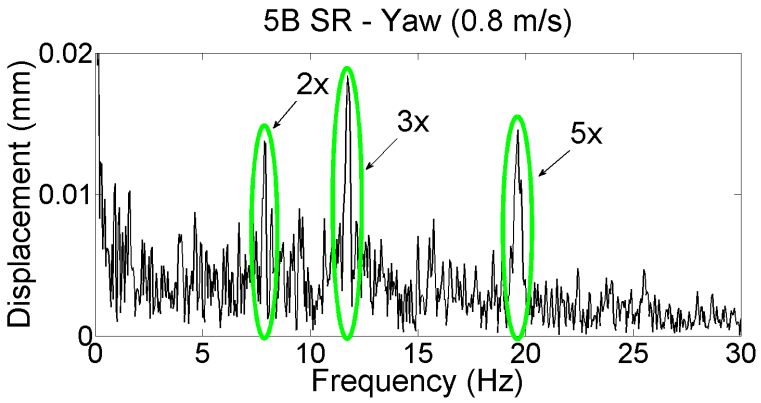

(b)

Figure 6.17: Yaw Energy Spectrum of: a)3 Bladed Single Rotor Turbine and b)5 Bladed Single Rotor Turbine at $0.8\,^{\mathrm{m}}/_{\mathrm{s}}$.

SINGLE ROTOR (SR)								
Tow Velocity	0.4 m/s	0.5 m/s	0.6 m/s	0.8 m/s	0.4 m/s	0.5 m/s	0.6 m/s	0.8 m/s
	Roll Mean (°)				Roll Standard Deviation (°)			
2B SR	80.08	78.64			5.18	11.30		
3B SR	11.78	13.11	6.59	1.97	1.39	1.69	1.67	3.14
4B SR	67.99	67.47	76.76	71.49	4.40	5.02	7.53	7.22
5B SR	71.73	61.64	60.90	14.41	10.03	11.37	24.58	29.45
	Pitch Mean (°)				Pitch Standard Deviation (°)			
2B SR	-16.71	-12.90			1.57	2.14		
3B SR	-18.71	-20.97	-10.37	-0.32	3.20	4.84	2.82	5.73
4B SR	-21.96	-21.30	-10.39	8.12	2.33	3.09	3.20	18.12
5B SR	-19.87	-16.91	13.42	22.00	7.65	4.13	8.40	24.11
	Yaw Mean (°)				Yaw Standard Deviation (°)			
2B SR	-2.70	-3.52			1.19	1.46		
3B SR	-4.73	-4.74	-3.79	-2.56	1.49	1.33	1.56	1.60
4B SR	-3.22	-3.22	-2.51	-1.09	1.47	1.43	1.46	1.64
5B SR	-9.51	-7.97	-3.61	-5.00	1.39	1.44	1.57	1.87

Table 6.4: SR Turbine Mean and Standard Deviation.

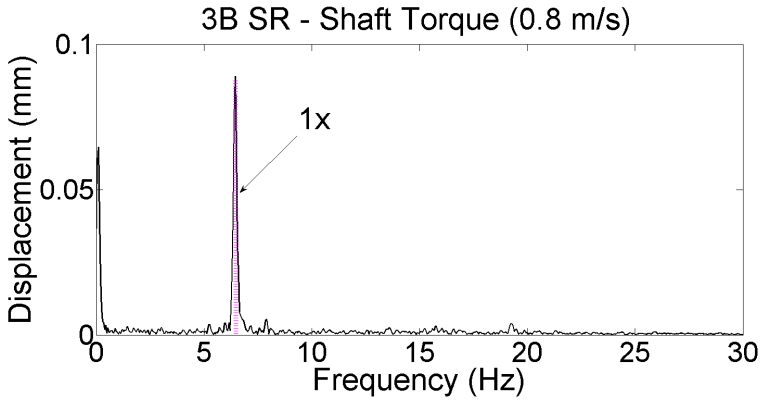

(a)

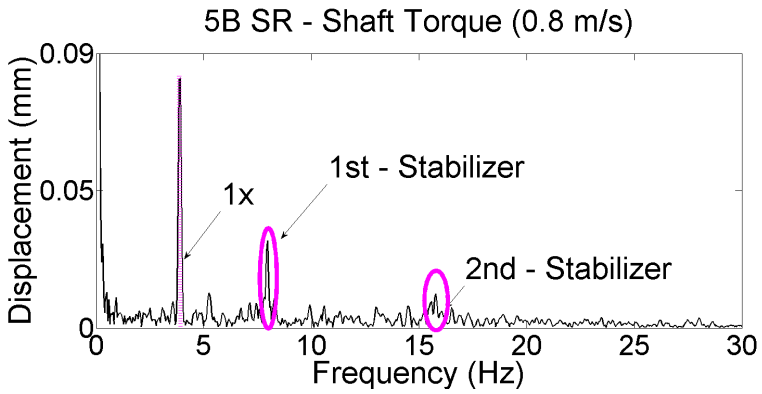

(b)

Figure 6.18: Roll Energy Spectrum of the a) 3 Bladed Single Rotor Turbine and b) 5 Bladed Single Rotor Turbine at$0.8\,{}^{\mathrm{m}}/_{\mathrm{s}}$.

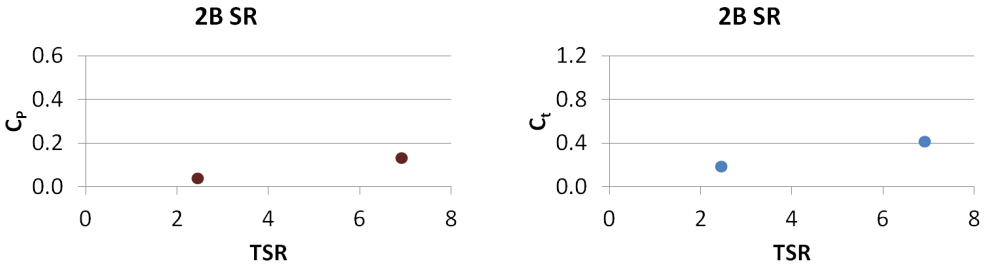

(a)

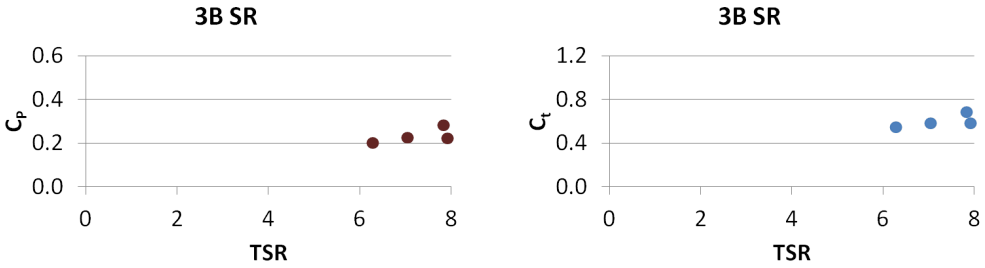

(b)

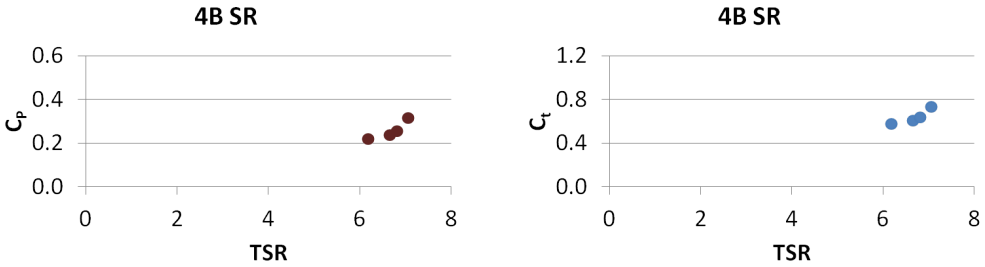

(c)

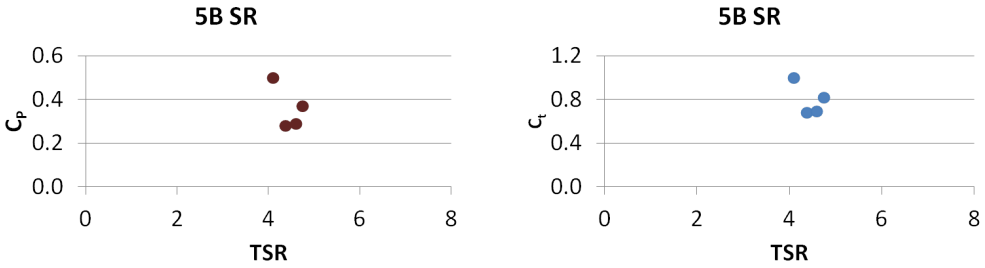

(d)

Figure 6.19: Experimental C_p and C_t curves for SR Turbines with different Number of Blades: a) 2 Bladed, b) 3 Bladed, c) 4 Bladed and d) 5 Bladed.

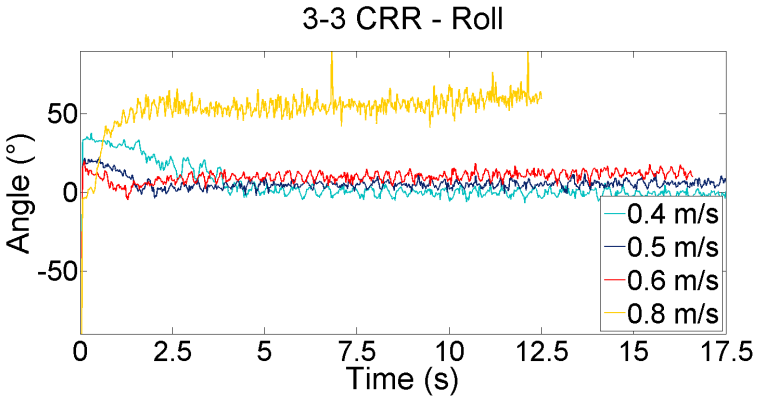

Figure 6.20: 3-3 Contra Rotating Rotor Turbine in Roll Motion

In any turbine, deviations from the theoretical predictions may be expected if it fails to maintain accurate alignment with the flow, either in yaw or pitch. Here the standard deviation values showed that oscillations in yaw and pitch increase with flow velocity, in most of the cases (Table 6.4). From the mechanical vibration analysis (obtained in order to employ the tolerance charts presented in Section 4.7.4), the turbines experienced vibrations of approximately 0.15 mm RMS velocity in pitch and yaw motions; however, this were smaller in yaw motion f (0.02 mm RMS). Such oscillations can affect the mechanical performance of the turbine. Blade deflections under load, as mentioned in Section 6.2.4, were predicted to take place at higher flow rates and might cause the efficiency of the turbine to be further compromised.

6.4.2 Dynamic Response: CRR Turbines

In contrast with SR turbines, contra-rotating turbines can counter-act the reaction torque with the use of a second rotor. To apply a load torque a mechanical brake was operated in the prototypes, which provided a fairly accurate response at low velocities. The torque was more difficult to modulate in other cases creating variation in roll motion, as observed in Figures 6.20 and 6.21.

The roll frequency domain analysis of the 2-3 CRR and 3-3 CRR turbines shows that the dominant frequencies of the energy spectrum are related to the angular velocity of the upstream $(1xu)$ and to a lesser extent, the downstream rotor $(1xd)$(Figure 6.22). The second and third harmonics are also present in the spectra, along with blade interactions which are clearly depicted in both scenarios.

When the turbine experienced balance problems (i.e. the torques exerted by the two rotors were unequal) a different pattern emerged. For example, in Figure 6.23 the amplitude at the frequencies of the upstream and downstream rotor decreased greatly while other harmonics

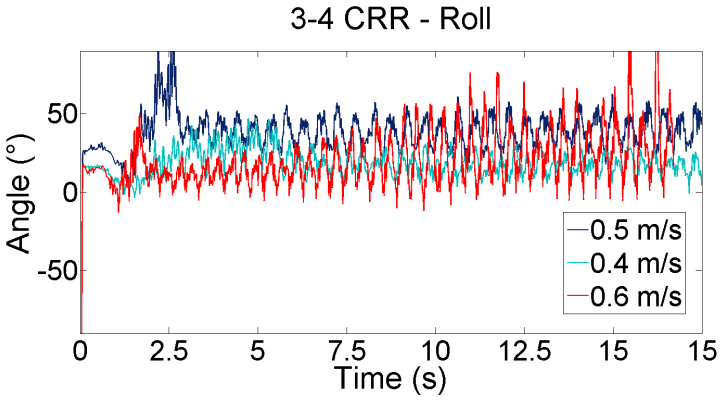

Figure 6.21: 3-4 Contra Rotating Rotor Turbine in Roll Motion.

appeared in the spectrum (e.g. $3xd$ denoting misalignment in the system caused by the downstream rotor). The lack of balance was confirmed by observation that the upstream rotor ran considerably faster than the downstream rotor.

The same effect was seen with 3-4 CRR turbines, where it was observed that the dominant frequency belongs to the downstream rotor$(1xd)$ (Figure 6.24). The reason is that the torque generated by a rotor with higher solidity was more difficult to counter-act with the mechanical brake utilised. The limitations of such brakes can be avoided with the use of electromechanical dynamometer brakes, certainly at larger scales.

In general, pitch alignment improves as the prototypes are tested at higher flow velocities (Figure 6.5). In the FFT analysis, similarities are also observed between the roll and pitch spectra; however, the amplitudes of the peak frequencies in pitch were slightly higher. A noticeable feature was the disappearance of the blade – blade frequency (Figure 6.22(b). At a lower level the frequencies of $5xd$ and $6xu$ are present in the spectrum, suggesting a machine part failure (possibly an early sign of blade failure). A similar pattern is observed in the pitch energy spectrum of the 3-4 CRR turbine; but, it is observed that not a single frequency of the upstream rotor is found in the spectrum, highlighting a balance problem of the rotors (Figure 6.26).

Yaw alignment and yaw oscillations of CRRs are conjectured to be satisfactory for almost all of the situations (Table 6.5). It is clear that the 2-3 configuration are the one which presents highest misalignments amongst the CRR turbines. In the frequency domain analysis, it appears that the devices suffer misalignment problems due to excessive axial looseness $(3x)$, as was observed earlier for SR turbines. An example of this can be shown in Figure 6.28.

Additional information regarding the frequencies of the shaft vibrations is shown in Figures 6.29(a) and (b). It is observed that the amplitudes of the peak frequencies related to the shaft's torque are considerably lower than those perceived in roll motion spectra (e.g. Figure 6.24).

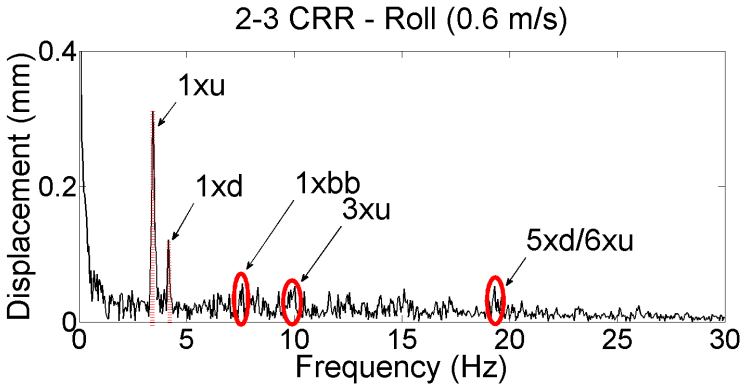

(a)

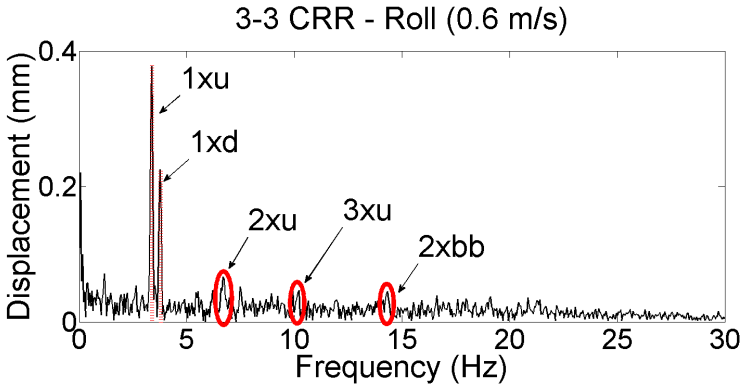

(b)

Figure 6.22: Roll Energy Spectrum of: a) 2-3 Contra Rotating Rotor Turbine and b)3-3 Contra Rotating Rotor Turbine at $0.6\,{}^{\mathrm{m}}/_{\mathrm{s}}$.

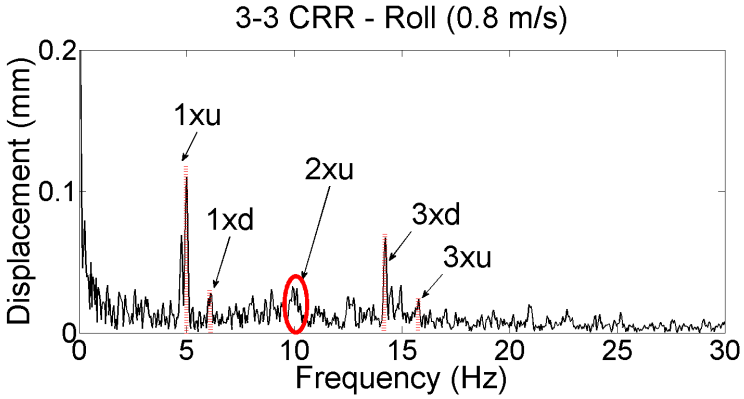

Figure 6.23: Roll Energy Spectrum of the 3-3 Contra Rotating Rotor Turbine at $0.8\,{}^{\mathrm{m}}/_{\mathrm{s}}$.

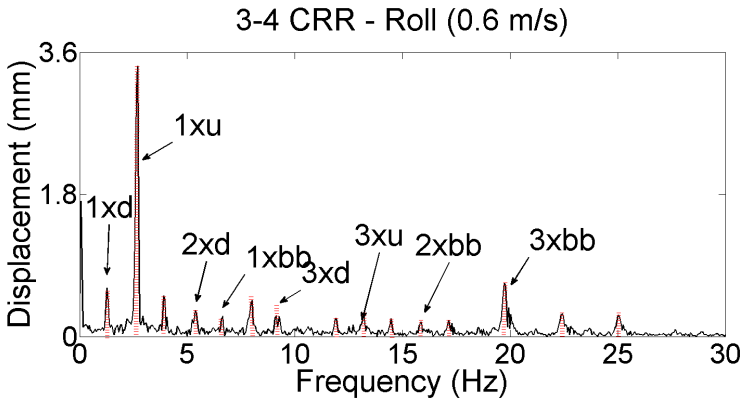

Figure 6.24: Roll Energy Spectrum of the 3-4 Contra Rotating Rotor Turbine at $0.6\,^{\mathrm{m}}/_{\mathrm{s}}$.

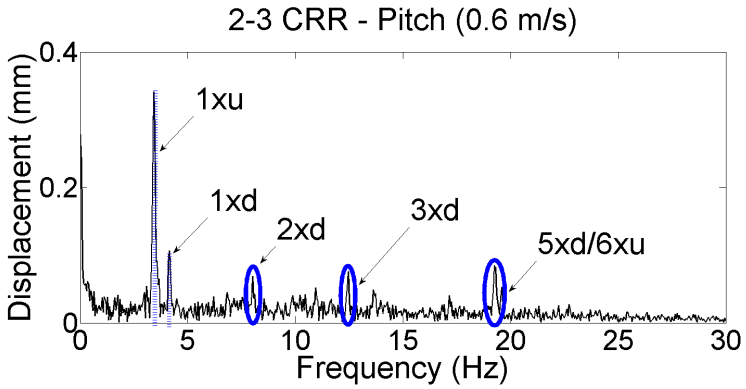

Figure 6.25: Pitch Energy Spectrum of the 2-3 Contra Rotating Rotor Turbine at $0.6\,^{\mathrm{m}}/_{\mathrm{s}}$.

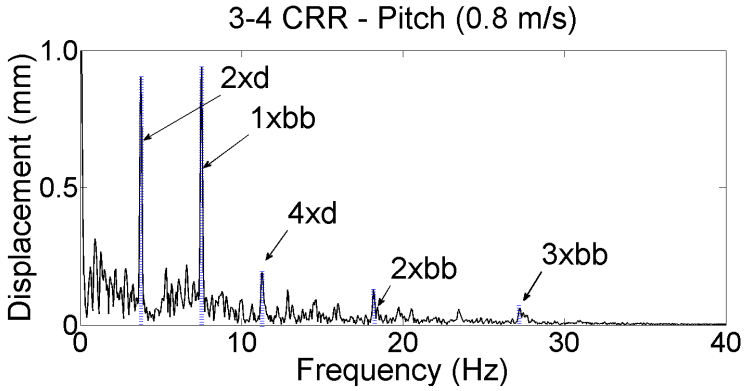

Figure 6.26: Pitch Energy Spectrum of the 3-4 Contra Rotating Rotor Turbine at $0.8\,^{\mathrm{m}}/_{\mathrm{s}}$.

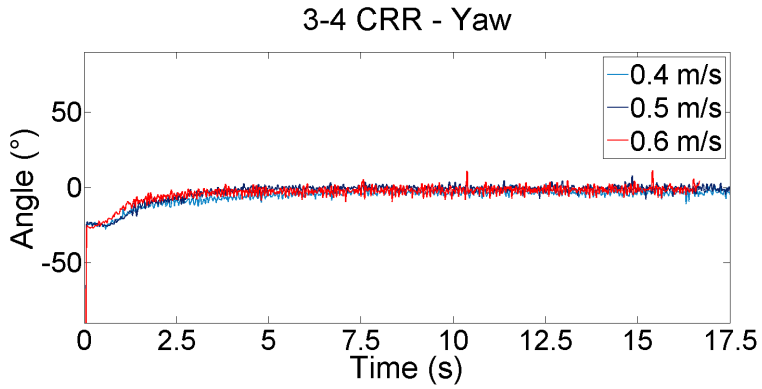

Figure 6.27: 3-4 Contra Rotating Rotor Turbine in Yaw Motion.

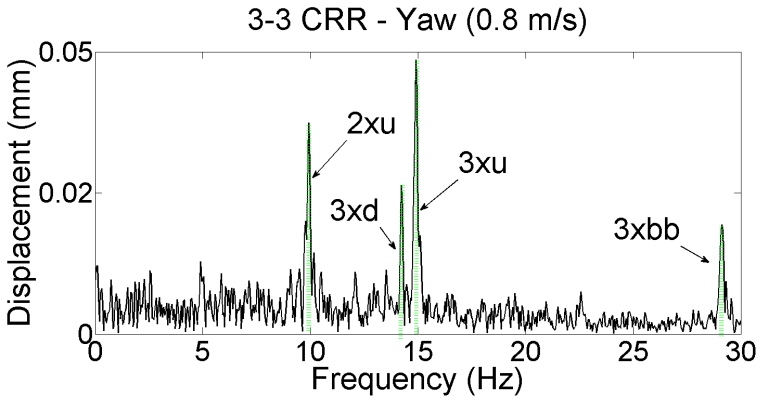

Figure 6.28: Yaw Energy Spectrum of the 3-3 Contra Rotating Rotor Turbine at $0.8\,\mathrm{m/s}$.

CONTRA ROTATING ROTOR (CRR)								
Tow Velocity	0.4 m/s	0.5 m/s	0.6 m/s	0.8 m/s	0.4 m/s	0.5 m/s	0.6 m/s	0.8 m/s
	Roll Mean (°)				Roll Standard Deviation (°)			
2-3 CRR	-1.63	26.44	50.29	**Blade Fail.**	2.87	4.08	3.12	**Blade Fail.**
3-3 CRR	0.21	5.01	10.31	55.73	3.57	2.20	2.75	4.93
3-4 CRR	18.76	38.72	20.87	61.99	7.41	8.79	16.55	18.82
	Pitch Mean (°)				Pitch Standard Deviation (°)			
2-3 CRR	-22.96	-8.89	-2.66	**Blade Fail.**	1.33	1.17	3.43	**Blade Fail.**
3-3 CRR	-23.19	-17.51	-12.33	-8.63	6.24	6.72	7.62	7.44
3-4 CRR	-9.99	-4.49	5.22	26.08	2.40	1.75	3.76	19.44
	Yaw Mean (°)				Yaw Standard Deviation (°)			
2-3 CRR	-5.55	-4.37	-4.23	**Blade Fail.**	1.04	1.46	1.59	**Blade Fail.**
3-3 CRR	-3.13	-2.98	-3.51	-1.82	2.53	2.55	2.52	2.29
3-4 CRR	-4.01	-0.92	-2.35	-2.36	2.27	1.75	2.44	2.19

Table 6.5: CRR Turbine Mean and Standard Deviation.

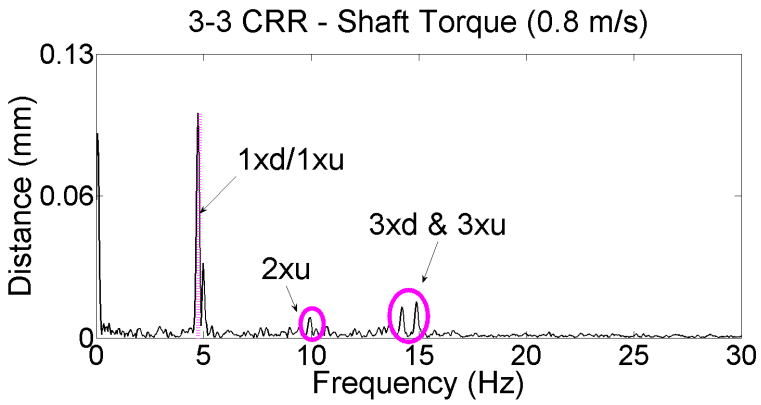

(a)

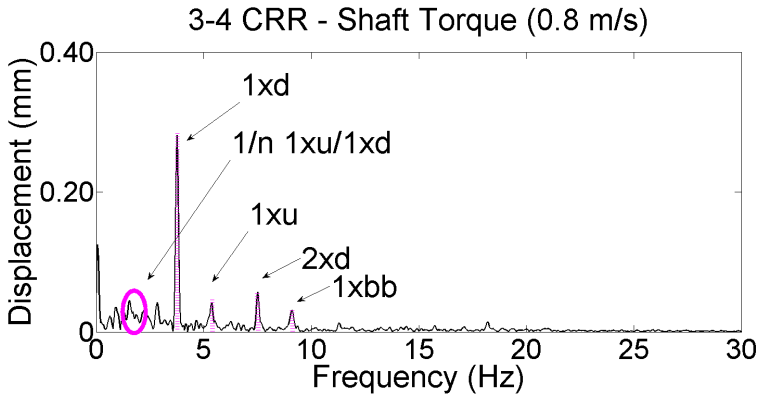

(b)

Figure 6.29: Torsion Energy Spectrum of: a) 3-3 Contra Rotating Rotor Turbine and b) 3-4 Contra Rotating Rotor Turbine at $0.8\,{}^{\mathrm{m}}/_{\mathrm{s}}$.

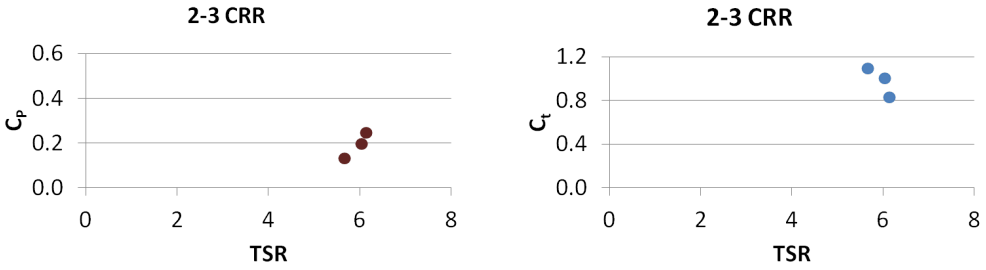

(a)

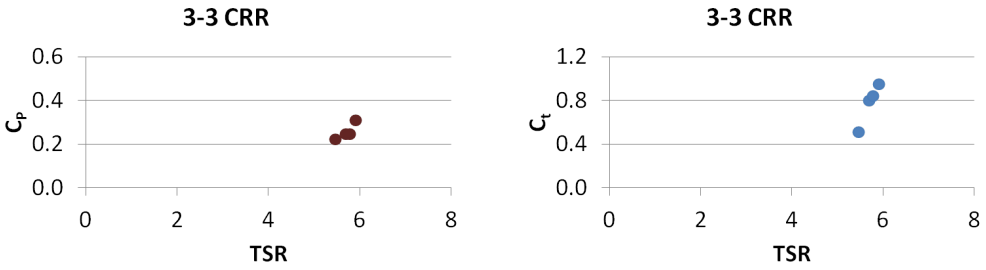

(b)

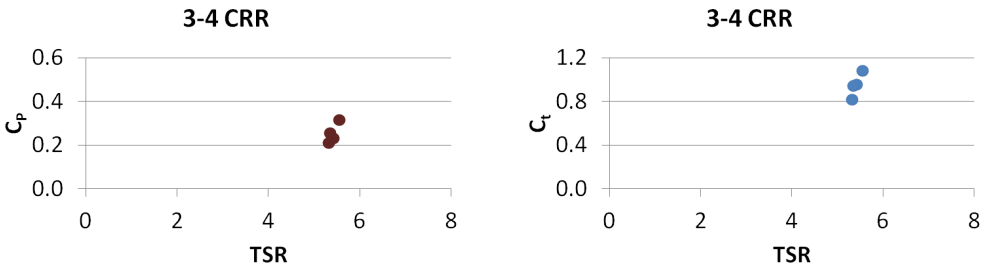

(c)

Figure 6.30: Experimental C_p and C_t curves for CRR Turbines with different Number of Blades: a) 2-3 Configuration, b) 3-3 Configuration and c) 3-4 Configuration.

It was found that the coefficients C_p and C_t of the CRR turbines were about 0.3 and 0.93, respectively. When the magnitudes of thrust and power coefficients were compared to single rotors with the same pitch and yaw characteristics, for example the case of 3-3 CRR turbine and 3-bladed SR turbines, it was found that the former produced 30% more thrust than single rotor turbines. This value was found to be in agreement with the studies undertaken by Kumar et al. (2012) which reported an increase in thrust of 35%. Also, C_p increased by 10%, a similar result to that obtained by O´Doherty et at. (2009). C_p and C_t curves of each of the contra rotating rotor turbines can be found in Figure 6.30.

SIDE BY SIDE ROTOR (SSR)								
Tow Velocity	0.4 m/s	0.5 m/s	0.6 m/s	0.8 m/s	0.4 m/s	0.5 m/s	0.6 m/s	0.8 m/s
	Roll Mean (°)				Roll Standard Deviation (°)			
2-2 SSR	-5.01	-30.35			6.05	8.81		
3-3 SSR	-1.33	1.62	11.13	Blade Fail.	1.33	5.00	7.84	Blade Fail.
	Pitch Mean (°)				Pitch Standard Deviation (°)			
2-2 SSR	-6.25	38.16			2.75	10.36		
3-3 SSR	-18.97	-3.99	5.32	Blade Fail.	1.46	2.07	1.95	Blade Fail.
	Yaw Mean (°)				Yaw Standard Deviation (°)			
2-2 SSR	-9.51	2.89			2.15	6.12		
3-3 SSR	-10.13	-3.84	-1.91	Blade Fail.	1.56	2.27	2.28	Blade Fail.

Table 6.6: SSR Turbine Mean and Standard Deviation.

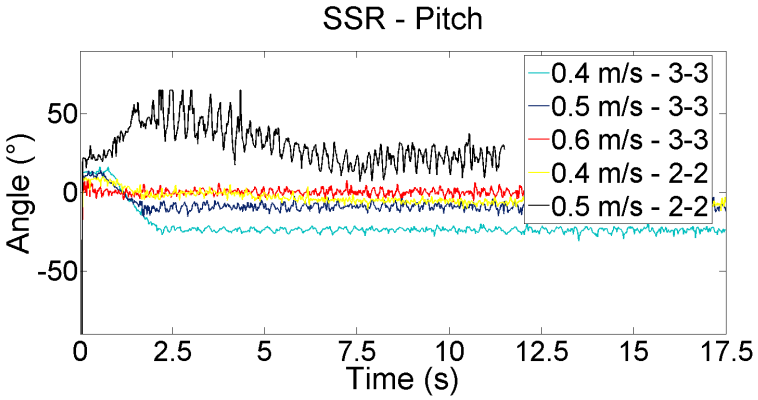

Figure 6.31: Side by Side Rotor Turbines in Pitch Motion.

6.4.3 Dynamic Response: SSR Turbines

In the SSR configuration two similar rotors were placed side by side in the same plane; if set to contra rotate, their net reaction torque can (in theory at least) be reduced to zero. The results show that the 3-3 SSR turbines generally present more satisfactory results than the 2-2 SSRs, being relatively stable through the entire set of trials (Table 6.6). The pitch behaviour follows the same pattern as seen already; the device improves its alignment as the flow velocity increases (Figure 6.31). The same pattern is visualised in yaw motion, and as expected, the 3-3 SRR device aligns with the flow more readily than SR turbines (Figure 6.32).

In the frequency domain results (Figures 6.33 and 6.34), the spectrum of the 3-3 SSR at $0.5\,^{\mathrm{m}}/_{\mathrm{s}}$ shows the first $(1xr)$, second $(2xr)$ and third harmonic $(3xr)$ of the right rotor and the first $(1xl)$ harmonic $(1xl)$ of the left rotor, suggesting a slight misalignment. The effects of vortex shedding are noticed in the spectral analysis even with the use of a streamlined strut (Figure 6.33). It is evident that the yaw spectrum of the 3-3 SSR device running at $0.5\,^{\mathrm{m}}/_{\mathrm{s}}$ contains the $3x$ harmonic of both rotors (Figure 6.34).

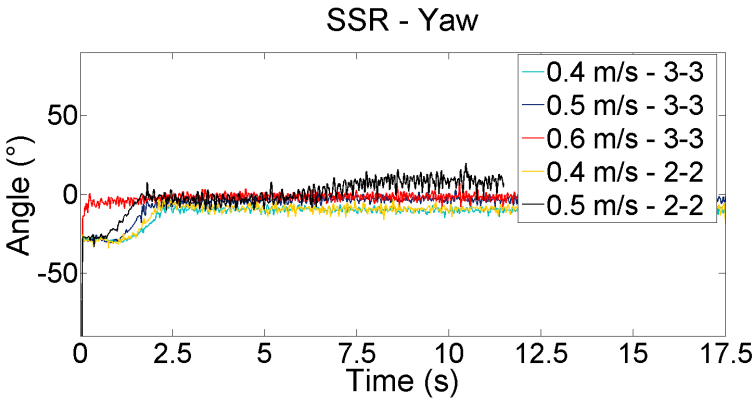

Figure 6.32: Side by Side Rotor Turbines Yaw Motion.

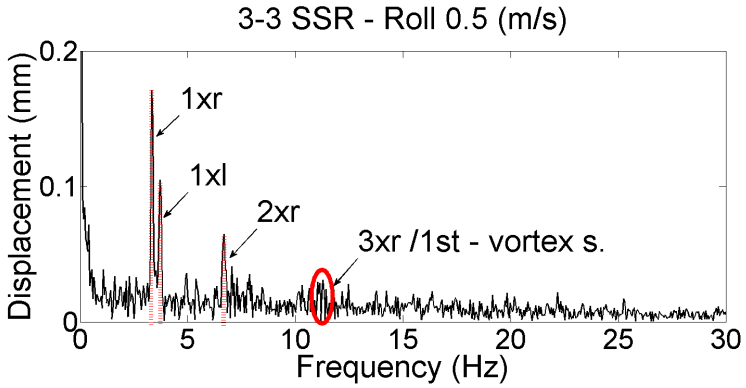

Figure 6.33: Roll Energy Spectrum of the 3-3 Side by Side Rotor Turbine at $0.5\,^{\mathrm{m}}/_{\mathrm{s}}$ ..

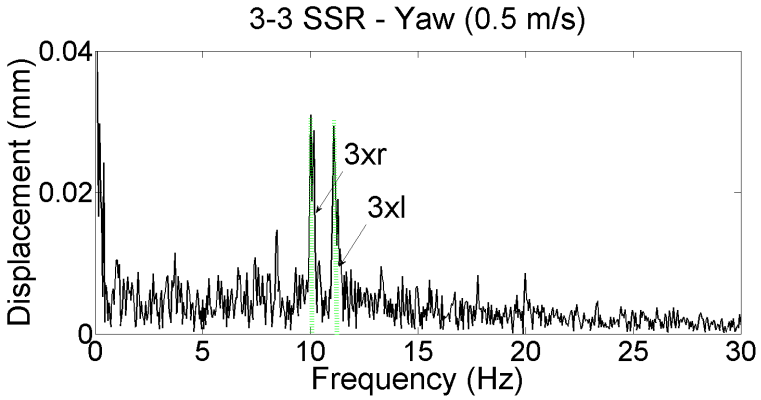

Figure 6.34: Yaw Energy Spectrum of the 3-3 Side by Side Rotor Turbine at $0.5\,^{\mathrm{m}}/_{\mathrm{s}}$.

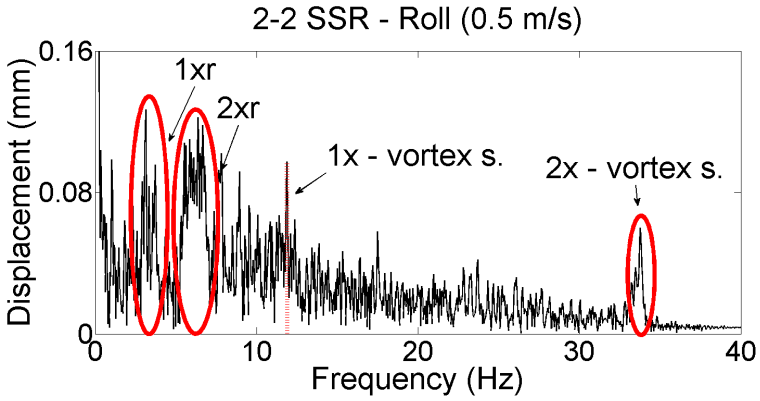

Figure 6.35: Roll Energy Spectrum of the 2-2 Side by Side Rotor Turbine at $0.5\,^{\mathrm{m}}/_{\mathrm{s}}$.

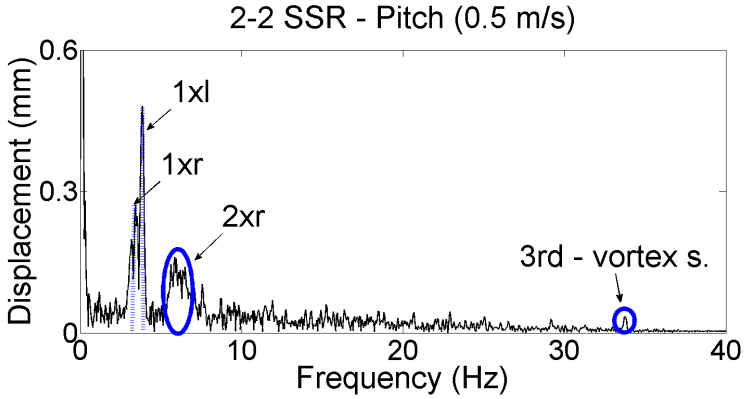

Figure 6.36: Pitch Energy Spectrum of the 2-2 Side by Side Rotor Turbine at $0.5\,^{\mathrm{m}}/_{\mathrm{s}}$.

The 2-2 SSR configuration performed relatively poorly during the tests. Its instabilities are shown through the frequency domain analysis in Figures 6.35, 6.36 and 6.37. It is clear that the first $(1xr)$ and second $(2xr)$ harmonics of the right rotor are present in the spectrum. With no corresponding contribution from the left rotor, pointing to a lack of balance (Figure 6.35). Figure 6.36 shows the pitch frequencies of 2-2 SSR at $0.5\,^{\mathrm{m}}/_{\mathrm{s}}$. Although the oscillation of the left rotor is greater than the right, the second harmonic of the right rotor indicates some mechanical play or axial movement which causes unsteadiness in the entire device. As it has been observed in wind turbine systems (Larsen et al., 2007), instability of the system related to teeter angles caused by 2 bladed systems influences the steadiness of this type of tethered turbine. The last highlights the advantages of CRR devices, where even if there is clear evidence of unbalance, the system is unlikely to undergo such severe roll and pitch motions as seen in SSR configurations.

As expected, an approximate doubling of thrust loads in SRR turbines (compared to SR turbines working in similar conditions) was obtained. Therefore, C_t values were similar to those presented in Section 6.4.1. C_p values for the individual rotors varied around 0.2, with 2-2 SSR turbines presenting slightly lower values. There are good reasons for this; first the 2-2 SSR

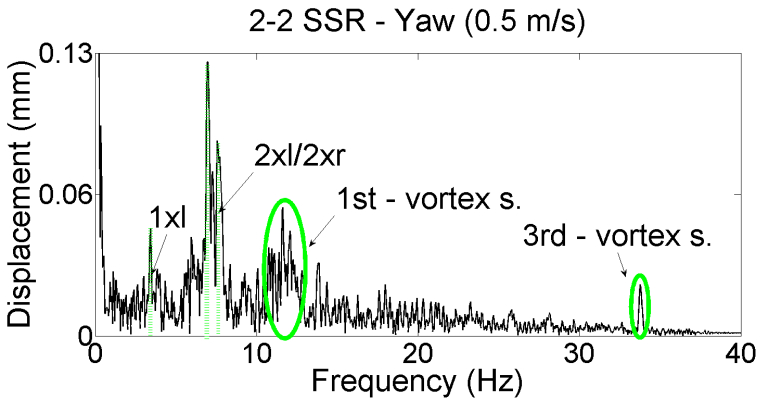

Figure 6.37: Yaw Energy Spectrum of the 2-2 Side by Side Rotor Turbine at $0.5\,\mathrm{m/s}$.

turbines never reached an accurately aligned position in pitch and yaw; and additionally, they suffered from oscillations in both motions.

Finally, the mechanical vibrations were substantial, reaching values of up to $0.5\,\mathrm{mm}$ at velocities of $0.5\,\mathrm{m/s}$. This vibration magnitude was not seen in other devices when they were tested at such velocities and they had even lower values at flow velocities of $0.8\,\mathrm{m/s}$.

6.5 Blade Failure Results and Discussion

As mentioned earlier, the purpose of using the Veroblue resin to fabricate the rotor blades of the prototypes was to induce failure during the tests. Therefore, it was possible to study the signal changes in both time and frequency domains before and after a blade collapsed.The reason to use a material with low tensile strength was to simulate the real life event of a collapsed blade during turbine operation. Therefore, it is possible to study the turbine's dynamic response changes before and after the event which in the future could be used as a warning mechanism.

A few examples of blade failure occurrences during the experimental trials are presented in the following sections. In order to complement the results contained in Figures 6.4, 6.5 and 6.6; a summary of the blade failure results is given in Table 6.7.

6.5.1 Dynamic Response: SR Turbines

Blade failure was observed during one of the tests of the 5 bladed and 3 bladed SR configurations at flow velocities of $0.8\,\mathrm{m/s}$ and $0.6\,\mathrm{m/s}$, respectively. The oscillations in roll and pitch are

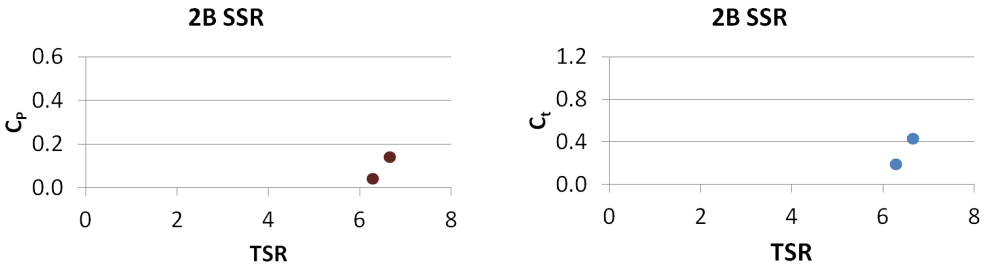

(a)

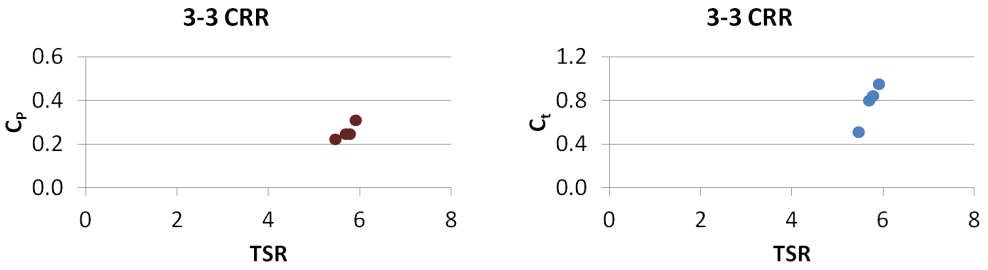

(b)

Figure 6.38: Experimental C_p and C_t curves for SSR Turbines with different Number of Blades: a) 2-2 Configuration and b) 3-3 Configuration.

BLADE FAILURE								
Tow Velocity	0.4 m/s	0.5 m/s	0.6 m/s	0.8 m/s	0.4 m/s	0.5 m/s	0.6 m/s	0.8 m/s
	Roll Mean (°)				Roll Standard Deviation (°)			
3B SR	11.78	13.11	6.59	1.97	1.39	1.69	1.67	3.14
3B SR			**19.06**				**13.37**	
5B SR	71.73	61.64	60.90	14.41	10.03	11.37	24.58	29.45
5B SR				**6.82**				**9.30**
2-3 CRR	-22.96	-8.89	-2.66	**67.45**	2.87	4.08	3.12	**23.05**
3-3 SSR	-1.33	1.62	11.13	**29.61**	1.33	5.00	7.84	**30.73**
	Pitch Mean (°)				Pitch Standard Deviation (°)			
3B SR	-18.71	-20.97	-10.37	-0.32	3.20	4.84	2.82	5.73
3B SR			**-19.60**				**21.24**	
5B SR	-19.87	-16.91	13.42	22.00	7.65	4.13	8.40	24.11
5B SR				**19.19**				**25.25**
2-3 CRR	-22.96	-8.89	-2.66	**3.42**	1.33	1.17	3.43	**14.31**
3-3 SSR	-18.97	-3.99	5.32	**40.46**	1.46	2.07	1.95	**25.46**
	Yaw Mean (°)				Yaw Standard Deviation (°)			
3B SR	-4.73	-4.74	-3.79	-2.56	1.49	1.33	1.56	1.60
3B SR			**-3.66**				**5.29**	
5B SR	-9.51	-7.97	-3.61	-5.00	1.39	1.44	1.57	1.87
5B SR				**-3.94**				**2.11**
2-3 CRR	-5.55	-4.37	-4.23	**0.43**	1.04	1.46	1.59	**3.81**
3-3 SSR	-10.13	-3.84	-1.91	**10.40**	1.56	2.27	2.28	**26.27**

Table 6.7: Mean and Standard Deviation of various blade failure cases.

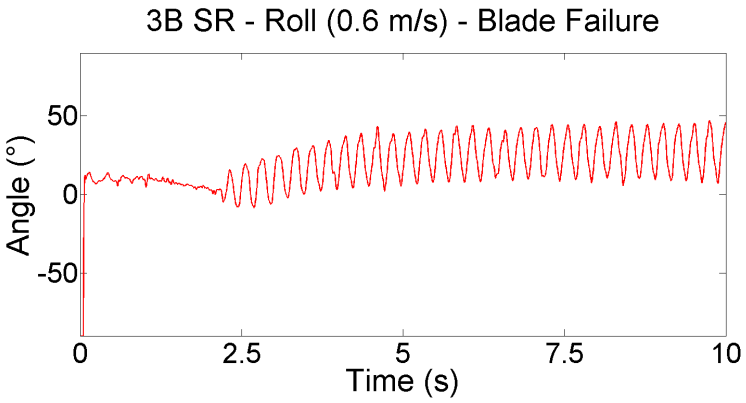

Figure 6.39: 3 Bladed Single Rotor Turbine in Roll Motion at $0.6\,{}^{\mathrm{m}}/_{\mathrm{s}}$ during blade failure.

recorded in Table 6.7, showing the expected contrast with normal operating modes. An example of the roll motion during failure is presented in Figure 6.39. From the frequency domain analysis in Figure 6.40, it can be observed that the amplitude of peak frequencies increased substantially compared to the cases shown in Figures 6.15 and 6.13. Vibration magnitudes of up to 1.5 mm RMS were obtained from the energy spectra after blade failure.

6.5.2 Dynamic Response: CRR Turbines

During the experimental tests, the 2-3 CRR configuration presented a failure case at flow velocities of $0.8\,{}^{\mathrm{m}}/_{\mathrm{s}}$. It is observed in Table 6.7 that high variations of roll motion were encountered during this mode, but pitch variations were lower than for the SR or the SSR turbines in corresponding cases. A similar pattern is also denoted in the yaw motion.

When referring to the frequency domain analysis, it is evident that for the "damaged case" (Figure 6.42(a)) the amplitude of the peak frequencies $1xu$ and $1xd$ have a large magnitude before blade failure occurs. After the blade fails, the existence of the frequency ${}^{1}/_{\mathrm{n}}\,1x$ is visible in the spectrum which usually denotes friction in the shaft. The $2xd$ and $4xu$ harmonics are also present denoting backlash and resonance. Also, only the $1xu$ frequency is denoted in the spectrum.

6.5.3 Dynamic Response: SSR Turbines

When the 3-3 SSR device was tested at velocities of $0.8\,{}^{\mathrm{m}}/_{\mathrm{s}}$, it was observed that oscillations of the device increased substantially as depicted in Table 6.7. When the device lost a blade, it started to roll continuously until the damaged rotor reached the free surface (Figure 6.43) and reached a pitch angle of $40°$.

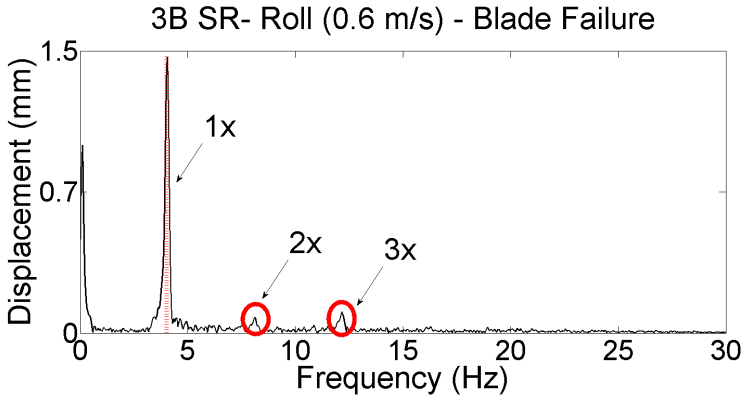

(a)

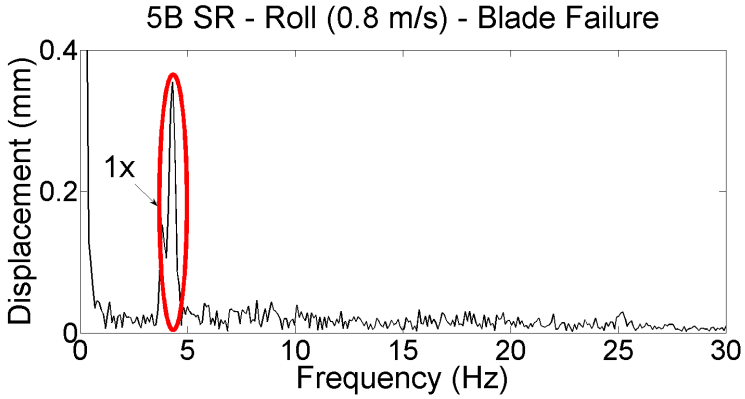

(b)

Figure 6.40: Roll Energy Spectrum of the : a) 3 Bladed Single Rotor Turbine at $0.6\,^{\mathrm{m}}/_{\mathrm{s}}$ and b)5 Bladed Single Rotor Turbine at $0.8\,^{\mathrm{m}}/_{\mathrm{s}}$.

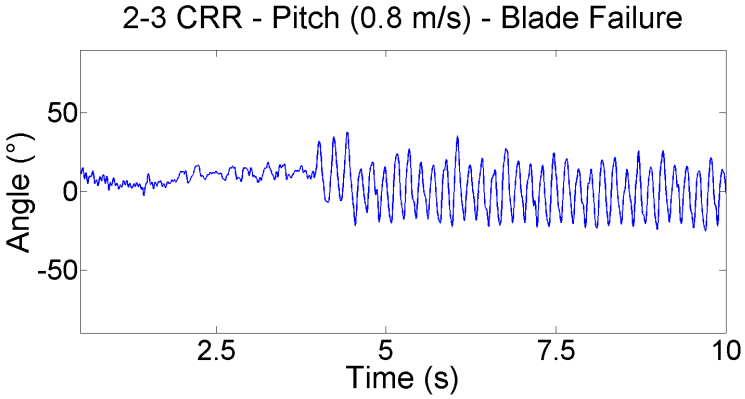

Figure 6.41: 2-3 Contra Rotating Rotor Turbine in Pitch Motion at $0.8\,^{\mathrm{m}}/_{\mathrm{s}}$ during blade failure.

(a)

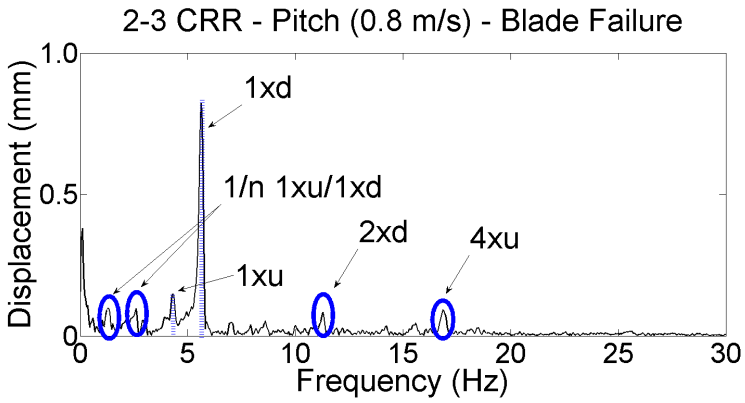

(b)

Figure 6.42: Pitch Energy Spectrum of the 2-3 Contra Rotating Rotor Turbine at $0.8\,{}^{\mathrm{m}}/_{\mathrm{s}}$. The case (a) represents the spectrum of the device with a blade failure. The case (b) represents the same case before the turbine has suffered any damage.

(a)

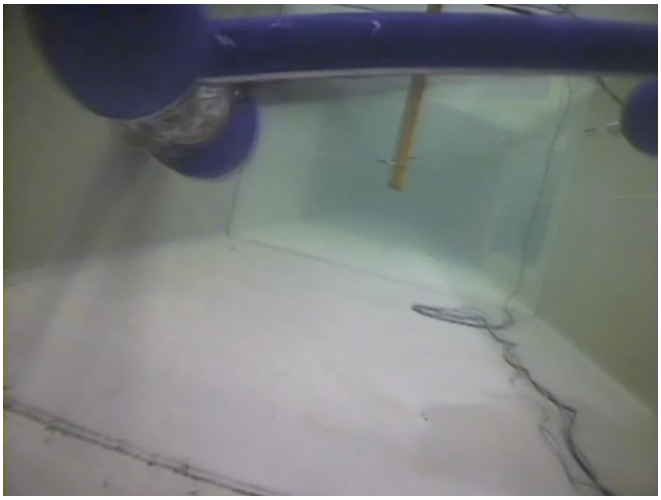

(b)

Figure 6.43: 3-3 SSR at $0.8\,{}^{\mathrm{m}}/_{\mathrm{s}}$: a) Before Blade Failure and b) After Blade Failure.

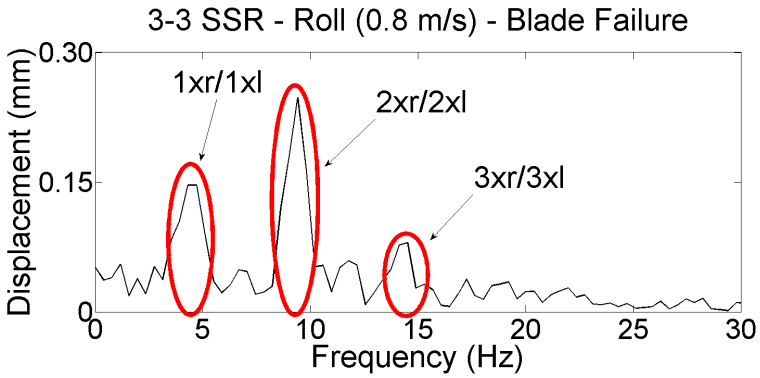

Figure 6.44: Roll Energy Spectrum of the 3-3 Side by Side Rotor Turbine at$0.8\,^{\mathrm{m}}/_{\mathrm{s}}$.

In the frequency domain, the effects of the blade failure can be noticed in Figure 6.33(b) where the appearance of the $3rd$ harmonic is present in the spectrum. This frequency denotes misalignment (obvious in the time domain data), and a corresponding decrease in the amplitude of the dominant frequency $1x$; thus, the mechanical looseness of the machine is visible (Figure 6.33(b)). In this case, instead of visualising an increment of the amplitude of the dominant frequency $(1x)$ indicates unbalance in the system, as seen previously.

6.6 Summary

Experimental results from testing, employing the methodology developed in Chapter 4, showed the dynamic motions and mechanical condition of various tethered turbine configurations. In these tests, model turbines were constructed with specially designed blades manufactured by rapid prototyping techniques. The material used permitted investigations of system behaviours during spontaneous blade failure, induced by running at high flow velocities. Configurations tested were single-rotor turbines (SR), co-axial contra-rotating turbines (CRR) and turbines with two rotors turning side-by-side (SSR).

The findings of this experimental work suggest that the single bladed rotor turbines present an adequate behaviour if these are conditioned with suitably sized stabilisers. For example, the results of this chapter showed that a 3 bladed turbine presented adequate roll alignment (a change of only $9°$ was observed within the flow speed range) and roll variation (with an average of $\pm 2°$). Yaw motions were also satisfactory with values of around $4°$ and oscillations in the range of $\pm 1.5°$ (Figure 6.12(a) and Table 6.4). Also, as the number of blades increased in the rotor, yaw alignment became poor and a larger period of time to achieve steadiness was observed (e.g. Figure 6.12(a)). This was expected since as the solidity increases in a turbine the shaft torque tends to increase, thus, it is more difficult to counter-act the forces in the

system.

Moreover, an interesting characteristic was shown in the frequency domain analysis. The appearance of similar vibration frequencies at identical flow velocity conditions was observed for a range of turbine configurations. Such frequencies were associated with the vibration of the stabilisers, because as the single bladed turbines presented certain misalignments, there was a shedding of vortices from the stabilisers, causing the vibrations observed. As expected, the magnitude and the appearance of harmonics of the frequency changed as the flow speed increased (as observed in Figures 6.13), denoting larger vibrations of the system.

The results of this chapter showed that unbalanced forces between rotors exist in 2-2 SSR. In some cases, the system rolls continuously until one of the rotors reaches the free surface. As it has been observed in wind turbine systems (Larsen et al., 2007), instability of the system related to teeter angles caused by 2 bladed systems influences the steadiness of this type of tethered turbine. In contrast, 3 bladed systems proved to be a steadier option showing low dynamic oscillations and mechanical vibrations (i.e. an average of $\pm 4^{\circ}$ of roll, pitch and yaw oscillations).

As far as stability is concerned, the CRR configurations tested were the most favourable within this gamut of options. The reason is that the thrust load generated by high solidity ratio rotors improve the capability of the turbine to align adequately in yaw and pitch motions. Moreover, CRR turbines are not influenced by external components that could generate resonant additional resonant responses (e.g. connecting struts or stabilisers). The main disadvantage encountered with the use of CRR turbines is that a lack of balance could create large roll oscillations and also high mechanical vibrations.

Photo-polymer resin was used in the fabrication of the small turbine blades used in the experimentation presented in this chapter. The mechanical properties of photo-polymer resins are far from those of materials typically used for tidal turbine blades but were employed to induce and observe blade failure and thus, investigate the dynamic response and mechanical vibrations during such an occurrence.

According to this experimentation it was found that as the blade failed, oscillations in pitch and roll increased by up to 10 times; however, in this case the turbines did not roll continuously, they remained under eccentric motions (out of round) and that is the reason why the oscillations are so large (as observed in Figures 6.39 and 6.41). Single rotor and side by side rotor turbines were the most severely affected as expected due to a change in the inertial forces. Contra-rotating arrangements also suffered but to a lesser degree, due to the presence of a second rotor able to counter act the imbalance in forces. Blade failure on twin-rotor SSR turbines caused a continuous roll of the entire system which was brought about by the physical

separation of the undamaged and damaged rotors creating unequal forces in different sections of the system.Therefore, the work presented in this thesis suggests that blade failure can be detected with the use of the methodology proposed in this thesis, for both single and contra-rotating turbines. The reason is that a different behaviour was presented by SSR turbines. According to the results obtained for 2-2 SSR and 3-3 SSR turbines, the frequency and time domain results show similar information when there is unbalance of the turbine and blade failure (e.g. continuous roll until one of the rotors is projected in the free surface). Therefore, these results suggest that if SSR turbine systems are used, additional instrumentation will be required to differentiate both situations.

Chapter 7

Dynamic Response Assessment of Scaled Up Tethered Turbines

It was identified in the previous chapter that contra-rotating turbines were the most effective configurations in terms of dynamic motions and mechanical vibrations. Although it was clearly possible to identify inherent responses of tethered devices in laboratory tests, the results in chapter 5 showed that a turbulent environment had significant effects on the turbine's performance. Moreover, the dimensions of conventional tank testing facilities usually limit the rotor diameter; so achieving dynamic similarity, based on scaling parameters such as the Reynolds Number, is complicated. In that context, this chapter introduces experimental tests for a scaled up contra-rotating device. The turbine is deployed in two contrasting locations: a river and an energetic tidal stream. This experimental programme aims to clarify the stability effects of a device under different turbulent flow conditions; for example, when the site is affected by marine traffic in combination with river and tidal flows.

7.1 Motivation and Objectives

As concluded in Chapter 6, contra-rotating devices provided the best responses in terms of alignment, oscillations and mechanical vibrations, in most of the cases. It was noted that 2-3 CRR turbines presented blade failures at a lower speed compared to other CRR configurations, so it was conjectured that high solidity rotors would be a more feasible solution. This series of experiments therefore featured a scaled up 3-4 CRR turbine.

The aim of this last set of experiments is to verify the application of the methodology de-

veloped in Chapter 4 in testing under real environmental conditions. It must be noted that the work presented on this chapter and throughout the thesis is not related to the development of the CoRMaT turbine, developed by Clarke et al. (2007b). The investigation and results presented in this chapter are uniquely associated to the appraisal of the dynamic response of a flexibly moored contra rotating turbine. Therefore, a fully equipped tethered tidal turbine of $1.1\,\mathrm{m}$ rotor diameter developed by the Energy Systems Research Unit (ESRU) within Strathclyde University was used. A permanent magnet generator was installed in the mid section of the turbine. Unlike conventional generators, both windings and magnetic parts were designed to rotate; the electrical output was removed by slip rings. Neutral buoyancy was accomplished by placing two buoyancy chambers in the front and back sections. In order to asses the dynamic response, the turbine was instrumented to measure roll, pitch and yaw. Additionally, the flow velocity; the angular velocity of the rotors, the electric voltage and current were measured.

Before the turbine was deployed in the Sound of Islay, tests were undertaken in Kyles of Bute in order to pre-test the turbine's instrumentation and performance. This stage was also carried out to test the submerged components and the continuity of the data acquisition module. But, the dynamic response analysis was focused on the results obtained from the second deployment which took place in the Sound of Islay, an open tidal site, which due to its geometry is considered as one of the most suitable places in Scotland to extract tidal energy. There are plans to lodge a large tidal turbine farm of $10\,\mathrm{MW}$capacity in the near future (Hammerfest Strom, 2012a). The third set of experiments was undertaken in the River Thames. The Thames carries a large volume of marine traffic which creates random wave strikes from the passing vessels; thus, it is an excellent location to study the dynamic response of tethered turbines deployed in confined turbulent environments. As discussed in Section 2.1.3, the flow velocity will be affected in both the bottom and top sections of the water column by the seabed roughness and the wave induced particle velocities, respectively. To quantify and mitigate surface wave interference, the turbine was submerged at several depths through the water column.

The remainder of this chapter is organised as follows: Section 7.2 describe the characteristics of the Sound of Islay and Thames River. Section 7.3 details the station keeping system designed for each location. Sections 7.4 and 7.5 present the turbine's design characteristics and the instrumentation used in the trials, respectively. Sections 7.6, 7.7 and 7.8 present the device's operational parameters and dynamic and mechanical responses in time and frequency domains in the two environments. A summary is given in Section 7.9.

7.2 Site Specification

As described in Section 4.3, sites specifications must first be considered. The Sound of Islay was chosen due to the convenient tidal flow speeds and water depth characteristics of the area. Maxwell et al. (2008) reported maximum flow velocities of approximately $2\ {}^{\mathrm{m}}/_{\mathrm{s}}$. The maximum tidal range was $2\ \mathrm{m}$ with an average water depth of $12\ \mathrm{m}$ (Figure 7.1). Furthermore, the area possesses low levels of wave energy densities due to its sheltered position. The precise location was in the Bunnahabhain Bay close to the Destillery (Figure 7.1).

The second test site was located at the Temple steps on the Victoria Embankment in the River Thames in London, UK (Figure 7.2), which provided convenient access while avoiding interference with other activities in the river. The maximum flow velocities recorded during testing in the Thames reach $1.5\ {}^{\mathrm{m}}/_{\mathrm{s}}$ when the ebb tide runs with the river flow (Environment Agency, 2012). As mentioned previously, the site is ideal to study the potential instability of a turbine in low velocity conditions, when exposed to transient waves.

7.3 Mechanical Design of the 3-4 CRR Turbine

The rotor diameter of $1.1\,\mathrm{m}$, coupled with a large hub to accommodate the generator was compact and easily handled but was not likely to produce optimum performance. The reason is that the ratio of blade diameter between the nacelle size was lower than it would be in comparison to the full scale turbine. Also the ability of the turbine to self align with the flow might be impaired, compared to a device with larger blades. However, it would give clear indications of any inherent stability issues with the design. NREL S814 blade profiles were used in both rotors (see Section 4.4.2). Static balancing was achieved by equipping the turbine with two rotors of identical masses. It was calculated that the rotor operated at Reynolds Numbers between 1.18×10^5 and 2.96×10^5 at flow velocities of $0.4\ {}^{\mathrm{m}}/_{\mathrm{s}}$ and $1\ {}^{\mathrm{m}}/_{\mathrm{s}}$, respectively. Similarly, the Froude number was calculated to range between 0.045 and 0.16, for the same flow speeds (Section 4.4.3).

The turbine was expected to produce a power output of $150\ \mathrm{W}$ and a thrust load of $271\ \mathrm{N}$ at optimum conditions, with a flow velocity of $1\ {}^{\mathrm{m}}/_{\mathrm{s}}$. Such calculations were estimated using the maximum C_p and C_t coefficients obtained in Clarke et al. (2008).

As mentioned in Section 4.4.5, an electromechanical method may be used to control turbine operations, and such a system was designed for the 3-4 CRR turbine turbine. A peak power tracking system was used to vary the impedance of the electric circuit. The system consisted of pulse width modulator, connected between the power source and the load (Gitano-Briggs,

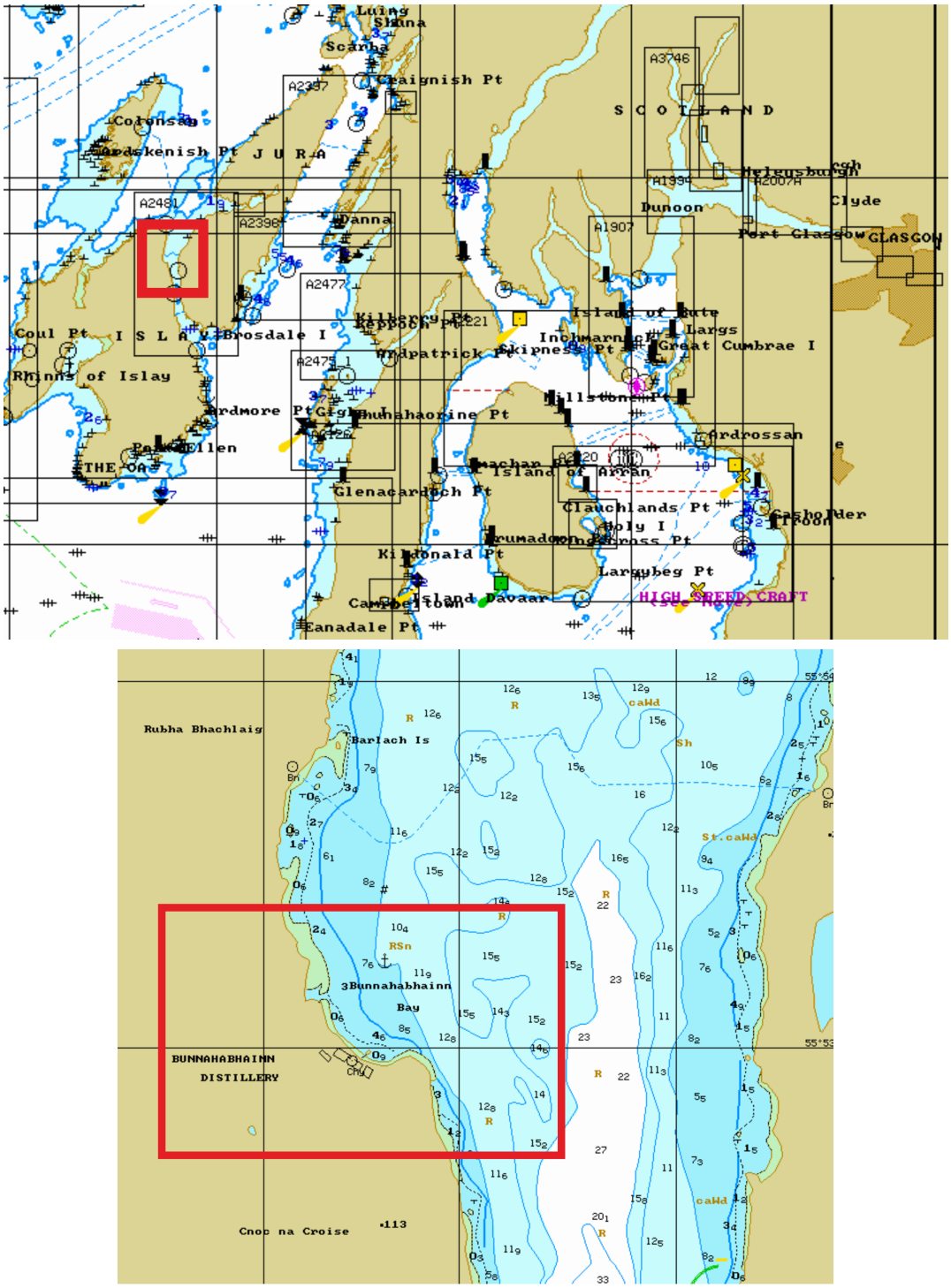

Figure 7.1: Sound of Islay: Installation Area.

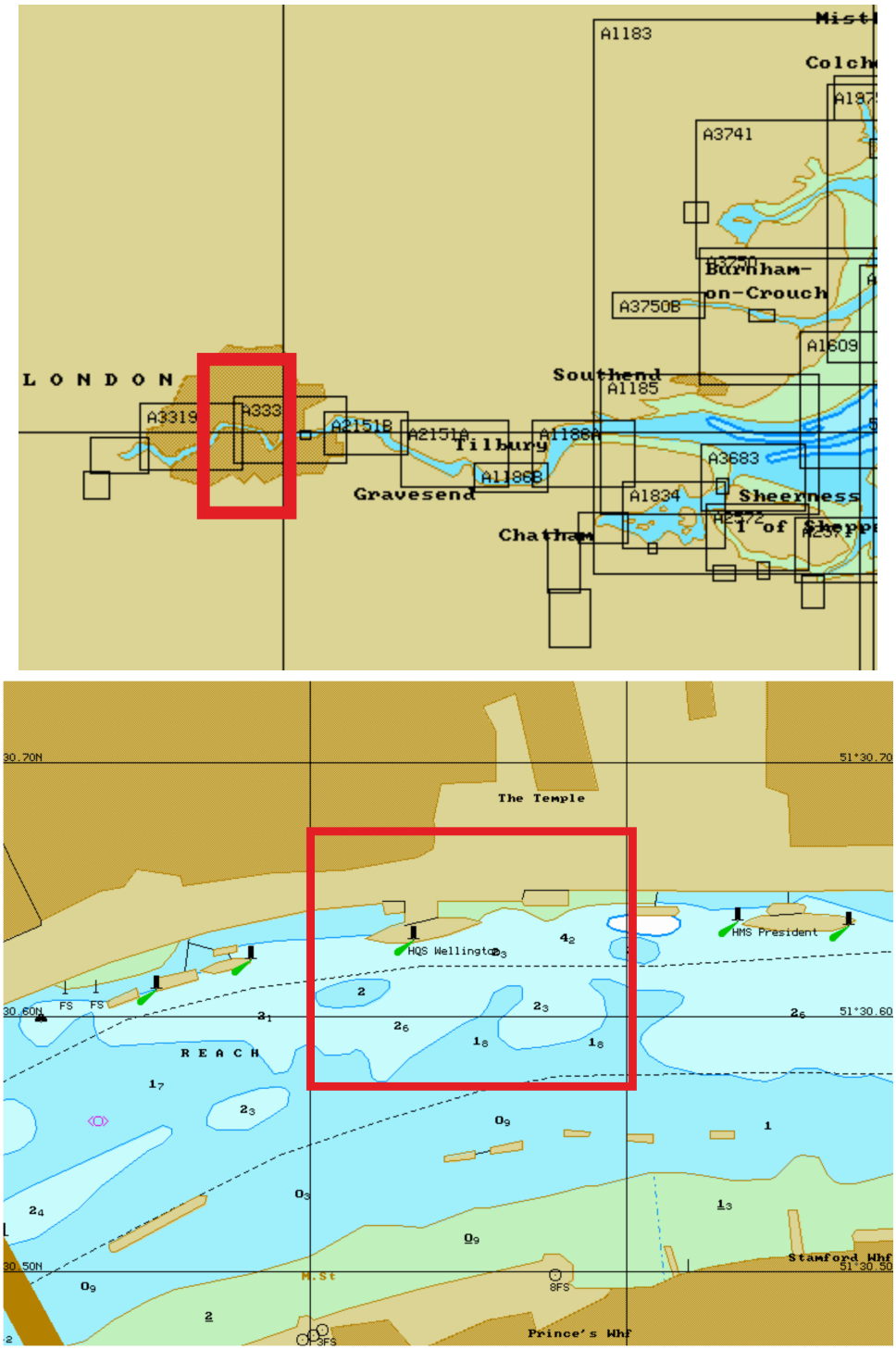

Figure 7.2: River Thames: Installation Area.

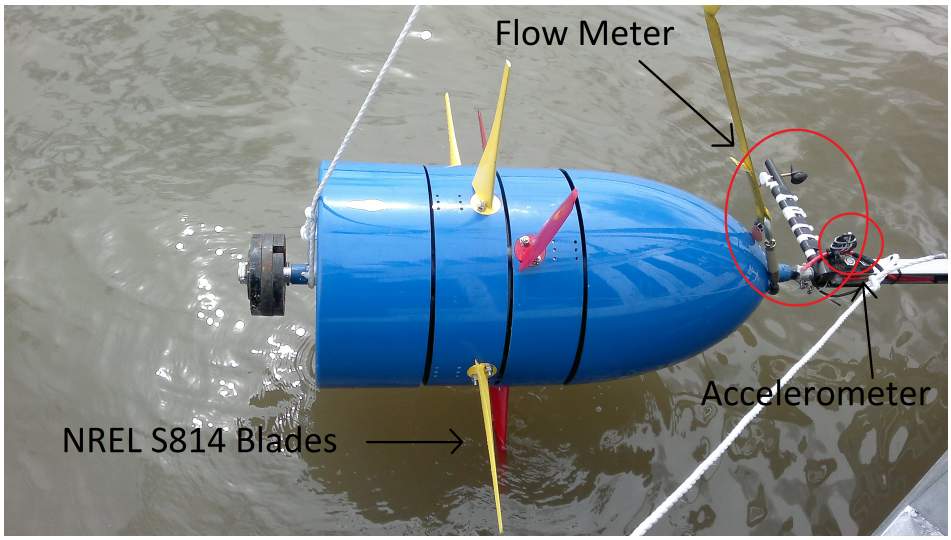

(a)

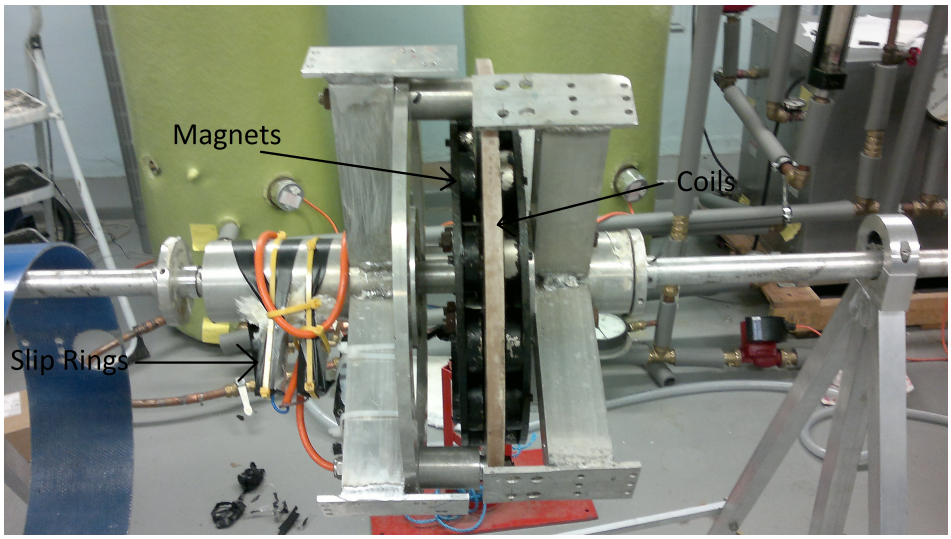

(b)

Figure 7.3: Contra-Rotating Turbine's Generator.

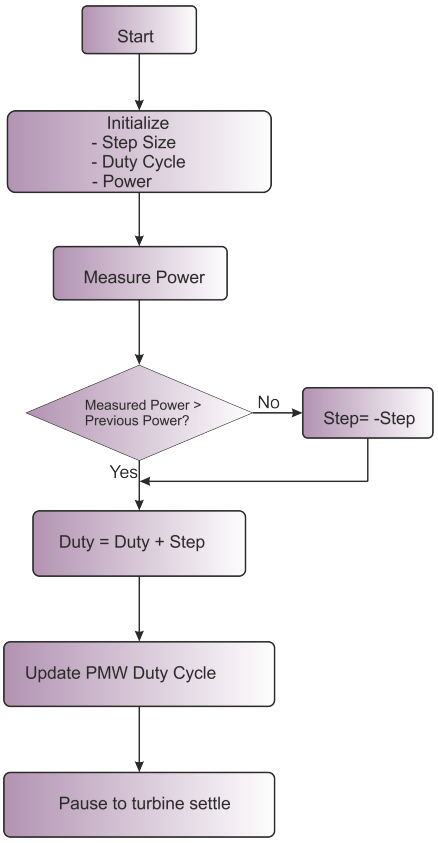

Figure 7.4: Peak Power Tracking Flux Diagram , based on Gitano-Briggs (2010).

2010). In order to reach the maximum power conditions, a gradient method is applied to the Supervisory Control and Data Acquisition system. The technique consists of increasing gradually the duty cycle. The power output is monitored through every step and if it has a lower magnitude than the previous value, the duty cycle is increased, and vice versa. A flow diagram is depicted in Figure 7.4.

7.4 Support Mechanism

Two different support structures were employed in the two test locations. Firstly, a gravity base foundation was utilised to anchor the device to the seabed in the Sound of Islay, consisted of a series of high density tubular sections which provided sufficient holding capacity, as illustrated in Figure 7.5(b).The taut mooring line composed of steel wire was connected from the anchor to the front part of the turbine's nacelle (Figure 7.5(a)). The turbine was then connected to the surface buoy by means of a tubular section, as it is observed in Figure 7.5(a). As concluded in Section 3.5.2, the angle formed between the mooring line and the seabed dictates the size of the surface buoy. Therefore, the mooring line was designed to work at a large angle of $45°$, in order to minimise the diameter of the buoyant section.

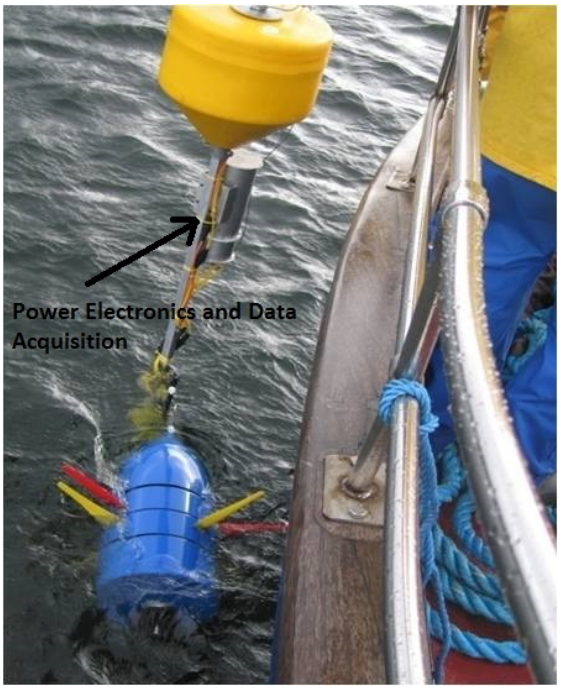

(a)

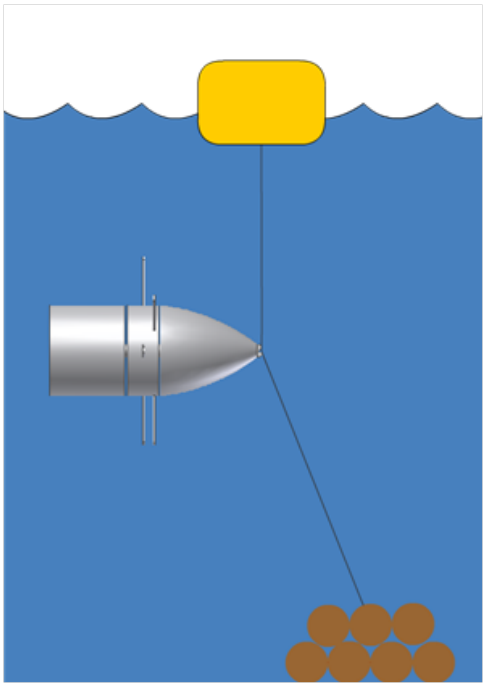

(b)

Figure 7.5: 3-4 CRR turbine installation in the Sound of Islay.

(a)

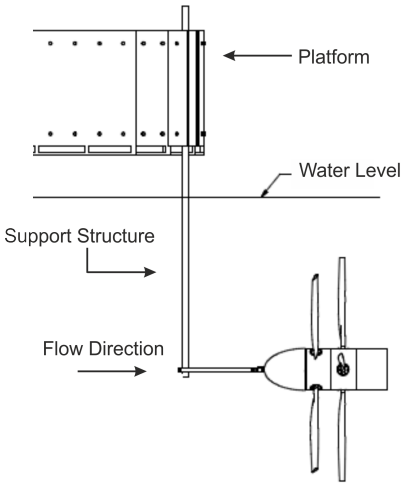

(b)

Figure 7.6: 3-4 CRR turbine installation in the River Thames.

The consent to deploy the turbine in the River Thames was given with the premise that seabed connections would not be utilised in the location. Therefore, during this test stage the device was installed from a platform located alongside the Head Quarter Ship Wellington. A tubular structural support of $88.9\,\mathrm{mm}$ outside diameter, $9.5\,\mathrm{mm}$ wall thickness and $4.5\,\mathrm{m}$ length was used to fix the device to the ship's platform, as depicted in Figure 7.6(b). The tubular section was selected according to the limit criteria established in Section 3.4.2. Hence, it was possible to deploy the turbine at a variety of water depths from $1\,\mathrm{m}$ to $2.5\,\mathrm{m}$, below the surface.

The device was fixed to the platform in such a way that it was able to rotate freely about its three main rotational axes (i.e. roll, pitch and yaw). An unfastened collar was fitted at the bottom of the pole to provide a free yaw movement. To restrain heave movement along the pole, a collar was located in both upper and lower parts. The roll and pitch motions were

unrestricted with the use of a swivel fixed to the main strut (Section 4.4.7). The arrangement is illustrated in Figure 7.6(a) and (b).

7.5 Instrumentation

The device was instrumented according to the general specifications made in Section 4.5. The electronic device to measure inclination in the Sound of Islay tests was a 2 axis accelerometer (Stand Alone Inclinometer Sensor SCA121). This had an accuracy of $0.1°$ and was able to operate in temperatures between -40C and 85C. Its maximum frequency response was 18 Hz. The dimensions of the instrument are $30\,\mathrm{mm}\times30\,\mathrm{mm}\times13\,\mathrm{mm}$; thus, it was easily accommodated in the system. The accelerometer used during the Thames River tests was similar to the one described in Section 5.2.3.

To measure the axial load (Section 4.5.2), an "S" type stainless steel load cell was located between the turbine and the structural support (Figure 7.7, beside the swivel). The principle of operation of a load cell is similar to a strain gauge; thus, the axial force (tension or compression) is calculated through an analogue voltage signal. The Vishay Instruments model 620 was chosen given its capability of measuring loads of up to $1000\,\mathrm{kg}$ (Figure 7.8). The input voltage required was from -10 to $+10\,\mathrm{V}$. The maximum frequency response of the device is $30\,\mathrm{Hz}$ and, the working temperature range is between $-30°\mathrm{C}$ and $90°\mathrm{C}$. The calibration processes for the load cell and the accelerometers were undertaken as described in Section 4.5.5.

The angular velocity of the rotors was measured with electromagnetic tachometers (Section 4.5.3). Eight magnets were installed on the circumference of the external part of each hub section (Figure 7.9). To activate the magnets, a magnetic reed switch was installed in close proximity. Thus, an entire revolution generated eight voltage pulses. The device is able to operate with a frequency of 400 Hz , and an operating temperature between $-40°\mathrm{C}$ to $125°\mathrm{C}$.

A stream flow meter was installed at the front of the turbine to measure the relative velocity of the fluid flow (Section 4.5.3). The principle of operation consists of digital voltage pulses created by the propeller each $180°$ (Figure 7.7). The pulse counts are correlated by eq. 7.1 to obtain the corresponding velocity (Geopacks, 2012).

$$V = 0.000854C + 0.05 \tag{7.1}$$

where V represents the velocity in (m/s), and C designates the number of pulses per second.

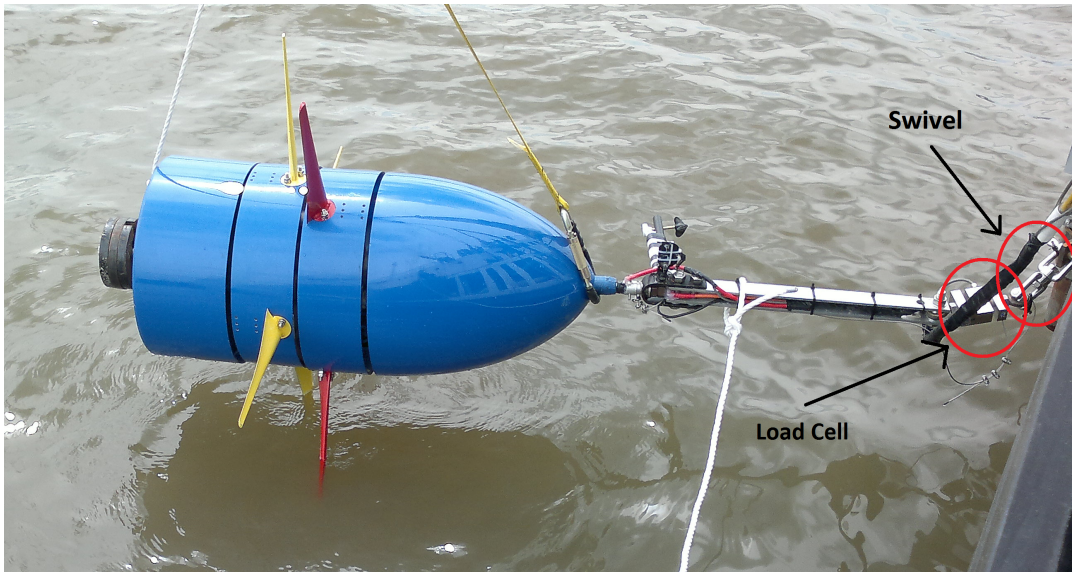

(a)

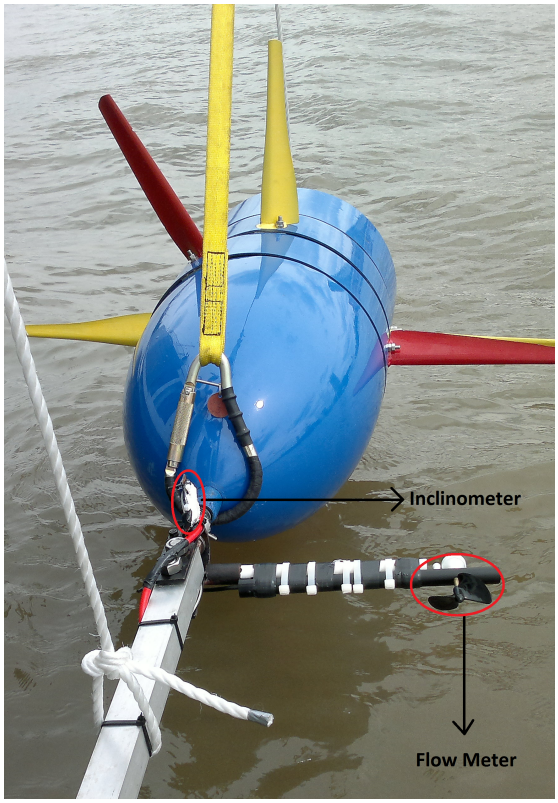

(b)

Figure 7.7: Turbine Installation from the Wellington Ship and Instrumentation.

Figure 7.8: “S” type load cell, model 620, taken from Vishay Measurements Group (1989).

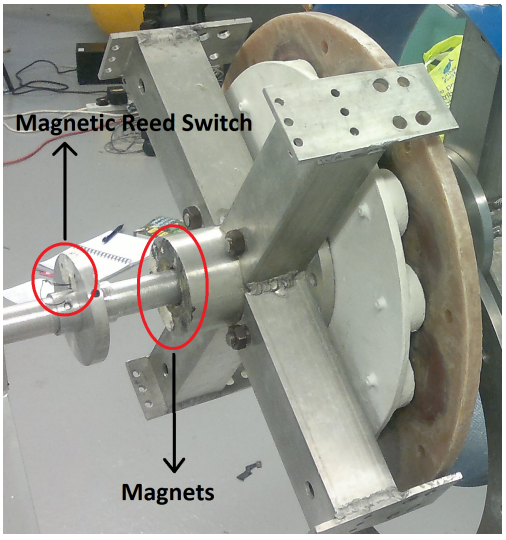

Figure 7.9: Magnetic Relays on Turbine.

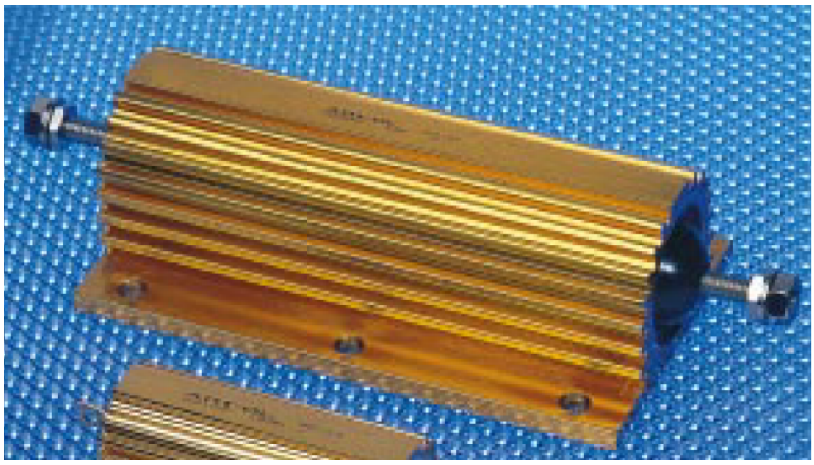

Figure 7.10: Resistive Element.

A 20 ampere current sensor was included within the system's power electronics (Section 4.5.3). The power output obtained from the generator was AC but it was rectified to DC and eq. 7.2 was utilised to obtain the magnitude of the electrical current (according to Phidgets (2012)).

$$A = 0.05(X - 500) \tag{7.2}$$

where A corresponds to the direct current in amps and X represents the analogue signal. The power was dissipated through resistive elements (Figure 7.10) during the Sound of Islay trials. However, the load was connected to a series of batteries on board of the Wellington Ship in the River Thames tests.

The electrical connections and waterproofing techniques were based on the specifications established in Section 4.5.4 and the procedures followed in Section 5.2.3. The data acquisition procedures followed the specifications of Section 4.5.6, but they were different in each location. During the Sound of Islay trials, the turbine was moored remotely from the monitoring site; thus, a landward SCADA system was not suitable. Therefore, a data logger "GigaLog E" was installed in the surface buoy as shown in Figure 7.5(b); a telemetry acquisition module was included as a supplementary data collection system and the data was sent via Bluetooth. In both instances, the data was sampled at a frequency rate of $100\,\mathrm{Hz}$.

During the Thames River tests, the SCADA system was connected to the shore: the power and data lines were taken on board the Wellington Ship where the data was collected and monitored. The data acquisition module employed during the River tests was similar to the one described in Chapter 5, and a sampling rate of $300\,\mathrm{Hz}$ was used. Four depths of immersion were considered in the experiments: $1\,\mathrm{m}$, $1.5\,\mathrm{m}$, $2\,\mathrm{m}$ and $2.5\,\mathrm{m}$ measured at the hub axis. For

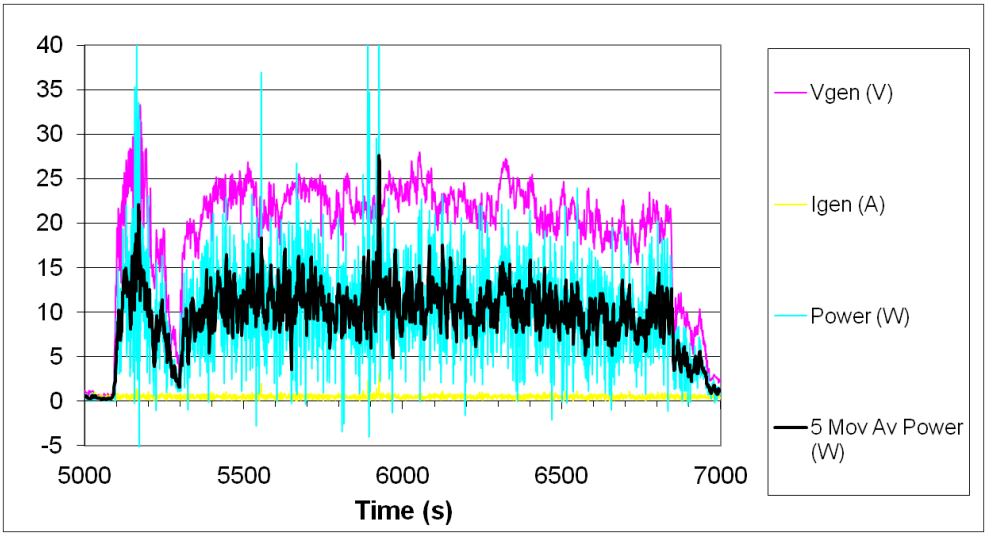

Figure 7.11: System Performance.

each test run, the data was captured for a period of 30 minutes. An Intel(R) Core (TM) 2 Duo (model P7450) with a CPU clock speed of $2.13\,\mathrm{GHz}$, with $3.6\,\mathrm{GB}$ in RAM running under Windows 7 and Labview 8.5 were used for the data capture.

7.6 System Performance

Figure 7.11 shows the parameters measured during the sea trials. The power coefficient obtained from such measurements was recorded as between 0.21 and 0.28. Clearly, the device was not working at the optimal conditions (indicated also by a mean tip speed ratio around 8). This might have been due to the efficiency of the generator itself; but some uncertainty must attach to the original BEM - based performance predictions. From the thrust loads acquired, C_t oscillated around 0.38 at TSR of around 4, but the whole performance curves of the turbine are shown in Figure 7.12.

7.7 Results and Discussion of the Dynamic Response in the Sound of Islay

7.7.1 Dynamic Response in Time Domain

A time domain representation of the 3-4 CRR turbine and the surface mooring buoy is observed in Table 7.1 and Figures 7.13 and 7.14. It is seen that the turbine has more fluctuations

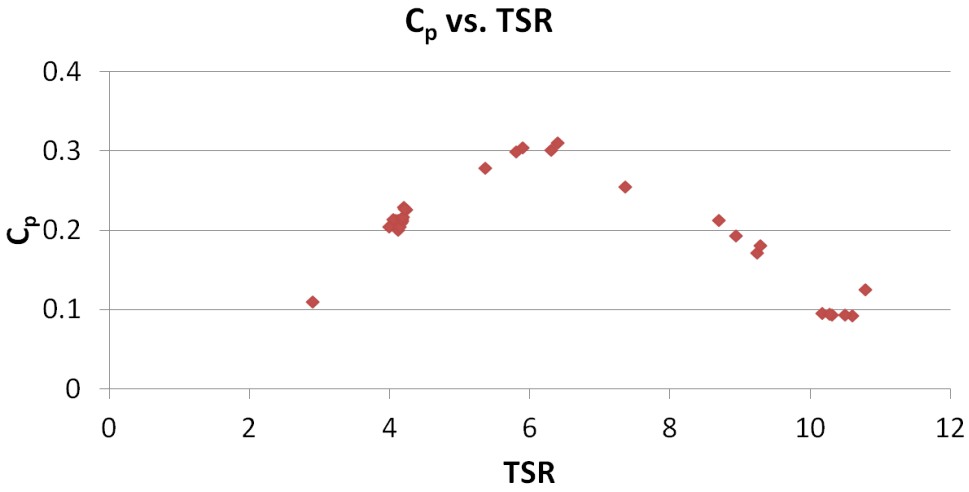

(a)

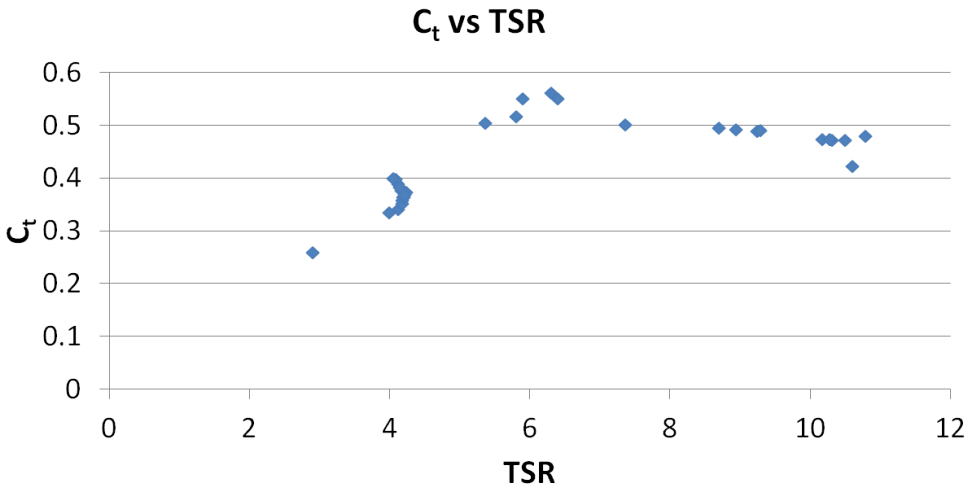

(b)

Figure 7.12: Performance Curves of a 1.1m rotor diameter 3-4 CRR Turbine: a) Cp vs. TSR and b) Ct vs. TSR.

Sensor	Mean	Standard Deviation
Surface Buoy (Roll)	-5.16	1.65
Surface Buoy (Pitch)	-1.14	1.37
Turbine (Roll)	15.96	3.67
Turbine (Pitch)	6.03	1.94

Table 7.1: Time Domain Characteristics at the sea trials.

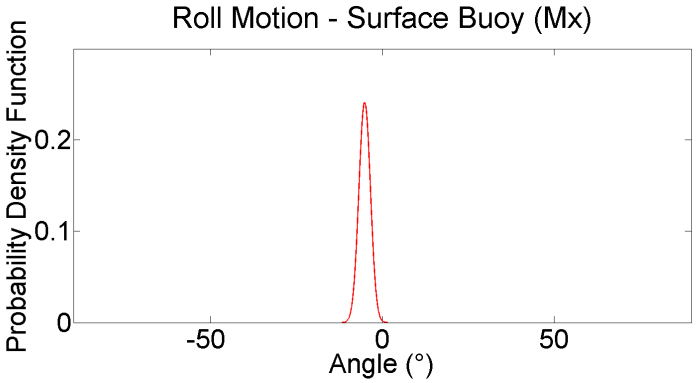

(a) Skewness = -0.04, Kurtosis = 3.06

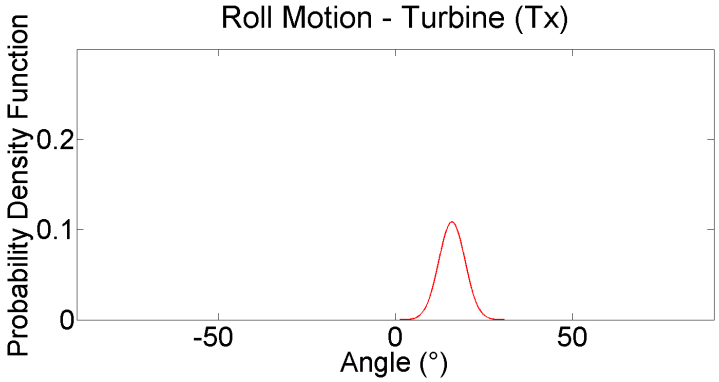

(b) Skewness = 0.07, Kurtosis = 2.97

Figure 7.13: Roll of Turbine and Surface Buoy.

in roll but still maintains its behaviour under a tolerance of around $\pm 8°$; therefore, it is observed that the turbine's roll motions present a mesokurtic behaviour. It is observed that the device maintains a pitch angle of approximately $6°$ through the entire period of time, due to inaccuracies in ballasting. In this case, both kurtosis and skewness values are farther away from expected values (as stated in Section 4.6.2). The fluctuations of the surface buoy are very moderate here but in general would of course reflect the local wave intensity.

7.7.2 Mechanical Vibrations in Frequency Domain

As discussed in Chapters 5 and 6, the dominant frequencies of a system reveal the condition of a device during a given operational period. Figure 7.15(a) shows the existence of four

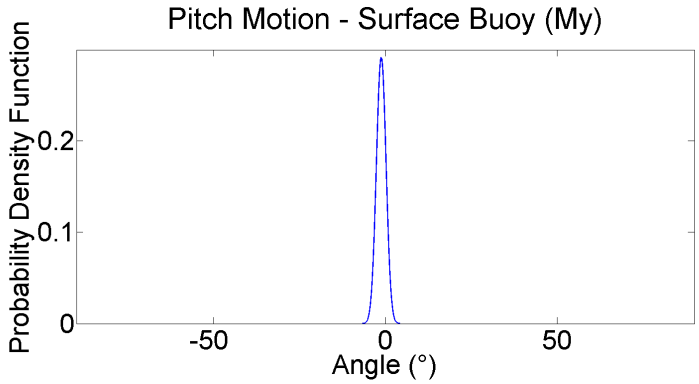

(a) Skewness = -0.02, Kurtosis = 3.02

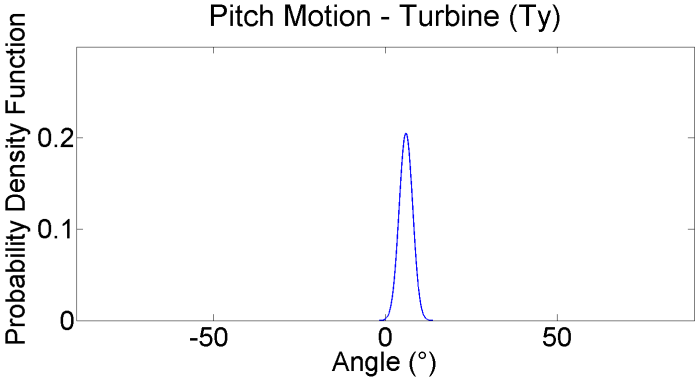

(b) Skewness = -0.22, Kurtosis = 4.67

Figure 7.14: Pitch of Turbine and Surface Buoy.

dominant frequencies in the roll spectrum. The angular velocity of the upstream rotor ($1x$) is visible, and is generally related to device misalignment. To a lesser extent the $5x$ frequency of the upstream rotor is observed, which would generally be linked to a machine component problem. The third peak frequency found is identified to be the result of the permanent magnet generator non-uniformities. Finally, blade-blade interactions are the source of the last minor peak frequency identified.

The peak frequencies of the pitch motions are presented in Figure 7.15(b). It is observed that the vibration levels in the pitch motion are substantially higher than the ones obtained in the roll fluctuations; for example, in the case of the $1x$ the amplitude of the pitch motion is 2.8 times higher than that of the roll spectrum. The low frequency of the pitch motions is very likely to be related to the oversize nacelle. A more resonant frequency is recognised to come from the mooring pole connecting to the surface buoy and located upstream of the turbine, creating shed vortices which impinge on the rotor. The angular velocity of the upstream rotor ($1x$) is also found in the pitch spectrum, suggesting misalignment. The frequencies of the combined rotor speeds and of blade-to-blade interactions have an insubstantial presence in the spectrum. According to the vibration charts described in Section 4.7.4 and found in Goldman (1999), the vibration levels are situated in the “rough” area.

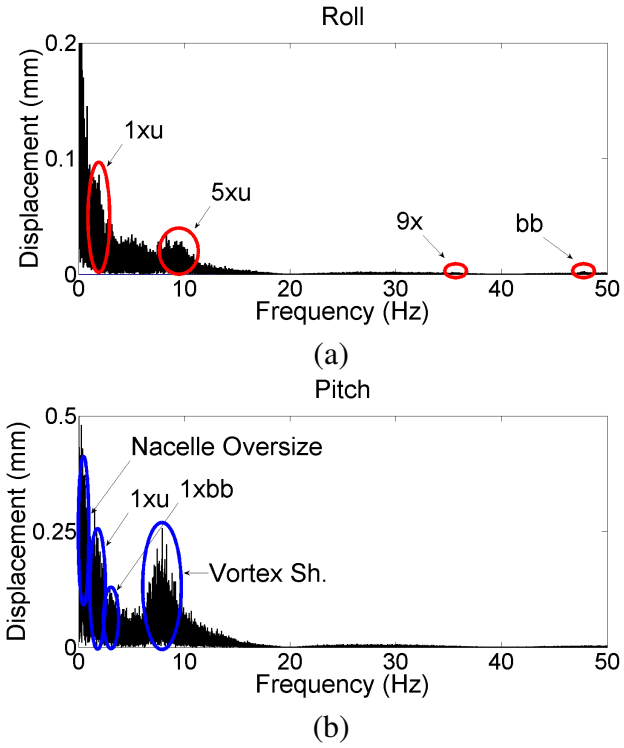

Figure 7.15: Frequency domain analysis of: a) Roll and b) Pitch. The energy spectrums were obtained at average flow velocity conditions of $0.5\,^{\mathrm{m}}/_{\mathrm{s}}$.

7.8 Results and Discussion of the Dynamic Response in the River Thames

The results reported in the following sections give an insight into the effects of underwater wash from passing vessels and the surface waves on the performance of a submerged turbine. In order to clarify the results, the nomenclature used to specify each test condition is as follows: neap +1 - 1e; where, "neap +1" is related to the tidal cycle which varies accordingly to Table 7.2. "1e" is related to the distance between the free surface and the hub height of the turbine and to the flow direction; in this case it means $1.0\,\mathrm{m}$ and the letter "e" specifies a flow running in the *ebb* direction. Conversely if the flow is in the *flood* direction the nomenclature will change to "f"; for example, "neap +1 - 1f".

7.8.1 Flow Speed

Peak velocities of the river in the ebb direction were higher than those recorded at flood conditions since the tidal flow was running in the direction of the river course. The maximum velocity recorded at the ebb tide was of $1.2\,^{\mathrm{m}}/_{\mathrm{s}}$ at $1\,\mathrm{m}$ depth. An example of the flow speed variation through time is depicted in Figure 7.16. Conversely, the maximum velocity obtained

Tidal Cycle	Flow Direction
Neap+1	Flood
Neap+1	Ebb
Neap+2	Flood
Neap+2	Ebb
Neap+3	Flood
Spring	Flood
Spring+1	Ebb
Spring+3	Flood

Table 7.2: River Thames Tidal Cycles.

Tidal Cycle	Flow Direction	Deployment Depth
Neap+1	Ebb	1.0 m
Neap+2	Flood	2.0 m
Neap+2	Ebb	1.5 m
Neap+3	Flood	1.5 m
Spring	Ebb	1.0 m

Table 7.3: Detected Wave Strikes on the River Stream.

at flood tides was of 0.52 $^{\mathrm{m}}/_{\mathrm{s}}$ with an average magnitude of 0.48 $^{\mathrm{m}}/_{\mathrm{s}}$ through the entire sets of tests. The low flow velocities detected at the site would make the turbine particularly sensitive to sudden disturbances. Thus, it was an ideal location to test the methodology proposed in Chapter 4.

7.8.2 Turbulence Intensity

The maximum turbulence was observed in the flood tide regime (Figure7.17(b)) with an average value of 6.9%. The maximum intensity observed in the ebb tide was 5%. Both values were obtained closer to the free surface. The results were fairly representative values obtained

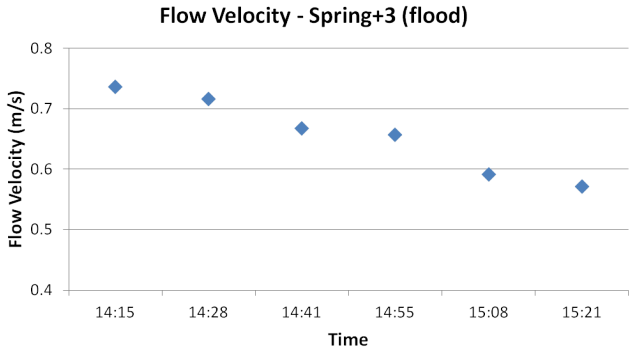

Figure 7.16: Flow Velocity measured during the Spring+3 tidal cycle.

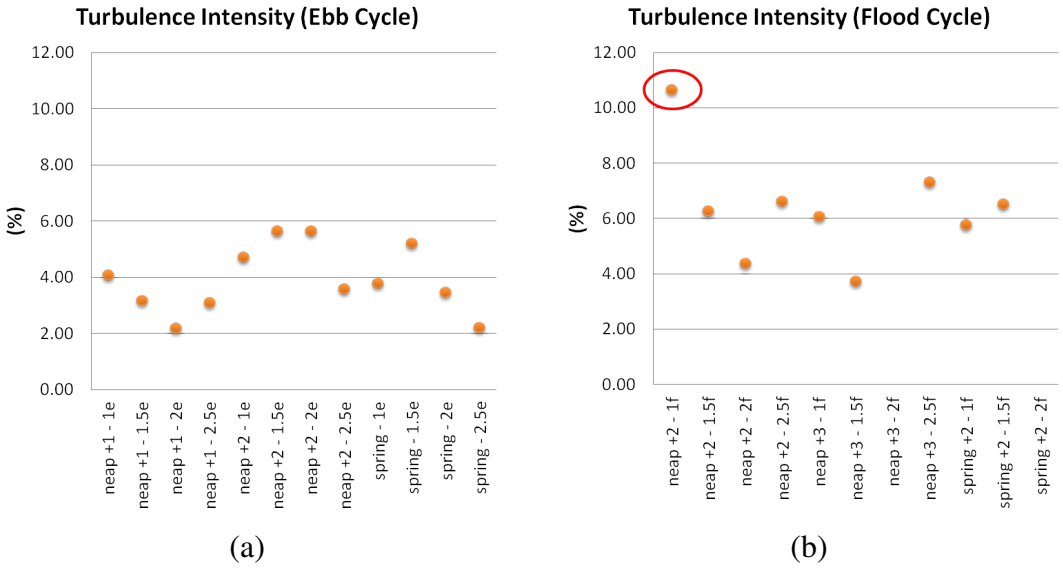

Figure 7.17: Turbulence Intensity : a) Ebb Cycle and b) Flood Cycle.

for tidal sites, as stated by Rose et al. (2010).

Most of the turbulence intensities calculated from the flood tide were within 4% and 8%, higher than those obtained at ebb regimes (i.e. 2% to 6%) as might be expected, given the relatively at low flow velocities. Turbulence intensity measurements recorded with the flow meter, described in Section 7.5, gave an insight of the environmental conditions of the site; however, it must be remembered that accurate site monitoring should be undertaken with additional equipment (e.g. ADCPs), as stated by Venugopal et al. (2011).

7.8.3 Dynamic Response in Time Domain: Roll

In the same way as in Chapters 5 and 6, the evaluation of the dynamic motions of the device was carried out following the basis of the methodology developed in Chapter 4. Figures 7.18 represent the average magnitudes and the roll oscillations of the 3-4 CRR turbine in various tidal regimes. The device showed roll motions of $-3°$ to a maximum roll angle of $24°$ (the mean angle is an irrelevance, relating simply to the position of the sensor within the turbine nacelle). No significant change in the roll motions of the device was detected when it was deployed during ebb and flood tides or when the device was installed in deeper waters. The standard deviations through the entire trial remained small; the device swiftly achieved its stability point and it remained in position, subject to maximum roll oscillation of $\pm 8°$. Figures 7.19(a) and (b) depict the impact of a wave strike, after which the 3-4 CRR turbine returned rapidly to its original equilibrium position.

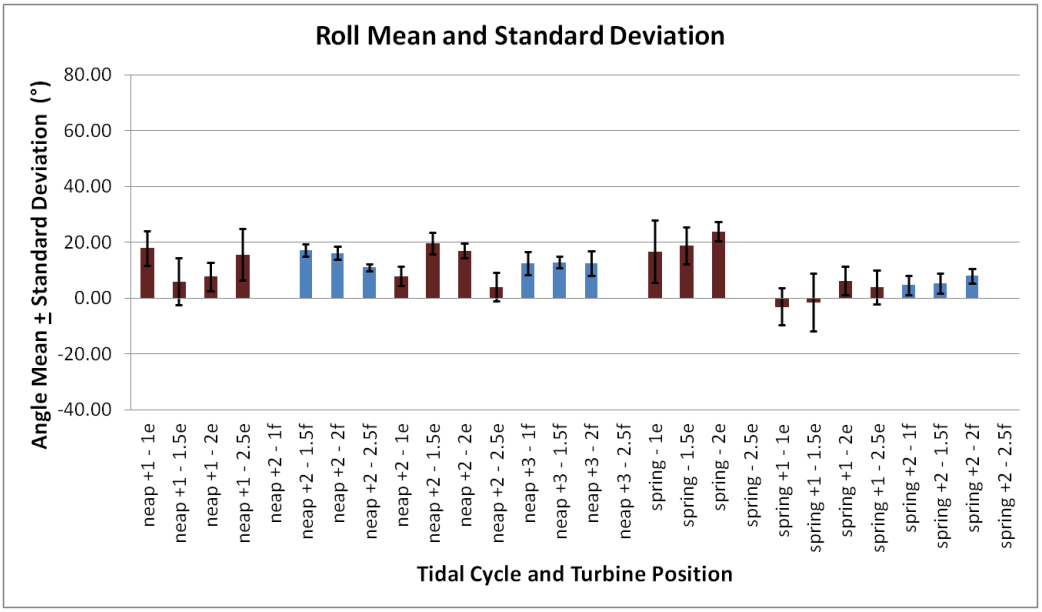

Figure 7.18: Roll: Mean and 1D Standard Deviation. The bars in blue represent "flood conditions" and the bars in brown represent "ebb conditions".

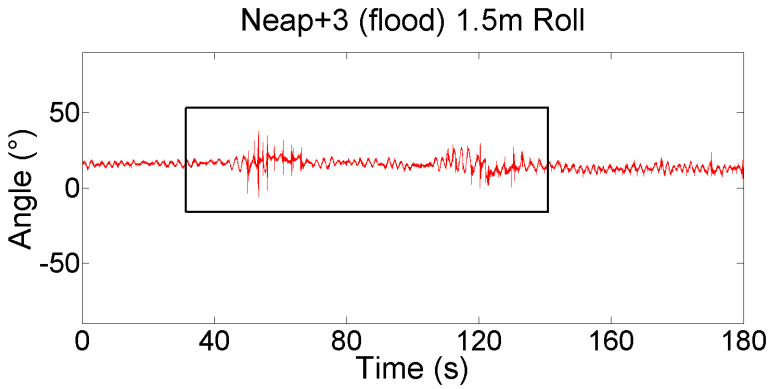

(a)

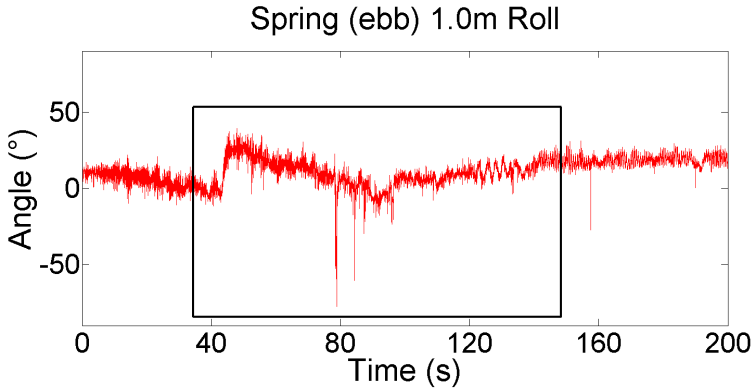

(b)

Figure 7.19: Roll Motion: a) Neap+3 (flood) and b) Spring (ebb).

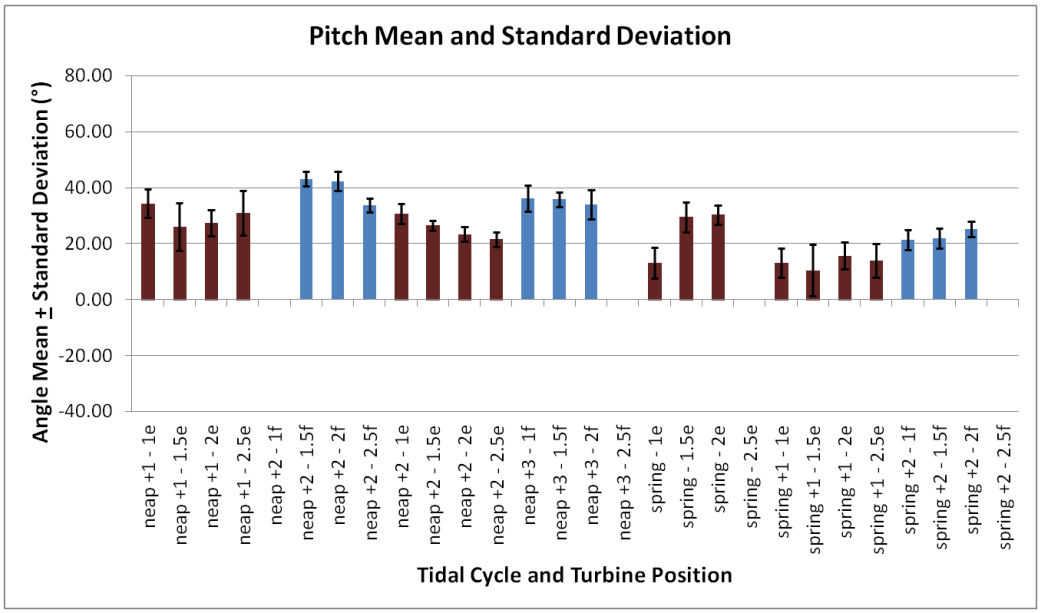

Figure 7.20: Pitch : a) Mean and b) Standard Deviation. The bars in blue represent "flood conditions" and the bars in brown represent "ebb conditions".

7.8.4 Dynamic Response in Time Domain: Pitch

The results of the mean and fluctuating pitch motions are shown in Figure 7.20. It is clear that the alignment of the device improved as the velocity of the stream increased (i.e. moving from neap to spring tides). The best alignment was achieved with around $10°$ pitch and similarly to the roll motions, once the device reached a stability point, it fluctuated around its average position by only a small amount approximately $\pm\ 5°$. The only critical case was observed in the motions for the Spring+2 tide at $1.5\,\mathrm{m}$ below the free surface, where, several underwater wave strikes were observed. Similarly to the case for roll, there was no correlation found between the position of the device in the water column and the device's alignment. However, it is evident that a ballasting problem occurs especially during low flow velocities, as was detected in previous chapters. Figures 7.21(a) and (b) depict the impact of a wave strike, after which the turbine returned rapidly to its original equilibrium position.

7.8.5 Dynamic Response in Time Domain: Yaw

The calculated mean and yaw variations of the 3-4 CRR turbine during the river tests are observed in Figure 7.22. In general, the device self aligned with the flow quite accurately. A notable misalignment of approximately $70°$ occurred in the Neap+2 tide. One possible explanation is that the collar responsible for allowing free movement of the device in yaw had locked onto the supporting structure. In addition, the standard deviation values showed a

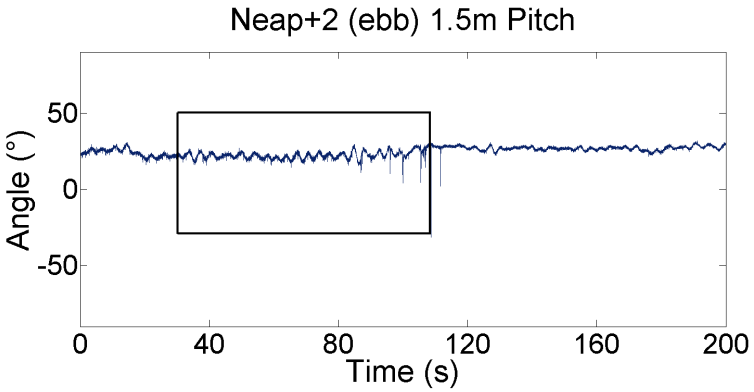

(a)

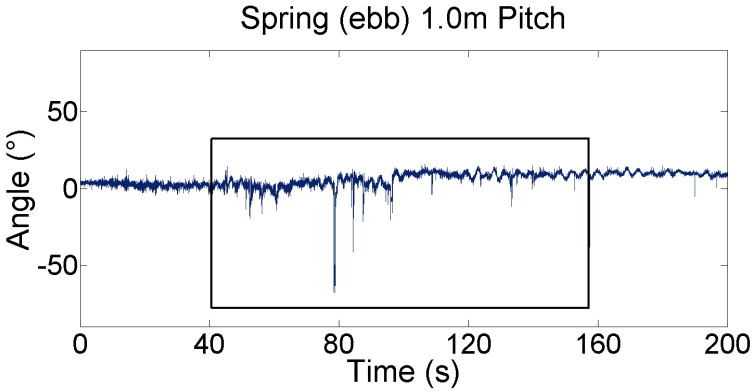

(b)

Figure 7.21: Pitch Motion: a) Neap+2 (ebb) and b) Spring (ebb).

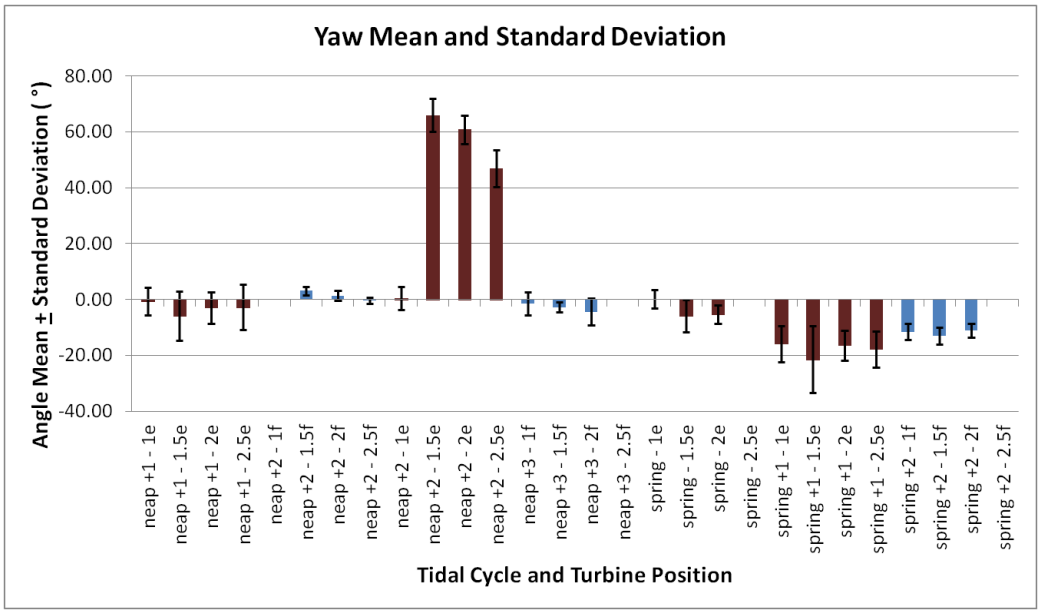

Figure 7.22: Yaw : a) Mean and b) Standard Deviation. The bars in blue represent "flood conditions" and the bars in brown represent "ebb conditions".

high fluctuation of yaw motions at Spring+2 tide at 1.5 m and Spring tide at 1 m. This was related to high turbulence in the water created by wash from passing vessels. Finally, it was also found that the yaw motions are similar to the one obtained on roll and pitch ($\pm 10°$ on the ebb tides and $\pm 2°$ in the flood tides). Figures 7.23(a) and (b) depict the impact of a wave strike.

7.8.6 Frequency Domain Analysis: Roll

A frequency domain analysis was carried out to obtain the mechanical vibrations related to the 3-4 CRR turbine at several depths in the water column. According to the vibration tolerance charts first shown in Section 4.7.4, it was estimated that the peak frequencies of the energy spectra were located between the"rough" and "extremely rough" sections (Figures 7.24, 7.26 and7.28).

A correlation was found between the vibration levels and the level of the turbine in the water column. The highest levels were found close to the free surface in ebb tides (Figure 7.24(d), (h) and (i)). In contrast, much lower levels were found in neap tides and when the device was installed at 1.5 and 2 m below the free surface (see Figure 7.24(a),(b),(f),(g),(l) and (m)). There is no clear explanation for this, other than the presence in some cases of high levels of turbulence from river traffic or other sources.

A distinct roll frequency was associated with the angular velocity of either the first or second

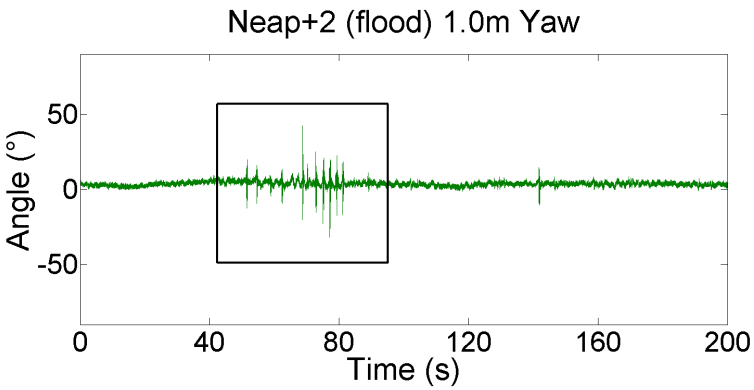

(a)

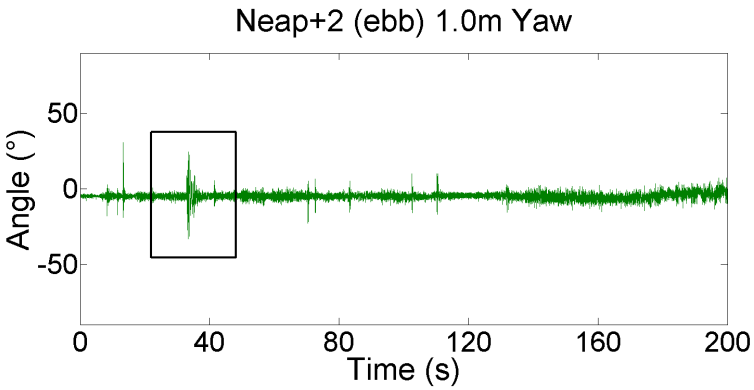

(b)

Figure 7.23: Yaw Motion: a) Neap+2 (flood) and b) Neap+2 (ebb).

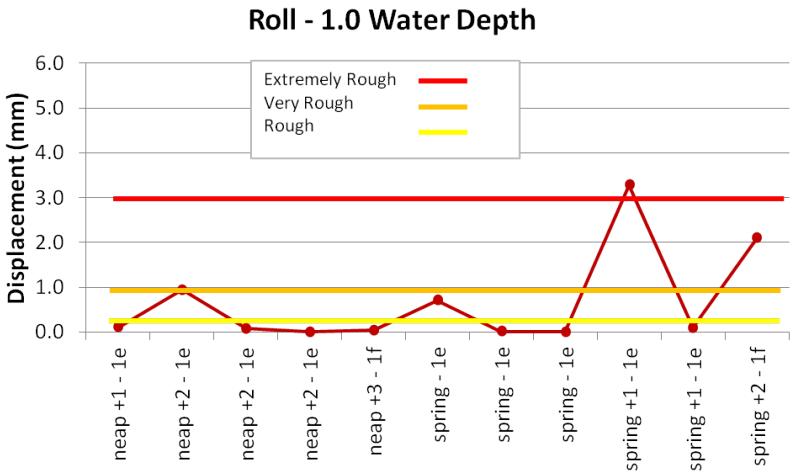

(a)

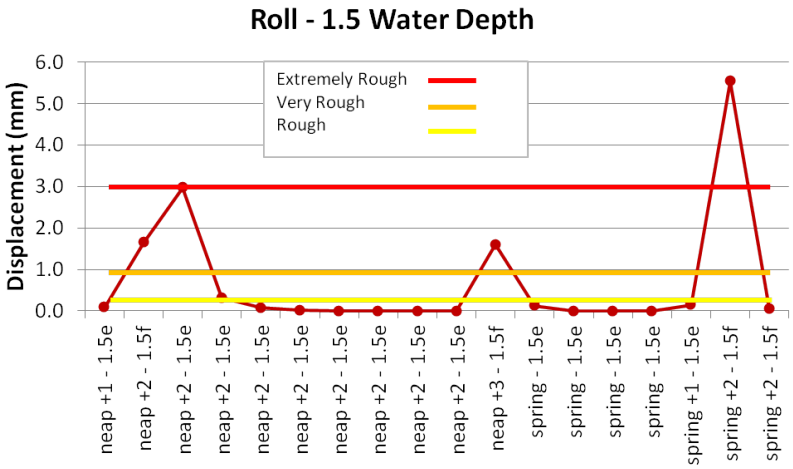

(b)

Figure 7.24: Roll Motion Vibration Level.

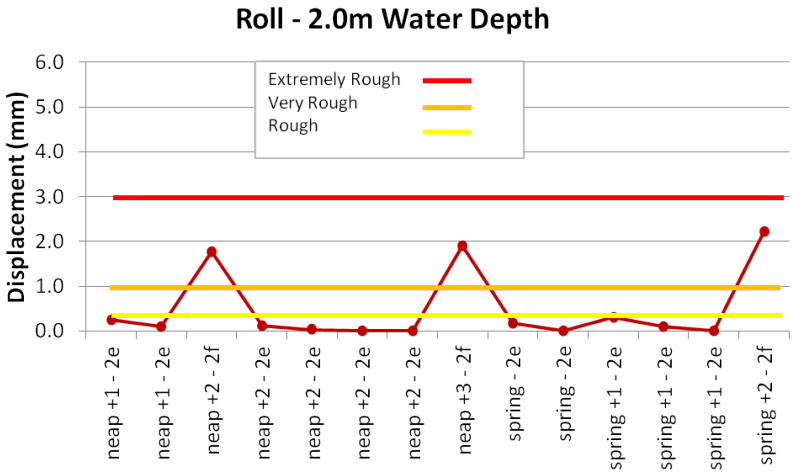

(c)

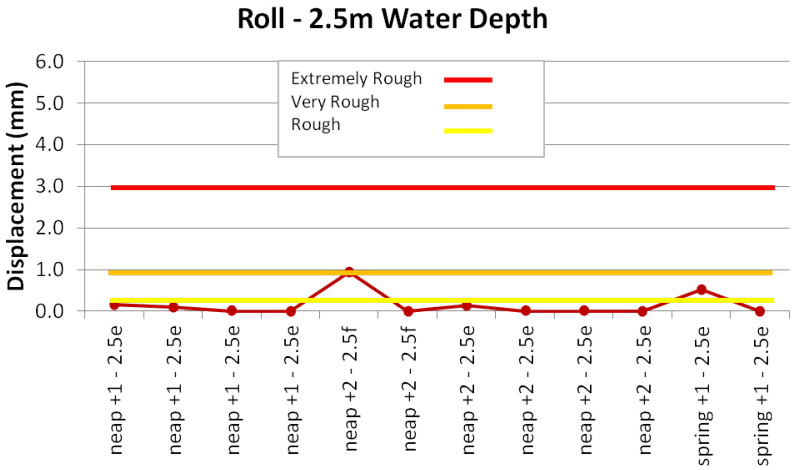

(d)

Figure 7.23: Roll Motion Vibration Level. (Cont)

rotor ($1xu$ or $1xd$). It is clearly visible in some of the spectra, notably during flood tide periods (Figure 7.24(a),(b),(f),(g),(k) and (m)); however, two more cases are observed in ebb tides during the Spring cycle (Figure 7.24(h) and (l)). A frequency relating to shaft friction $(^1/_{\mathrm{n}}\,1x)$ is apparent in Figures 7.24(e), (j) and (l). A particularly high amplitude of this frequency is clearly evident during Neap+2 at $1.5\,\mathrm{m}$ (Figure 7.24(e)). This could perhaps be related to a ship wash backlash in the turbine mechanism (Table 7.3).

The appearance of multiple harmonics ($3x, 4x, 5x$, ...,etc.) is evident in Figures 7.24 (c), (d), (e) and (h), but the peaks are relatively small. They appear to be prominent when the device is located closer to the free surface. The appearance of vortex shedding from the turbine's supporting structure in ebb tides is depicted in Figure 7.24(d), (i) and (j). The same pattern is also visible in the spectra under the wave strike effects and ebb tide conditions (Figures 7.24(c), (e) and (h)). Finally, blade interactions are just visible in Figures 7.24(g), (h) and (k), although they are of a very small amplitude.

7.8.7 Frequency Domain Analysis: Pitch

Similarly to the roll frequency analysis, the strongest vibrational frequencies are detected in neap tide tests, but this time there is a little distinction between ebb and flood conditions. Again, the greatest disturbances in the spectrum are obtained when the device is deployed close to the free surface.

The peak frequencies identified mostly in the spectral analysis are angular velocity of upstream or downstream rotors ($1xu$ or $1xd$), as shown in Figure 7.26. Shaft friction problems $(^1/_{\mathrm{n}}\,1x)$ are also present (Figures 7.26(a), (b) and (e)) which record information gathered during ebb conditions. The appearance of several harmonics ($4x, 5x,$ etc.) is again apparent, shown in Figures 7.26(b) and (e), and occur in similar conditions to those observed in roll. The effects of vortex shedding is visible in the pitch spectra of Figures 7.26(a) and (b), which refer to ebb conditions.

7.8.8 Frequency Domain Analysis: Yaw

The yaw energy spectra show a similar pattern to those presented for roll. The majority of the highest vibration frequencies are detected in the upper part of the water column (Figures 7.28(a), (d), (e), (f), (g) and (h)).

Once more, the most recurrent vibration frequency in each of the yaw energy spectra is the angular velocity of the turbine's rotors $(1x)$. It is evident that the disturbance is more extreme

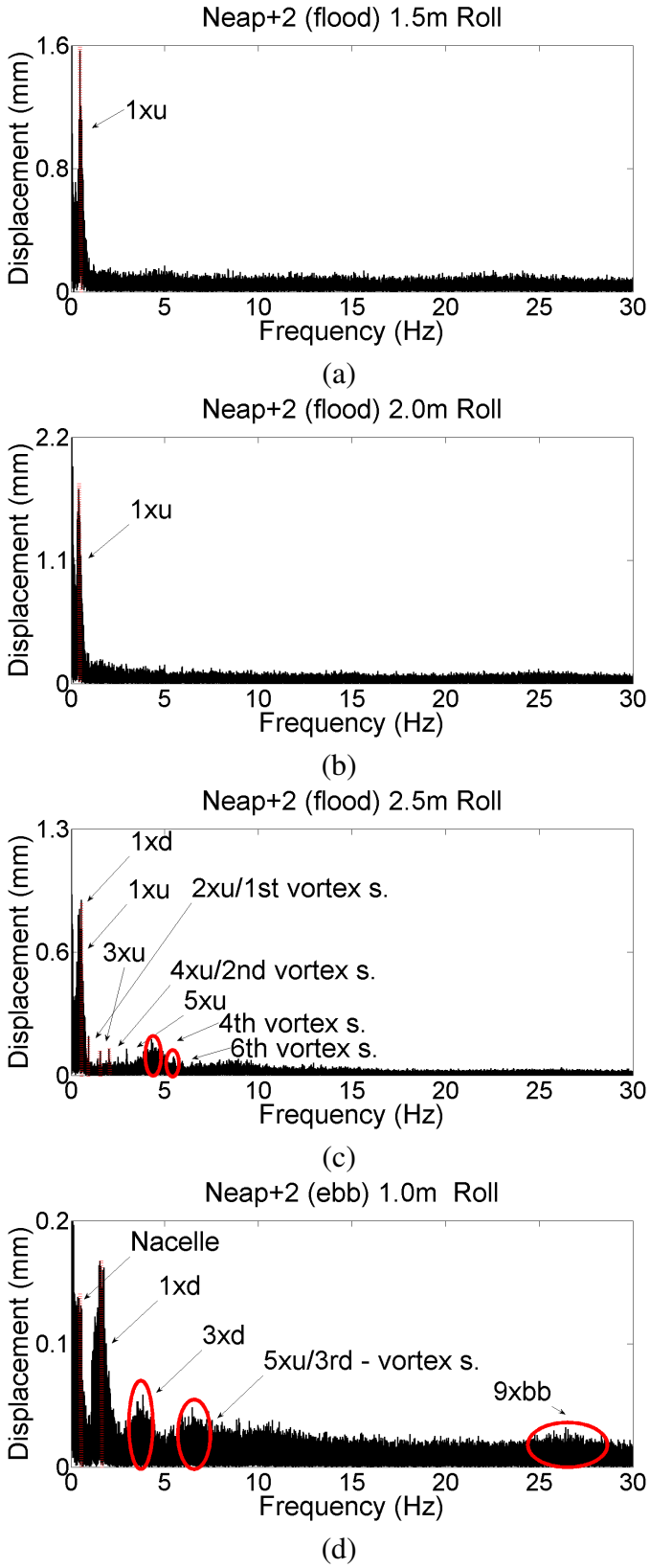

Figure 7.24: Roll energy spectrums of the tidal cycle.

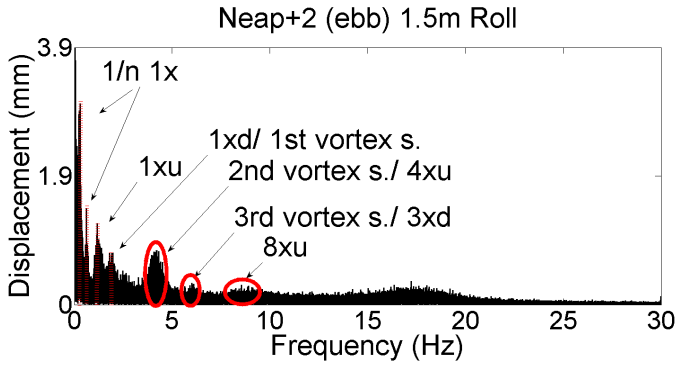

(e)

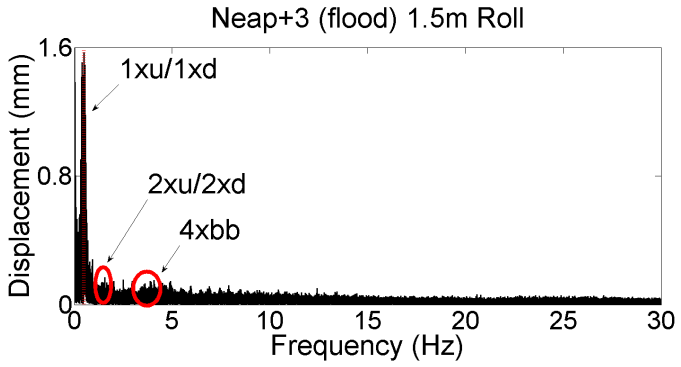

(f)

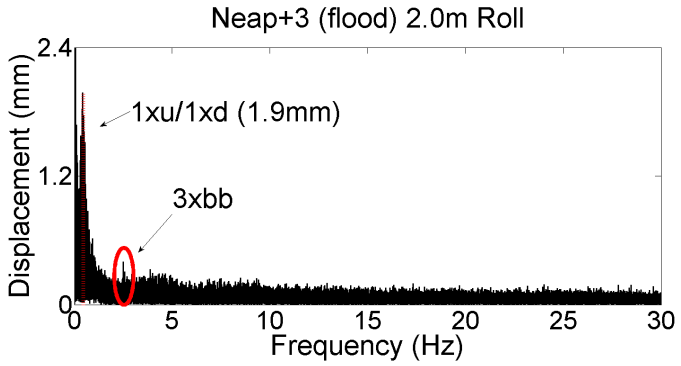

(g)

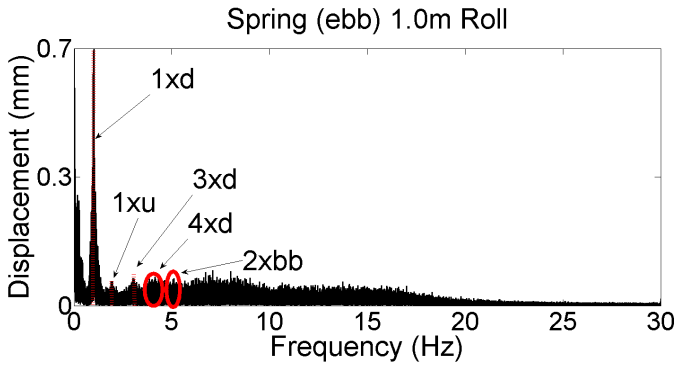

(h)

Figure 7.24: Roll energy spectrums of the tidal cycle. (Cont.)

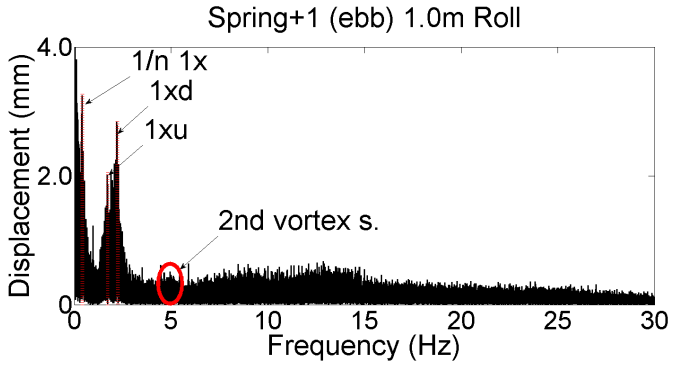

(i)

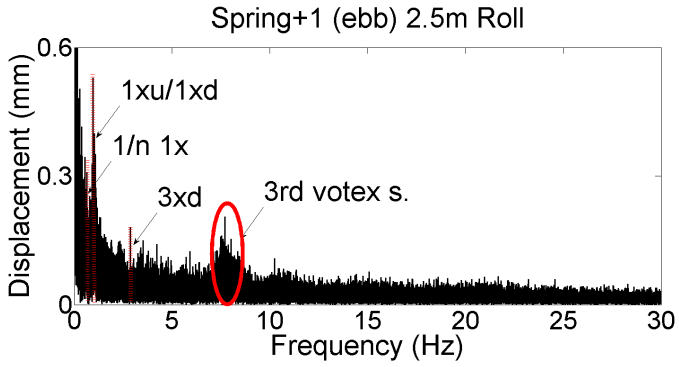

(j)

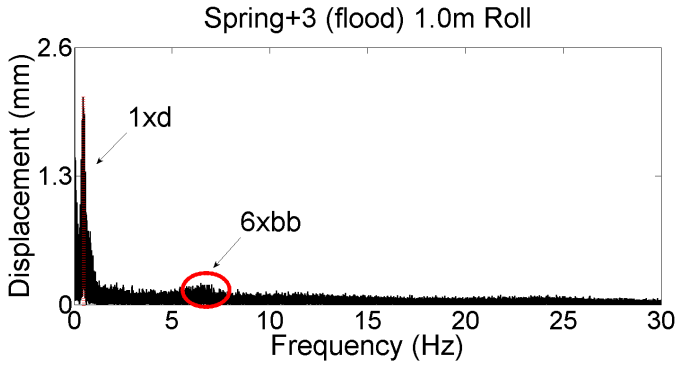

(k)

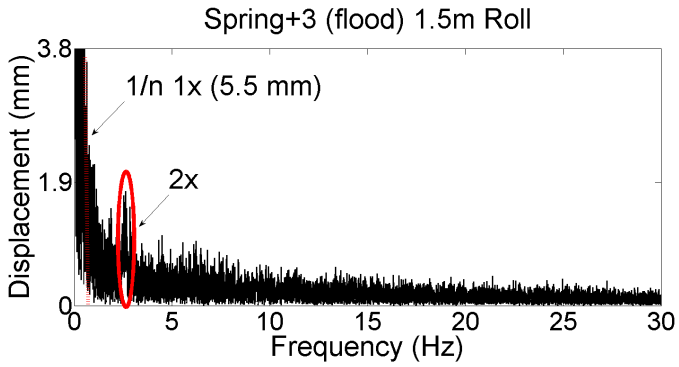

(l)

Figure 7.24: Roll energy spectrums of the tidal cycle. (Cont.)

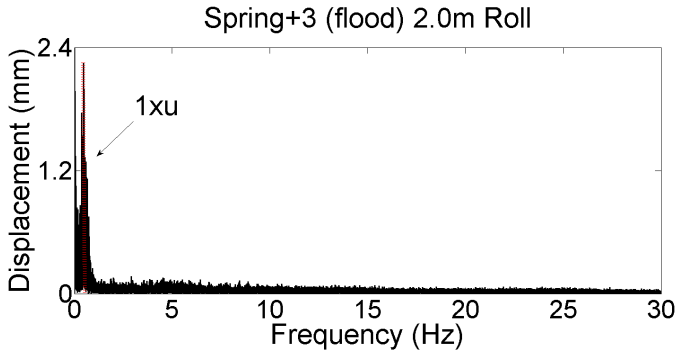

(m)

Figure 7.24: Roll energy spectrums of the tidal cycle. (Cont.)

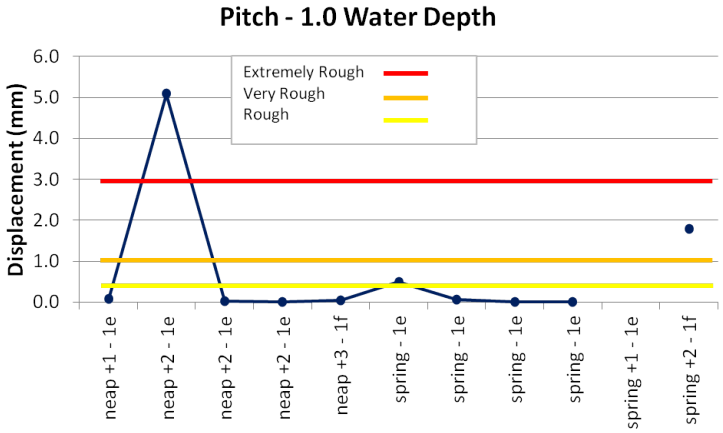

(a)

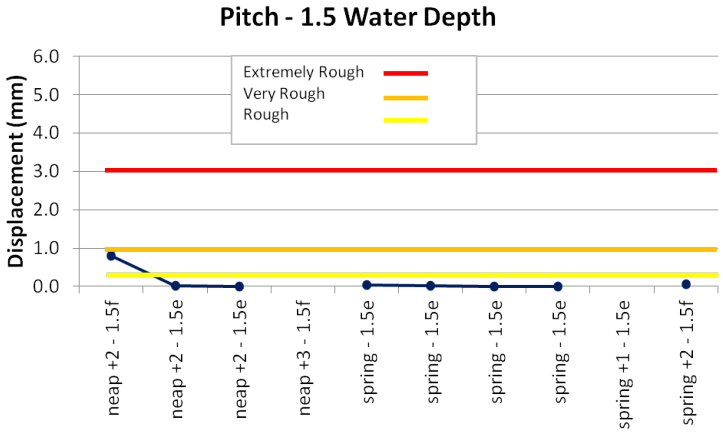

(b)

Figure 7.25: Pitch Motion Vibration Level.

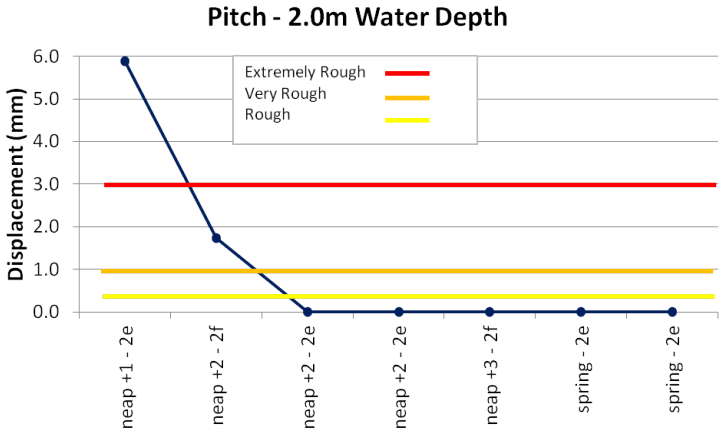

(c)

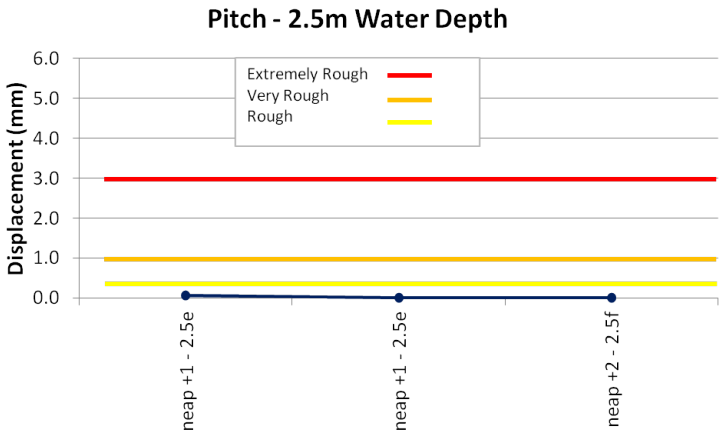

(d)

Figure 7.25: Pitch Motion Vibration Level. (Cont.)

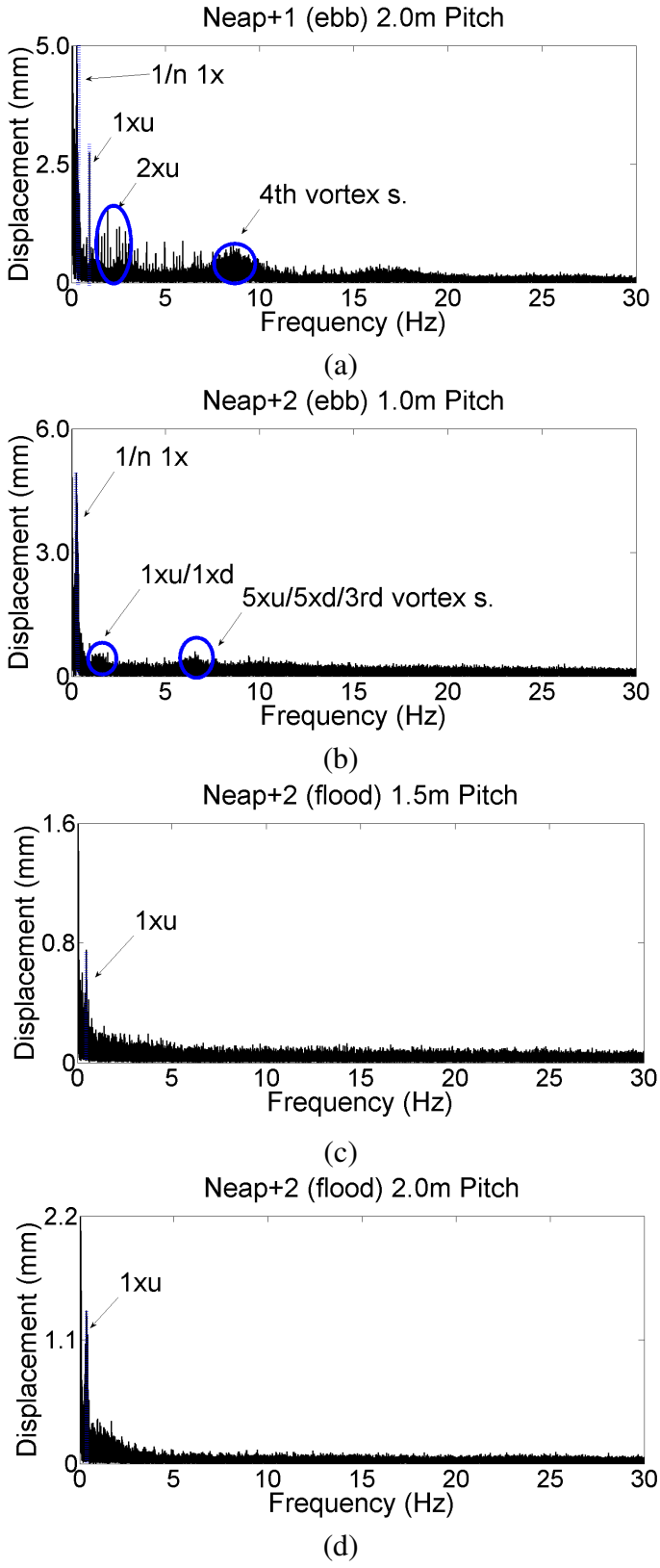

Figure 7.26: Pitch energy spectrums of the tidal cycle.

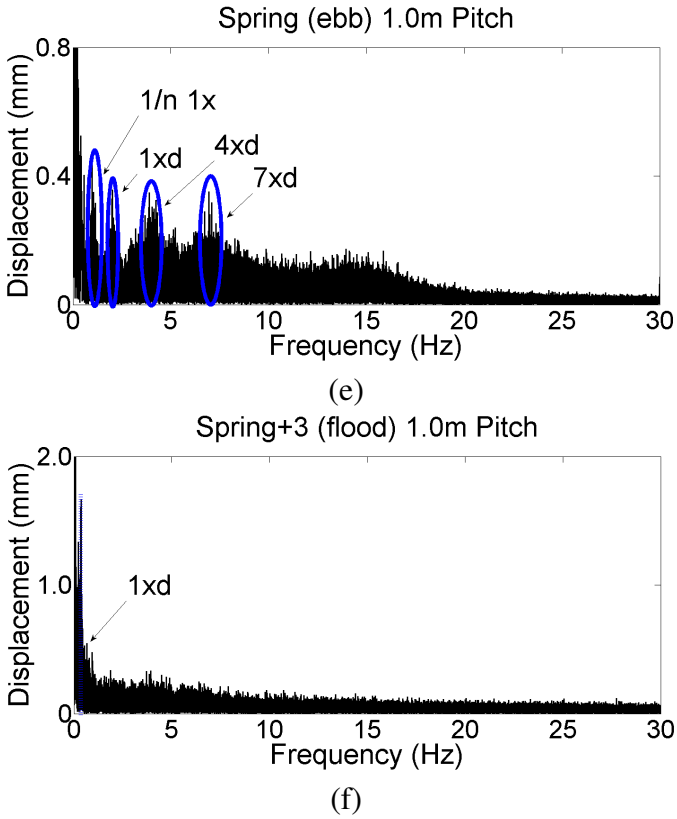

Figure 7.26: Pitch energy spectrums of the tidal cycle. (Cont.)

during ebb conditions than during flood tides (Figure 7.27), contrary to the results found for roll motions. However, the amplitudes are never high. An imbalance of the machine $(1/n\,1x)$ is also observed in Figures 7.28 (d) and (i), the first case being the most affected. Again, it is conjectured that a ship wash is responsible for such a disturbance.There are no discernible frequencies related to blade interactions. However, there are various cases where the support structure's vortex shedding is depicted in the yaw frequency spectra, e.g. Figures 7.28 (b), (c), (d), (g) and (i)). Von Karman Vortices appear during flood conditions in deep water ($2\,\mathrm{m}$ immersion) and closer to the free surface during ebb conditions where the flow is more turbulent.

The second harmonic of the rotor speed $(2x)$ is related to mechanical play or backlash in the turbine. This frequency is mostly identified during records from the flood tides (Figures 7.28(c),(e) and (f)). The 3rd harmonic $(3x)$ is also evident in the yaw spectra as found in Chapter 6. Higher harmonics $4x$ and $5x$ are observed during flood conditions with a very low amplitude.

Moreover, a large amount of insignificant low frequencies are found in some of the spectra (such as Figure 7.26(a)). These signals have a frequency of around $0.5\,\mathrm{Hz}$ between each peak and are likely to reflect ripples from continuous wave patterns.

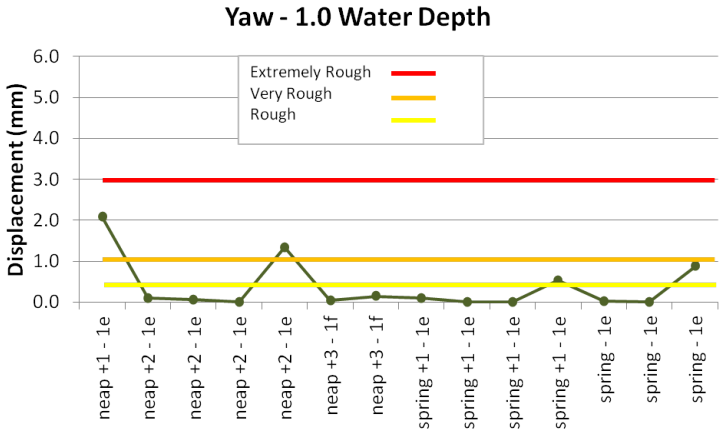

(a)

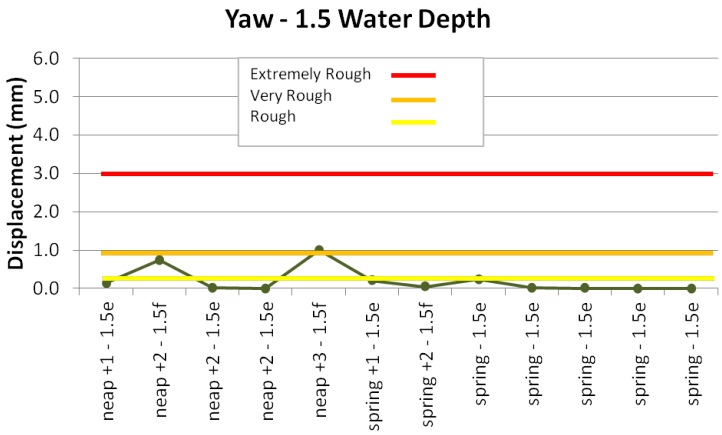

(b)

Figure 7.27: Yaw Motion Vibration Level.

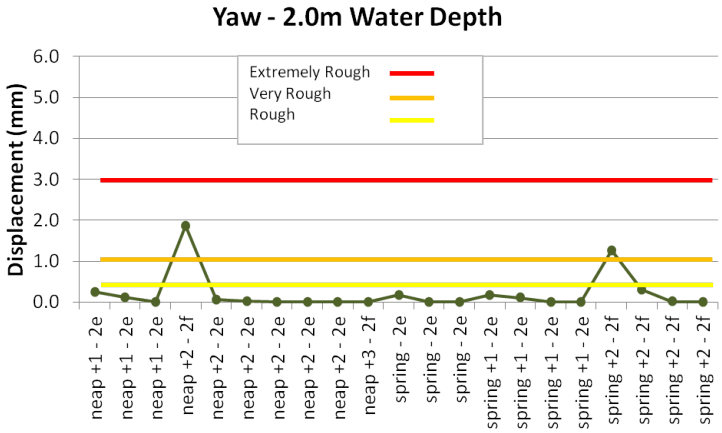

(c)

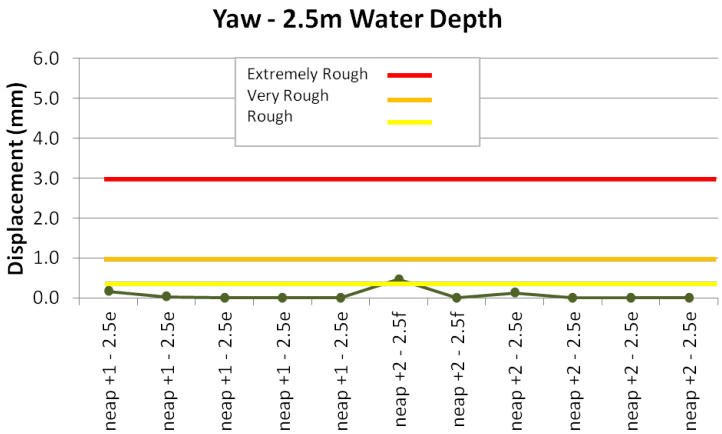

(d)

Figure 7.27: Yaw Motion Vibration Level. (Cont.)

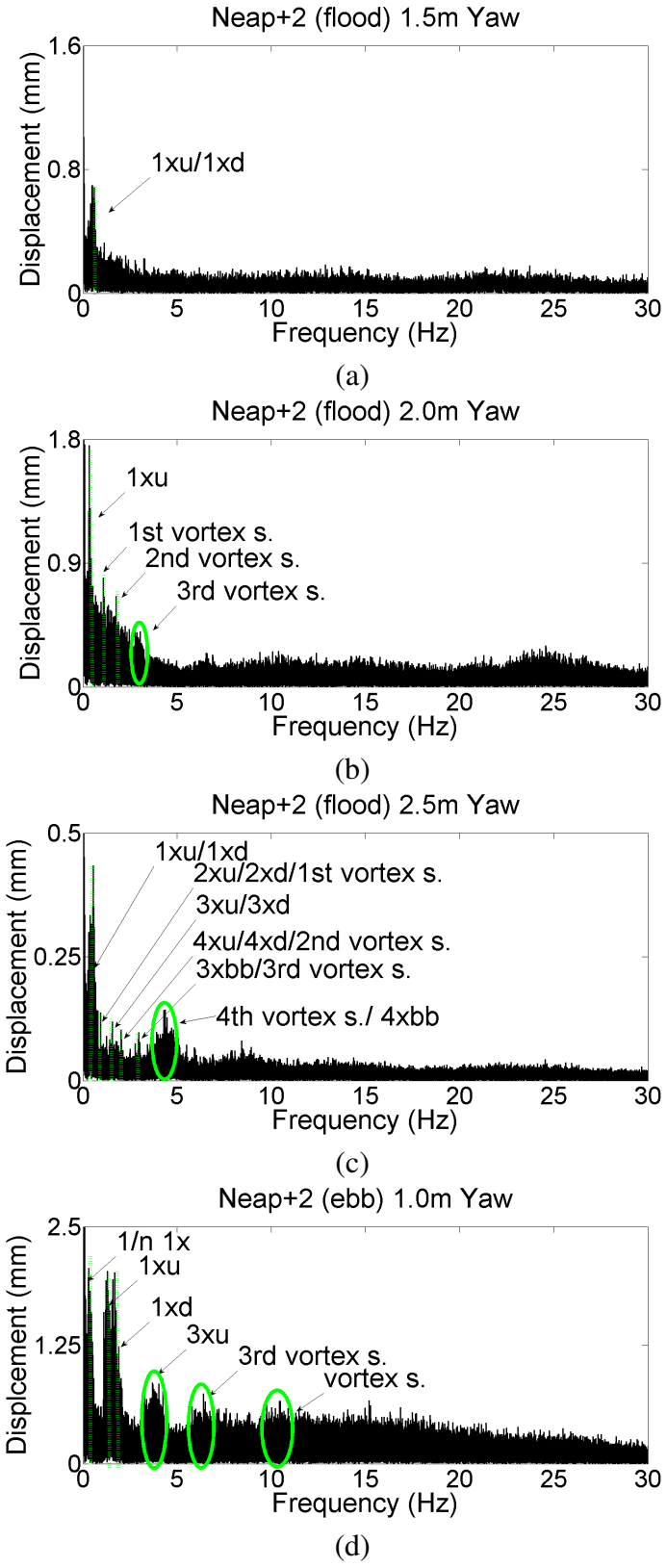

Figure 7.28: Yaw energy spectrums of the tidal cycle.

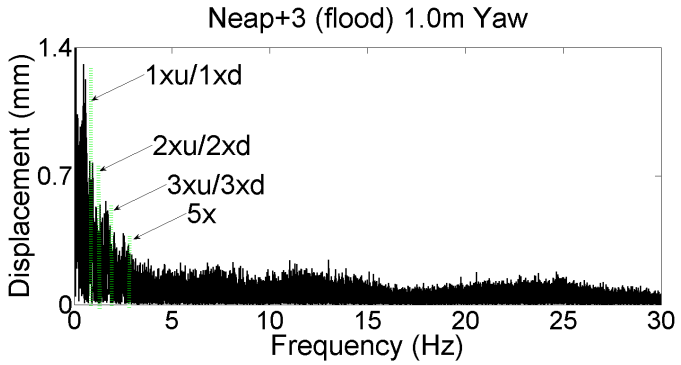

(e)

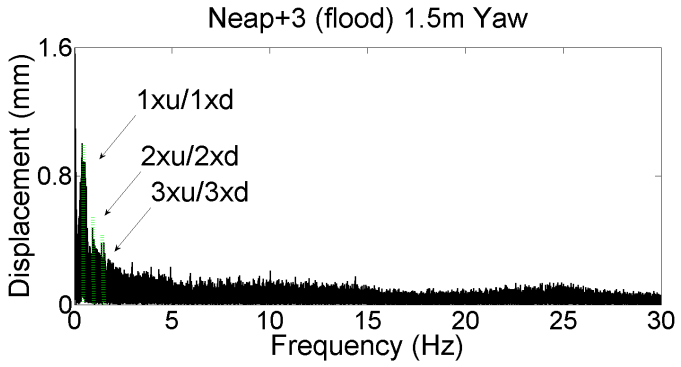

(f)

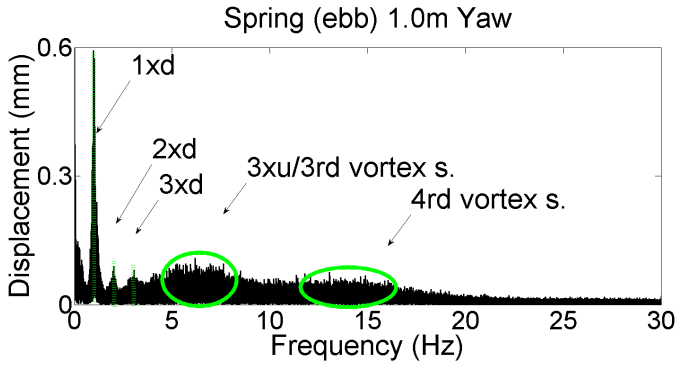

(g)

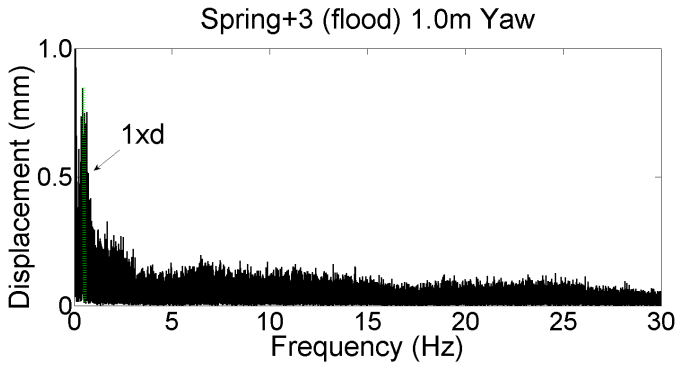

(h)

Figure 7.28: Yaw energy spectrums of the tidal cycle. (Cont.)

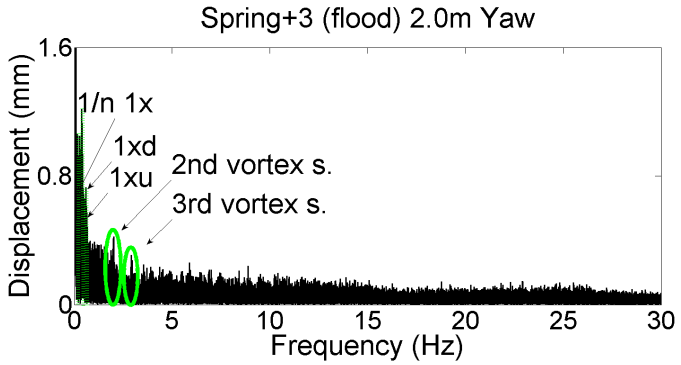

(i)

Figure 7.28: Yaw energy spectrums of the tidal cycle. (Cont.)

Event	Tidal Cycle	Flow Direction	Deployment Depth
1	Neap +2	Flood	1.5 m
2	Neap +2	Flood	2.0 m
3	Neap +2	Ebb	1.0 m
4	Neap +3	Flood	1.5 m
5	Spring	Ebb	1.0 m

Table 7.4: Highest Vibrations on the same Tidal Cycle.

Overall, five particular experimental occurrences are identified where high vibrations occurred about the three rotational axes (Table 7.4). It is observed in Table 7.4 and in Table 7.3 that the greatest disturbances were found on three occasions where high intensity wave strikes were recorded. No obvious wave strikes occurrences were observed for the 1st and 3rd event, rather an underwater turbulence generated by a series of passing vessels distant from the turbine installation. As before, most of the significant frequencies are prominent when the device is located closer to the free surface and under flood conditions.

7.9 Summary

The methodology developed in Chapter 4 was utilised in this chapter to measure the dynamic response of scaled up tethered turbines. A 3-4 bladed contra-rotating turbine was deployed at two different sites, an open tidal flow location and a heavily navigated river stream. As expected, it was found that the roll and pitch oscillations were lower in sheltered locations than with a high volume of marine traffic (River Thames).

The upstream rotor frequency was observed in the roll energy spectra as expected (Section 4.7.1). The pitch energy spectra showed frequencies caused by von Karman vortex shedding. According to published tolerance charts, the magnitude of the peak frequencies was found to

be in the “rough” segment during the sea trials, and mostly in the “very rough” areas for the river spectra.

This was a test of a complete TEC system, with electrical power take off. It was not a properly scaled model, its geometry being compromised by the need to accommodate a large permanent-magnet generator. Therefore, from a stability point of view it represented an extreme case , made more extreme by relatively low flow velocities and high levels of turbulence.

Chapter 8

Implication to Operation of Tethered Turbines at Full Scale

The study of support structures in Chapters 2 and 3 gave insight into the advantages and disadvantages of using tethered tidal turbines compared to rigidly mounted devices. It was determined that substantial research into the dynamics of such systems should be investigated is required before full scale devices could contemplate the use of flexible moorings. Therefore, an extensive investigation of the dynamic response of tethered turbines was undertaken in Chapters 5, 6 and 7 according to the methodology proposed in Chapter 4. This chapter discusses a number of issues arising from these investigations and presents the implications for the operation of full scale tethered turbines.

8.1 Tethered Turbine Configurations

As discussed in Chapters 2 and 3, there are various types of tidal energy devices and numerous structural supports for each of them. In deep water locations, it is likely that tethered turbines will be seen as one of the most effective options, as has already been observed in the development of oil and gas technology and is now being discussed for wind (e.g. floating wind turbines).

The work undertaken in this thesis has focused on the evaluation of horizontal axis tidal turbines. In order to provide a generic approach, several rotor configurations (i.e. single bladed, contra rotating and side by side turbines) were studied as tethered turbines in order to identify both positive and negative effects with their use.

In general, it was found that the use of 2 bladed rotors presented higher dynamic instabilities compared to higher solidity turbines with larger number of blades. There are two main aspects for this; first, since the thrust loads are only distributed over 2 sections, the blades are under higher stress which lead to rapid failure (as observed in Chaper 6). In the case of contra rotating systems, a 2-3 bladed configuration was able to withstand higher loads; however, it was demonstrably more fragile than other systems (e.g. 3-3 and 3-4 CRR turbines). Secondly, teeter angles generated by 2 bladed turbines induce unsteadiness in the system, as was observed with 2 bladed single rotor and side by side turbines (Sections 6.4.1 and 6.4.3). Therefore, it is likely that higher solidity ratio full scale turbines will present better dynamic responses than 2 bladed devices.

Indubitably, there are advantages with the use of a single rotor configuration, the most obvious being the simplicity of its design. In testing, it was found for a 3 bladed turbine it was possible to counter act its torque by the use of small stabilisers. Even in the event of blade failure, it was found that the turbine describe an eccentric motion and, mooring line tangling was avoided.

Unfortunately, there are also negative characteristics associated with the use of single rotor turbines in flexibly moored systems. Passive stabilisers cannot prevent the transmission of reaction torque to the mooring under all circumstances. Also, in Chapter 6, it was observed that its use caused the appearance of peak frequencies on the energy spectra. Therefore, such frequencies could lead to resonance on full scale systems. This would be a major problem with high solidity ratio turbines which will require larger stabilisers in order to compensate the generated torque to avoid a continuous roll, as observed with 5 bladed single rotor systems in Section 6.4.1.

In the case of contra rotating systems, it was found as expected that a small increase of power was obtained in comparison with single-rotor turbines. However, this is a minor factor and the main benefit is seen in the ability to counter act torque with the use of a second rotor. Peak vibrational frequencies are only associated with each of the rotors and their super-harmonics, avoiding resonance problems from other sources (e.g. stabilisers). As with single rotor systems, it was observed that contra rotating turbines also describe eccentric motions when blade failure occurs; thus, avoiding mooring line knotting.

It could be argued that this a potential problem with contra rotating systems would be failure to achieve torque equalisation between rotors. In this case, significant roll oscillations would be produced (as observed in Figure 6.21); however, results from Chapters 5, 6 and 7 showed that a contra rotating turbine is unlikely to go under continuous roll motions. Another point is that mooring lines in contra rotating systems would require to withstand greater tensile loads than single rotor turbines since they produce higher thrust loads (around 30% higher).

Turbines with two rotors in the same plane (side by side) have the obvious advantage of generating twice the power of single rotor turbines. The additional structural elements (i.e. the connections between rotors) give only a small increment in thrust loads; therefore, the station keeping system would not be heavily compromised. However there is the possibility of fluid/structure interaction between these structural elements and the rotor blades, producing cyclic loads and hence (possibly) cyclic oscillations of the entire system. As with single rotor turbines, it was found that a 3 bladed configuration would be the most stable. Table 8.1 provides a summary of the points discussed in this section. Table 8.1 provides a summary of the points discussed in this section.

8.2 Small and Medium Scale Tethered Tidal Turbines

As seen in the previous chapter there are more significant advantages and fewer disadvantages with the use of contra rotating turbines in tethered systems. Therefore it was conjectured that 3-3 or 3-4 configurations would be ideal to examine as larger scale devices. Since it is known that higher solidity ratio turbines would present better alignment properties, a 3-4 configuration was selected for real sea condition tests.

Chapters 5, 6 and 7 presented the analysis of a 3-4 contra rotating turbine at different scales. As mentioned in Chapter 4, Froude number was easily scalable and the values achieved during laboratory and real conditions oscillated around 0.15. In the case of Reyolds number, the disparity between the two cases was considerable; but, as stated in McCombes et al. (2010) Reynolds scaling is usually impossible to achieve and does not influence greatly the performance of turbines. Similarity of inflow turbulence was achieved between the flume and real sea conditions with 7% and 6% on average, respectively.

Since water depth and other conditions were in some cases restrictive, three station keeping systems were used during the experimental phases. Steel wire mooring lines were used during the tests of small scale turbines working under pure tension in both tow and flume tanks and free from external disturbances (e.g. mammal interaction, debris, etc.). In a similar manner, a larger scale turbine was deployed in a very unstable environment by means of flexible linkages which allowed the turbine to move freely in the three rotational angles; therefore, it could be considered that the turbine was mounted similarly to the small scale prototypes. The main difference is that this time, the turbine was subjected to random events (e.g. wave strikes from marine traffic). A more realistic approach to full-scale deployment of a tethered turbine was employed during the Sound of Islay tests. In contrast to the two approaches described earlier, the turbine was moored to the seabed with a steel wire mooring line with a surface buoy producing an upward force, giving freedom to deploy the turbine at the desired height

Turbine Configuration	Advantages	Disadvantages
Single Rotor Turbines	• Cheaper device in terms of number of blades and simplicity of system. • 3 blade systems require small stabilisers to provide an adequate dynamic response. • Eccentric motions when blade fails (but avoiding continuous roll).	• 2 bladed systems exhibit instability due to teeter angles, possibly leading to blade failure • High solidity rotors (4 or 5 blades) will require larger stabilisers in order to avoid continuous roll problems. • Stabilisers increase the mass of the system; therefore, more robust station keeping systems would be required. • Stabilisers could produce resonant frequencies in the system.
Contra Rotating Turbines	• A second rotor counter balances the torque of the system; therefore, no additional members are required in the system. • Even if the torque is not perfectly balanced it is unlikely to generate continuous roll motions. • Eccentric motions when blade fails (avoiding continuous roll). • Power output increases slightly compared to single rotor turbines.	• 2 -3 or 2-2 bladed configurations are affected by the 2 bladed teetering angles in their dynamic motions. They are also fragile compared to other contra rotating turbines. • If torque of both rotors is not counteracted correctly, several frequencies appear in the energy spectra which could lead to resonance problems. • The turbine generates around 30% more thrust than single rotor turbines.
Side by Side Turbines	• Double power generation. • 3 bladed turbines presented adequate dynamic responses. • Minimal increase in drag force from extra structure (5% according to the configuration presented in Chapter 6).	• Teetering angles of 2 bladed systems induce unsteadiness. • Vortex shedding frequencies created by the connecting strut. • Potential for instability due to blade/structure interaction. • Blade failure and instability show similar dynamic responses (e.g. continuous roll) leading to possible line tangling.

Table 8.1: Advantages and disadvantages of several tethered turbine configurations.

(mid part of water column). The main difference would be reflected in surge motions (tensile and compressive loads measured by means of load cells); fortunately, during the Sound of Islay tests, the environmental conditions remained reasonably calm . Therefore, the results obtained from the three approaches should be comparable between each other.

Power coefficient of the larger scale contra rotating turbine was between 0.21 and 0.26. Such values were similar to those predicted by Clarke et al. (2008) at the same tip speed ratio conditions, and reflect the non-optimal geometry of this prototype device, with a large hub and short blades. Thrust coefficients matched the theoretical values in most of the cases (Ct =~ 0.38). In the case of the small scale turbines power and thrust coefficients were around 0.24 and 0.95, respectively. These had a nacelle/blade diameter ratio of around 0.15 – 0.25 (according to private communications), which is representative of full-scale designs but far from the value seen on the 1m diameter turbine used in the river and sea trials (0.40). Of course for very small scales, measured power coefficients tend to be low because of Reynolds number effects on the blades, and high frictional losses.

Differences between dynamic responses were examined in Chapters 5, 6 and 7. As expected, the electro-mechanical control used in the larger contra rotating turbine gave more consistent equalisation of torque between the two rotors, producing lower roll variations even in turbulent environments, such as the River Thames. The purely mechanical brakes fitted to the small scale turbines were more difficult to control, giving significant roll oscillations even in tow tank testing.

Pitch and yaw deviations in the larger turbine were in some cases extremely high (e.g. $40°$ and $70°$, respectively) due to the large nacelle diameter and the relatively short length of the turbine blades; despite this, pitch oscillations in this case were only half those obtained in flume tanks at the same flow velocity. One reason may be that in the outdoor trials there was a large distance between the seabed and the turbine; thus, turbulent effects from the bottom layer were avoided. The importance of deploying a turbine with sufficient clearance between it and the seabed was therefore highlighted.

Yaw variations were similar in the three test regimes. This indicated that the thrust load created was more than adequate to align the turbine to be parallel with the flow direction. Certainly ship washes increased temporarily such variations and created misalignments, as observed in Figures 7.19, 7.21 and 7.23; but satisfyingly, the turbine went back to its stable position after a few seconds.

Rotor Diameter	3-4 CRR Turbine of 0.3 m		3-4 CRR Turbine of 1 m	
	Source of frequency	Displacement (mm)	Source of frequency	Displacement (mm)
Flow Velocity	0.4 m/s		0.4 m/s	
Roll	1xd	2.27	n.a.	n.a.
Pitch	1xd	1.02	n.a.	n.a.
Yaw	1xu	0.04	n.a.	n.a.
Flow Velocity	0.5 m/s		0.5 m/s	
Roll	1xd	2.97	1xu	0.94
Pitch	1xd	0.43	Vortex Sh.	0.002
Yaw	4xd	0.01	1xu	0.47
Flow Velocity	0.6 m/s		0.6 m/s	
Roll	1xd	3.47	n.a.	n.a.
Pitch	1xd	1.02	n.a.	n.a.
Yaw	3xu	0.02	n.a.	n.a.
Flow Velocity	0.8 m/s		0.8 m/s	
Roll	1xd	1.08	1xu	0.15
Pitch	1xd	0.9	1xu	0.07
Yaw	1xbb	0.02	1xu	0.17

Table 8.2: 3-4 Contra Rotating Turbine Mechanical Vibrations.

8.3 Vibration Analysis of Small and Medium Scale Tethered Tidal Turbines

In order to assess the impacts on a tethered turbine; roll, pitch and yaw motions were not only studied in time domain; additionally, the peak frequency amplitudes were studied throughout the thesis. In order to compare turbine prototypes at different scales, the peak frequency amplitudes of both 3-4 contra rotating turbines (0.3m and 1m of rotor diameter) were compared during similar flow conditions (e.g. flow velocity and turbulence intensity). 2.5m water depth data related to the 1.0m rotor were considered in order to compare similar conditions between laboratory and real sea events.

It was identified that the main source of vibration was related to the angular velocity of the rotors (i.e. 1xu or 1xd). As observed in Chapter 7, most of the peak vibrations that were within the "extremely rough" intensity belonged to either "wave strike" or 1m water depth location occurrences; therefore, all the cases presented in Table 8.2 are below such level.

The major vibration intensities are noted in the roll energy spectra, being those of the small scale turbine within the "very rough" level and substantially higher than those presented by the 1.0 m turbine. Similarly, pitch vibrations are higher in the small turbine than in the larger scale device. These results can be associated with a correct torque compensation between

rotors on the design of the larger scale turbine; respectively. However, full scale turbines might not be able to avoid vibrations in the yaw energy spectrum. Observed behaviour in sea trials could be related to significant turbulence effects from the 3 principal directions. Contrast this to the relatively confined conditions in flumes, where the turbulence in the "x" direction (i.e. north to south – flow direction) is far greater than that in the "y" (i.e. east to west) or "z" (i.e. upwards to downwards) directions.

To a small extent and with fewer appearances, Strouhal vortices were also observed in some of the energy spectra (Chapter 8.2). As stated in Table 8.1, frequencies related to vortex shedding might not be expected in contra rotating turbines, due to the lack of transverse structural members. However, vortex shedding from mooring lines might have an influence on tethered configurations if large diameter cables are used. Moreover, if the turbines are kept on station with tubular sections (e.g. rigid structures such as frameworks of monopiles), an influence of vibration from the structural struts should be expected. There is the further consideration that as turbines are scaled up, the angular velocity of the rotor will decrease making it more likely to generate resonant frequencies closer to those created by vortex shedding from structural supports. To minimise vibrations, streamlined struts or shrouds may be used in the structural support systems.

8.4 Final Assessment of Tethered Tidal Turbines

According to the work presented during this thesis, it can be concluded that 3 bladed tethered tidal converter designs, including 3-4 contra rotating turbines, will be a feasible solution to extract energy from marine currents. In order to minimise unsteadiness of the device it is recommended that, just as wind turbine designs, 3 bladed systems are used, at least when tethered designs are considered. Also, higher solidity ratio turbines will provide more accurate alignments to the flow direction due to higher thrust loadings therefore, power losses due to misalignment will decrease.

According to the results of Chapter 7, tethered turbines would benefit from deployment far from surface interactions (e.g. wave strikes). Therefore, due to the flexibility of a flexible mooring, such configurations are likely to be re-designed if required (adjusting line dimensions) which is inconceivable with rigidly mounted structures. However, one of the main disadvantages related to small and medium scale tethered turbines or turbine with a high aspect blade/nacelle ratio is that random events generate high vibrations in the machine which will lead to faster mechanical system failure (e.g. bearing failure, backlash on the machine). But it was discovered that as the tethered turbine is scaled up, the magnitude of such vibrations decreases, a satisfactory indication in the case of full scale systems.

If a tethered system is designed to be kept on station by mooring lines and consists of a contra rotating rotor, it would be possible to get rid of undesirable sources of vibration such as those generated by rigid structures or connecting parts (as in the case of twin rotor arrangements). In this case, developers should also consider the use of synthetic ropes or hybrid configurations comprising them in order to avoid possible failure due to tangling. Similarly, it would be recommended that catenary lines would be carefully used or perhaps not used at all. The reason is that due to surge motions generated by marine traffic, animal life, and so on, the catenary system would need to be reinforced either with a stiffer chain or with external elements to increase the mass of the system; therefore, it is possible that the system would be as heavy as a rigid foundation at the end. Also, steel wires could degrade due to continual twisting motions during the turbine's operation.

As with the River Thames, small establishments situated along similar river paths (even if affected by a tidal regime) would benefit from a source of free and clean energy. In this case, small tethered turbines will be able to provide such requirements without the need of large structural connecting elements.

Chapter 9

Conclusions and Recommendations

This chapter presents the conclusions of the investigation carried out and identifies areas for future research to be undertaken to extend and built upon the outcomes presented in this thesis.

9.1 Conclusions

The main objective of this thesis was to develop an experimentally-based methodology to study the dynamics and vibrations of tethered systems. In order to ensure its viability, the dynamic response of various types of small scale tethered turbines has been undertaken. The same process has been applied to a scaled up tethered tidal turbine deployed in outdoor turbulent environments.

Overall, it was concluded that the use of the methodology proposed in Chapter 4 of this thesis is suitable to monitor the dynamic response of tethered devices at various model scales. The information obtained from accelerometers must be studied in both time and frequency domains in order to perceive each of the parameters that influence the dynamic response of tethered turbines. From the results obtained it was concluded that:

- The use of rigid foundations such as framework or minipile structures should not ruled out during initial design stages. It has been proved that such structures can support severe loads associated with marine turbines with minimum mechanical stresses. However, it was observed that their used is limited to shallow water locations as it has been observed in wind and oil technology (Chapter 2 and 3).
- The stresses and dimensions on a quadpod configuration are lesser than those obtained

in tripod configurations; however, due to the costs associated with additional members the system becomes economically feasible only at high flow conditions (Chapter 3).

- Flexible mooring structures have lesser material costs, do not have water depth limitations and allow the turbine to align to the flow; however, high stresses on the lines mean that they will need to be changed frequently (Chapter 3).

- The dynamic response of tethered turbines is highly influenced by environmental conditions. For example, in Chapter 5 the use of a flume tank provided similar flow conditions to real scenarios, at least in terms of turbulence. But due to high blockage ratios, yaw and pitch motions showed distinct differences. Thus, in order to predict the dynamics of a turbine, it is necessary to understand the way in which the system relates to its environment (Chapter 5).

- Higher solidity rotors achieve better dynamic stability than 2 bladed single rotor turbines. Teeter angles created in 2 bladed systems induce instability on the devices (Chapter 6).

- Single-rotor turbines can be used as tethered configuration but in order to produce reactive torque compensation, stabilisers must be included in the design. The main disadvantage in their use is that the stabilisers produce their own characteristic frequencies of oscillation, leading to possible resonance problems (Chapter 6).

- Co-axial contra-rotating turbines showed a much better dynamic response. But in order to minimise roll motions, accurate torque equalisation controls must be integrated in the design (Chapter 6).

- Twin-rotor co-planar turbines will be compromised by vortex shedding from the connecting structural member. Tests pointed to instability in the device, especially in the case of two-bladed turbines (Chapter 6).

- The number of peak frequencies (harmonics) decreases and present a delineated shape when the turbine presents better dynamic response characteristics; thus, there is a lesser risk of resonance problems (Chapter 6)

- During blade failure, eccentric motion was observed for single and contra-rotating turbines, in the time domain. The axis of rotation traced out a conical surface behind the mooring point (Chapter 6).

- The use of the methodology to monitor side by side turbines must be complemented with the use of other sensors to detect blade failure, since the dynamic response reported during blade failure and unbalanced conditions presents similar signals in both time and frequency domains which have been quantified in this work.

- Vortex shedding was observed in a number of cases and will occur if support structures are not properly designed with streamline sections or any other type of protection. This has been characterised and measured in the thesis (Chapters 6 and 7).
- Wave strikes can influence the roll, pitch and yaw oscillations of a turbine but usually the turbine will return to its steady conditions after a few seconds, at least for a co-axial contra rotating configuration. The extent of these have been evaluated in the research presented here (Chapter 7).
- If wave strikes occur during slow flow speeds, the disturbance to the turbines can be severe. This is therefore of particular concern at times of 'slack water' (Chapter 7).
- The existence of a highly turbulent environment is visualised as random energy in the frequency analysis of the signals which has been presented in the results of this thesis (Chapters 5 and 7).
- Yaw measurements have proved that even if the turbine goes under severe misalignment due to external effects, they recover rapidly and align accurately to the flow. Therefore, complex controls could be avoided in tethered designs 5, 6 and 7.
- Nacelle/blade diameter ratio lesser than $0.15 - 0.25$ can cause large pitch oscillations which in turn affect the performance of the turbine (Chapter 8).
- As tethered turbines are scaled up, mechanical vibrations have lesser magnitudes. This was associated with the use of suitable torque control equalisation. However, thrust loads also play an important roll in device stability which will be larger on full scale systems. This gives confidence to developers of tethered turbines Chapter 8).
- The use of synthetic mooring lines directly coupled to the turbine is highly recommended in order to avoid the rapid failure of steel wire ropes or chains if the turbines are subjected to excessive roll motions. (Chapter 8)

9.2 Contributions

This thesis advances current knowledge in the tidal technology field with the following key contributions:

- Development of a novel methodology to study the dynamics and vibrations of tethered TECs.

- First reported demonstration of the dynamic response and the mechanical vibrations of several tethered small scale turbines operated in various flow conditions within a repeatable and controllable environment, where blade failure effects were also studied.
- First reported demonstration of the dynamic oscillations and mechanical vibrations of a larger contra rotating turbine at sea and in a turbulent river environments, where the effects of wave strikes created by passing vessels were also studied.
- Demonstration of the dynamic response of several rotor blade configurations with different solidity ratios and how 2 bladed systems present specifically instability problems.

9.3 Recommendations

There is a clear and urgent need for the development of sophisticated analytical tools to predict the behaviour of the complete system of a neutrally buoyant tidal turbine and its flexible mooring system. Such tools must consider coupling effects between the hydrodynamic behaviour of the turbine and its mooring, in response to incoming turbulence or other transient effects. In that regard, the rotational angles of floating turbines could be coupled through dynamic libraries to software specialised on cable dynamics, similar to what has been done for flexibly moored OWTs (Appendix B).The effects of using different rotor configurations and numbers of blades could then be examined, as in the work described in this thesis.

Another option is to use the information obtained in this work and to undertake a modal analysis with the use of the experimental data. According to Piersol and Paez (2002) in order to carry this analysis several parameters must be firstly established. For example, the modal parameters could be obtained through the frequency domain analysis where the peak frequencies can give an insight of the number of modal frequencies in the analysis. However, other modal identification models can also be utilised (e.g. Stability Diagrams). The models can then be validated through several procedures; for example, modal vector consistency or finite element analysis.

Moreover, structural elements of the station keeping itself should be investigated. For example, scaling up the stiffness and damping of different mooring line arrangements. Similarly, snap loads during surge motions should also be widely investigated since this will give an indication on the replacement of mooring line sections.

9.3.1 Tolerance Charts and Condition Monitoring

The use of tolerance charts has been proved to be practical throughout the thesis; however, it was observed that the available tolerance charts had been made to study rotordynamic machines fixed rigidly; therefore, they do not represent accurately the intensity of a tethered turbine's behaviour. In that regard, the author believes that investigation and development of novel tolerance charts focused on tethered marine turbines should be created. To facilitate that process, comparative experimental tests with rigidly mounted tidal turbines and flexibly moored turbines should be carried out to investigate the differences between the systems. Similarly, matching up loading frequencies (e.g. thrust loads) and mechanical vibrations should also be considered in future work tasks.

Furthermore, the use of other signal processing tools should be further investigated in order to compare and benchmark the methodology presented in this thesis. For example, the use of the Wavelet signal processing tool could be employed in the analysis. This tool is usually used for the analysis of video processing or biomedical imaging but due to the facility to undertake Fourier Transforms with different appliances (e.g. windowing functions and filters), it can be a useful tool in the analysis of the dynamics of tidal turbines.

The methodology proposed in this thesis should be extended and applied to larger scale tidal turbines and also to rigidly mounted turbines, to confirm its validity.

Appendix A

Drawings

Drawings can be found in the following pages.

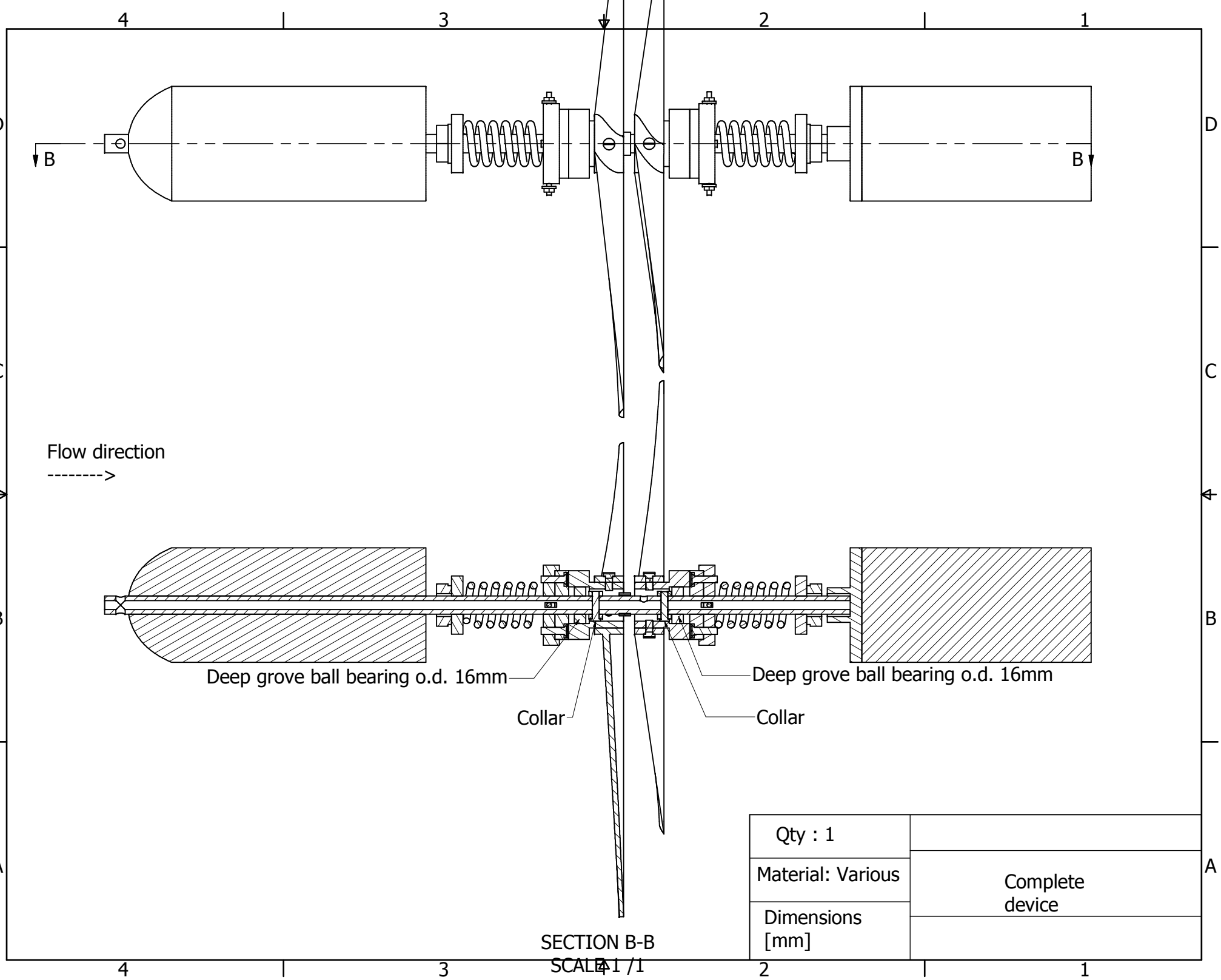
4
3
2
1
D
C
B
A
B
B
Flow direction
-------->
Deep grove ball bearing o.d. 16mm
Deep grove ball bearing o.d. 16mm
Collar
Collar
SECTION B-B
SCALE 1 /1
Qty : 1
Material: Various
Dimensions [mm]
Complete device

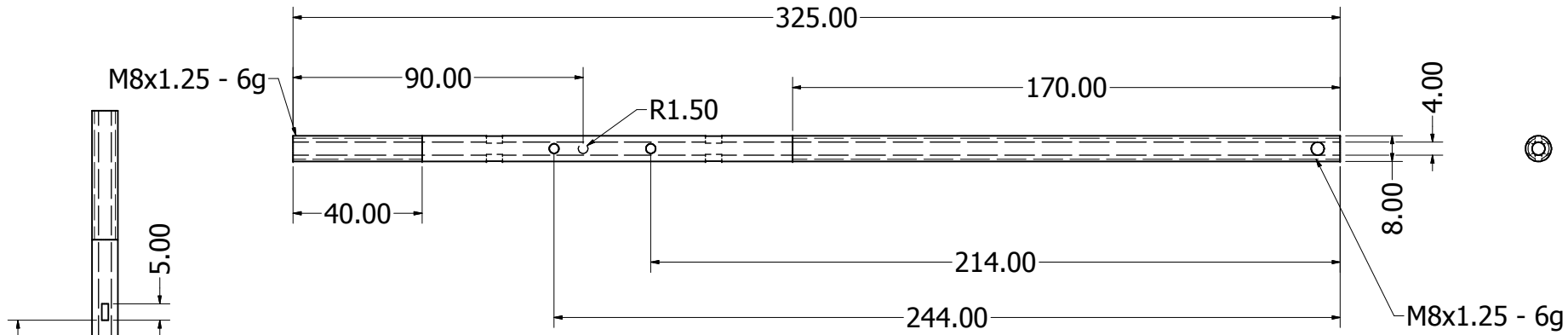

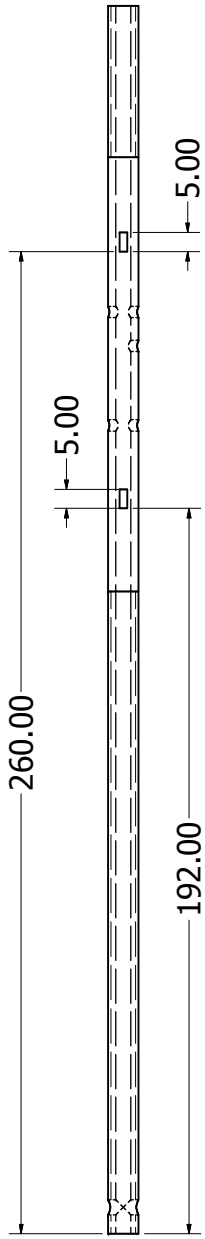

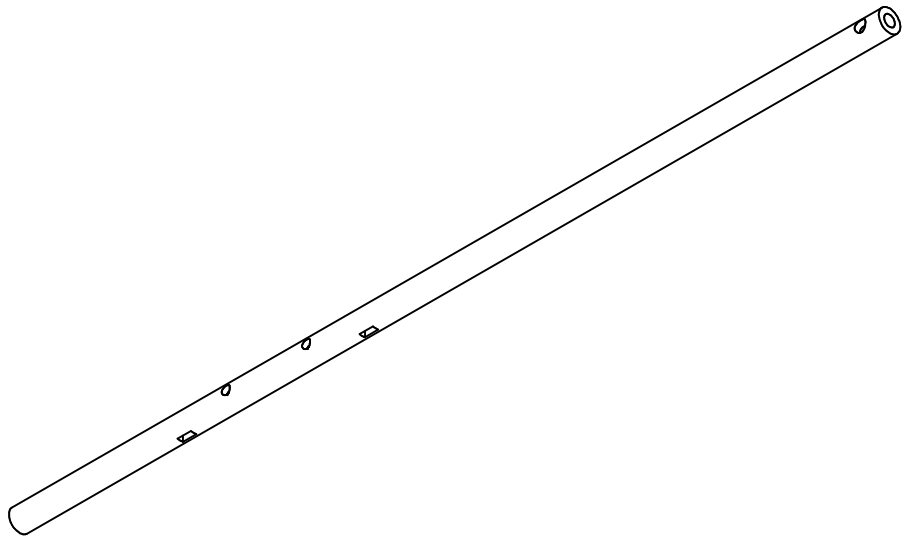

Qty : 1	
Material: Aluminium	Shaft
Dimensions [mm]	

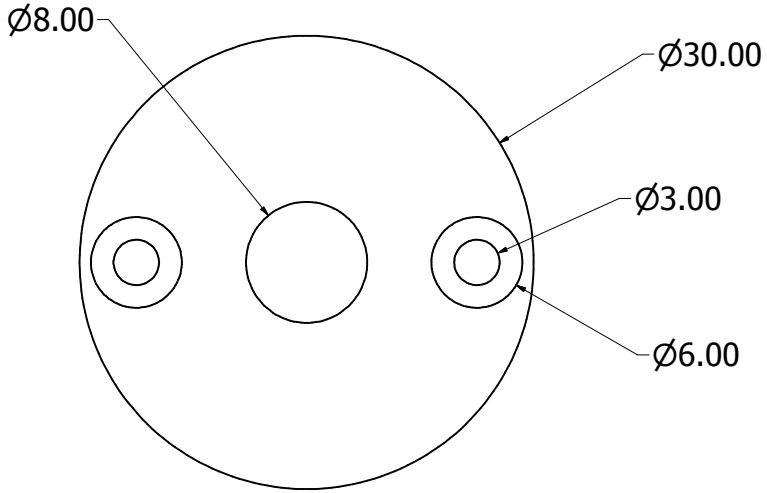

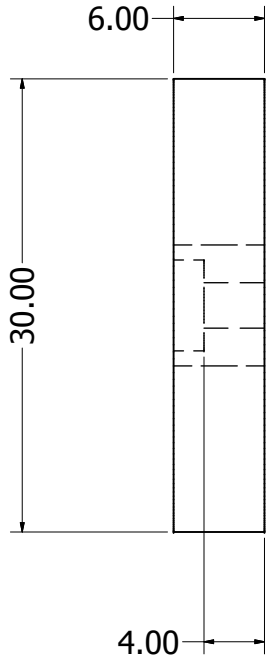

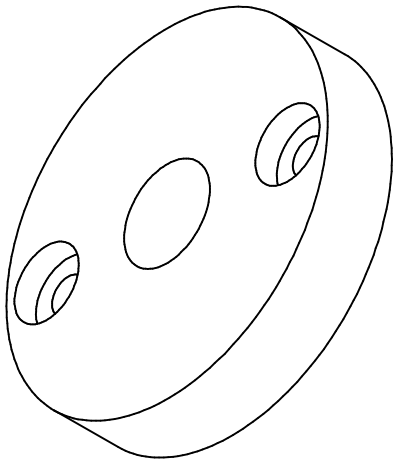

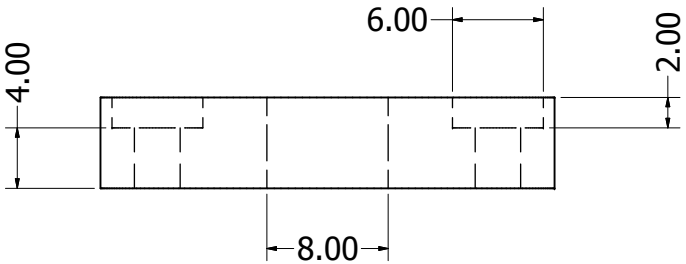

Qty : 2	
Material: Brass	Friction Disc
Dimensions [mm]	

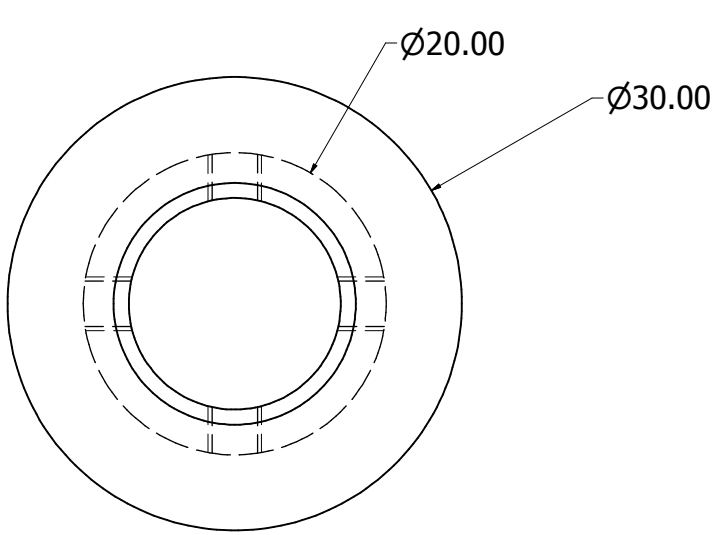

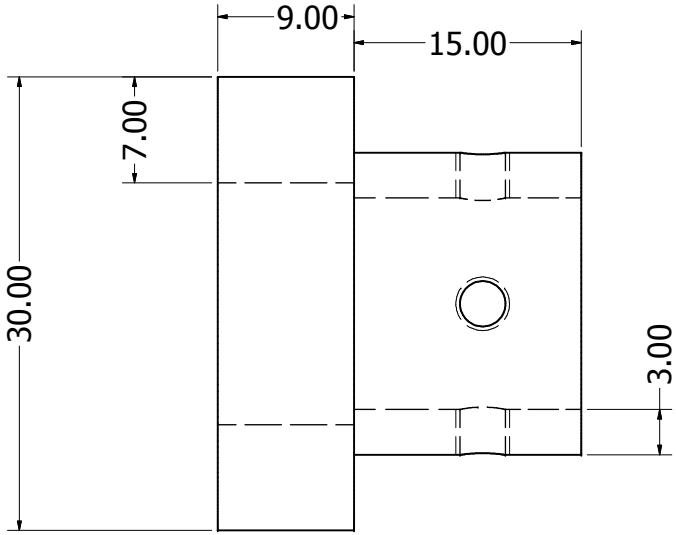

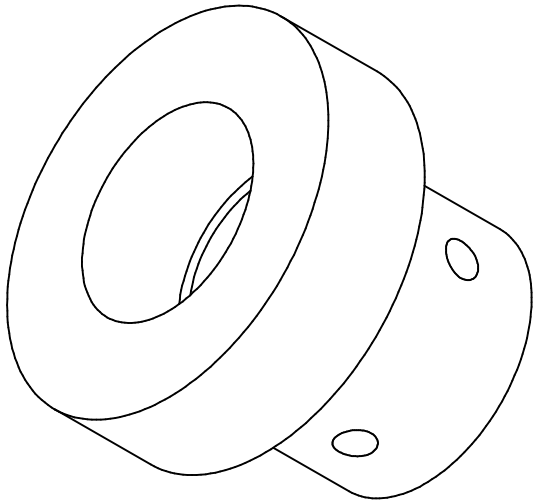

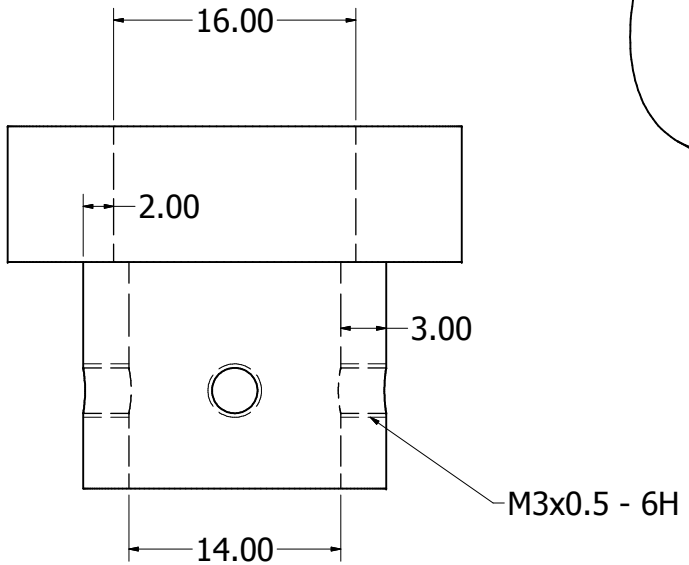

Qty : 1	
Material: Aluminium	Hub - 4 blades
Dimensions [mm]	

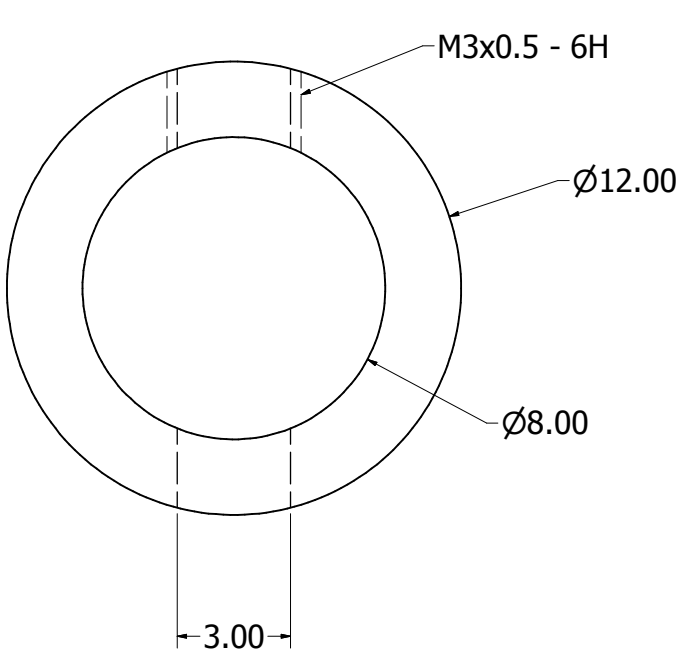

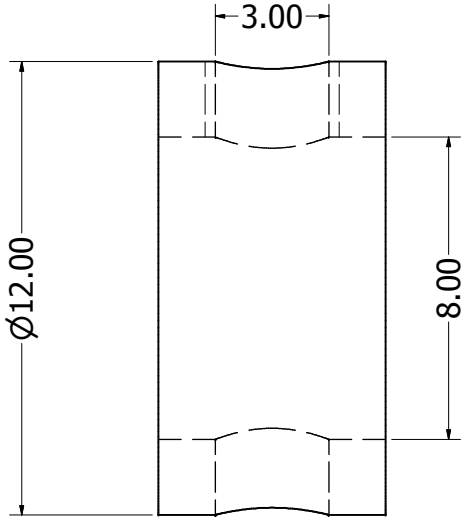

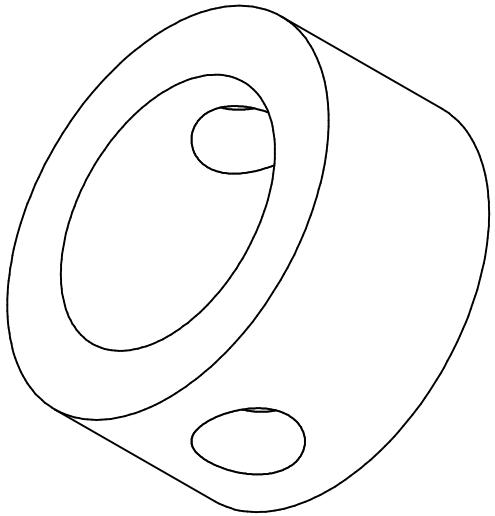

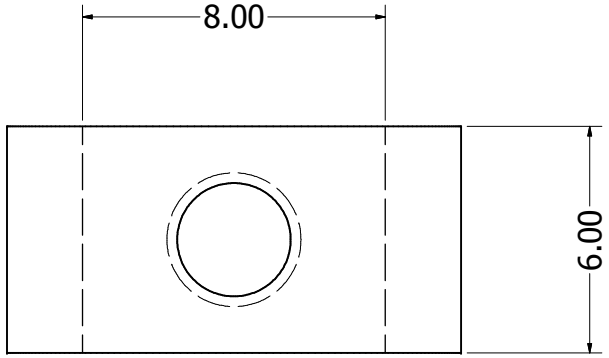

Qty : 2	
Material: Aluminium	Collar
Dimensions [mm]	

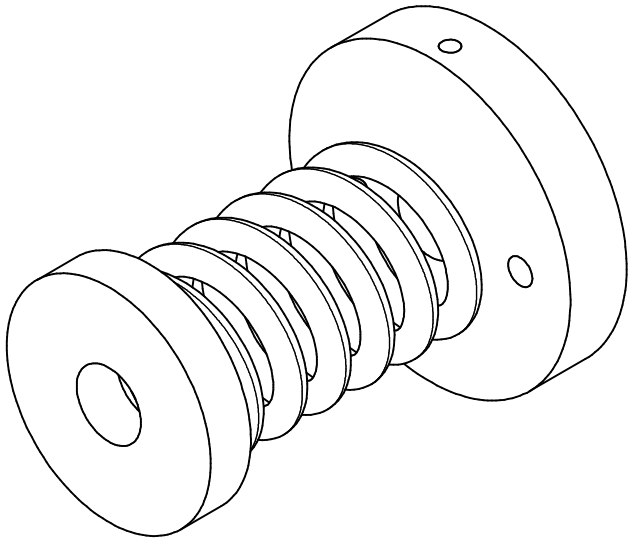

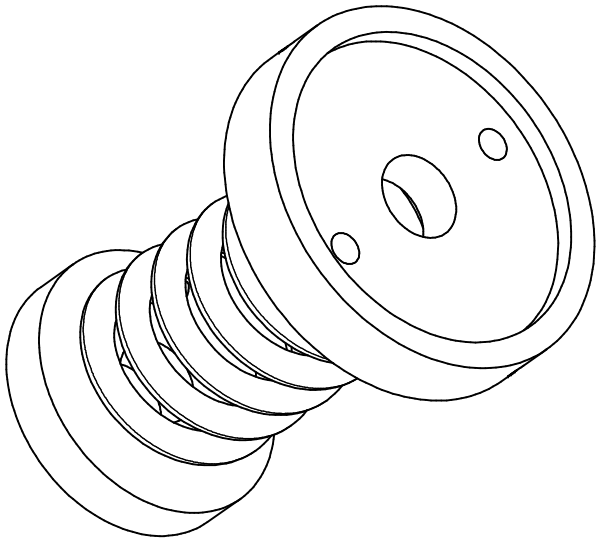

Qty : 2	
Material: Aluminium	Spring & Support
Dimensions [mm]	Isometric view

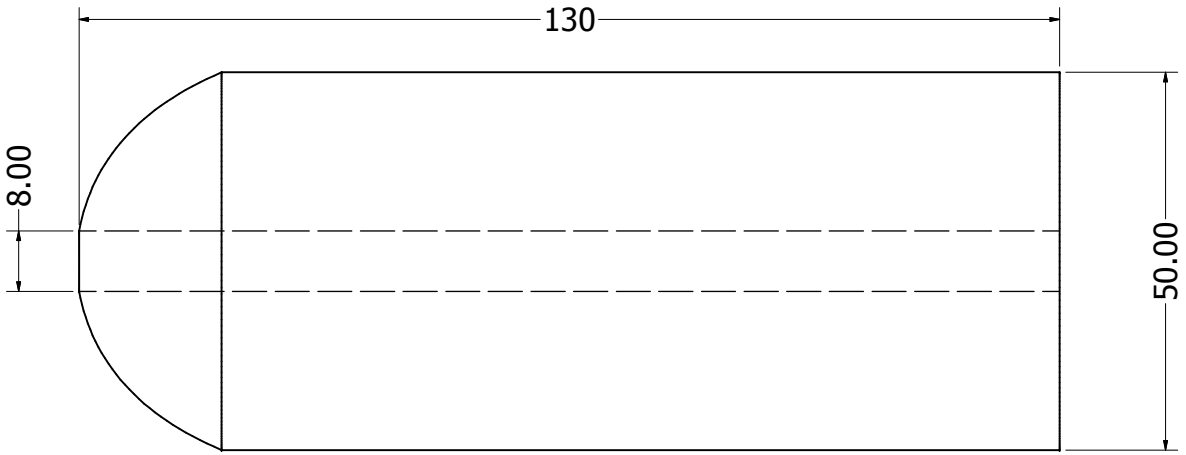

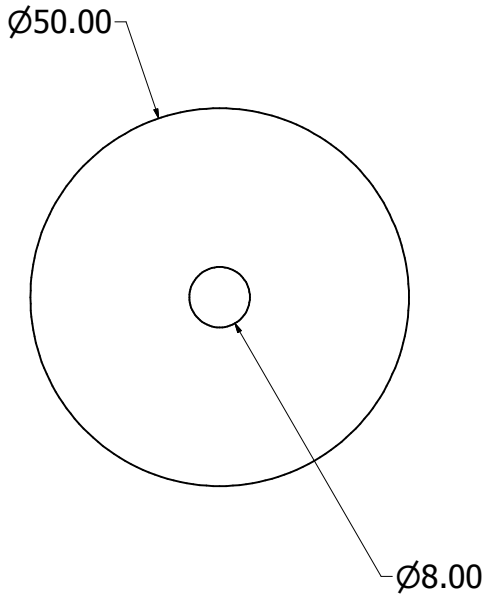

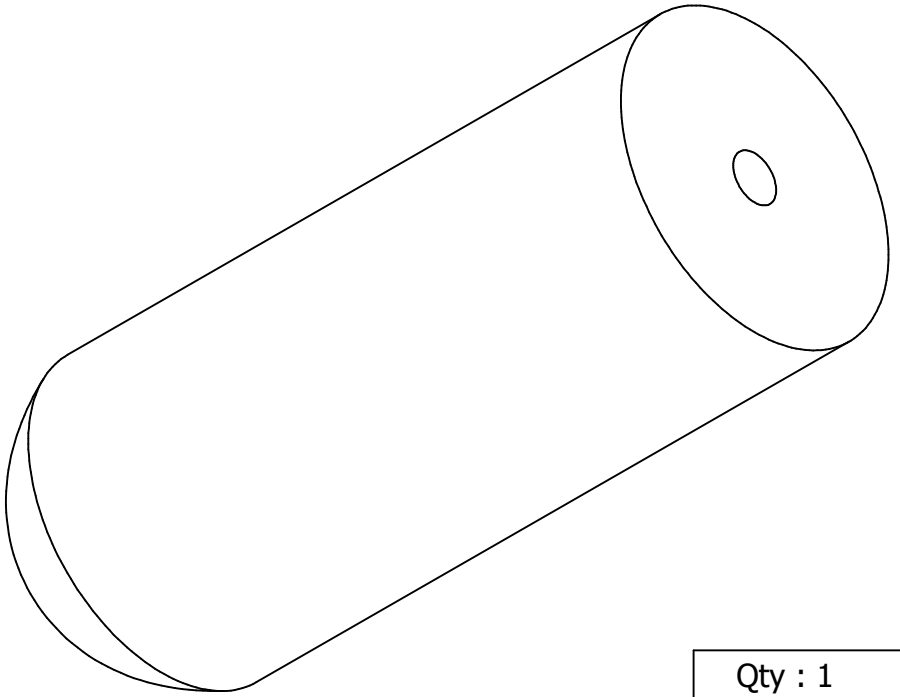

Qty : 1	
Material: Divinycell	Nacelle
Dimensions [mm]	

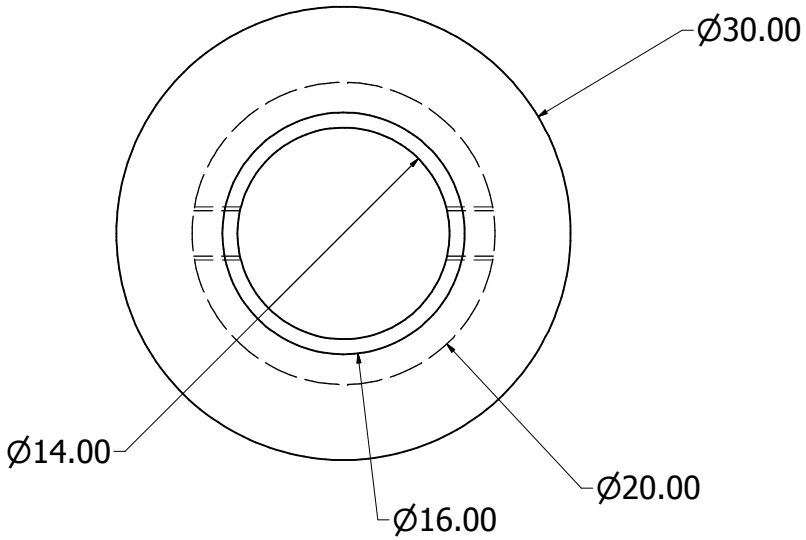

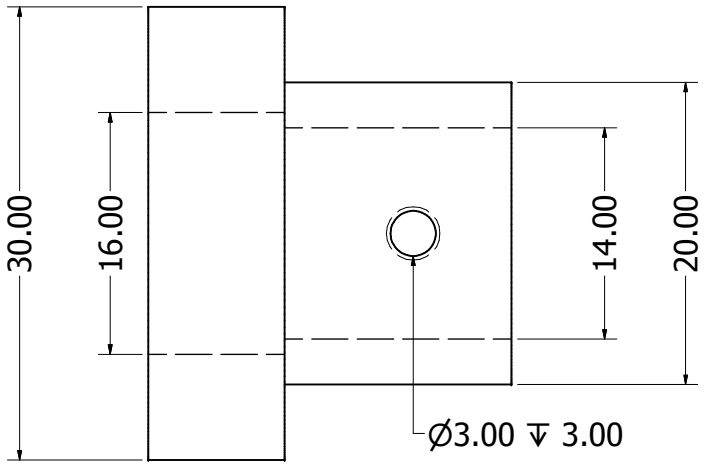

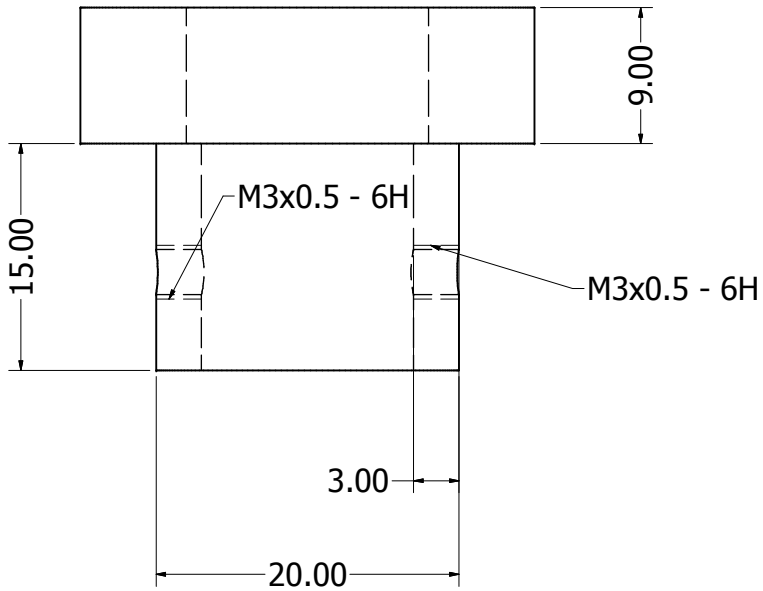

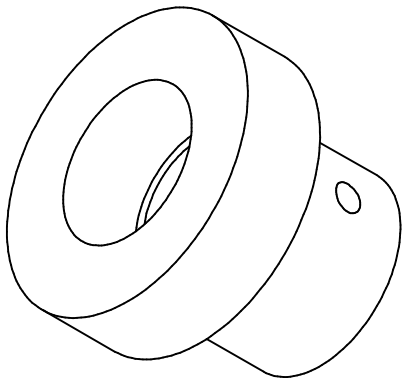

Qty : 1	
Material: Aluminium	Hub_2 blades
Dimensions [mm]	

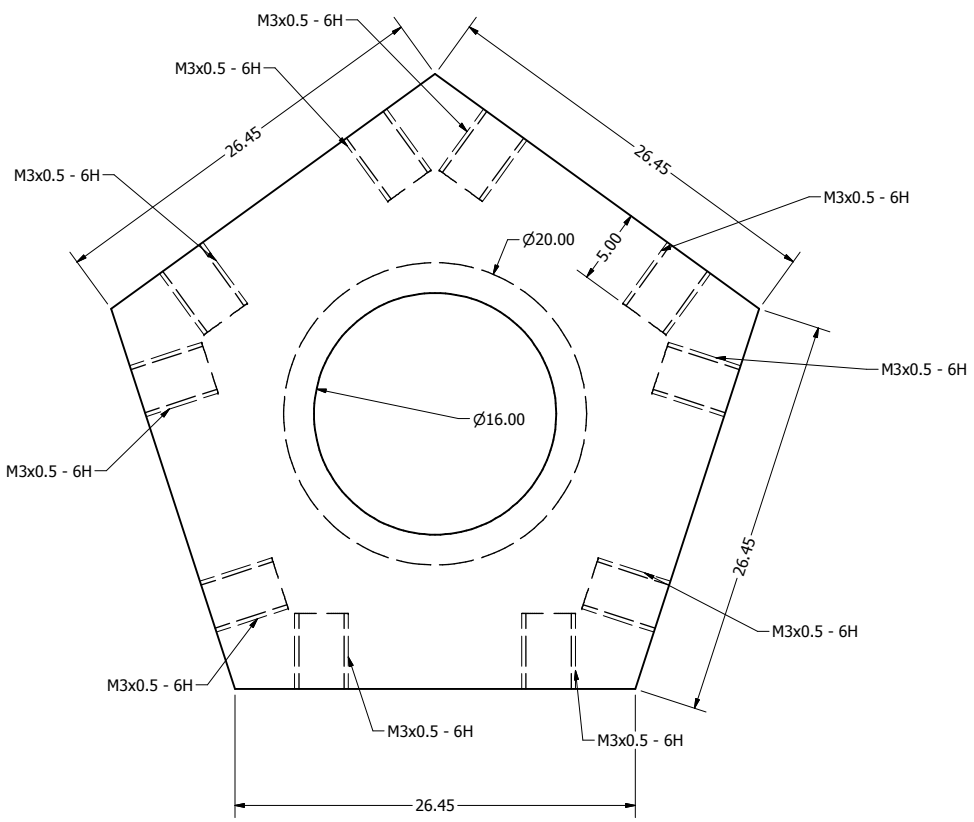

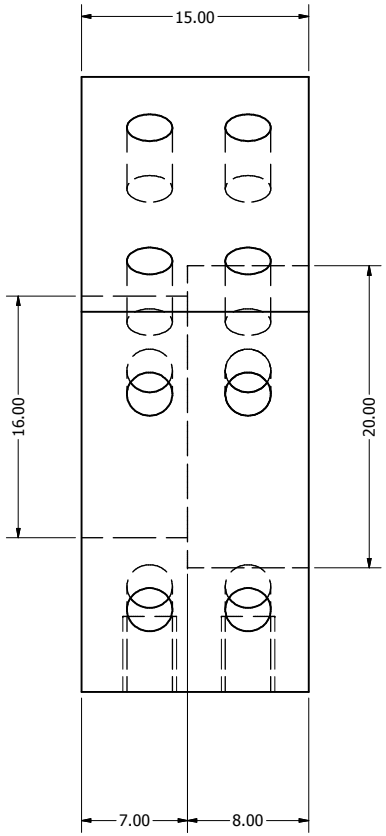

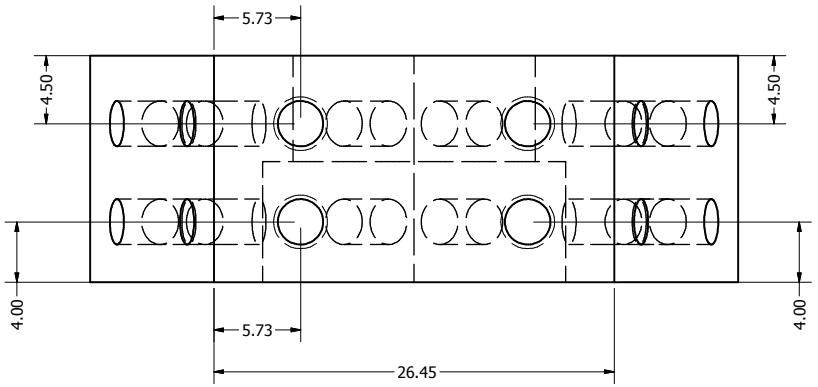

DRAWN Steph	18/08/2010	
CHECKED		TITLE
QA		
MFG		
APPROVED		
		SIZE C / DWG NO / REV
		SCALE / SHEET 1 OF 1

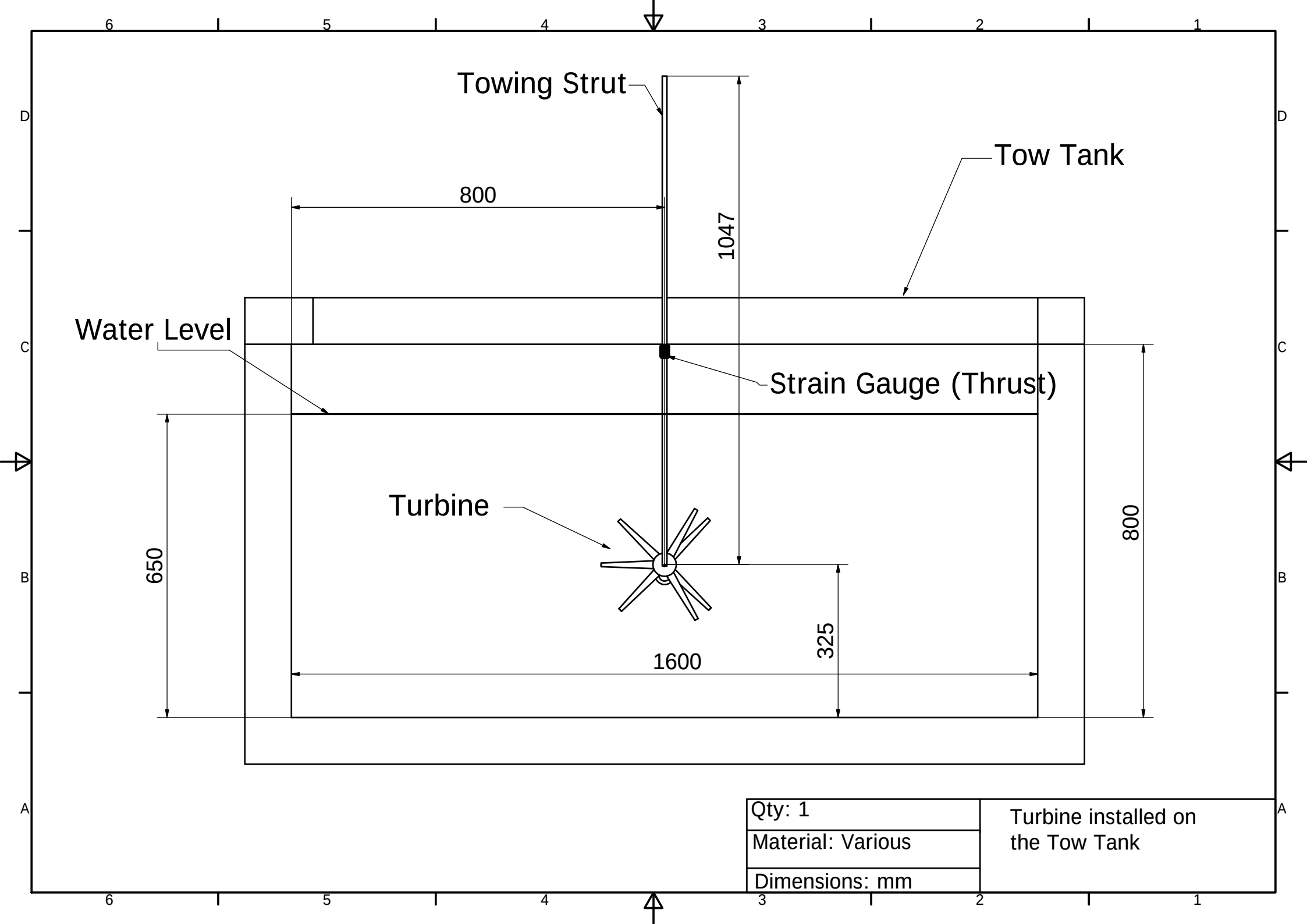
Towing Strut
Tow Tank
800
1047
Water Level
Strain Gauge (Thrust)
Turbine
650
800
325
1600
Qty: 1
Material: Various
Dimensions: mm
Turbine installed on the Tow Tank

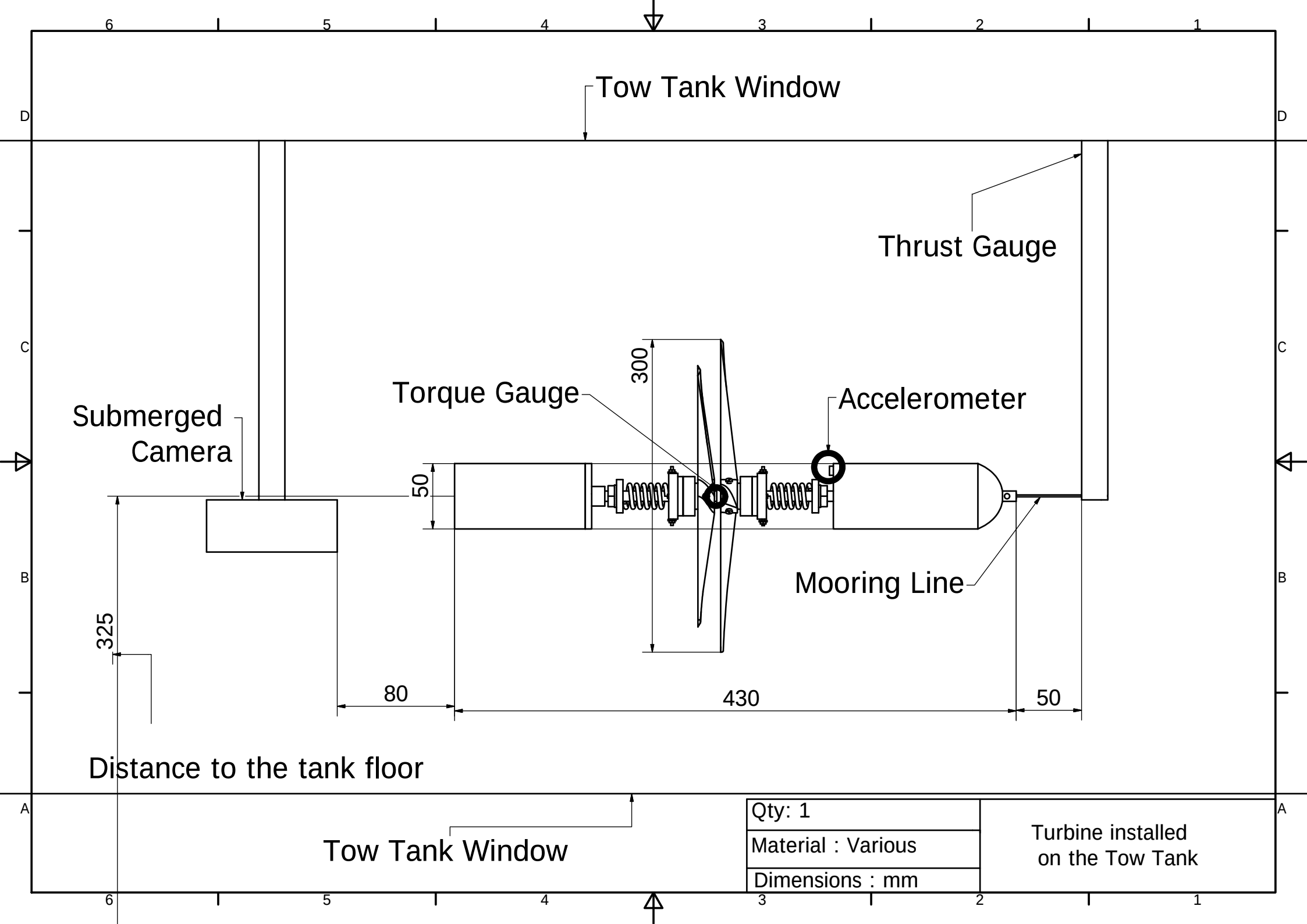
Tow Tank Window
Thrust Gauge
Torque Gauge
300
Accelerometer
Submerged
Camera
50
Mooring Line
325
80
430
50
Distance to the tank floor
Tow Tank Window
Qty: 1
Material : Various
Dimensions : mm
Turbine installed
on the Tow Tank

Appendix B

Existent Models to Evaluate Tethered Turbine Rotors

B.1 Dynamic Analysis Models to Study Tethered Wind Turbines

As it was discussed in Chapter 2, wind turbine technology evolved from using rigid foundations to a new stage where the turbines are attempted to be fixed to the seabed by mooring lines. Although the idea seems to be feasible (as it happened in the oil and gas industry), the interaction of random wind and waves motion coupled to rotordynamics of the turbine itself makes of it a difficult system to study. Thus, various models have been recently propose to examine the dynamics of floating OWTs (e.g. Wayman et al. (2006), Jonkman and Buhl (2007b), Nielsen et al. (2006), or Knauer (2007)).

The studies carried out by NREL (Jonkman and Buhl (2007a), Jonkman and Buhl (2007b) and Wayman et al. (2006) to mention a few) use the aerodynamics and structural dynamics code FAST coupled to other modules to complete the dynamic analysis of the full system. The core of the FAST code is Aerodyn which calculates de aerodynamic forces of the rotor using Blade Element Momentum (Section B.3). The aerodynamic forces are linked to the dynamic system obtained with Kane's method. This is solved through a 4th order Runge Kutta method for the first 3 time steps and then a prediction-corrector method is applied until the simulation is complete. The code involves 22/24 DOF (depending on the number of blades; 2 or 3), those include two flexible bodies: blades and tower. The edgewise and flapwise modes of the blades, the fore-aft and side to side modes for the tower are some of the DOF taken into account through the analysis. The nacelle, generator, hub, tail, and so forth are the rigid bodies

that complete the entire system. Turbulences can be set up in the model along with options that include three different control techniques.

The models proposed by Wayman et al. (2006) andJonkman and Buhl (2007b) integrate FAST to a the hydrodynamic software "WAMIT" to obtain hydrodynamic coefficients such as added mass, damping and stiffness of the structural system's ballast, in order to include the coefficients in the dynamic equations. After, those modules are coupled to a quasi-static analysis of the mooring line system.

Differently, models proposed by Knauer (2007) and Nielsen et al. (2006) integrate similar aeroelastic models such as Flex 5 and HAWC2. In order to carry out a complete dynamic analysis of the mooring lines and the rotordynamics, the studies of Knauer (2007) and Nielsen et al. (2006) coupled the aeroelastic routines with external hydrodynamic software to combine the dynamic motions of the structural system. For example, Nielsen et al. (2006) based its study on the SIMO/RIFLEX software which is able to undertake the analysis of floating bodies and additionally, it integrates the dynamics of slender bodies (e.g. mooring lines) through the use of dynamic libraries. As it can be observed there is a large amount of packages dedicated to undertake dynamics analysis of offshore structures, as it will be described in the next section. Thus, the last approaches should be consider as strategies to develop a model to study the dynamics of tethered turbines.

B.2 Hydrodynamic Software Packages

There is a large amount of software available for the analysis of offshore structures; for example, Orcaflex developed by Orcina, Zenmoor from the Company Zentech Ltd., Atkin's Quantitative Wave Analysis (AQWA) from ANSYS and Ariane-3D Dynamic. Due to the versatility, it is found that the most suitable programs to integrate a couple analysis of turbines are Orcaflex or the AQWA since they are capable to accept and communicate through their dynamic link libraries based on well known programming languages such as FORTRAN and C++. In both packages, it is also possible to generate a radiation/diffraction analysis of the structure in an environment of regular or irregular waves in time and frequency domain which can be coupled to a module of cable dynamics.

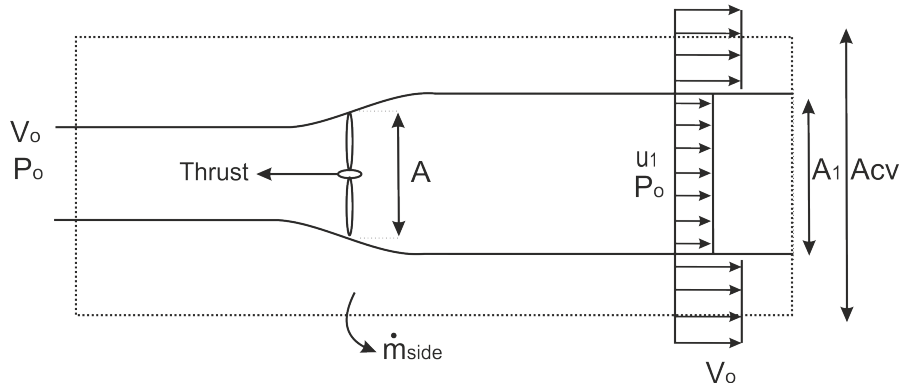

Figure B.1: Control volume around a wind turbine rotor, based on Hansen (2008)

B.3 Blade Element Momentum

The theory for an ideal wind turbine is described by a 1D momentum model. Basically, the theory assumes an inviscid and incompressible fluid. The turbine rotor is considered as a thin disk that does not opposes the fluid flow through it, similar to a porous disc. Finally, the far upstream and downstream flow pressures are consider to have a static free stream pressure (Hansen, 2008). The equations of the flow energy can be obtained through the volume control shown on Figure B.1. The control volume allows to obtain an approximation of the power output and thrust by a calculating the energy of the fluid through the Bernoulli equation. By introducing the axial induction factor which correlates the flow velocity at the rotor and the flow velocity far upstream the rotor, the equations to calculate power output and thrust can be obtained and applied as shown in Chapter 3.

As it can be observed, the power characteristics of a turbine can be approximated with the momentum theory; however, up to this point the analysis has not considered the solidity of the rotor, and the blade profile geometry (e.g. chord and twist distributions). Therefore, the analysis of the turbine can be complemented with the analysis of the several annular sections to calculate the corresponding normal and tangential forces according to the aerodynamic characteristics of the blade profile.

Figure B.2 describes the distribution of aerodynamic forces that occur on an 2D airfoil section. The lift and drag forces affecting the airfoil section are directly related to the angle of attack formed between the chord section of the foil and the relative velocity of the flow stream. This angle is in turn related to the local geometrical pitch angle and the angle (ϕ) that is formed between the rotor plane and the relative velocity of the fluid. Therefore, the final angle of attack is calculated by:

$$\alpha = \phi - \theta \tag{B.1}$$

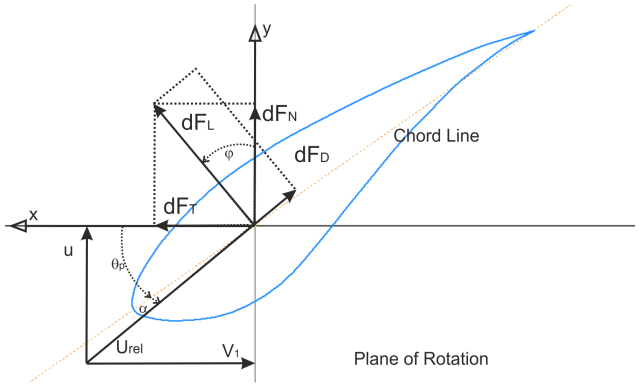

Figure B.2: Resultant Projection of Lift and Drag Forces,based on Manwell et al. (2009)

where α corresponds to the angle of attack and θ symbolizes the local pitch which relates the geometrical pitch angle and the corresponding blade twist. The twist angle for the airfoil S814 utilized on this experimental test was obtained from Giguère and Selig (1999).

Once the angle of the attack is known for the specific flow conditions, the aerodynamic lift and drag coefficients were obtained form the tests files contained in the code FAST developed by the NREL (Jonkman and Buhl, 2005). Thus, the normal and tangential forces for each blade section can be obtained with the use of the Equation B.2 to the Equation B.5.

$$L = 0.5\rho v^2 c C_l \tag{B.2}$$

$$D = 0.5\rho v^2 c C_d \tag{B.3}$$

$$C_N = Lcos\phi + Dsin\phi \tag{B.4}$$

$$C_T = Lsin\phi - Dcos\phi \tag{B.5}$$

where L and D are the lift and drag aerodynamic forces created on the airfoil respectively. ρ represents the density of salt water. c corresponds to the chord length of the foil and v expresses the undisturbed flow velocity. C_l and C_d are the corresponding lift and drag coefficients obtained from the characteristic tables of the S814 airfoil. Finally, C_N and C_T are the normal an tangential coefficients of each blade element respectively. This coefficients can the be used to calculate the normal and tangential forces as $F_n = 0.5\rho v^2 C_N c$; where c represents the chord length of the section. Similarly, the tangential force (F_t) is calculated but in this

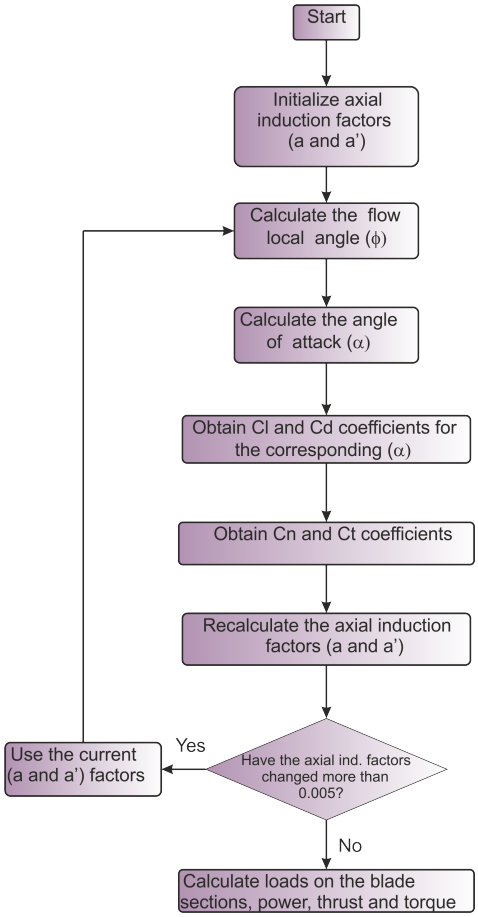

Figure B.3: BEM Algorithm, based on Hansen (2008)

occasion the C_T coefficient should be employed. Finally, the axial induction factors are recalculated and the iterative process is repeated until the axial induction factors become similar between iterations.

One of the main limitations of the model arise with assumption of independence between blade sections. This means that the resultant forces acting on one section do not have any relation to the following elements. In addition, the theory assumes to have an infinite number of blades; but, this postulation can be rectified by using the appropriate correction factors (e.g. Prandtl tip loss factor). Finally, wake effects are not considered in this analysis; however, some calculations considering swirl effects can be found on the model developed by NREL (Laino and Hansen, 2002). To sum up, the algorithm that was followed to compute the blade loads can be depicted on the following figure. The underlying concepts and theory used on this section were based from Hansen (2008) and Moriarty and Hansen (2005).

Appendix C

Results

C.1 Probability Density Functions

C.2 Frequency Domain Analysis

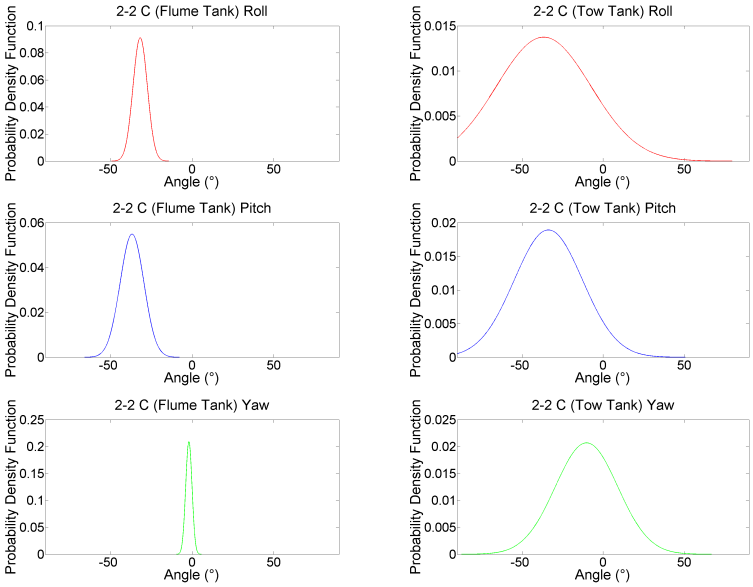

(a) (b)

Figure C.1: 2-2 C: a) Flume Tank and b) Tow Tank

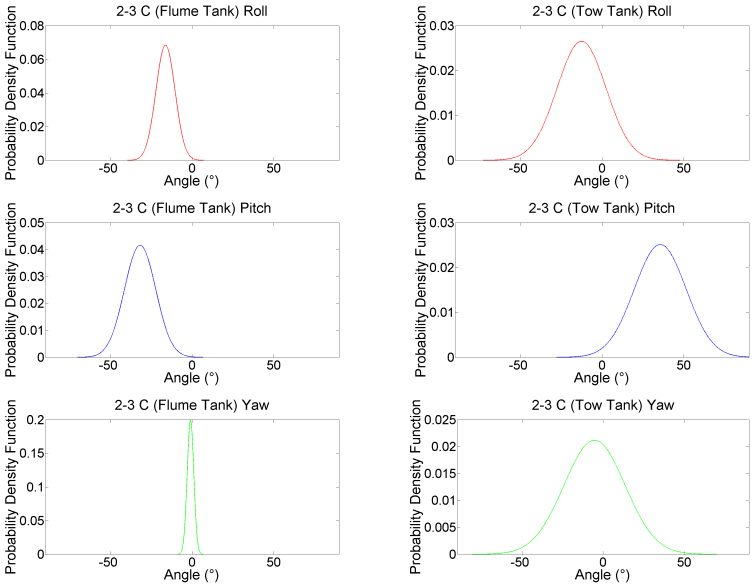

(a) (b)

Figure C.2: 2-3 C: a) Flume Tank and b) Tow Tank

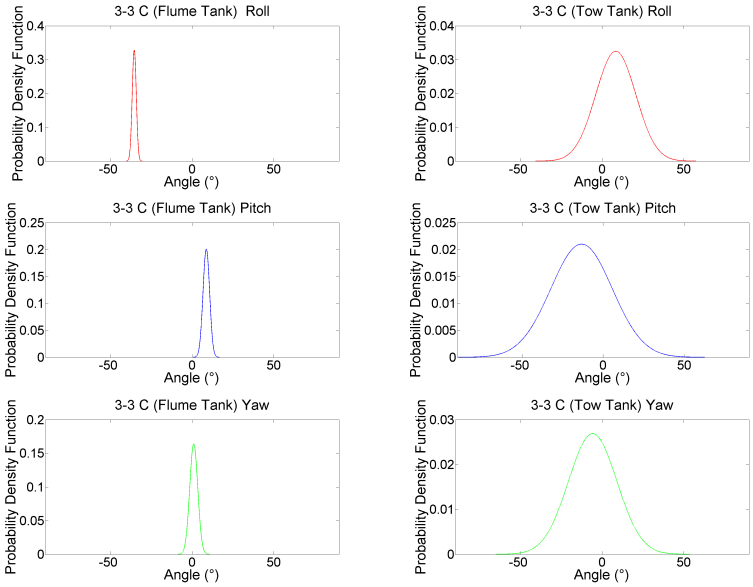

(a) (b)

Figure C.3: 3-3 C: a) Flume Tank and b) Tow Tank

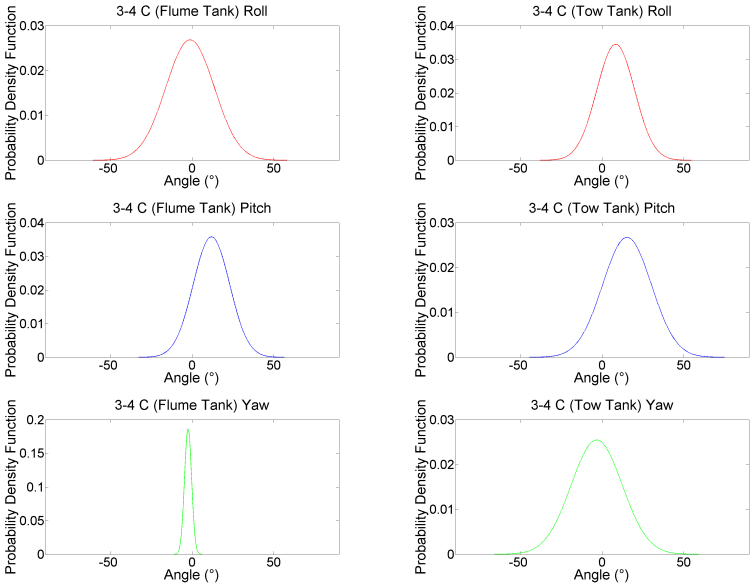

(a) (b)

Figure C.4: 3-4 C: a) Flume Tank and b) Tow Tank

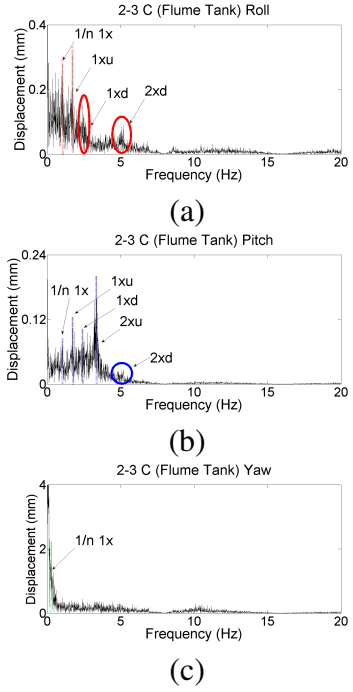

Figure C.5: 2-3 C Flume Tank FFT's: a) Roll b) Pitch and c) Yaw

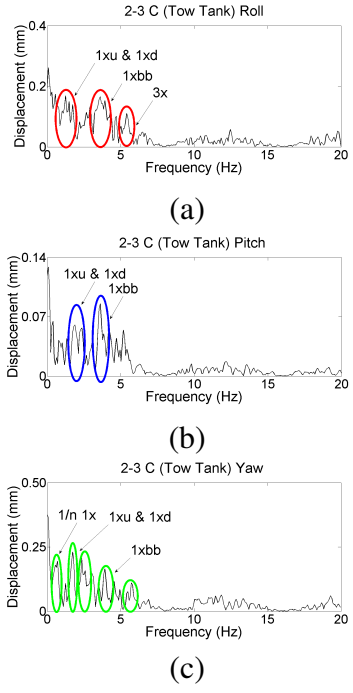

Figure C.6: 2-3 C Tow Tank FFT's: a) Roll b) Pitch and c) Yaw

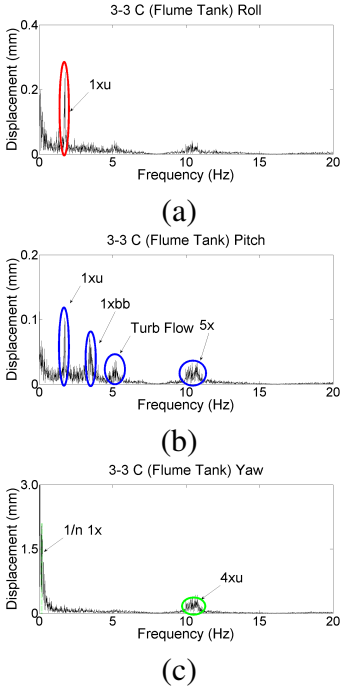

Figure C.7: 3-3 C Flume Tank FFT's: a) Roll b) Pitch and c) Yaw

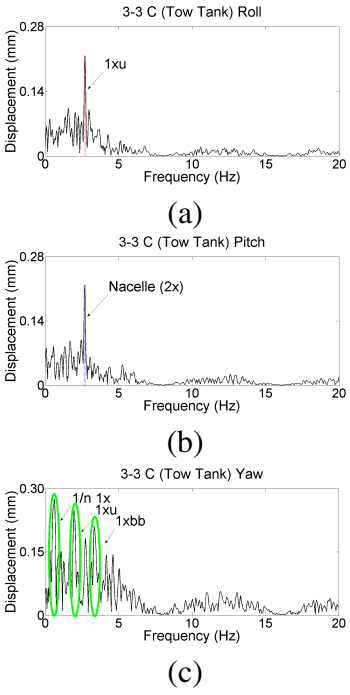

Figure C.8: 3-3 C Tow Tank FFT's: a) Roll b) Pitch and c) Yaw

Bibliography

4C Offshore, June 2012. Turbines v39-500kw.
URL http://www.4coffshore.com/windfarms/turbine-vestas-v39-500kw-tid56.html

Adams, M. L., 2005. Rotating Machinery Vibration: From Analysis to Troubleshooting. Marcel Dekker Inc.

Alstom, June 2012. Power–renewables.
URL http://www.alstom.com/power/renewables/ocean-energy/tidal-energy/

Analog Devices, 2007. ADXL33O - Small, Low Power, 3-Axis +/-3 g iMEMS® Accelerometer. Analog Devices, One Technology Way, P.O. Box 9106, Norwood, MA 02062-9106, U.S.A.
URL http://www.analog.com/static/imported-files/data_sheets/ADXL330.pdf

Ansys, April 2012. Ansys - aqwa features.
URL http://www.ansys.com/Products/Other+Products/ANSYS+Aqwa/Features

Bai, Y., 2003. Marine Structural Design. Elsevier.

Baltazar, J., Falcão de Campos, J., Bosschers, J., 2005. A study on the modeling of marine propeller tip flows using bem. In: Congreso de Métodos Numéricos en Ingeniería, SEMNI, Granada, Spain.

Batten, W., Bahaj, A., Molland, A., Chaplin, J., Feb. 2006. Hydrodynamics of marine current turbines. Renewable Energy 31 (2), 249–256.

Batten, W., Bahaj, A., Molland, A., Chaplin, J., 2008. The prediction of the hydrodynamicperformance of marine current turbines. Renewable Energy 33, Issue 5, 1085–1096.

Bradley, A., August 2006. Application Guide - Condition Monitoring. Rockwell Automation, Milwaukee, WI, USA.

Budynas, R. G., Nisbett, J. K., 2011. Shingley's Mechanical Engineering Design. McGraw Hill.

Bulder, B., Henderson, A., Huijsmans, R., Peeringa, J., Pierik, J., Snijders, E., van Hees, M., Wijnants, G., Wolf, M., 2003. Floating offshore wind turbines for shallow waters. In: European Wind Energy Conference.

Bureau Veritas and MCS, April 2012. Applications.
URL http://www.dredgingengineering.com/moorings/mooringsonline/ARI/ARI.htm#Applications

Byrne, B., Houlsby, G., 2006. Assessing novel foundation options for offshore wind turbines. In: World Maritime Technology Conference. London, UK.

Chakrabarti, S. K., 2002. The theory and Practice of Hydrodynamics and Vibration. World Scientific Publishing Co. Pte. Ltd.

Chen, L., McKerrow, P., 2007. Modelling the lama coaxial helicopter. In: Proceedings of the Australasian Conference on Robotics and Automation. Brisbane, Australia.

Chitode, J. S., 2009. Digital Signal Processing. Technical Publications Pune.

CJ Day Associates, 2001. Tidal turbine installation at fixed navigation marks. Tech. rep., Department of Trade and Industry.

Clarke, J., Connor, G., Grant, A., Johnstone, C., 2005. Developments of a contra-rotating tidal current turbine and analysis of performance. In: Proceedings of the 7th European Wave and Tidal Energy Conference. Porto, Potrugal.

Clarke, J., Connor, G., Grant, A., Johnstone, C., Mackenzie, D., 2007a. Development of a contra-rotating tidal current turbine and analysis of performance. In: Proceedings 7th European Wave and Tidal Energy Conference (EWTEC). Porto, Portugal.

Clarke, J., Connor, G., Grant, A., Johnstone, C., Ordonez-Sanchez, S., 2008. Contra-rotating marine current turbines: Performance in field trials and power train developments. In: Proceedings of the 10th World Renewable Energy Congress.

Clarke, J., Connor, G., Grant, A., Johnstone, C., Ordonez-Sanchez, S. E., 2010. Analysis of a single point tensioned mooring system for station keeping of a contra-rotating marine current turbine. IET Renewable Power Generation 4, 473–487, iSSN 1752-1416.

Clarke, J. A., Connor, G., Grant, A. D., Johnstone, C. M., Jan. 2007b. Design and testing of a contra-rotating tidal current turbine. Proceedings of the Institution of Mechanical Engineers, Part A: Journal of Power and Energy 221 (2), 171–179.

Cognity, July 2012. 3d print.
URL http://www.cognity.com/rapid-prototyping-3d-printer

Connor, G., D., G. A., Johnstone, C. M., 2008. Development of a european tidal energy road map. In: Proc. 2nd International Conference on Ocean Energy, Brest, France. Glasgow UK.

Cotrell, J., 2002. The mechanical design, analysis, and testing of a two-bladed wind turbine hub. Tech. rep., National Renewable Energy Laboratory.

Dawson, T. H., 1983. Offshore Structural Engineering. Prentice Hall Inc.

EMEC, April 2012. Tidal developers.
URL http://www.emec.org.uk/tidal_developers.asp

Environment Agency, 2012. Thames barrier project pack 2012. Tech. rep., The Environment Agency.

EPRI, 2006. Instream tidal power in north america - environmental and permitting issues. Tech. rep., Electric Power Research Institute (EPRI) , Inc. and Devine Tarbell & Associates, Inc.

EquiMar, September 2012. Equimar project deliverables.
URL http://www.equimar.org/

Fitzgerald, J., Bergdahl, L., 2007. Considering mooring cables for offshore wave energy converters. In: 7th European Wave and Tidal energy Conference. IST/IDMEC.

Fitzgerald, J., Bergdahl, L., Jan. 2008. Including moorings in the assessment of a generic offshore wave energy converter: A frequency domain approach. Marine Structures 21 (1), 23–46.

Fonseca, N.and Pascoal, R., Morais, T., Dias, R., 2009. Design of a mooring system with synthetic ropes for the flow wave energy converter. In: Volume 4: Ocean Engineering; Ocean Renewable Energy; Ocean Space Utilization, Parts A and B. ASME, pp. 1189–1198.

Fraenkel, P., 2005. Marine current turbines: pioneering the development of marine kinetic energy converters. In: Proceedings of the symposium on Fluid machinery for Wave and Tidal Energy: State of the Art and New Developments, Institute of Mechanical Engineers.

Fraenkel, P. L., Jan. 2007. Marine current turbines: pioneering the development of marine kinetic energy converters. Proceedings of the Institution of Mechanical Engineers, Part A: Journal of Power and Energy 221 (2), 159–169.

Francis, M., Hamilton, M., 2007. Srtt floating tidal turbine production design study with independent verification. Tech. rep., Scotrenewables Ltd Heriot-Watt University (ICIT).

Frohboese, P., Schmuck, C., 2010. Thrust coefficients used for estimation of wake effects for fatigue load calculation. In: European Wind Energy Conference.

Fulton, G., 2007. Semi-submersible platform and anchor foundation systems for wind turbine support. Tech. rep., NREL/SR-500-40282 (2007).

Fulton, G., Malcolm, D., Elwany, H., Stewart, W., Moroz, E., Dempster, H., 2005. Semi-submersible platform and anchor foundation systems for wind turbine support. Tech. rep., National Renewable Energy Laboratory (NREL).

Galloway, P. W., Myers, L. E., Bahaj, A. S., 2011. Experimental and numerical results of rotor power and thrust of a tidal turbine operating at yaw and in waves. In: World Renewable Energy Congress.

Gao, Z., Moan, T., 2009. Mooring system analysis of multiple wave energy converters in a farm configuration. In: Proceedings of the 8th European Wave and tidal Energy Conference.

Geopacks, September 2012. Home - stream flowmeter.
URL `http://www.geopacks.com/default.aspx`

Ghassemi, H., Jan. 2009. Hydrodynamic performance of coaxial contra-rotating propeller (ccrp) for large ships. Polish Maritime Research 16 (1), 22–28.

Giguère, P., Selig, M., 1999. Design of a tapered and twisted blade for the nrel combined experiment rotor. Tech. rep., National Renewable Energy Laboratory (NREL).

Gitano-Briggs, H., 2010. Wind Power. InTech.

Goldman, S., 1999. Vibration Spectrum Analysis - A Practical Approach. Industrial Press Inc.

Gooch, S., Thomson, J., Polagye, B.and Meggitt, D., 2009. Site characterization for tidal power. In: In Proceedings of Oceans 2009.

Hammerfest Strom, April 2012a. Product.
URL `http://www.hammerfeststrom.com/products/`

Hammerfest Strom, May 2012b. Research and development.
URL `http://www.hammerfeststrom.com/`

Hansen, M. O. L., 2008. Aerodynamics of Wind Turbines. Earthscan.

Harris, R., Johanning, L., Wolfram, J., 2004. Mooring systems for wave energy converters: A review of design issues and choices. In: 3rd International Conference on Marine Renewable Energy, Blyth, UK.

Harris, S. T., 2003. Signals and Sytems with MATLAB. Orchard Publications.

Hau, E., 2006. Wind turbines: fundamentals, technologies, application, economics. Springer.

Heinzel, G., Rudiger, A., Schilling, R., 2002. Spectrum and spectral density estimation by the discrete fourier transform (dft), including a comprehensive list of window functions and some new at-top windows. Tech. rep., Max Planck Society.

Henriques, J., Marques da Silva, F., Estanqueiro, A., Gato, L., Dec. 2009. Design of a new urban wind turbine airfoil using a pressure-load inverse method. Renewable Energy 34 (12), 2728–2734.

Hochart, C., Fortin, G., Perron, J., Ilinca, A., 2008. Wind turbine performance under icing conditions. Wind Energy 11, 319–333.

Huang, M., Aggidis, G. A., Feb. 2008. Developments, expectations of wave energy converters and mooring anchors in the uk. Journal of Ocean University of China 7 (1), 10–16.

Jardine, R., 2009. Review of technical issues relating to foundations and geotechnics for offshore installations in the ukcs. Tech. rep., Imperial College London.

Johanning, L., Smith, G. H., Wolfram, J., 2005. Towards design standards for wec moorings. In: 6th European Wave and Tidal Energy Conference.

Johanning, L., Smith, G. H., Wolfram, J., 2006. Mooring design approach for wave energy converters. Journal of Engineering for the Maritime Environment 220, 159–174.

Johanning, L., Wolfram, J., 2005. Challenging tasks on moorings for floating wecs. In: International Symposium on Fluid Machinery for Wave and Tidal Energy: State of the Art and New Developments.

Johnson, R., 2010. USG Shaft Wall Systems. USG Design Studio.

Johnson, W., 1994. Helicopter Theory. Dover Publications.

Jonkman, J. M., Buhl, M.L., J., 2007a. Development and verification of a fully coupled simulator for offshore wind turbines. In: 45th AIAA Aerospace Sciences Meeting and Exhibit.

Jonkman, J. M., Buhl, M.L., J., 2007b. Loads analysis of a floating offshore wind turbine using fully coupled simulation. In: WINDPOWER Conference and Exhibition.

Jonkman, J. M., Buhl, M. L., 2005. Fast user's guide. Tech. rep., National Renewable Energy Laboratory.

Jukola, H., Ronkainen, T., 2006. Contra-rotating propellers - combination of dp capability, fuel economy and environment. In: Dynamic Positioning Conference. Houston, U.S.A.

Kehtarnavaz, N., Kim, N., 2005. Digital Signal Processing System Level Design using Labview. Elsevier Inc.

Knauer, A.and Hagen, E., 2007. Simulation of floating wind turbine concept. In: European Offshore Wind Energy Conference and Exhibition (EOW).

Kumar, P. S., Bensingh, R. J., Abraham, A., 2012. Computational analysis of 30kw contra rotorwind turbine. ISRN Renewable Energy Volume 2012, 1–5.

Laino, D., Hansen, A., December 2002. Aerodyn User's Guide. Windward Engineering L.C. and National Renewable Energy Laboratory, Salt Lake City, UT84117. U.S.A.

Larsen, T. J., Madsen, H. A., Thomsen, K., Rasmussen, F., 2007. Reduction of teeter angle excursions for a two-bladed downwind rotor using cyclic pitch control. In: European Wind Energy Conferece.

Lee, K., 2005. Responses of floating wind turbines to wind and wave excitation. Master's thesis, Department of Ocean Engineering, Massachusetts Institute of Technology, Cambridge, Massachusetts, USA.

Mackie, G., 2008. Development for evopod tidal stream turbine. In: Proceedings of the International Conference on Marine Renewable Energy. The Royal Institute of Naval Architects.

Macnaughton, D., Fraenkel, P., Paish, O., Hunter, R., Derrick, A., 1993. Tidal stream turbine development. In: International Conference on Renewable Energy - Clean Power. pp. 67 – 71.

Malhotra, S., 2011. Wind Turbines. In Tech.

Manwell, J. F., McGowan, J. G., Rogers, A. L., 2009. Wind Energy Explained: Theory, Design and Applications. John Wiley and Sons Ltd.

Marine Current Turbines, September 2012. Technology development.
URL `http://www.marineturbines.com/SeaGen-Products/SeaGen-S`

Marine Environmental Research, 2011. Tidal resource.
URL `http://www.renewables-atlas.info/`

MARINET, September 2012. Access.
URL http://www.fp7-marinet.eu/

Marion Harrald, C. A., Davies, I., September 2010. Scottish marine and freshwater science volume 1 no 18: Further scottish leasing round (saltire prize projects): Regional locational guidance. Web only publication.
URL http://www.scotland.gov.uk/Publications/2010/09/17095123/0

Masters, I., Orme, J., 2006. Analysis and comparison of support structure concepts for tidal stream turbines. In: World Maritime Technology Conference.

Maxwell, P., Owen, A., Ogilvie, M., Scott, B., 2008. Islay community tidal energy project. Tech. rep., The Robert Gordon University.

McCombes, T., Johnstone, C., Holmes, B., Myers, L. E., Bahaj, A., Kofoed, J., 2010. Best practice for tank testing of small marine energy devices. deliverable d3.4. Tech. rep., Equitable Testing and Evaluation of Marine Energy Extraction Devices in terms of Performance, Cost and Environmental Impact (EQUIMAR).

Mokwa, R. L., 1999. Investigation of the resistance of pile caps to lateral loading. Ph.D. thesis, Virginia Polytechnic Institute.

Molland, A. F., Bahaj, A. S., Chaplin, J. R., Batten, W. M. J., Jan. 2004. Measurements and predictions of forces, pressures and cavitation on 2-d sections suitable for marine current turbines. Proceedings of the Institution of Mechanical Engineers, Part M: Journal of Engineering for the Maritime Environment 218 (2), 127–138.

Moriarty, P. J., Hansen, A. C., December 2005. Aerodyn Theory Manual. National Renewable Energy Laboratory, 1617 Cole Boulevard, Golden, Colorado, U.S.A.

Morton, K. M., 2004. Tidal and marine current energy resource in ireland. Tech. rep., Queens University Belfast, Natural Power Consultants for the Sustainable Energy Authority of Ireland.

Nautricity, April 2012. Cormat.
URL http://www.nautricity.com/cormat/

Nicholson, J. W., 2006. The Chemistry of Polymers. The Royal Society of Chemistry.

Nielsen, F. G., Hanson, T. D., Skaare, B., 2006. Integrated dynamic analysis of floating offshore wind turbines. In: Proceedings of the international Conference on Offshore Mechanics and Arctic Engineering.

Nihoul, J. C. J., 1982. Hydrodynamics of semi-enclosed seas: proceedings of the 13th International Liège Colloquium on Ocean Hydrodynamics. Elsevier Oceanography Series.

Norris, J., Dronio, E., 2007. Update on emec activities, resource description, and characterisation of wave-induced velocities in a tidal flow. In: Proceedings of the European Conference of Wave and Tidal Energy.

Object-Geometries, 2010. Fullcure materials. Tech. rep., Object Geometries Ltd.

Oceanflow Energy, April 2012. Technology.
URL http://www.oceanflowenergy.com/technology.html

O'Doherty, D., Mason-Jones, A., O'Doherty, T., Byrne, C., 2009. Considerations of improved tidal stream turbine performance using double rows of contra-rotating blades. In: Proceedings of the 8th European Wave and Tidal Energy Conference, Uppsala, Sweden.

Openhydro, September 2012. Development (emec).
URL http://www.openhydro.com/development.html

Orcina, April 2012. Applications.
URL http://www.orcina.com/SoftwareProducts/OrcaFlex/Applications/index.php

Ordonez-Sanchez, S., Grant, A., Johnstone, C., 2010. Contra rotating marine turbines tank tests to analyse system dynamic response. In: International Conference in Ocean Energy.

Patel, M. H., 1989. Dynamics of Offshore Structures. Butterworths & Co. Ltd.

Pelamis, May 2012. Global resource.
URL http://www.pelamiswave.com/global-resource

PelaStar, 2012. Anchors. Tech. rep., Glosten Solutions, Inc.

Phidgets, September 2012. Products - 20 amp current sensor ac/dc.
URL http://www.phidgets.com/products.php?category=8

Piersol, A. G., Paez, T. L., 2002. Harris' Shock and Vibration Handbook. McGraw-Hill Inc.

Polagye, B., Previsic, M., 2006. System level design, performance, cost and economic assessment - tacoma narrow washington tidal in-stream power plant. Tech. rep., Electric Power Research Institute.

Principle Power, May 2012. Products.
URL http://www.principlepowerinc.com/products/windfloat.html

Ramachandran, G., Bredmose, H., Sørensen, J., Jensen, J. J., 2011. Response of response of a tlp floating wind turbine subjected to combined wind and wave loading. In: International Workshop on Water Waves and Floating Bodies.

Rangel-Ramírez, J. G., Sørensen, J. D., 2008. Optimal risk-based inspection planning for offshore wind turbines. Steel Structures 8, 295–303.

Ricci, P., Villate, J. L., Scuotto, M., Zubiate, L., Davey, T., Smith, G. H., Smith, H., Huertas-Olivares, C., Neumann, F., Stallard, T., Bittencourt Ferreira, C., Flinn, J., Boehme, T., Grant, A., Johnstone, C., Retzler, C., Sorensen, H. C., 2009. Global analysis of pre-normative research activities for marine energy - deliverable d1.1. Tech. rep., Equitable Testing and Evaluation of Marine Energy Extraction Devices in terms of Performance, Cost and Environmental Impact (Equimar).

Rogers, L., 1979. The application of vibration signature analysis and acoustic emission source location to on-line condition monitoring of anti-friction bearings. Tribology International 12, 51–58.

Rose, S., Johnstone, C., Grant, A., 2010. Investigating the wake of a marine energy converter through flume channel testing. In: World Renewable Energy Congress XI, Abu Dhabi, UAE.

Rosler, J., Hardens, H., Baker, M., 2007. Mechanical Behaviour of Engineering Materials. Springer.

Savin, A., Svensson, O., Stro?mstedt, E., Bostro?m, C., Leijon, M., 2009. Determining the service life of a steel wire under a working load in the wave energy converter (wec). In: Volume 4: Ocean Engineering; Ocean Renewable Energy; Ocean Space Utilization, Parts A and B. ASME, pp. 839–844.

Schilling, R. J., Harris, S. L., 2005. Fundamentals of Digital Signal Processing Using Matlab. Cengage Learning.

Scotrenewables, April 2012. The concept.
URL `http://www.scotrenewables.com/technology-development/the-concept`

Sinclair, K., Bowen, A., 2008. Testing small wind turbines at the national renewable energy laboratory: Nrel/cp-500-43452. In: Wind Power.

SKF Group, June 2012. Products.
URL `http://www.skf.com/portal/skf/home/products?maincatalogue=1&lang=en&newlink=1_1_7`

SMD, April 2012. Design development.
URL http://smd.co.uk/products/renewables/design-development.htm

Somers, D. M., 1997. Design and Experimental Results for the S814 Airfoil. Airfoils Inc. and National Renewable Energy Laboratory (NREL).

Somers, D. M., Tangler, J. L., 1995. Wind-tunnel test of the s814 thick-root airfoil. Tech. rep., National Renewable Energy Laboratory (NREL).

Spiegel, M. R., Stephens, J. L., 1999. Schaum's Outline of Theory and Problems of Statistics. McGraw Hill.

Stallard, T., 2011. Summary of performance limits and guidelines for assessing devices in terms of performance increase required to attain a target unit electricity cost. deliverables - d7.5.1-2. Tech. rep., Equitable Testing and Evaluation of Marine Energy Extraction Devices in terms of Performance, Cost and Environmental Impact (EQUIMAR).

Statoil, May 2012. Technology and innovation.
URL http://www.statoil.com/en/TechnologyInnovation/NewEnergy/RenewablePowerProduction/Offshore/Hywind/Pages/HywindPuttingWindPowerToTheTest.aspx

Stegemann, D., 1998. Monitoring and vibrational diagnostic of rotating machinery in power plants. In: Power Station Maintenance - Profitability Through Reliability. First IEE/IMechE International Conference on (Conf. Publ. No. 452). pp. 39 – 44.

Suzuki, K., Yamaguchi, H., Akase, M., Imakita, A., Ishihara, T., Fukumoto, Y., Oyama, T., 2011. Initial design of tension leg platform for offshore wind farm. Journal of Fluid Science and Technology, 6, Issue 3, 372–381.

Swanturbines, April 2012. Technology.
URL http://www.swanturbines.co.uk/technology.htm

Sway, May 2012. Home.
URL http://sway.no/

Tangler, J. L., Somers, D. M., 1995. Nrel airfoil families for hawt. Tech. rep., National Renewable Energy Laboratory.

Thomson, J., Polagye, B., Richmond, M., Durgesh, V., 2010. Quantification of turbulence for tidal power applications. In: MTS/IEEE Oceans Conference.

Tocardo, May 2012. Technology.
URL http://www.tocardo.com/digi_cms/5/technology.html

Trantina, G., Nimmer, R., 1994. Structural Analysis of Thermoplastic Components. McGraw-Hill Inc.

Tronix, June 2012. Lines.
URL http://www.tronixpro.com/index.php/brands/tronixpro/accessories/lines/item/164-wire-trace-with-crimps

Ultramarine, April 2012. Moses - technical information.
URL http://www.ultramarine.com/hdesk/document/document.htm

Vanzwieten, J., Driscoll, F., Leonessa, A., Deane, G., 2006. Design of a prototype ocean current turbine-part i: mathematical modeling and dynamics simulation. Ocean Engineering 33, 1485–1521.

VanZwietena, J., Driscolla, F., Leonessaa, A., Deaneb, G., 2006. Design of a prototype ocean current turbine-part ii: flight control system. Ocean Engineering 33, 1522–1551.

Venugopal, V., Davey, T., Smith, H., Smith, G., Holmes, B., Barrett, S., Prevosto, M., Maisondieu, C., L., C., L., B., Lawrence, J., Girard, F., 2011. Wave and tidal resource characterisation. Tech. rep., Equitable Testing and Evaluation of Marine Energy Extraction Devices in terms of Performance, Cost and Environmental Impact (EQUIMAR).

Verdant Power, April 2012. What we do.
URL http://verdantpower.com/what/

Vickers, A., Johanning, L., 2009. Comparison of damping properties for three different mooring arrangements. In: 8th European Wave and Tidal Conference.

Vishay Measurements Group, 1989. Strain gage selection: Criteria, procedures, recommendations, tn-505-4. Tech. rep., Measurements Group Inc., 1 Scarsdale Road, Toronto, ON M3B2R2.

Vishay Presicion Group, June 2012. Product "m-coat w1".
URL http://www.vishaypg.com/micro-measurements/list/product-11033/

Vø lund, P., Dec. 2005. Concrete is the future for offshore foundations. Wind Engineering 29 (6), 531–539.

Wayman, E. N., Sclavounos, P. D., Butterfield, S., Jonkman, J., Musial, W., 2006. Coupled dynamic modeling of floating wind turbine systems. In: Offshore Technology Conference (OTC).

Westgate, Z., DeJong, J., 2005. Geotechnical considerations for offshore wind turbines. Tech. rep., Massachusetts Technology Collaborative Renewable Energy Trust.

White, F. M., 1991. Viscous Fluid Flow. McGraw-Hill Inc.

Wowk, V., April 2009. A brief tutorial on machine vibration. Machine Dynamics Inc., 1021 Commercial Drive SE Rio Rancho, NM 87124 PO Box 66479 Albuquerque, NM 87193-6479.

Yuan, Y., Cui, J., Mang, H. A., 2009. Computational Structural Engineering. Springer.

Zaayer, M. B., 2003. Comparison of monopile, tripod, suction bucket and gravity base design for a 6 mw turbine. In: European seminar offshore wind energy in mediterranean and other european seas. pp. 255–269.